DOE/EV/06020-1
UC-11

DOE/EV/06020--1

DE82 015891

Final Report
Vaporization, Dispersion, and Radiant Fluxes From LPG Spills
Technical Report

Published: May 1982

Prepared by: Applied Technology Corp.
P.O. Box FF
Norman, OK 73070
Under Contract No. DE-AC05-78EV-06020

Prepared for:

U.S. Department of Energy
Assistant Secretary for Environmental
Protection, Safety and Emergency Preparedness
Office of Operational Safety
Washington, DC 20545

DISCLAIMER

Technical Report Documentation Page

1. Report No.	2. Government Accession No.	3. Recipient's Catalog No.
DOE/EP-0042	DOE/EP-0042	

4. Title and Subtitle	5. Report Date
Vaporization, Dispersion, and Radiant Fluxes from LPG Spills	December, 1981
	6. Performing Organization Code
7. Author(s) J: R. Welker and W. D. Cavin	8. Performing Organization Report No. ATC-112-FR-D
9. Performing Organization Name and Address Applied Technology Corp. 401 West Main Street, Suite 220 Norman, OK 73069	10. Work Unit No. (TRAIS)
	11. Contract or Grant No. DE-AC05-78EV-06020
12. Sponsoring Agency Name and Address U. S. Department of Energy (EP-32) Operational Safety Programs Washington, DC 20545	13. Type of Report and Period Covered Final Report Task D
	14. Sponsoring Agency Code

15. Supplementary Notes
This report was prepared under the cognizance of Dr. John M. Cece, Operational Safety Programs, U. S. Department of Energy (EP-32).

16. Abstract

Both burning and non-burning spills of LPG (primarily propane) were studied. Vaporization rates for propane spills on soil, concrete, insulating concrete, asphalt, sod, wood, and polymer foams were measured. Thermal conductivity, heat transfer coefficients, and steady state vaporization rates were determined.

Vapor concentrations were measured downwind of open propane pools 25, 100, 400, and 1600 ft^2 in area. A Gaussian dispersion model modified for area sources provided a good correlation of measured concentrations.

Emitted and incident radiant fluxes from propane fires were measured. Simplified flame radiation models were adequate for predicting radiant fluxes; the maximum effective flux emitted at the flame surface was about 50,000 Btu/hr-ft^2.

A few tests in which propane was sprayed into the air showed that at moderately high spray rates all the propane flashed to vapor or atomized; no liquid collected on the ground.

17. Key Words	18. Distribution Statement
Liquefied petroleum gas, vapor dispersion, vaporization rates, boiloff rates, flame radiation, LPG, LPG fires, LPG spills, fire modeling.	This document is available from: National Technical Information Service 5285 Port Royal Road Springfield, VA 22161

19. Security Classif. (of this report)	20. Security Classif. (of this page)	21. No. of Pages	22. Price
Unclassified	Unclassified		

METRIC CONVERSION FACTORS

Approximate Conversions to Metric Measures

Symbol	When You Know	Multiply by	To Find	Symbol
	LENGTH			
in	inches	*2.5	centimeters	cm
ft	feet	30	centimeters	cm
yd	yards	0.9	meters	m
mi	miles	1.6	kilometers	km
	AREA			
in^2	square inches	6.5	square centimeters	cm^2
ft^2	square feet	0.09	square meters	m^2
yd^2	square yards	0.8	square meters	m^2
mi^2	square miles	2.6	square kilometers	km^2
	acres	0.4	hectares	ha
	MASS (weight)			
oz	ounces	28	grams	g
lb	pounds	0.45	kilograms	kg
	short tons (2000 lb)	0.9	tonnes	t
	VOLUME			
tsp	teaspoons	5	milliliters	ml
Tbsp	tablespoons	15	milliliters	ml
fl oz	fluid ounces	30	milliliters	ml
c	cups	0.24	liters	l
pt	pints	0.47	liters	l
qt	quarts	0.95	liters	l
gal	gallons	3.8	liters	l
ft^3	cubic feet	0.03	cubic meters	m^3
yd^3	cubic yards	0.76	cubic meters	m^3
	TEMPERATURE (exact)			
°F	Fahrenheit temperature	5/9 (after subtracting 32)	Celsius temperature	°C

*1 in = 2.54 (exactly). For other exact conversions and more detailed tables, see NBS Misc. Publ. 286, Units of Weights and Measures, Price $2.25, SD Catalog No. C13.10:286.

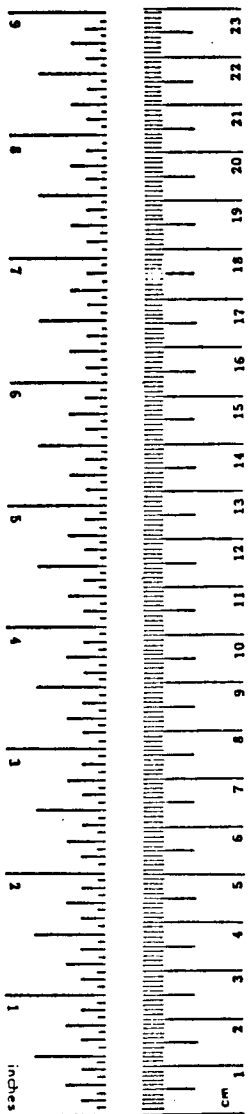

Approximate Conversions from Metric Measures

Symbol	When You Know	Multiply by	To Find	Symbol
	LENGTH			
mm	millimeters	0.04	inches	in
cm	centimeters	0.4	inches	in
m	meters	3.3	feet	ft
m	meters	1.1	yards	yd
km	kilometers	0.6	miles	mi
	AREA			
cm^2	square centimeters	0.16	square inches	in^2
m^2	square meters	1.2	square yards	yd^2
km^2	square kilometers	0.4	square miles	mi^2
ha	hectares (10,000 m^2)	2.5	acres	
	MASS (weight)			
g	grams	0.035	ounces	oz
kg	kilograms	2.2	pounds	lb
t	tonnes (1000 kg)	1.1	short tons	
	VOLUME			
ml	milliliters	0.03	fluid ounces	fl oz
l	liters	2.1	pints	pt
l	liters	1.06	quarts	qt
l	liters	0.26	gallons	gal
m^3	cubic meters	35	cubic feet	ft^3
m^3	cubic meters	1.3	cubic yards	yd^3
	TEMPERATURE (exact)			
°C	Celsius temperature	9/5 (then add 32)	Fahrenheit temperature	°F

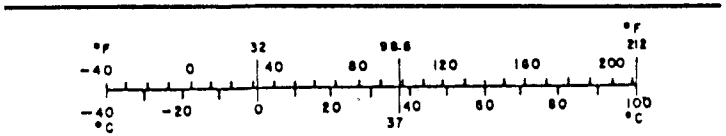

TABLE OF CONTENTS

TABLE OF CONTENTS--Continued

LIST OF FIGURES

LIST OF FIGURES--Continued

LIST OF FIGURES--Continued

LIST OF TABLES

EXECUTIVE SUMMARY

INTRODUCTION

In 1979 and 1980, tests were performed to determine the effectiveness of some fire control and extinguishing agents for liquefied petroleum gas (LPG) fires (Johnson, et al. 1980). Those tests required that LPG be spilled, ignited, and then attacked with fire fighting agents. The sequence followed during the tests was much the same as expected for an accidental spill and fire, and it was possible to obtain information on dispersion of LPG vapor and radiation from LPG fires during the same test series.

The fire control tests did not require a sudden release of LPG, so there were some limitations on the information that could be gained without major modifications to the test program. The most important limitation was that the LPG was spilled slowly, so that transient behavior could not be studied. Therefore vapor dispersion and flame radiation studies were made only for steady state conditions. "Steady state" refers to the vaporization rate of fuel. Both vapor concentrations and flame radiation fluctuated during the tests because of atmospheric properties.

In addition to the observations made in conjunction with the fire control tests, small scale tests were conducted to study the vaporization of LPG spilled on solid

surfaces and the behavior of LPG leaking from containers at high pressure and ambient temperatures.

This report is divided into four sections, each of which discusses one of the subject areas. Each section is written as a separate report. The LPG used in all tests was commercial propane, generally more than 97 percent pure if supplied at ambient temperature and 80 percent pure if supplied as a refrigerated liquid.

I. DISPERSION OF VAPORS FROM LPG SPILLS

Propane was unloaded into concrete pits 5, 10, 20, and 40 ft square from either ambient temperature or refrigerated storage. Filling time for a depth of 3 inches was about a half hour to 2 hours, so the pools had reached approximately steady vaporization rates before dispersion tests began. Five gas sensors were placed in the vapor plume downwind of the spill as near the mean plume centerline as could be determined from wind direction measurements. Concentrations were measured for periods from 10 to 20 min for most tests. Wind speed, wind direction, and propane vaporization rate were measured during the tests. The dispersion data in this report are primarily averages of the measured data for the test durations.

Figure S-1 shows the average propane concentration downwind of a 5-ft square pit containing propane. Similar plots were obtained for all of the tests. A Gaussian

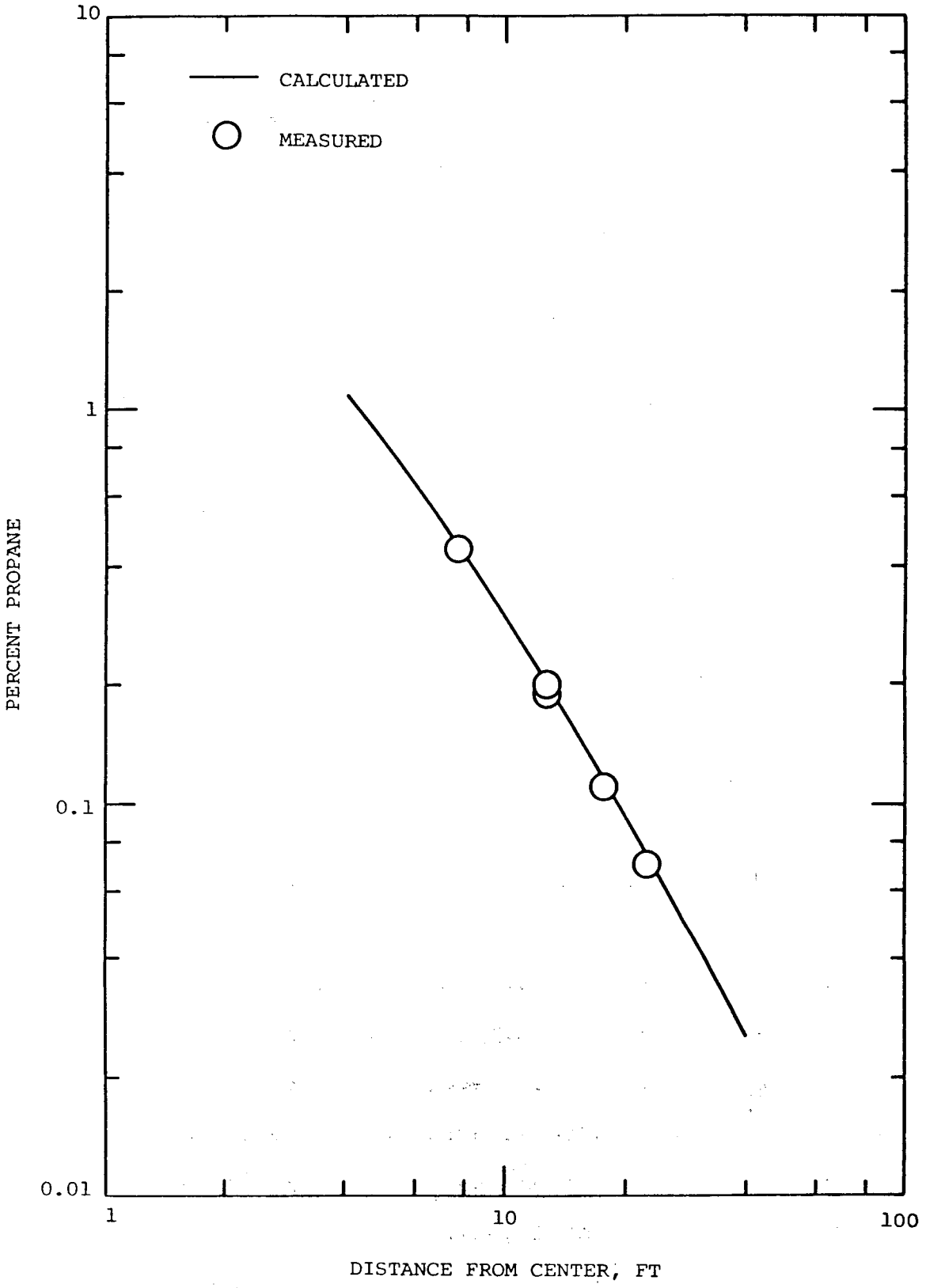

FIGURE S-1. COMPARISON OF AVERAGE MEASURED AND CALCULATED PROPANE CONCENTRATIONS, RUN 275-1.

dispersion model modified for area sources was used to predict the concentration based on the vaporization rate, the wind velocity, and atmospheric stability. The atmosperhic stability class was determined on the basis of wind direction fluctuations. The line drawn through the data in Figure S-1 shows the calculated concentration. Similar calculations were made for all tests and compared with the test data. Ratios of calculated concentration to measured concentration were determined for each data point. The average of the ratios was 1.03, with a standard deviation of 0.54. The fact that the average is so near 1.0 is somewhat surprising because propane vapors are usually thought to layer along the ground significantly. The apparent lack of layering is apparently due to the quite low vaporization rates (about 5 lb/ft^2-hr) and moderately high wind speeds. Layering was pronounced in one test on the 40-ft pit where the atmosphere was stable and the wind speed was very low. The rather high standard deviation of calculated to measured propane concentration is not surprising because of variation in atmospheric properties and the difficulty of obtaining accurate data for very low vaporization rates and low propane concentrations.

The lack of layering during these tests should not be taken as an indication that propane vapors will not form layers. Low wind speeds, stable atmospheric conditions and high vaporization rates will all tend to cause layering,

especially where the terrain is suitable. Larger spills or higher vaporization rates from pressurized releaes can lead to formation of large plumes whose behavior cannot be adequately predicted by simple Gaussian models, but will require models where gravity effects are taken into account.

Tests using liquefied natural gas (LNG) have shown that the concentration of gas downwind of an LNG spill can be reduced by covering the pool with high expansion foam, even though the vaporization rate was increased. Figure S-2 shows the results of a single test in which high expansion foam was applied to a pool of propane. The vapor concentration increased sharply as foam was applied, reflecting a vaporization rate more than double that before foam application.

Peak concentrations measured during the tests were usually three to four times the average concentration. In one test a peak concentration 35 times the average was measured, but the reason was because the sensor was off the plume centerline and was contacted infrequently during the test by short puffs of vapor. The average concentration was therefore abnormally low.

II. RADIATION FROM LPG FIRES

Radiation fluxes were measured for fires burning above pits 5, 10, 20, and 40 ft square at steady state burning rates. Both narrow and wide angle radiometers were

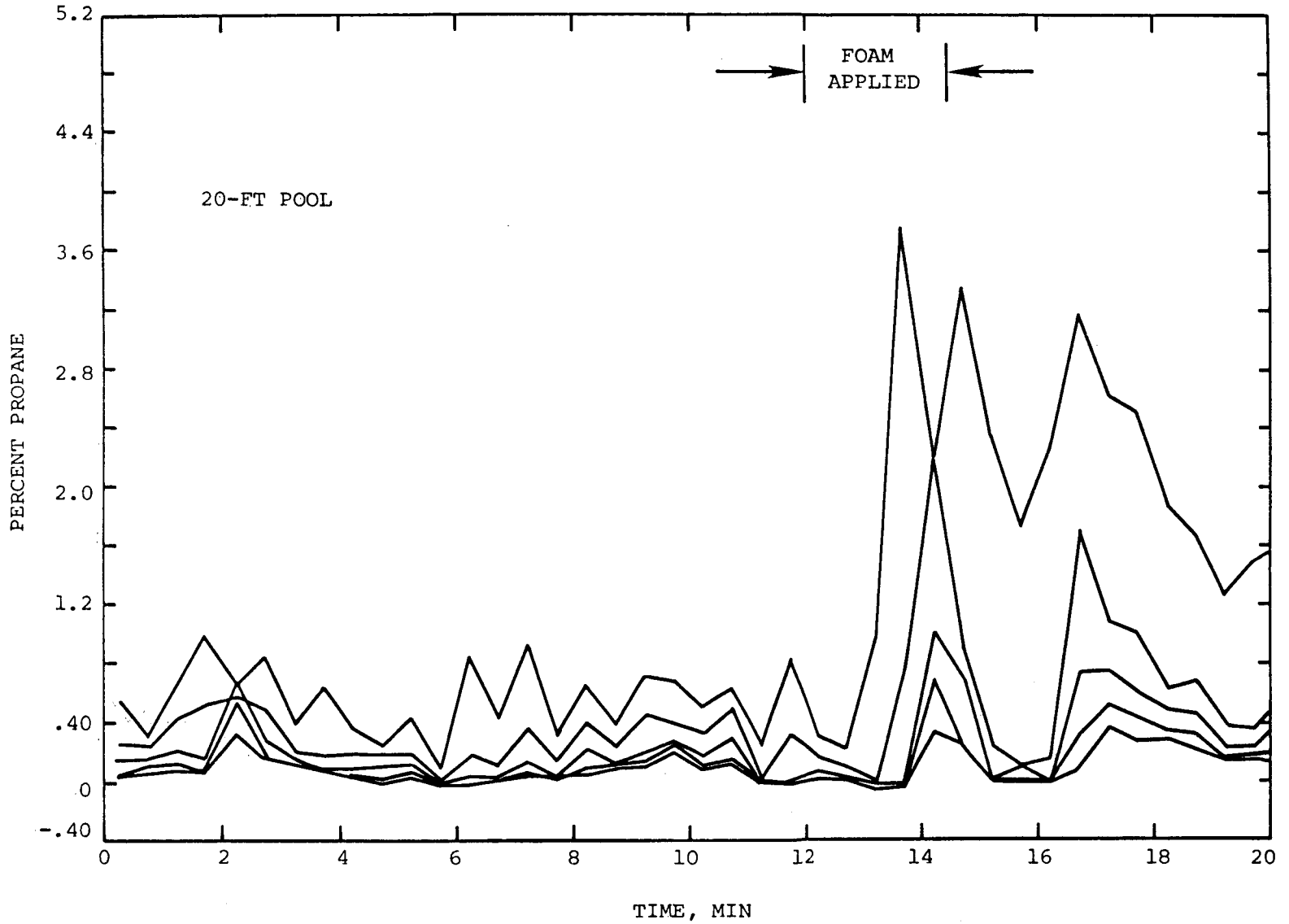

FIGURE S-2. VAPOR CONCENTRATION DOWNWIND OF PROPANE POOL SHOWING EFFECTS OF APPLICATION OF HIGH EXPANSION FOAM.

used, so that both the effective flame surface flux and the incident flux at a given location could be measured. The measurement period was usually about half a minute, although tests as long as 10 minutes were run to investigate time effects. Fluxes were measured during the steady state part of the burn, before the fire was attacked with fire fighting agents. Results were obtained for a wide range of wind speed and wind direction.

The flame radiation was modeled assuming the flame to be a surface emitter. The effective surface flux was determined on the basis of narrow angle radiometer measurements to be

$$q = 50{,}000 \left[1 - \exp\ (-0.126\ D)\right]$$

where q is the effective surface flux in Btu/hr-ft^2, and D is the width of the square pit in feet. The radiant heating rates expected at the wide angle radiometers were calculated based on a tilted cylinder model. The flame height and tilt angle were predicted from literature correlations. The basic input data to the model were flame base size, average wind speed, average wind direction relative to the radiometer, and distance from the fire to the radiometer. Figure S-3 is a comparison of the measured and calculated fluxes. Ratios of calculated flux to measured flux were determined for each run. The average of the ratio was 1.0 with a standard deviation of about 16 percent. The close

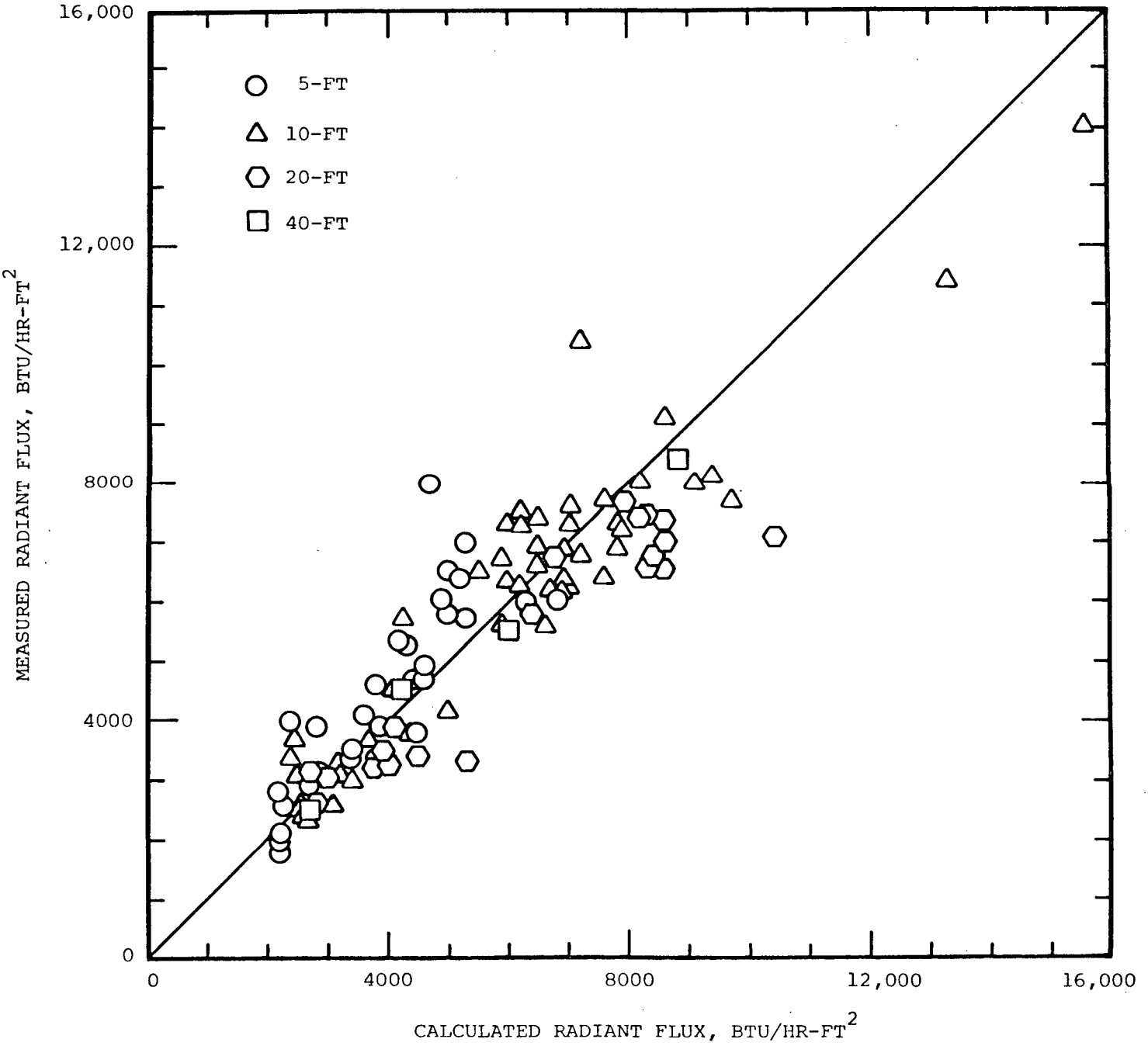

FIGURE S-3. COMPARISON OF MEASURED AND CALCULATED RADIANT FLUXES.

comparison of measured and calculated fluxes indicates that the simplified surface emission model is adequate for predicting radiant fluxes for propane fires.

III. VAPORIZATION OF PROPANE FROM SPILLS ONTO SOLID SURFACES

If LPG is spilled on a solid surface in the open atmosphere, it begins to boil. After about 15 minutes the solid cools enough that the vaporization rate, which has been decreasing, becomes relatively constant. Active boiling has stopped, but vaporization continues until all the LPG is gone. Tests were run to determine the vaporization rates for propane and to determine the physical properties of the solid substrates onto which it was poured. Two general types of tests were performed; closed tests in which a polystyrene foam lid was placed over the test pit, and open tests in which the pool surface was exposed to wind and/or solar radiation during the test. In some of the latter tests, steady state vaporization rates were measured as well as transient rates.

In a closed test the vaporization rate decreases continuously. After a short time, the vaporization rate is inversely proportional to the square root of elapsed time and the total quantity vaporized is proportional to the square root of elapsed time. The proportionality constants are related to the thermal conductivity, heat capacity, and

density of the solid, so if density and heat capacity are measured independently, the effective thermal conductivity of the solid can be determined.

When propane is first spilled, the boiling rate is limited by the heat transfer coefficient between solid and liquid. The effective heat transfer coefficient can be derived from the vaporization data taken during the first few minutes of a closed test once the thermal conductivity has been determined. A mathematical model can then be used to describe the vaporization curve. Figure S-4 shows the weight of propane vaporized during a test in which perlite concrete was used as the solid substrate. The line drawn through the data is from the mathematical model, using the thermal conductivity and heat transfer coefficient derived from the vaporization data. The model reproduces the data very accurately.

Thermal conductivities and heat transfer coefficients were determined for gravel concrete, sand concrete, concrete containing vermiculite and perlite as fillers, clay soil, plywood, and asphalt containing crushed rock aggregate. The thermal conductivities determined from the vaporization data were higher than those found from literature sources for similar materials. Temperature measurements in some of the substrate materials indicate that the thermal conductivity is higher when the substrate is cold than when the substrate is at ambient temperature, which may be the

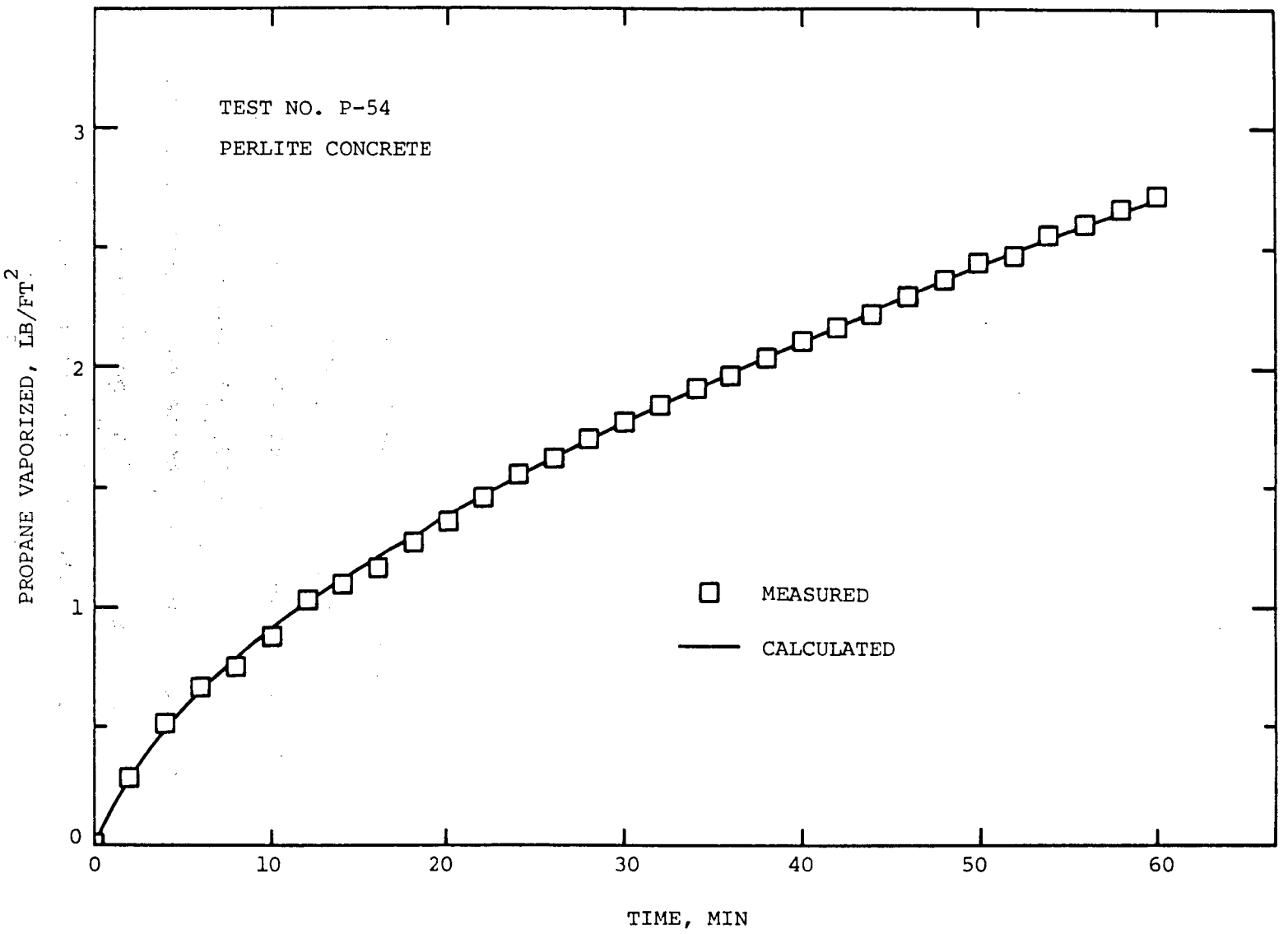

FIGURE S-4. COMPARISON OF MEASURED AND CALCULATED WEIGHT OF PROPANE VAPORIZED FOR TEST NO. P-54.

reason the effective thermal conductivities were higher than those found in the literature. Literature values were generally available for ambient temperature, but not for lower temperatures.

A few tests were run to investigate the behavior of propane when it was spilled onto surfaces covered with small rocks. When poured onto granite chips with a typical thickness of about 0.15 inches, the additional heating from the chips was rapid enough that the chips were cooled in the time required to pour the propane. When propane was poured onto larger marble chips, the time required for cooling the chips was about 3 minutes. A first-order heat transfer model could reproduce the results successfully.

Heat transfer coefficients were in the range to be expected based on correlations in the literature. Boiling of propane spilled onto ambient temperature solids is generally within the transition region between nucleate and film boiling. Variations in heat transfer coefficients can be substantial in the transition region. Tests on similar materials under similar conditions gave relatively reproducible results. Heat transfer coefficients were usually larger for higher density substrates, which would be expected because active boiling would occur longer than for low density substrates. Low density substrates would cool more quickly, thus reducing boiling at the interface to a shorter period.

Mass transfer factors were derived from the steady state vaporization rate data. Figure S-5 is a correlation of the mass transfer factors as a function of the Reynolds number. The propane vaporization data include results from tests on circular pits 5 ft^2 in area up to tests on square pits 400 ft^2 in area. Some data points from earlier vaporization rate measurements on hexane and carbon disulfide are included. They show good agreement with the propane test results even though the boiling points are much higher. Heat transfer coefficients for transfer between the cold pool and warm atmosphere could not be determined from the available data.

The temperature of the open propane pools dropped substantially below the boiling point when the pools were allowed to vaporize for more than a few minutes. The steady state temperature depended primarily on wind velocity, but the presence of solar radiation also affected pool temperature. Shallow pools respond to wind and solar radiation changes more rapidly than deep pools.

IV. SPILLS OF PRESSURIZED PROPANE

Most propane is transported and stored in the United States as a pressurized liquid at ambient temperature. About one-third of the liquid vaporizes when the pressure is reduced to atmospheric pressure under equilibrium conditions. In nearly all accidental releases, the propane

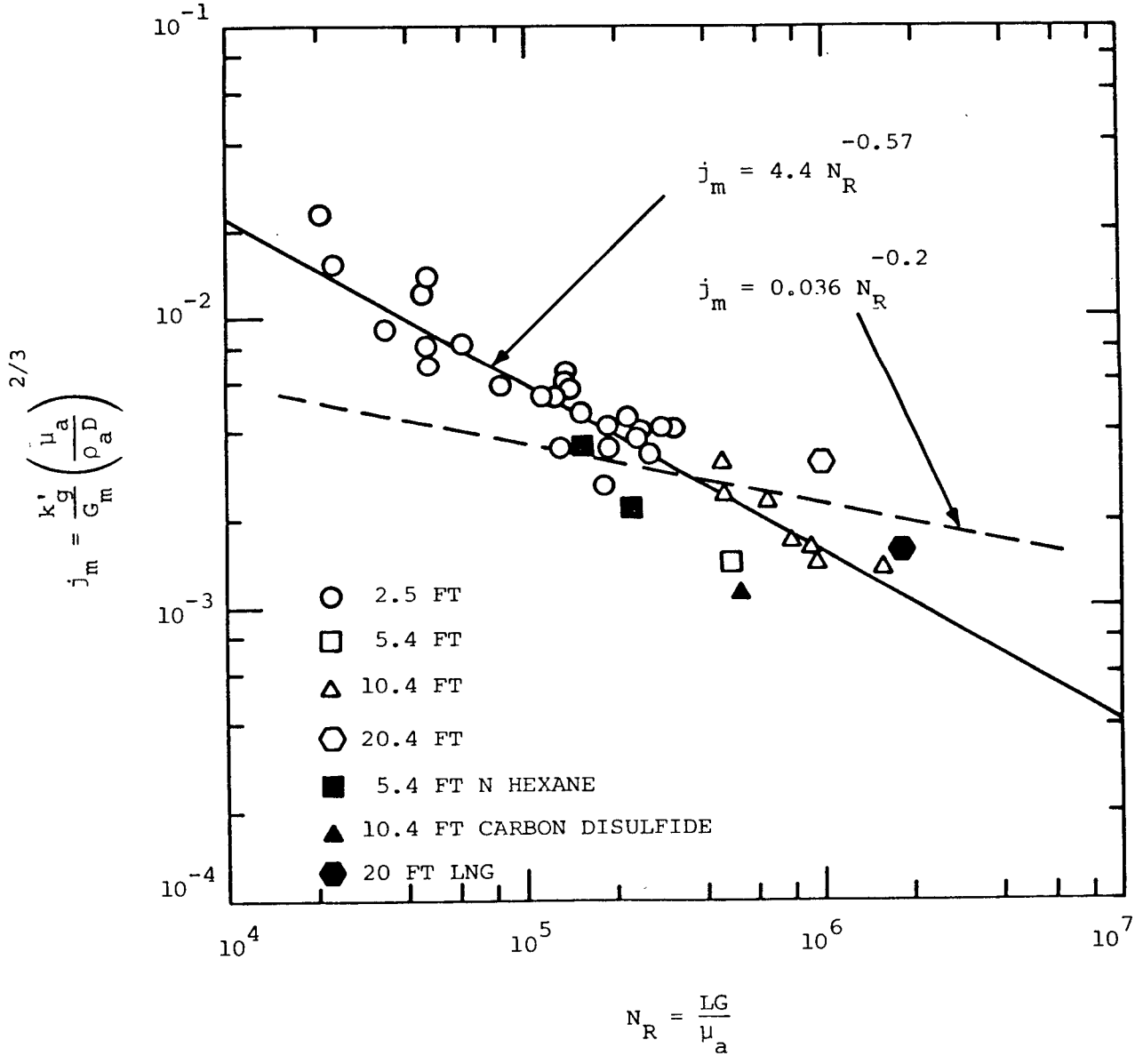

FIGURE S-5. MASS TRANSFER FACTORS FROM PROPANE VAPORIZATION.

discharges at high velocity, atomizing the liquid as it sprays into the atmosphere.

A brief series of tests was run in an effort to determine the fraction of liquid that would fall to the ground as it was released from high pressure storage at ambient temperature. Liquid propane was flashed through horizontal tubes into the open atmosphere at rates up to 180 lb/min. No liquid propane accumulated in the specially designed, insulated tray placed beneath the discharge plume in any test. The plume temperature dropped as low as $-70^{\circ}F$, indicating the lack of equilibrium. The liquid was partially atomized and partially vaporized as it sprayed from the discharge tubes, and the droplets that were formed during discharge were so small that they vaporized before they reached the ground. There was not even a marked tendency for the plume to fall to the ground during the brief discharge.

The results of these brief tests and other observations during the test program indicate that accidental spills of propane from ambient temperature storage will not cause liquid accumulation except if there is a large quantity spilled, the spill duration is long, and the spray is directed downward to a solid surface that interferes with formation of the spray plume.

REPORT I

DISPERSION OF VAPORS FROM LPG SPILLS

INTRODUCTION

In a study of LPG fire control and extinguishment, approximately 100 tests were run in which propane was spilled into concrete or earthen pits and ignited (Johnson, et al., 1980). Propane concentrations downwind of the spills were measured before ignition for 21 of the tests.

Vapor dispersion measurements were run on spills in pits 25, 100, 400, and 1600 ft^2 in area. Concentrations were measured at approximately ground level as nearly directly downwind from the pits as possible.

PROCEDURE AND MEASUREMENT

Propane was unloaded into concrete pits directly from either pressurized or refrigerated storage. Because of large losses due to flashing and atomizing of the liquid, ambient temperature storage was used only for the smaller test pits. Purity was greater than 97 percent for the ambient temperature propane and 80 percent for refrigerated propane. The time required for filling the pits ranged from about a half hour to about two hours, so when concentrations were measured, the vaporization rates were at or approaching steady state. The pools of liquid propane, usually about 3 inches deep, were subcooled and had ceased boiling. The

pits were nominally 5, 10, 20 and 40 ft square and 2 ft deep.

In most tests, 5 catalytic bead gas sensors were placed downwind of the pools after unloading had been completed. The placement was as near the centerline of the propane plume as could be determined from observing the plume and considering the average measured wind direction. The gas sensors were calibrated immediately before they were placed in order to minimize the effects of zero drift. Both wind speed and wind direction were monitored continuously during the tests. The propane evaporation rate was measured using a bubbler connected to a low pressure transducer. The pool temperatures were measured using a thermocouple. The fire control report by Johnson, et al. (1980) contains more detail on the liquid measuring technique and the pit design.

The gas sensors measured concentrations continuously, and the outputs were recorded by strip chart recorders. In addition, outputs were recorded in digital form on magnetic tape at intervals of about 2 sec. Figure 1 shows an example of the output of a strip chart recorder.

RESULTS

The gas concentration at a fixed point varies during a test because of atmospheric turbulence and changes in wind speed and wind direction. Atmospheric turbulence causes smaller fluctuations in concentration, but the changes are

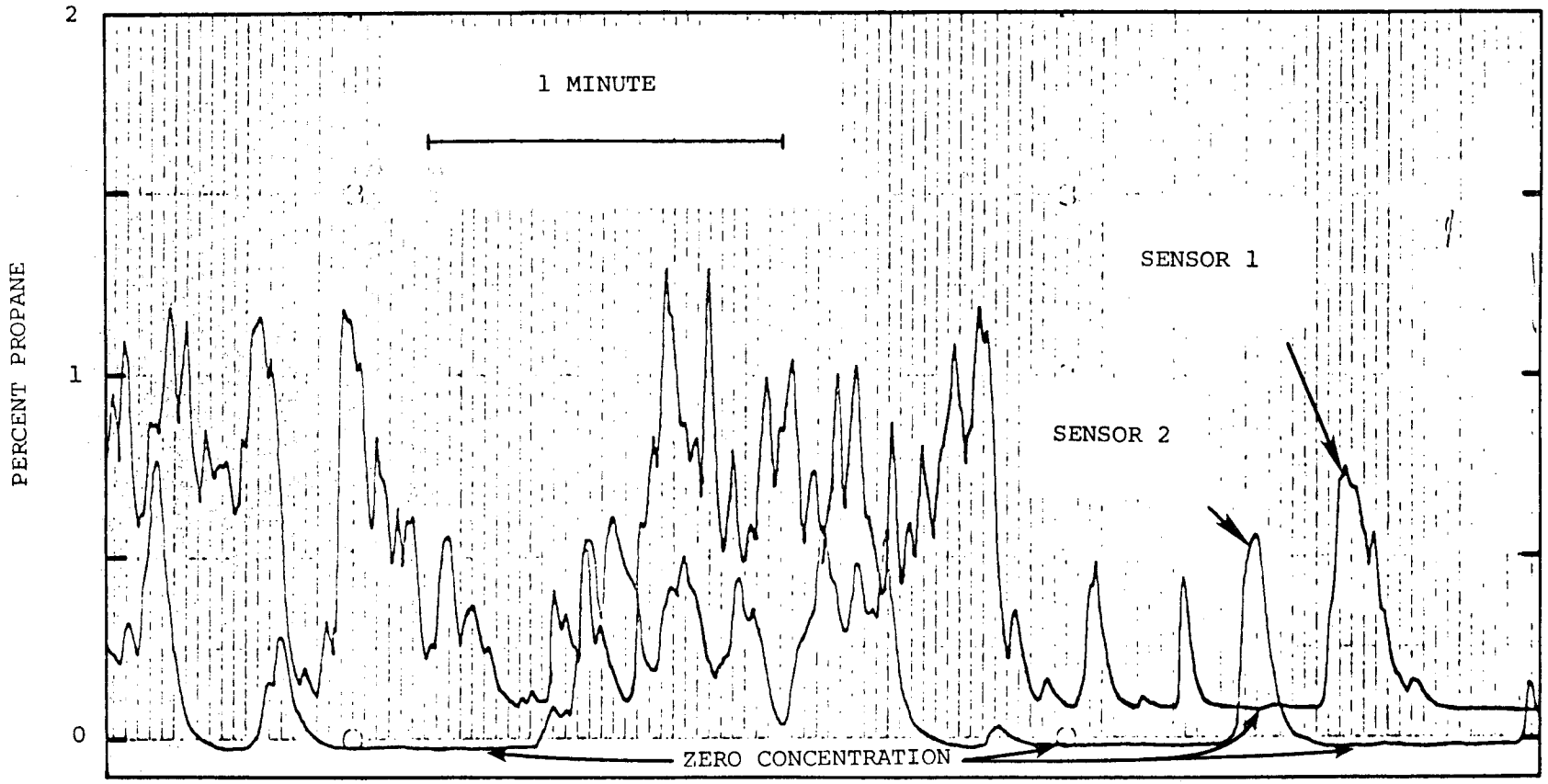

FIGURE 1. SAMPLE OF STRIP CHART RECORDING OF PROPANE CONCENTRATIONS. (THE RECORDER PENS ARE OFFSET BY ABOUT THE DISTANCE OF THE TWO PEAKS MARKED "SENSOR 1" AND "SENSOR 2.")

more rapid than those caused by changes in the average wind velocity and direction. The turbulence also results in changes in instantaneous wind speed and direction, but not in average wind speed and direction. There is a relationship between wind speed and turbulence level, but the average wind speeds during the tests reported here did not change substantially during most of the tests, so no changes in turbulence level would be expected during a test. Wind direction changes were related to the atmospheric turbulence rather than changes in average wind direction during the tests.

The test period was usually about 10 to 20 minutes, although a few longer runs were made. No differences in average gas concentrations were noted that could be attributed to test length. The gas sensors frequently exhibited a zero drift during the tests. In most tests, there were enough points where no gas was present at the sensor to enable a correction for zero drift to be made. In all cases where zero drift could be measured from the records, the change was found to be linear with time. In the few cases where no zero points could be found for data measured during the test, the zero reading at the end of the test was used as the basis of constructing a linear zero drift line.

The causes of zero drift were apparently from both the sensors themselves and from the electronic control and measurement portion of the circuit. Small zero drifts were

noted on all sensors; one channel of measurement and control showed large zero drifts on nearly every test, regardless of which sensor head was attached to it.

The average gas concentrations were calculated from the instantaneous readings by simply averaging the instantaneous readings over the period of the tests. The concentrations on the digital data printout were simply summed and then divided by the number of points in the sum to get the average. A zero drift correction was applied where zero drift had occurred. The correction was based on the zero reading at the end of the run and zero points throughout the run. Concentration averages were found in two other ways for a few of the tests. One of the ways was a graphical integration of the data as recorded by the analog recorder. The strip chart record was averaged by measuring the area under the concentration-time trace with a planimeter and dividing by the time covered by the test. The digital data were then used to reconstruct a second concentration-time curve, which was averaged using the same procedure. Both of these averages were the same as the average taken directly from digital data, within the limits of accuracy possible, so the concentrations reported for all tests were averaged from the digital data, which was the fastest analytical procedure.

Average wind speed and direction were also found by averaging the digital recordings. They were averaged over

the same period as the concentrations so that the results would be for consistent times. The standard deviation of wind direction was also determined directly from the digital data. Wind direction standard deviations are useful in estimating the atmospheric stability category, which is important in data correlations and predictions of vapor concentration.

Table 1 is a summary of the evaporation and wind data from the vapor dispersion tests. Because of the relatively short test duration and the slow evaporation rate at steady state, it was frequently impossible to measure the evaporation rate accurately, so the evaporation rate data are missing for a number of tests. The atmospheric stability listed for each run is based on the standard deviation of wind direction as recommended by Gifford (1968).

Table 2 is a summary of the average propane concentration downwind of the pool. The distances for which concentrations are given are measured from the center of the pool.

DISCUSSION OF RESULTS

Figure 1 shows a section of a strip chart recording of propane concentration. The data from the chart can be used to determine the average concentration through a graphical integration process, but it is easier to average the concentrations from tables of data. This procedure was

TABLE 1. SUMMARY OF WIND AND EVAPORATION DATA.

Run No.	Pit Width[a] ft	Evap. Rate lb/ft^2-hr	Wind Speed Ave. mi/hr	Wind Speed σ mi/hr	Wind Dir. Ave. Deg.	Wind Dir. σ Deg.	Stab.	Run Time min
275-1	5	5.98	10.1	2.6	205	20.8	B	18
276-1	5	--	20.6	4.2	8	12.2	D	19
281-2	10	4.50	6.9	2.1	200	20.4	B	51
285-1	10	--	10.9	2.2	54	13.6	D	20
291-1	10	--	14.0	3.4	180	16.4	C	17
292-1	10	--	17.5	4.0	193	15.7	C	10
293-1	10	--	19.9	4.4	185	13.6	D	17
293-2	10	--	20.8	4.6	182	13.4	D	10
296-1	10	5.62	9.6	2.3	212	14.4	D	9
297-1	10	4.61	9.7	2.9	226	15.5	C	20
297-3	10	4.03	8.2	2.4	212	13.6	D	10
297-4	10	--	8.5	2.3	207	15.2	C	11
298-1	10	4.36	4.5	1.3	214	18.7	C	19
298-2	10	3.45	4.8	1.5	226	22.5	B	12
302-1	10	5.80	16.7	3.5	138	13.6	D	15
313-1	20	--	15.5	3.1	349	10.2	D	28
334-1[b]	20	4.93	5.3	1.5	254	16.7	C	30
334-2[b]	20	10.9	6.2	1.7	264	18.7	C	6
347-1	40	--	14[c]	--	339	9.5	E	15
365-1	40	--	3.5[c]	--	335[c]	--	F	18
011-1	40	--	8.4	1.7	31	8.8	E	16

[a] Nominal size; actual pit width is 5 inches larger than nominal size.

[b] Following application of high expansion foam.

[c] Estimated from airport weather data.

TABLE 2. SUMMARY OF AVERAGE GAS CONCENTRATIONS DOWNWIND OF PROPANE POOLS[a]

Run No.	Dist. ft	Conc. %	Dist. ft	Conc. %	Dist. ft	Conc. %	Dist. ft	Conc. %	Dist. ft	Conc. %
275-1	7.7	0.44	12.7	0.19	17.7	0.11	22.7	0.07	12.7	0.20
276-1	7.7	0.54	12.7	0.20	17.7	0.16	22.7	0.08	12.7	0.26
281-2	15.2	0.45	25.2	0.24	35.2	0.19	55.2	0.08	25.2	0.24
285-1	15.2	0.38	25.2	0.18	35.2	0.12	--	--	55.2	0.06
291-1	15.2	0.69	25.2	0.51	35.2	0.30	55.2	0.16	25.2	0.39
292-1	10.2	0.89	15.2	0.61	25.2	0.40	35.2	0.21	55.2	0.14
293-1	10.2	0.64	15.2	0.63	25.2	0.35	35.2	0.24	55.2	0.10
293-2	10.2	0.60	15.2	0.58	25.2	0.32	35.2	0.21	55.2	0.11
296-1	10.2	1.35	15.2	1.02	25.2	0.40	35.2	0.24	55.2	0.15
297-1	10.2	0.45	15.2	0.13	25.2	0.11	35.2	0.05	--	--
297-3	10.2	0.68	15.2	0.35	25.2	0.25	35.2	0.14	55.2	0.06
297-4	10.2	0.61	15.2	0.30	25.2	0.23	35.2	0.13	55.2	0.06
298-1	10.2	1.71	15.2	1.06	25.2	0.37	35.2	0.27	55.2	0.09
298-2	10.2	1.20	15.2	0.71	25.2	0.31	35.2	0.19	55.2	0.07
302-1	10.2	0.90	15.2	0.63	25.2	0.47	35.2	0.29	55.2	0.11
313-1	30.2	0.40	50.2	0.29	90.2	0.09	130.2	0.05	210.2	0.03
334-1	30.2	0.54	50.2	0.29	70.2	0.16	90.2	0.10	110.2	0.08
334-2[b]	30.2	2.01	50.2	0.62	70.2	0.36	90.2	0.23	110.2	0.15
347-1	80.2	0.92	100.2	0.71	140.2	0.43	180.2	0.25	220.2	0.14
365-1	60.2	4.19	100.2	2.23	140.2	1.23	180.2	0.86	--	--
011-1	40.2	0.88	60.2	0.55	80.2	0.37	100.2	0.29	--	--

[a] Distances are measured from pool center; concentrations are in mole percent.

[b] Following application of high expansion foam.

followed for all tests. Notice that Figure 1 shows some points where the concentration apparently drops to zero and then rises again. These zero points may change during the test, but the change is approximately linear with time. The zero drift was corrected by assuming a linear change over the test period. Figure 2, which is plotted from 30-second averages of the data, shows how the corrections were made. The average gas concentration over a 30-sec interval was plotted as a function of time. Periods when short term average concentrations stayed constant or increased linearly without peaks corresponded to zero gas concentration at the sensor. These periods of zero gas concentration represent times when the wind direction changed enough that the sensor was no longer in the gas plume. At the end of each test, the gas sensor was removed from the plume before the pool was ignited. A separate baseline was established at that time, as illustrated in Figure 2. Calibration after test runs showed that the span had not changed, so no adjustment in span was required. The zero adjustment was equivalent to integrating the measured gas concentration above the baseline, as represented by the shaded areas in Figure 2. The curves such as those shown in Figure 2 are simplified by the averaging process; they were used only to establish the zero baseline. Actual average concentrations were determined by point-by-point data sampled at about 1- to 2-second intervals during the tests.

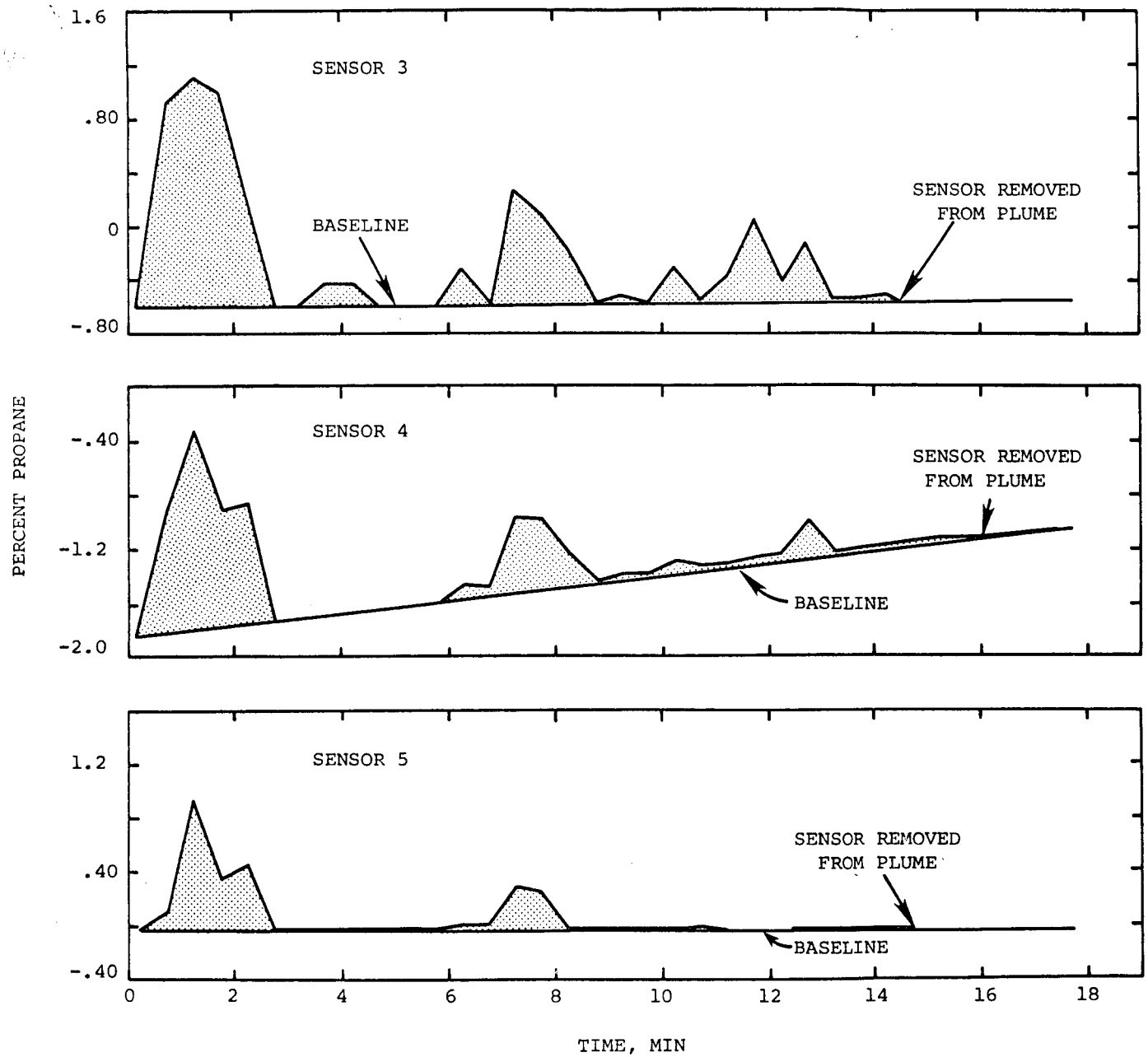

FIGURE 2. CORRECTION FOR ZERO DRIFT DURING VAPOR DISPERSION TESTS.

A simple Gaussian dispersion model can be used to predict the concentrations downwind of a propane pool based on the evaporation rate, the wind speed, and the atmospheric stability. Such a model, modified to account for source area, was used to predict concentrations for the conditions under which the tests were run. Figures 3 through 5 show the results of predictions for three of the tests. These three runs were chosen to illustrate cases in which the predicted concentrations were less than, about equal to, and greater than the measured concentrations. Similar curves were drawn for the other tests. In general, the slopes for all the calculated curves match the experimental data well. That result is to be expected because the curves for atmospheric stability parameters all have about the same slope for the distances of these tests. The Pasquill stability classes were used for the calculations; the stability parameters were extrapolated to the shorter distances of the tests.

The ratio of the calculated concentration, C_c, to the measured concentration, C_m, was calculated for each of the runs. The results are summarized in Table 3. The average of all the ratios is 1.03 and the standard deviation is 0.54. The relatively large standard deviation is not surprising because of the variation in atmospheric properties and the difficulty of obtaining accurate data for slow evaporation rates and low propane concentrations. The fact

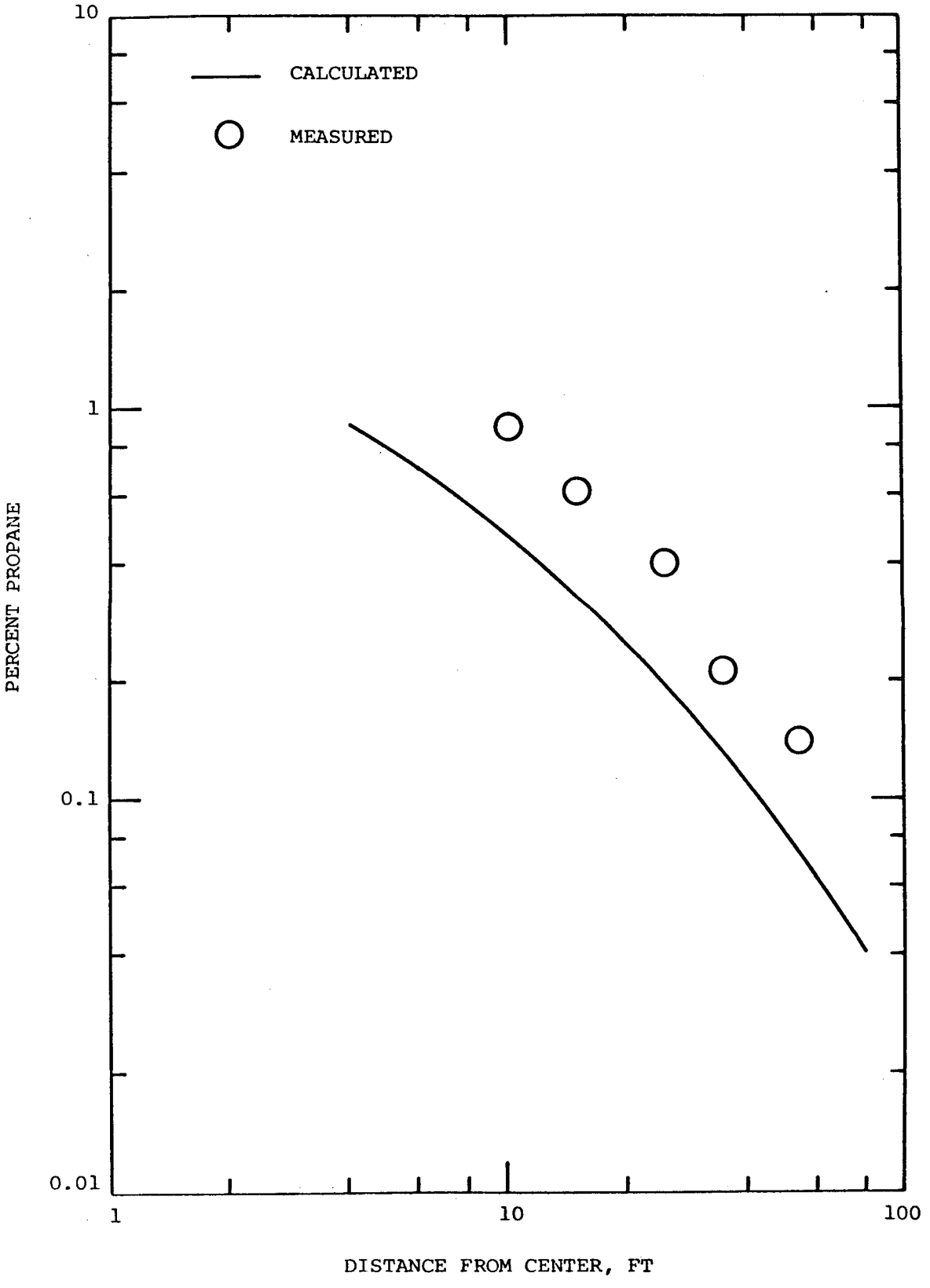

FIGURE 3. COMPARISON OF AVERAGE MEASURED AND CALCULATED PROPANE CONCENTRATIONS, RUN 292-1.

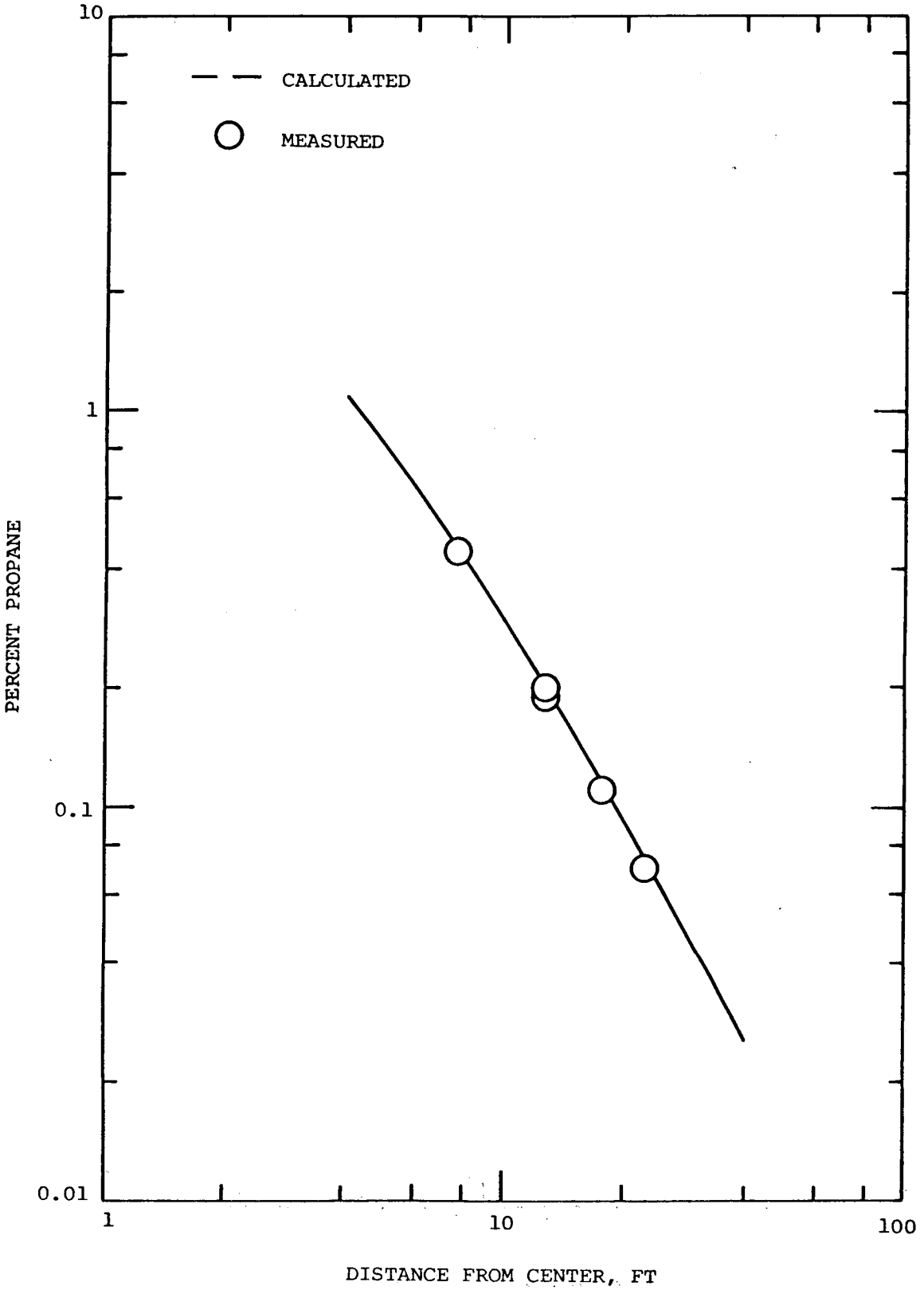

FIGURE 4. COMPARISON OF AVERAGE MEASURED AND CALCULATED PROPANE CONCENTRATIONS, RUN 275-1.

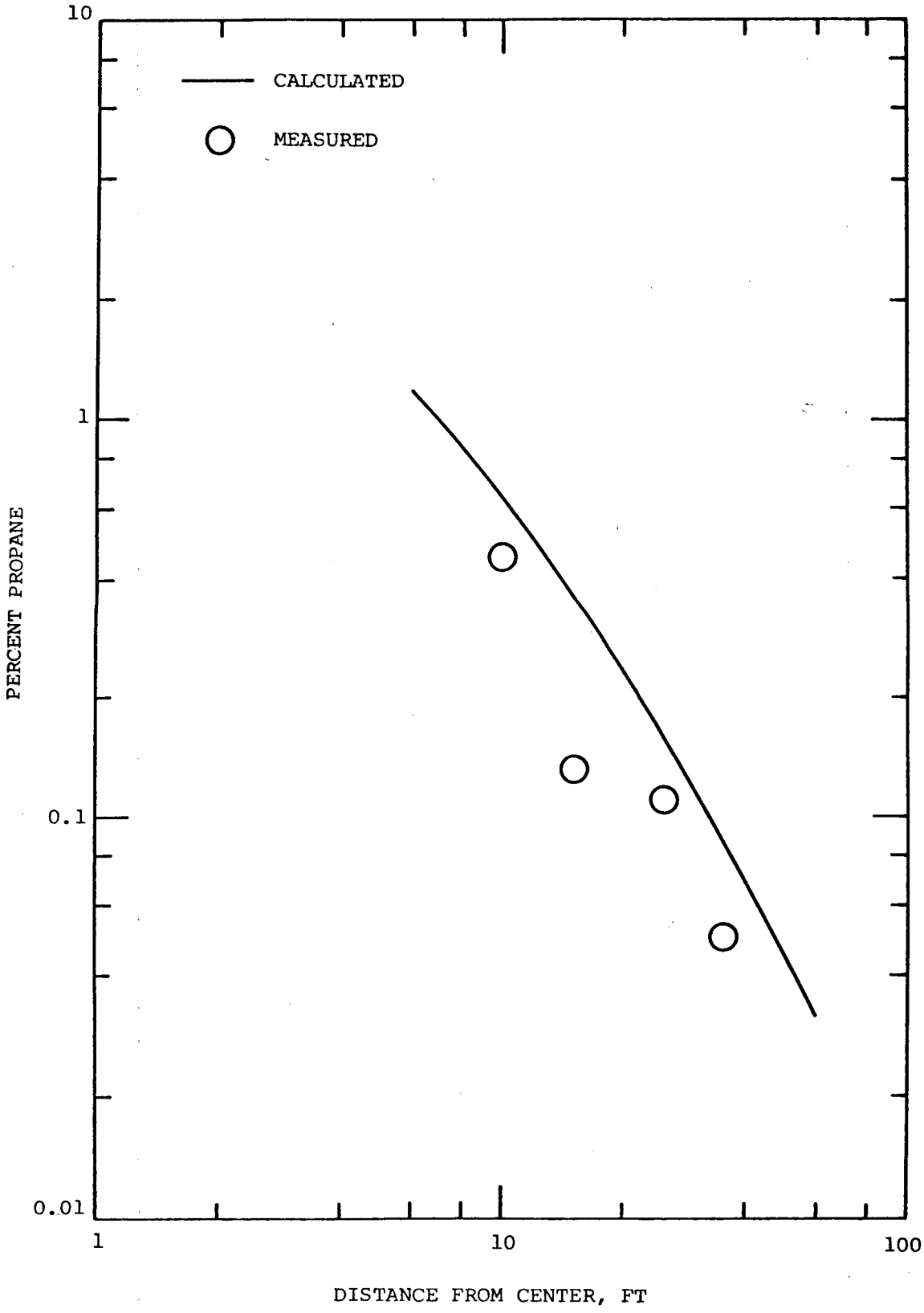

FIGURE 5. COMPARISON OF AVERAGE MEASURED AND CALCULATED PROPANE CONCENTRATIONS, RUN 297-1.

TABLE 3. RATIO OF PREDICTED CONCENTRATION TO MEASURED CONCENTRATION[a]

Run No.	Dist. ft	C_c/C_m	Dist. ft	C_c/C_m	Dist. ft	C_c/C_m	Dist. ft	C_c/C_m	Dist. ft	C_c/C_m
275-1	7.7	1.00	12.7	1.05	17.7	1.00	22.7	1.00	12.7	1.00
276-1	7.7	0.52	12.7	0.85	17.7	0.75	22.7	1.00	12.7	0.73
281-2	15.2	1.07	25.2	0.92	35.2	0.63	55.2	0.63	25.2	0.92
285-1	15.2	1.18	25.2	1.56	35.2	1.58	--	--	55.2	1.67
291-1	15.2	0.49	25.2	0.35	35.2	0.33	55.2	0.31	25.2	0.46
292-1	10.2	0.49	15.2	0.44	25.2	0.35	35.2	0.38	55.2	0.29
293-1	10.2	0.61	15.2	0.43	25.2	0.46	35.2	0.46	55.2	0.60
293-2	10.2	0.63	15.2	0.45	25.2	0.50	35.2	0.52	55.2	0.55
296-1	10.2	0.67	15.2	0.61	25.2	0.95	35.2	1.08	55.2	0.93
297-1	10.2	1.62	15.2	3.54	25.2	2.18	35.2	2.80	--	--
297-3	10.2	1.12	15.2	1.49	25.2	1.28	35.2	1.57	55.2	1.83
297-4	10.2	1.20	15.2	1.53	25.2	1.04	35.2	1.08	55.2	1.17
298-1	10.2	0.86	15.2	0.89	25.2	1.32	35.2	1.07	55.2	1.44
298-2	10.2	0.75	15.2	0.75	25.2	0.77	35.2	0.68	55.2	0.86
302-1	10.2	0.60	15.2	0.59	25.2	0.49	35.2	0.52	55.2	0.73
313-1	30.2	1.10	50.2	0.93	90.2	1.44	130.2	1.60	210.2	1.00
334-1	30.2	1.70	50.2	1.66	70.2	1.81	90.2	1.90	110.2	1.67
334-2[b]	30.2	0.86	50.2	1.45	70.2	1.50	90.2	1.52	110.2	1.67
347-1	80.2	0.67	100.2	0.72	140.2	0.86	180.2	1.12	220.2	1.57
365-1	60.2	0.93	100.2	1.17	140.2	1.62	180.2	1.88	--	--
011-1	40.2	0.80	60.2	0.87	80.2	1.00	100.2	1.07	--	--

[a] Distances are measured from pool center.

[b] Following application of high expansion foam.

that over the average of 21 tests the predicted concentrations were close to the measured concentrations is a little surprising. Propane vapors are more dense than air, particularly at the boiling temperature, and it was expected that concentrations would be higher than predicted from a model that assumed neutral buoyancy because the vapors would tend to layer and suppress dispersion. There would also be a tendency for dense vapors to disperse laterally under the influence of gravity. Because of the limited number of sensors available, it was not possible to monitor concentrations in enough locations to determine if lateral spread was occurring. However, it would require an unusual coincidence for lateral spread to compensate for layering in so many tests. Also, the slope of the concentration versus distance curves matches the predicted slopes, which would not be true if strong lateral spread occurred. Thus, for these relatively small tests and low evaporation rates, a Gaussian model modified for area sources but assuming neutral buoyancy provides satisfactory estimates of vapor concentrations.

Most of the propane pools were ignited as soon as the gas sensors could be removed from the plume. At the low evaporation rates and moderate wind velocities present during the tests, there was little burning of the vapor plume beyond the edges of the pit. One exception to this general statement occurred in Test 365-1. This test used the 40-ft

square pit. Propane was piped into the pit during the late afternoon of a day when the wind speed was quite low. Fuel unloading was quite slow because the excess flow valve on the storage tank would close periodically, requiring a waiting period for the pressure to equalize before flow could be restarted. Consequently, it was near sundown when the dispersion test began. About halfway through the dispersion test, the sensor nearest the pit (at 60 ft from pool center) increased its reading and then decreased sharply, indicating that it had been saturated with propane. (At concentrations above about 4 percent, the gas sensor output decreases as the concentration increases.) The wind speed decreased near the end of the run to about half a mile per hour and the wind direction sensor stopped functioning because there was insufficient wind to turn it. By the time the gas sensors had been removed from the test area and the pool was ignited, a flammable layer of vapor about a foot thick extended from about a pool diameter upwind to 3 or 4 pool diameters downwind. The width of the flammable layer was about 1 diameter in one crosswind direction and 2 diameters in the other crosswind direction. This flammable layer formed relatively quickly and covered an area about 10 times the pool area, illustrating the layering effect that can occur if wind speeds are low. The layering occurred with a very low vaporization rate, and it can be expected that layering will occur in the immediate area for faster

vaporization rates at higher wind speeds. These tests do not show the relationship between wind speed and vaporization rate that would result in layering or other gravity-induced effects. They do show that any gravity-induced effects are not important for the pool sizes and vaporization rates present during the tests unless the wind speed is very low (less than about 3 mi/hr).

In tests using liquefied natural gas, it has been shown that applying high expansion foam to the pool will reduce the methane concentration downwind of the pool. One similar test was run during the propane test series. Figure 6 shows the result. The concentration of propane at 5 locations is shown for a period of 20 minutes. (The concentrations are 30-sec averages taken from digital data records.) High expansion foam with an expansion ratio of about 500:1 was applied about 13 min after the start of the portion of the record shown. The propane concentration downwind of the pool increased immediately in response to the foam. The increase was caused primarily by the increased vaporization rate following foam application. Figure 7 shows the average concentrations for the five sensors. Concentrations following foam application were 2 to 3 times as high as before foam application. The vaporization rate more than doubled when foam was applied, indicating that increased vaporization is the most important factor in causing higher concentrations. The slope of the

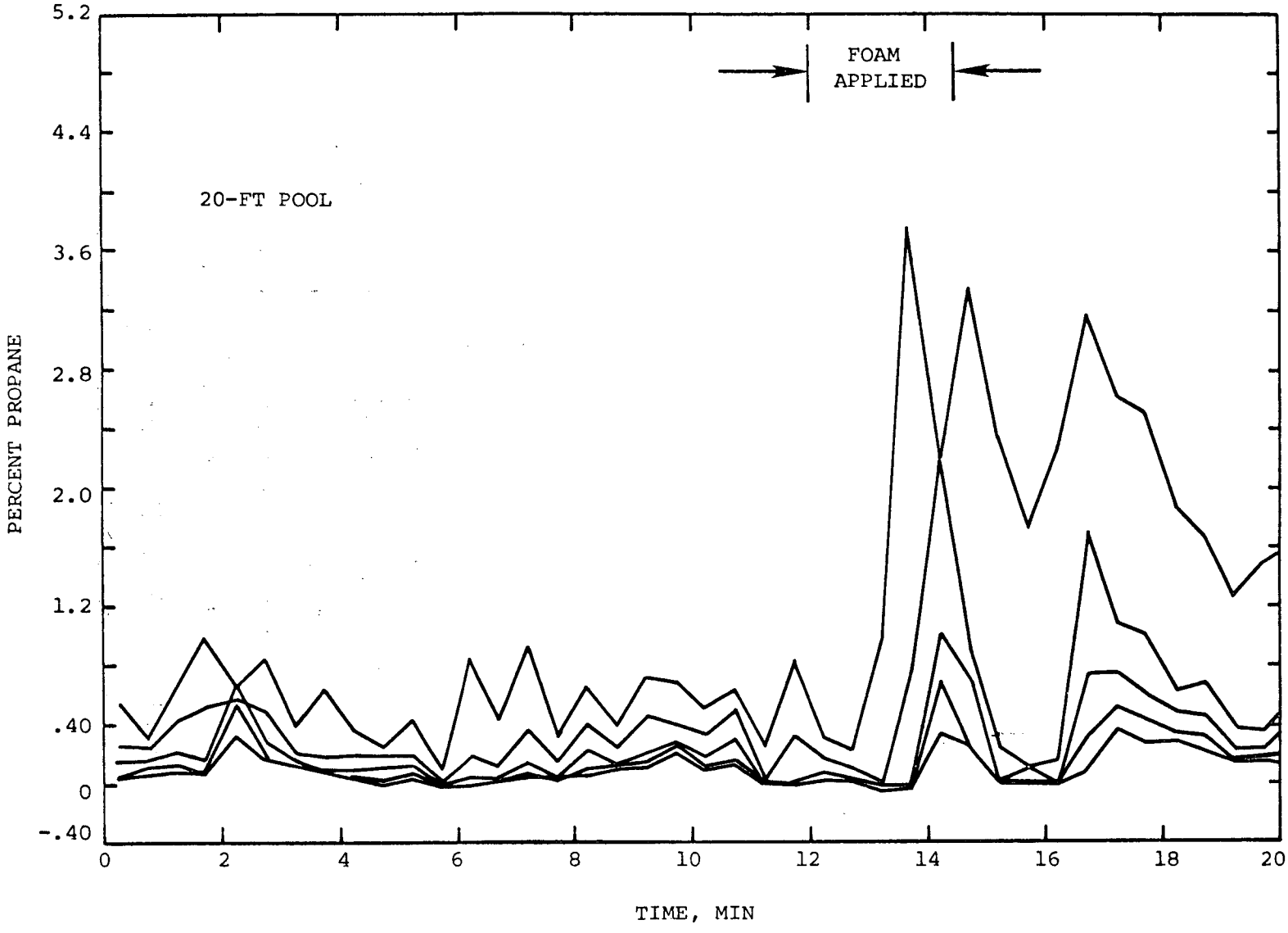

FIGURE 6. VAPOR CONCENTRATION DOWNWIND OF PROPANE POOL SHOWING EFFECTS OF APPLICATION OF HIGH EXPANSION FOAM.

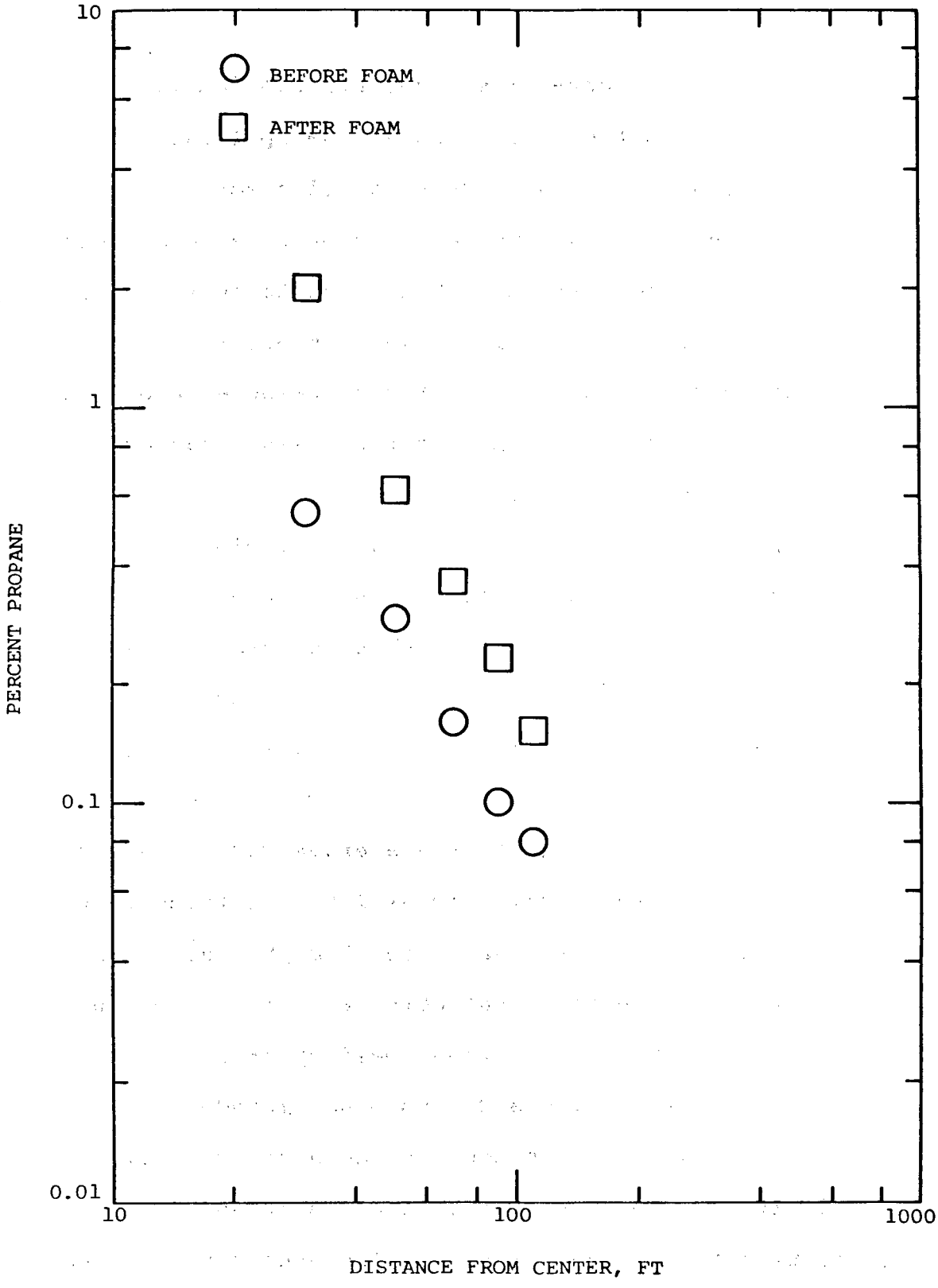

FIGURE 7. RESPONSE OF AVERAGE PROPANE CONCENTRATION TO APPLICATION OF HIGH EXPANSION FOAM.

average concentration curve after foam application is slightly steeper than the curve before foam application. Calculations using dispersion models for line sources indicate that the reason may be that the propane vapor does not penetrate the foam uniformly, but tends to be released near the downwind edge of the pit. That result is to be expected because foam was applied at the upwind edge of the pit and the foam layer was deeper at the upwind edge of the pit than at the downwind edge.

The propane concentrations shown in Table 2 and compared to calculated concentrations in Table 3 are averages. The data were also surveyed to determine the peak concentrations during the tests. Table 4 contains the results, presented in the form of peak-to-average concentration ratios. The results show peak concentrations from about 1.5 to 35 times as high as the average concentrations. The lower peak-to-average ratios generally were found when wind velocities were higher than 10 to 15 mi/hr, even though the atmosphere was moderately unstable (Pasquill B) during some of the tests. The faster wind speed apparently promotes more uniform mixing and less plume meandering.

At slower wind speeds the phenomena are a little different. If the atmosphere is stable, as in Run No. 365-1, the peak-to-average ratios are low even for low wind speeds. However, for unstable atmospheres, such as in Run No. 334-1, peak-to-average ratios are higher. The

TABLE 4. PEAK-TO-AVERAGE CONCENTRATION RATIOS FOR PROPANE SPILLS[a]

Run No.	Dist. Ft	C_p/C_a	Dist. Ft	C_p/C_a	Dist. Ft	C_p/C_a	Dist. Ft	C_p/C_a	Dist. Ft	C_p/C_a
275-1	7.7	2.6	12.7	3.7	17.7	6.6	22.7	5.4	12.7	4.7
276-1	7.7	1.8	12.7	2.3	17.7	4.1	22.7	8.1	12.7	2.2
281-2	15.2	3.0	25.2	4.2	35.2	5.4	55.2	8.5	25.2	4.2
285-1	15.2	4.2	25.2	5.6	35.2	4.8	--	--	55.2	6.0
291-1	15.2	1.8	25.2	2.1	35.2	2.0	55.2	3.3	25.2	1.9
292-1	10.2	1.8	15.2	1.8	25.2	2.2	35.2	2.8	55.2	2.6
293-1	10.2	1.7	15.2	1.6	25.2	2.2	35.2	2.2	55.2	2.8
293-2	10.2	1.9	15.2	1.9	25.2	1.9	35.2	2.3	55.2	2.2
296-1	10.2	2.0	15.2	2.1	25.2	2.7	35.2	4.2	55.2	3.9
297-1	10.2	3.3	15.2	9.4	25.2	6.5	35.2	9.8	--	--
297-3	10.2	2.5	15.2	2.9	25.2	3.1	35.2	3.9	55.2	4.2
297-4	10.2	2.3	15.2	3.5	25.2	3.4	35.2	3.7	55.2	5.2
298-1	10.2	3.6	15.2	5.8	25.2	12.4	35.2	15.3	55.2	35.0
298-2	10.2	5.3	15.2	6.6	25.2	7.5	35.2	5.7	55.2	8.6
302-1	10.2	1.7	15.2	1.8	25.2	3.0	35.2	2.9	55.2	3.0
313-1	30.2	1.9	50.2	1.8	90.2	3.0	130.2	2.8	210.2	3.3
334-1	30.2	7.8	50.2	9.2	70.2	9.9	90.2	9.7	110.2	7.3
334-2[b]	30.2	3.3	50.2	8.4	70.2	11.1	90.2	10.2	110.2	9.9
347-1	80.2	1.5	100.2	2.2	140.2	2.6	180.2	2.7	220.2	2.2
365-1	60.2	--	100.2	1.6	140.2	1.6	180.2	3.1	--	--
011-1	40.2	2.3	60.2	2.8	80.2	3.4	100.2	4.6	--	--

[a] Distances are measured from pool center.

[b] Following application of high expansion foam.

difference is due primarily to the difference in the magnitude of wind direction changes when the atmosphere is unstable.

In Run No. 298-1, the average wind direction did not correspond to the direction of the sensor array. As the distance from pool to sensor increased, the sensors were further from the plume centerline and the plume drifted across them less frequently. The average propane concentration measured during this test was therefore lower than would have been measured if the sensors had been on the centerline. In Run 298-1, the gas sensor 55 ft from the pit read zero during most of the test, and the few times the plume reached the sensor the concentrations were relatively high, causing high peak-to-average concentration ratios. These high peak-to-average ratios can be expected whenever concentrations are measured near the extreme edges of the path of a meandering plume.

CONCLUSIONS

Propane vapor concentrations were measured along the plume centerline for more than 20 tests in which propane was evaporating at steady state from pools up to 1600 ft^2 in area. A simple Gaussian model modified to account for area sources was found to be satisfactory for predicting the average concentrations using wind speed and vaporization rates taken during the tests. Atmospheric stability could

be estimated from the standard deviation of wind direction measurements. High expansion foam applied to the pool surface increased the vaporization rate and thereby increased vapor concentrations downwind of the pool.

REFERENCES

1. Johnson, D. W., et al., "Control and Extinguishment of LPG Fires," Report No. DOE/EV-6020-1, U. S. Department of Energy, Washington, DC (August, 1980).

2. Gifford, F. A., Jr., in Slade, D. H., (ed.), Meteorology and Atomic Energy, TID-24190, U. S. Atomic Energy Commission (July, 1968).

REPORT II

RADIATION FROM LPG FIRES

INTRODUCTION

During the study of LPG fire extinguishment and control, approximately 100 tests were run in which propane was spilled into concrete or earthen pits and ignited. When steady burning rates were reached the fires were extinguished or controlled (Johnson, et al., 1980). Radiometers were located near the test pits during the fires to measure radiation fluxes. Both narrow angle and wide angle radiometers were used.

Flame radiation tests were run on pits 25, 100, 400, and 1600 ft^2 in area. Generally radiation fluxes were measured from the crosswind direction; ranges of radiation recorded were from less than 2000 Btu/hr-ft^2 to nearly 14,000 Btu/hr-ft^2.

MEASUREMENT PROCEDURE

Two types of radiometers were used during the tests. The wide angle radiometers were Gardon-gage type instruments with a viewing angle of 150 degrees. They were water cooled continuously during the tests, and were allowed a long period of stabilization before a test began so that the cooling water was maintained at a constant temperature throughout a test. The water was not recirculated.

The wide angle radiometers were fixed at an elevation 5 ft above the top of the pit and were placed in a generally crosswind direction one and two pit widths from the edge of the pit. Figure 1 shows the general arrangement. The radiometer sensors were vertical and sapphire windows were used to protect the sensors from convective effects.

The narrow angle radiometer was placed one pit width from the edge of the pit 1.5 ft above the pit edge. It was aimed across the downwind edge of the pit at an upward angle of about 15 degrees to ensure that the entire viewing cone was filled with flame surface. In one 1600-ft^2 test a second narrow angle radiometer was located approximately 15 ft above the pit edge at a distance of about 175 ft from the pit. The viewing circle at that distance was less than 25 ft in diameter so that the entire viewing cone was filled with flame surface. (The same narrow angle radiometer was used for most of the tests to aid in determining fire control or extinguishment time, but the flames were not large enough to fill the entire viewing angle.) The narrow angle radiometers used calcium fluoride windows to protect the sensing element. The view restrictors were purged to prevent fogging of the window by dirt or fire fighting agents and cooled with water to provide stable view restrictor temperatures.

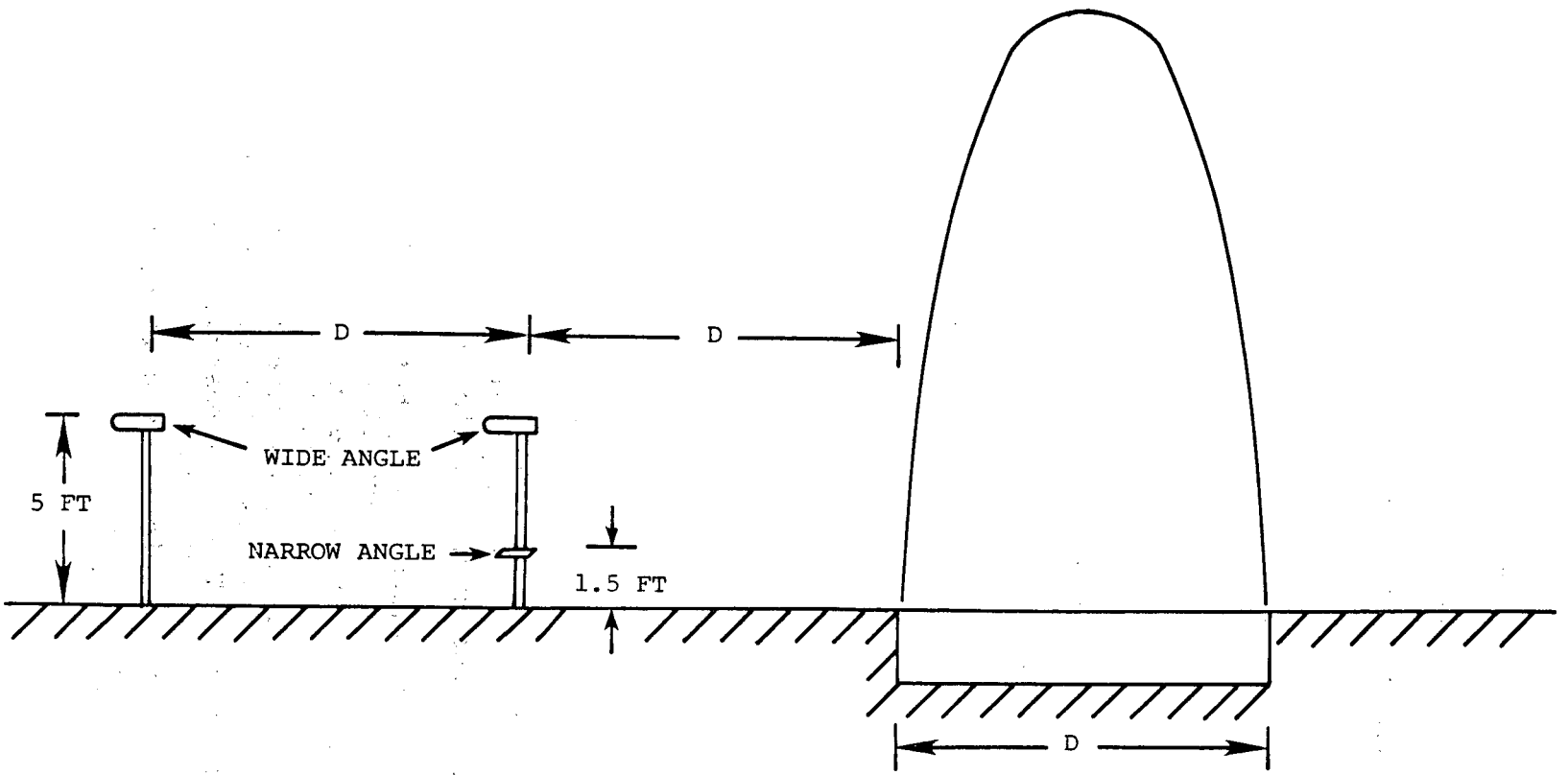

FIGURE 1. LOCATION OF RADIOMETERS NEAR TEST PIT.

All radiometers were insulated and wrapped with foil to reduce the heat input to the radiometer body. All electrical leads and water lines were either insulated and wrapped with foil or buried to protect them. The radiometer outputs were recorded in digital form on magnetic tape for all runs. During some runs, analog recordings were also made on a strip chart recorder. Figure 2 shows an example of the analog data.

RESULTS

As shown by the radiation flux recording in Figure 2, the radiant energy incident at some point near a propane fire varies during the fire's duration. Both short term and long term variations occur. Short term variations are due primarily to fluctuations in flame size and shape caused by turbulence within the flame. Some of the short term variations are too rapid to be detected by the radiometers; they are generally unimportant in practical heat transfer considerations because responses faster than a few seconds are seldom important. Short term fluctuations may have some important effects if rapid spectral flux measurements are made. In such measurements, misleading results may be inferred if the changes in both spectral and integrated fluxes due to flame turbulence are not properly accounted for.

Long term variations in radiant flux occur as the flame increases in size immediately after ignition and as

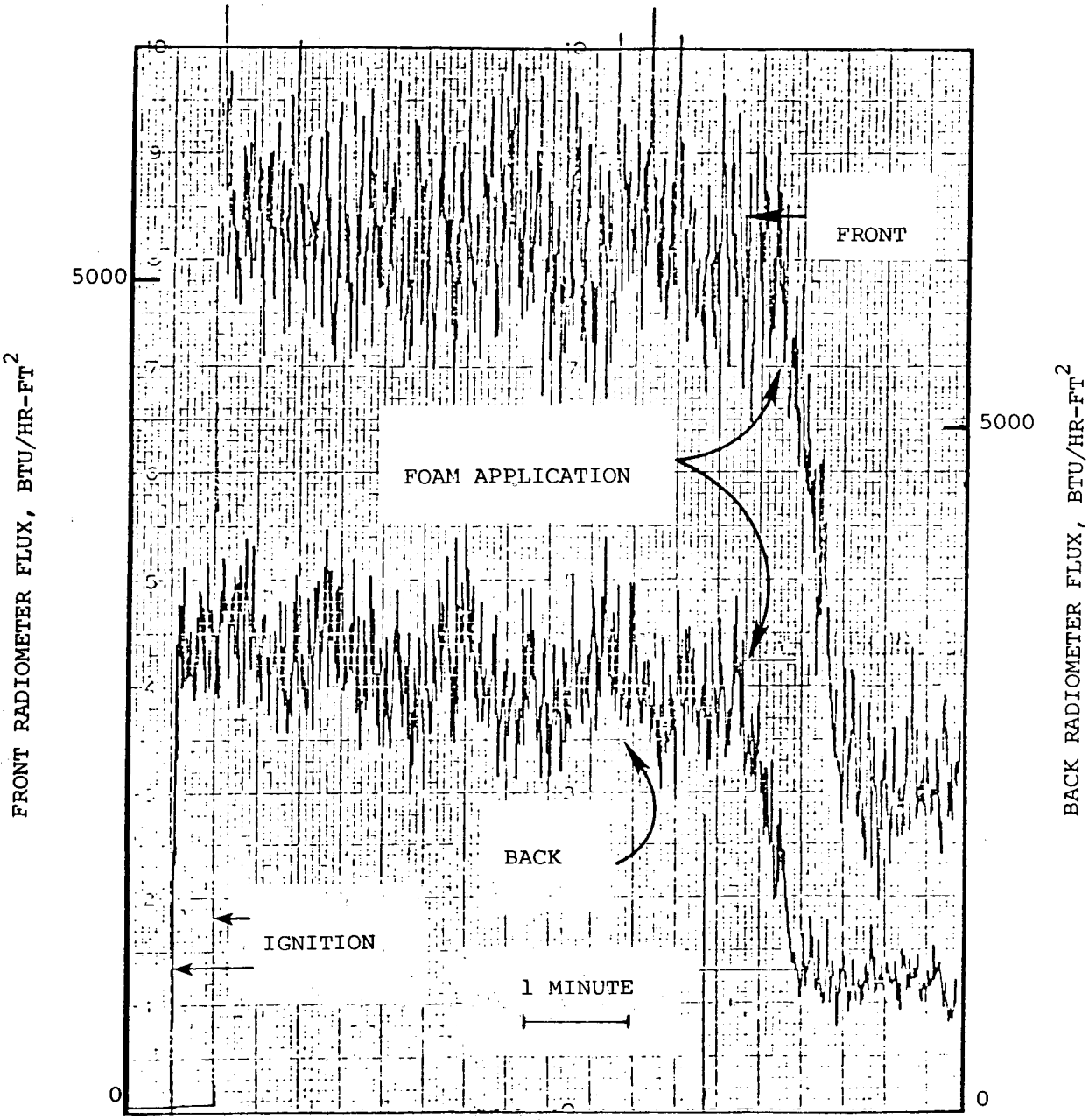

FIGURE 2. EXAMPLE OF RADIOMETER READINGS FROM LPG FIRES.

the flame size decreases during burnout (or fire control). Variations may also occur during burnout as the fuel composition changes. In outdoor tests such as these, the wind causes changes in radiant flux incident at a point because the flame is blown in different directions by the wind. The flame is tilted from vertical as the wind speed increases, and the flame is rotated around its base as the wind direction changes. Both the tilting and the rotation change the flame orientation with respect to a radiometer, so that incident flux readings vary.

Narrow angle flux measurements show short term variations in radiant flux caused by some of the same factors responsible for short term variations in radiant flux incident on a point near the fire. The long term variations for narrow angle radiometers are more noticeable for small fires than for large fires because the variations in flame tilt and direction cause the path length through the flame to change. As the fires become optically thick, the variations caused by path length changes become unimportant, so that the changes in long term flux readings by narrow angle radiometers are due more to changes in fuel composition or viewing position in the flame than to changes in path length due to changes in flame direction.

The radiation fluxes considered most important for assessing potential fire damage are those associated with the steady state portion of the fire. The radiation fluxes

discussed in this report were all measured during the steady state burning period. The duration of the measurement was usually about half a minute, although some measurements were made for periods of 10 minutes or longer. The short measurement period was a result of the desire to conserve fuel and the fact that the primary goal of the tests was to determine fire suppression parameters. The few longer duration tests were run to provide assurance that no erroneous interpretation of the results would occur. The longer duration data showed no phenomenological differences from the data of shorter duration tests. Because the radiation fluxes were measured during the steady burning portion of the tests, no data on flux changes during burnout were recorded.

Table 1 contains a summary of the radiation flux measurements. The pit dimensions shown in Table 1 are the nominal dimension. Actual pit widths were 5 inches greater than the nominal width. All pits were square. The pits were 2 ft deep and the fuel depth was usually 3 to 6 inches. All tests were run outdoors under ambient wind conditions. The wind speed and direction shown in the table were measured at a location near the instrument building. The short term fluctuations in wind direction and speed may be different at the test area, but the averages, as shown in Table 1, are not expected to be substantially different.

TABLE 1. SUMMARY OF RADIOMETER DATA

Run No.	Pit Width Ft	Wind Speed Mph	Wind Direction Degrees	Radiant Flux Measured Narrow Angle	Radiant Flux Measured Front Btu/hr-ft^2	Radiant Flux Measured Rear	Radiant Flux Calculated Front Btu/hr-ft^2	Radiant Flux Calculated Rear	Ratio, q_c/q_m Front	Ratio, q_c/q_m Rear
248-1	5	7.8	193	32,700	5,310	2,630	4,287	2,260	0.807	0.859
248-2	5	4.3	191	33,600	7,980	4,030	4,667	2,449	0.585	0.608
261-1	5	7.4	51	---	6,100	4,710	6,822	4,593	1.118	0.975
261-2	5	7.4	344	---	4,610	2,830	4,083	2,207	0.886	0.780
268-1A	5	10.1	161	---	5,960	3,770	4,854	2,969	0.814	0.788
268-1B	5	7.8	150	---	6,370	3,530	5,205	3,428	0.817	0.971
268-2	5	9.0	128	---	5,960	3,770	6,314	4,484	1.059	1.189
268-3	5	7.2	152	---	5,690	3,420	5,305	3,415	0.932	0.999
268-4	5	8.3	139	18,100	---	4,590	5,217	3,805	---	0.829
270-2A	5	18.3	154	26,900	4,740	3,180	4,422	2,805	0.933	0.882
270-2B	5	14.8	168	27,500	4,880	2,940	4,553	2,653	0.933	0.902
270-3B	5	6.1	171	27,800	6,500	3,890	5,048	2,825	0.777	0.726
270-3C	5	7.7	146	29,200	7,050	4,120	5,275	3,575	0.748	0.868
275-2	5	12.5	193	---	5,290	2,570	4,215	2,226	0.797	0.866
276-1B	5	20.6	355	---	3,930	2,120	3,874	2,216	0.986	1.045
276-2	5	20.6	358	---	3,520	1,770	3,831	2,218	1.088	1.253
276-3A	5	19.7	355	---	3,520	2,000	3,874	2,216	1.101	1.108
281-3	10	6.5	154	25,100	7,690	4,170	9,674	5,013	1.258	1.202
283-2	10	12.1	216	39,800	6,870	3,100	6,517	2,711	0.949	0.875
283-3	10	12.4	218	42,000	6,040	2,620	6,561	2,682	1.085	1.024
283-4	10	10.1	227	42,600	6,320	2,620	6,232	2,452	0.986	0.936

TABLE 1. SUMMARY OF RADIOMETER DATA--Continued

Run No.	Pit Width Ft	Wind Speed Mph	Wind Direction Degrees	Radiant Flux Measured Narrow Angle	Radiant Flux Measured Front Btu/hr-ft^2	Radiant Flux Measured Rear	Radiant Flux Calculated Front Btu/hr-ft^2	Radiant Flux Calculated Rear	Ratio, q_c/q_m Front	Ratio, q_c/q_m Rear
283-5	10	13.6	220	40,100	5,630	2,260	6,624	2,658	1.177	1.176
283-6	10	12.6	222	42,100	6,590	2,740	6,544	2,599	0.993	0.949
283-7	10	14.2	222	41,700	6,180	2,500	6,710	2,642	1.086	1.057
284-3	10	9.1	358	---	7,700	3,690	7,567	3,672	0.983	0.995
284-4	10	8.2	345	---	7,560	3,450	7,032	3,284	0.930	0.952
284-5	10	7.8	343	---	7,280	3,330	6,963	3,232	0.956	0.971
284-6	10	9.9	314	---	7,280	3,100	6,229	2,470	0.856	0.797
289-2	10	4.0	56	34,000	---	---	---	---	---	---
289-3	10	8.6	126	27,200	11,400	6,790	13,333	7,203	1.170	1.061
289-4	10	7.1	117	28,000	13,900	7,360	15,772	8,160	1.135	1.109
289-5	10	7.8	123	30,600	---	---	---	---	---	---
291-2	10	12.6	178	32,900	7,270	---	7,686	3,762	1.057	---
291-3	10	12.2	174	35,900	7,170	---	7,899	3,912	1.102	---
291-4	10	11.3	176	39,500	6,930	---	7,832	3,860	1.130	---
291-5	10	20.4	163	37,000	---	---	---	---	---	---
291-6	10	17.3	176	36,700	6,430	---	7,604	3,690	1.183	---
296-2A	10	4.4	233	44,900	6,320	2,380	5,985	2,608	0.947	1.096
296-2B	10	4.6	204	---	6,990	2,960	6,889	3,164	0.986	1.069
298-4	10	8.5	215	34,700	6,460	3,010	6,323	2,716	0.979	0.902
298-5	10	8.7	192	35,000	6,320	2,970	7,141	3,367	1.130	1.134
298-6	10	3.5	167	33,300	7,980	3,800	9,059	4,436	1.135	1.167
299-2	10	14.4	200	30,500	6,350	2,620	6,946	3,125	1.094	1.193
319-1	10	15.6	230	30,100	6,180	6,730*	6,884	6,773	1.114	1.006
319-2	10	6.7	257	27,500	6,460	10,400*	5,491	7,181	0.850	0.690

TABLE 1. SUMMARY OF RADIOMETER DATA--Continued

Run No.	Pit Width Ft	Wind		Radiant Flux Measured			Radiant Flux Calculated		Ratio, q_c/q_m	
		Speed Mph	Direction Degrees	Narrow Angle	Front Btu/hr-ft^2	Rear	Front Btu/hr-ft^2	Rear	Front	Rear
320-1	10	10.1	211	26,100	7,420	7,550*	6,517	6,181	0.878	0.819
323-1	10	8.7	154	20,700	8,100	5,630*	9,407	5,872	1.161	1.043
360-1	10	7**	14	---	9,060	5,710	8,598	4,336	0.949	0.759
360-2	10	7**	8	---	7,970	4,520	8,236	4,096	1.033	0.906
360-3	10	7**	308	---	6,730	3,450	5,870	2,375	0.872	0.688
360-4	10	7**	315	---	7,280	3,690	6,018	2,515	0.827	0.682
330-1	20	14.3	160	30,100	7,040	3,280	8,648	4,470	1.228	1.363
337-1	20	15.5	195	---	10,360	5,280	7,077	3,251	0.683	0.616
344-1	20	20.5	174	28,700	6,630	3,280	8,610	4,043	1.299	1.233
344-2	20	12.5	169	26,300	7,460	3,520	8,333	3,900	1.117	1.108
344-3	20	21.8	167	27,900	6,630	3,170	8,337	3,805	1.257	1.200
353-1	20	5**	160	35,600	7,410	3,400	8,150	3,844	1.100	1.131
353-2	20	6**	135	36,400	6,730	3,060	6,804	3,036	1.011	0.992
355-1	20	6**	158	35,100	7,680	3,170	7,873	3,685	1.025	1.162
355-2A	20	3.5**	163	33,600	7,410	3,870	8,612	4,099	1.162	1.059
355-2B	20	4**	162	34,100	6,870	3,280	8,432	4,005	1.227	1.221
002-1	20	6.5	53	29,200	5,800	2,580	6,442	2,803	1.111	1.086
365-2	40	0.8	59	---	8,450	4,502	8,784	4,195	1.040	0.932
011-2	40	7.8	55	49,600	5,540	2,510	5,990	2,682	1.081	1.069

*Radiometer in generally downwind direction from fire.

**Wind velocity estimated from airport weather data.

In a few tests, radiometer readings were not obtained for one or more radiometers. In the case of the narrow angle radiometers, data were sometimes taken with the radiometer located in a position where the viewing angle included background as well as the flame. These data were not included in Table 1. The rear radiometer was moved to a location downwind of the fire for a few tests. The purpose was to check fire control fluxes at that location. However, such data proved not to be useful, so the radiometer was moved back to its position 2 pit widths from the crosswind side of the pit.

Because of variation in wind direction, the "crosswind" and "downwind" sides of the pit are not exactly 90 degrees or 180 degrees from the wind direction. The radiometers were placed at a side of the pit that would usually be crosswind, i.e., they would view the flame at a direction 90 degrees from the wind direction. Once positioned, the wide angle radiometers were not moved until tests were run on a different pit. The narrow angle radiometers had to be repositioned and re-aimed for nearly every fire because of changes in flame tilt and flame direction. It was difficult to provide proper aiming of the narrow angle radiometer because the position could not be changed once the fire was started. Therefore, narrow angle radiometer data are less reliable than wide angle radiometer data.

SIMPLIFIED FLAME RADIATION THEORY

The data in Table 1 can be used to develop a method for predicting radiation fluxes from propane fires. The goal is to provide a relatively simple technique that will provide acceptable accuracy for engineering design purposes.

A turbulent flame burning propane is a reasonably complex system. The fuel vaporizes at a liquid pool surface and begins to mix with the surrounding air. Wind and buoyancy forces cause the flame to be turbulent, so that fuel and air are mixed throughout the flame volume. Combustion, which involves the breakdown of the fuel molecule and its reaction with oxygen from the air, may occur at any point in the flame column, although it does not occur at all points in the column simultaneously. The actual combustion zones are not very thick because the final mixing-combustion process takes place at the molecular level. (If mixing is complete before combustion, the resulting premixed flame has none of the red color characteristic of diffusion flames.) The combustion zones are probably less than a few centimeters thick, but there are many of them, so to the naked eye, and to most instruments, the flame appears to be continuous. In reality, for any given path through the flame, there are many constantly changing locations where combustion occurs.

As combustion occurs, energy is radiated from the flame from two types of sources: hot gases and hot carbon particles. The primary emission from hot gases is from

water and carbon dioxide. Emission from these two gases occurs in fairly broad bands. The bands are strongest at wavelengths of 2.7 microns and 4.3 microns. Radiation at these two wavelengths is invisible to the naked eye. The characteristic red-orange flame color originates from radiation emitted by hot carbon particles that are formed as the fuel molecules lose their hydrogen. Radiation from the hot carbon particles resembles the radiation from solid surface; it is distributed more or less along a continuum.

Because the flame emits (and absorbs) radiant energy throughout its volume, it is not strictly a surface emitter. Techniques were developed in the 1960's to describe the radiation process in flames based on the use of volume emission and absorption coefficients (Love, 1968; Shahrokhi, 1965; Pfenning, 1970). More recently similar methods that rely on use of flame temperatures have been considered (Markstein, 1974). Both methods require relatively sophisticated techniques for obtaining data that enables them to be used for predictive purposes. Either can be sufficiently simplified to enable relatively easy predictions of radiant fluxes to a flame's surroundings.

Starting with the assumption that the flame can be considered as a continuous absorbing, emitting medium, the radiant intensity at any point in the flame can be described by the basic transport equation

$$\frac{dI_\lambda(x)}{dx} = J_\lambda - \beta_\lambda I_\lambda(x) \qquad (1)$$

where $I_\lambda(x)$ = monochromatic radiant intensity at point x

x = distance within flame

J_λ = monochromatic volumetric emission coefficient

β_λ = monochromatic extinction coefficient

Equation 1 assumes isotropic emission within the flame and extinction proportional to local intensity. J_λ includes both the continuum radiation from hot carbon particles and the band radiation from emitting gases. β_λ includes absorption and scattering.

Application of Equation 1 to determine radiant fluxes from a fire requires knowledge of the emission and absorption coefficients. Such data are not available and cannot be easily obtained. Simplifications can be made that make predictions possible with more limited data. Assume that Equation 1 is to be applied to a flame having a hemispherical shape and that the radiant intensity is to be measured at the center of the flame. The monochromatic radiant flux at the center of the flame can be found by integrating Equation 1. Then

$$q_\lambda = \int_0^{2\pi} \int_0^{\pi/2} \left[\frac{J_\lambda}{\beta_\lambda} \left(1 - e^{-\beta_\lambda R} \right) \right] \sin\theta \cos\theta \, d\theta \, d\phi \qquad (2)$$

where R is the radius of the hemisphere and integration covers the entire hemispheric volume. The result is

$$q_\lambda = \frac{\pi J_\lambda}{\beta_\lambda}\left(1 - e^{-\beta_\lambda R}\right) \tag{3}$$

The total radiant flux may be found by integrating Equation 3 over all wavelengths where there is significant emission, giving

$$q = \int_{\lambda_1}^{\lambda_2} \frac{\pi J_\lambda}{\beta_\lambda}\left(1 - e^{-\beta_\lambda R}\right) d\lambda \tag{4}$$

Radiant emission from flames of other shapes to objects outside the flame can be found from equations similar to Equation 4. Assume that the form of Equation 4 can be used to describe the radiant energy emitted at a flame surface, and assume that the flame can then be considered as a surface emitter. The surface flux can then be written as

$$q_s = q_{sm}\left(1 - e^{-bD}\right) \tag{5}$$

where q_s = flux emitted from flame surface

q_{sm} = maximum surface flux for an optically thick flame

b = flame extinction coefficient

D = distance through the flame

The term q_{sm} is related to the integrated average of J_λ/β_λ and b is related to the integrated average of β_λ. The distance through the flame is most conveniently taken to be the distance across the fuel source. In the case of a pool fire, that distance is the diameter of a circular pool or the length of the side of a rectangular pool.

The radiant flux incident at some point outside a flame can be calculated as

$$q = F\, q_s \tag{6}$$

where F is a geometric view factor that can be calculated as

$$F_{dA_1 - A_2} = \int_{A_2} \frac{\cos \beta_1 \cos \beta_2}{\pi r^2}\, dA_2 \tag{7}$$

where dA_1 = target area, taken as a differential element

A_2 = emitting area of flame

r = distance from target element to flame along a line from dA_1 to dA_2

β_1 = angle between normal to dA_1 and the line from dA_1 to dA_2

β_2 = angle between normal to dA_2 and the line from dA_1 to dA_2

Figure 3 shows the geometry for a flame with a circular base. Equation 7 must be integrated over the entire emitting area of the flame that can be seen by the target

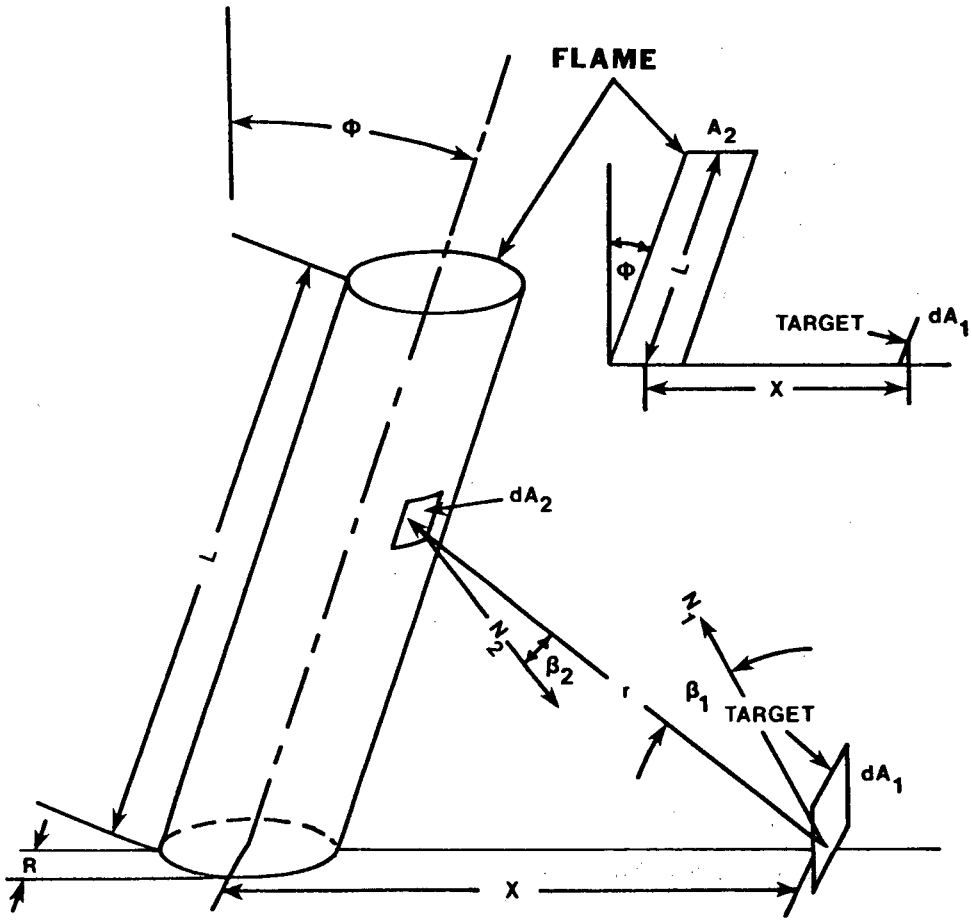

FIGURE 3. GEOMETRY USED FOR CALCULATION OF VIEW FACTORS.

element dA_1. The view factor depends only on the geometry of the flame-target system. Values of view factors for some target-flame systems are available in the literature (Rein, et al., 1970; Howell and Siegel, 1969; Raj, 1977, for example). Generalized computer solutions can be written to obtain view factors not otherwise available. Flame size, shape, and orientation with respect to the target must be known in order to calculate the view factors.

The flame height can be estimated from the correlation of Thomas (1963):

$$\frac{L}{D} = 42 \left(\frac{m}{\rho_a \sqrt{gD}} \right)^{0.61} \tag{8}$$

where L = flame height

D = pool diameter

m = burning rate

ρ_a = air density

g = gravitational acceleration

The pool diameter is the width for square pools and the equivalent diameter

$$D_{eq} = \frac{4 \text{ (pool area)}}{\text{pool perimeter}} \tag{9}$$

can be used for other rectangles.

The flame will be tilted by the wind, changing the flame target geometry. The flame angle can be estimated from Welker and Sliepcevich (1970):

$$\frac{\tan \phi}{\cos \phi} = 3.2 \left(\frac{D\ u\ \rho_a}{\mu_a} \right)^{0.07} \left(\frac{u^2}{gD} \right)^{0.7} \left(\frac{\rho_g}{\rho_a} \right)^{-0.6} \qquad (10)$$

where ϕ = flame angle measured from vertical

D = flame diameter

ρ_a = ambient air density

μ = ambient air viscosity

u = wind speed

g = gravitational acceleration

ρ_g = fuel vapor density

The units to be used in the foregoing equations can be any consistent system. The emission coefficient has units of energy/time-area-unit of solid angle-unit of wavelength, for example, and fluxes have units of energy/area-time. The extinction coefficients have units of length^{-1}. Equations 9 and 10 have empirical coefficients, and are written in dimensionless form so that any consistent set of units may be used.

Some of the radiant energy emitted by a fire is absorbed by the atmosphere. Absorption is strongest in wavebands centered near 1.9, 2.7, and 4.3 microns. These bands are due to absorption by water vapor and carbon dioxide in the atmosphere. Flames also emit radiation at these wavelengths, but the emission bands are wider than the absorption bands, so not all of the radiation emitted by a

flame in the emission bands is absorbed by the atmosphere. If an absorption band is particularly strong, all the radiation absorbed by that band will be absorbed fairly near the flame. The 2.7-micron and 4.3-micron bands are strong absorbers.

DISCUSSION OF RESULTS

Table 1 lists the radiation fluxes measured by narrow angle radiometers for fires in square pits from 5 to 40 ft wide. The radiometers were usually placed so that they viewed the flame across the downwind edge of the pit. Radiometer location was critical because if the fire was tilted too far by the wind or if the wind direction changed, the radiometer viewing cone might not be filled with flame and the radiometer readings would be erratic and inconsistent.

The windows on the narrow angle radiometers were made of calcium fluoride, which has a nearly flat transmission curve from about 2 microns to about 8 microns, and transmission from 1 micron to 2 microns averages about 80 percent. All the strong radiation from hydrocarbon fires is contained within the band from 1 micron to 8 microns. The narrow angle radiometers were calibrated at the factory using a blackbody source. Calibration was checked using a blackbody following the tests, and the calibration was identical. Calibration was performed on the basis of the

incident radiant flux, so that no corrections were required because of the small fraction of energy reflected or absorbed by the window. The flat transmission curve obviated a need to correct for transmission at various wavelengths, and because all the incident radiation struck the window at nearly right angles, no correction for reflection for grazing radiation was necessary.

The narrow angle radiometer data were used to determine values of q_{sm} for use in predicting radiant fluxes. The procedure followed was to average the measured narrow angle radiant fluxes for a period of half a minute to several minutes. The values thus obtained were used to determine the coefficients q_{sm} and b in Equation 5. The averaged narrow angle radiant fluxes varied from run to run, as shown in Figure 4. The solid line in Figure 4 is calculated from Equation 5 with q_{sm} of 50,000 Btu/hr-ft^2 and b = 0.126 ft^{-1}.

The measured narrow angle fluxes shown in Figure 4 vary substantially from the line drawn to represent the data, and some explanation is required. First, the data points are shown plotted as a function of flame diameter. There were actual fires from pools nominally 5, 10, 20, and 40 feet wide. However, the wind direction was frequently not perpendicular to the radiometer, so that the flame was blown in a direction that increased the viewing path length. The path lengths were corrected for the wind direction

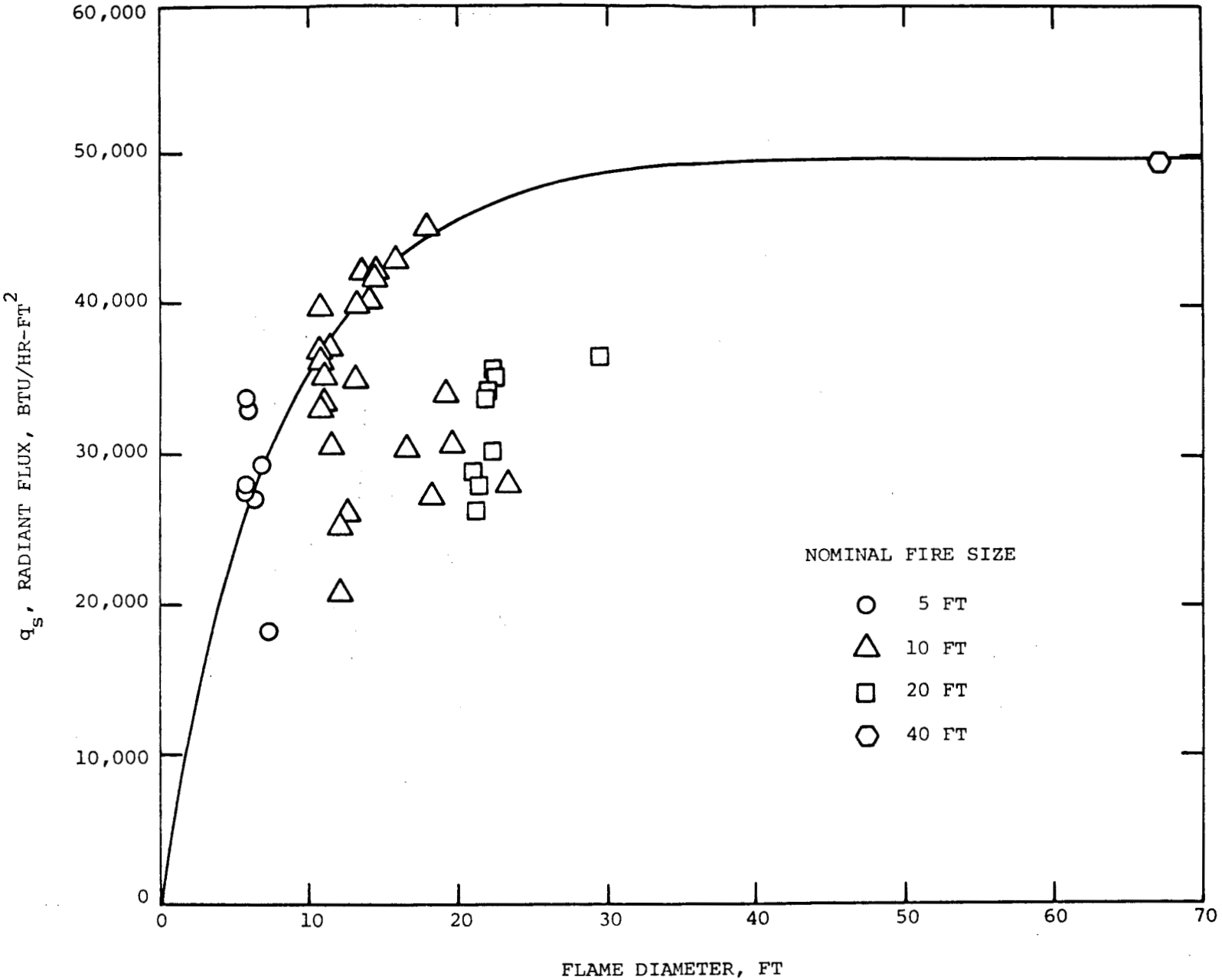

FIGURE 4. SURFACE RADIANT FLUXES FOR PROPANE FIRES.

effect, and the result is the "diameter" plotted in Figure 4.

Some of the narrow angle radiometer fluxes are well below the line. These are most likely tests where the full radiometer viewing cone was not completely filled by the flame. The line was drawn with a bias toward the higher fluxes because they were judged to be more reliable.

Narrow angle radiometer data were obtained for only one of the 40-ft tests. Both the narrow angle radiometer at the pit, and a second narrow angle radiometer about 175 ft away from the fire gave essentially the same readings. The reading at the longer distance was larger than the reading from the radiometer near the pit, but the difference was less than 2 percent.

The narrow angle radiometer fluxes were not corrected for atmospheric absorption for two reasons. First, no measurements were made of the spectral energy distribution. Second, the results from the 40-ft test indicate that absorption is relatively weak beyond the area immediately surrounding the fire. Standard methods of calculating the atmospheric transmissivity are based on blackbody radiators, and because the flame is not a blackbody radiator, the absorption may be less than predicted, particularly at longer distances from the fire, because both water vapor and carbon dioxide are relatively strong absorbers in their absorption wavebands.

The narrow angle radiometer data represent the effective surface radiant flux from the fire. As such, q_{sm} is an integrated average of the radiant fluxes from a number of reacting zones within the flame. The flux may vary with both time and position in the flame. Within the response capability of the radiometers, the time variation in flux for the 40 ft fires was less than 5 percent of the average. When the full viewing cone of the radiometer was viewing the fire, fluctuations in radiant flux from the 10- and 20-ft fires were usually less than 10 percent. Fluctuations from the 5-ft fires were a little larger. No long term changes in narrow angle radiometer readings were noted in the few fires that were monitored through burnout. However, the propane burned was nearly 98 percent pure, so no changes due to fuel composition would have been expected. The small difference between radiometer reading for narrow angle radiometers 40 ft and 175 ft from the fire indicates that there are no strong variations in radiant output in the portions of the flame where the flame is not broken up.

Table 1 also lists the results of wide angle radiometer measurements for propane fires. The wide angle radiometers were usually positioned one and two pit diameters from the edge of the pit. The location was chosen to be in the direction crosswind to the prevailing wind, but once the radiometers were positioned, they were not moved during the tests on a pit of given size. Average wind

direction varied during the tests, so the flame may have been blown toward or away from the radiometers during a test. Table 1 lists both wind speed and wind direction averaged over the same period that the radiometer readings were averaged. These are not necessarily the same averages as those measured for the full duration of the test (from ignition to extinguishment).

The wide angle radiometers used sapphire windows to protect the sensing element from convective effects. Corrections to the measured data were required to obtain the actual incident flux at the radiometer location. The transmissivity of the windows is best from about 1 micron to 4 microns. At wavelengths less than 1 micron and greater than 4 microns, transmission decreases. Factory calibrations of the wide angle radiometers was done using a group of tungsten filament lamps with quartz tubes surrounding the filament. The quartz tubes do not transmit beyond about 5 microns and transmission for quartz begins to decrease sharply at about 3.5 microns. Calibration checks were performed on each wide angle radiometer using a blackbody source. Checks were made both with and without the sapphire window. With the window removed, the blackbody calibration matched the factory calibration. However, with the window in place, a consistent difference was found. At a given radiometer output, the actual incident flux based on blackbody radiation, was about 20 percent greater than the flux

indicated by the factory calibration curves. Because the flame radiation is not blackbody radiation, additional corrections were required.

The windows were removed from the wide angle radiometers and the transmittance measured for radiation incident at several angles. Figure 5 shows the result. Measurement at wavelengths less than those shown by the solid lines were not possible with the equipment available, but manufacturers data indicate that the transmittance remains about constant at wavelengths down to 1 micron. The average transmittance of the windows for flame radiation was calculated from

$$\bar{\tau} = \frac{\int_{\lambda_1}^{\lambda_2} \tau_\lambda \, \varepsilon_\lambda \, d_\lambda}{\int_{\lambda_1}^{\lambda_2} \varepsilon_\lambda \, d_\lambda} \qquad (11)$$

where $\bar{\tau}$ = average transmittance for wavelengths between λ_1 and λ_2

τ_λ = transmittance at wavelength λ

ε_λ = emissive power of flame at wavelength λ

Spectral emission data were not available for propane, so data for large LNG fires (Raj, et al., 1979) were used to estimate $\bar{\tau}$. The error introduced by using LNG emission data instead of propane data is not expected to be large because the major emission bands are found at about the same wavelengths. The emission measurements for LNG were made from a distance of 775 ft, so there was little radiation

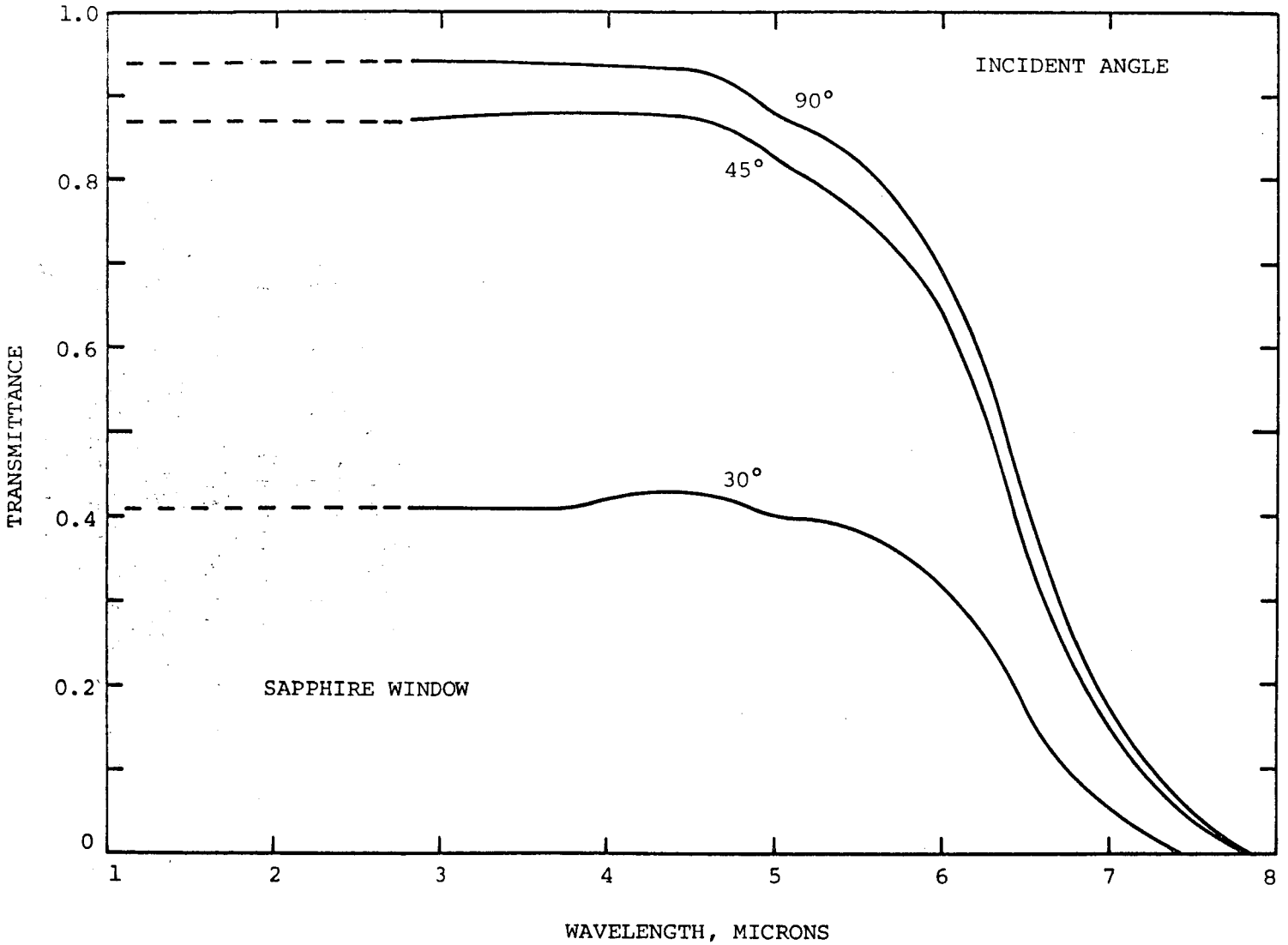

FIGURE 5. SPECTRAL TRANSMITTANCE OF SAPPHIRE RADIOMETER WINDOW.

detected at the wavelengths where atmospheric absorption is strong. Sapphire transmittances are high and relatively constant at those wavelengths where atmospheric absorption is strong, so the effect on average transmittance is minor. The average transmittances found from the sapphire transmittance data and LNG flame radiation are listed in Table 2.

TABLE 2. AVERAGE TRANSMITTANCE FOR FLAME RADIATION THROUGH SAPPHIRE WINDOWS.

Incident Angle	Average Transmittance
90	0.909
45	0.845
30	0.423
15	0.028

The average transmittance decreases rather sharply as the angle of incidence changes between 45 degrees and 15 degrees. At angles of incidence less than 15 degrees, sapphire reflects most of the incident radiation of all wavelengths. Correction to the wide angle radiometer data was required because of the reflection at low incident angles. The approximate incident angles for the radiation from the flames were calculated and the radiant flux data were corrected accordingly.

The wide angle radiometer fluxes shown in Table 1 have been corrected for both flame transmittance through the

radiometer window and incident radiation angle. Thus, the data listed represent the radiant flux incident at the radiometer location. No correction has been attempted for atmospheric absorption to determine what the flux might have been in the absence of absorption.

The narrow angle radiometer data were used in conjunction with Equations 5 and 6 to compare "predicted" and measured incident fluxes. Equations 5 and 6, combined with the narrow angle radiometer data, result in

$$q = 50{,}000\ F \left(1 - e^{-0.126\ D}\right) \qquad (12)$$

Equation 12 is a dimensional equation in which the incident flux is in Btu/hr-ft^2 and D must have the units of feet. (Other units may be used with suitable conversions.)

The procedure followed in predicting radiant fluxes required the calculation of radiant view factors. The flame height and angles required for the view factor calculations were obtained from Equations 8 through 10. A few flame length measurements were possible. The measured flame lengths are compared to the Thomas prediction in Figure 6, and the measured values are well represented by the Thomas equation. The measured values were taken from movies of the fires and were an average of the fluctuating flame length. Burning rates used in Equation 8 were calculated from

$$V = 0.13 + 0.32 \left(1 - e^{-0.208\ D}\right) \qquad (13)$$

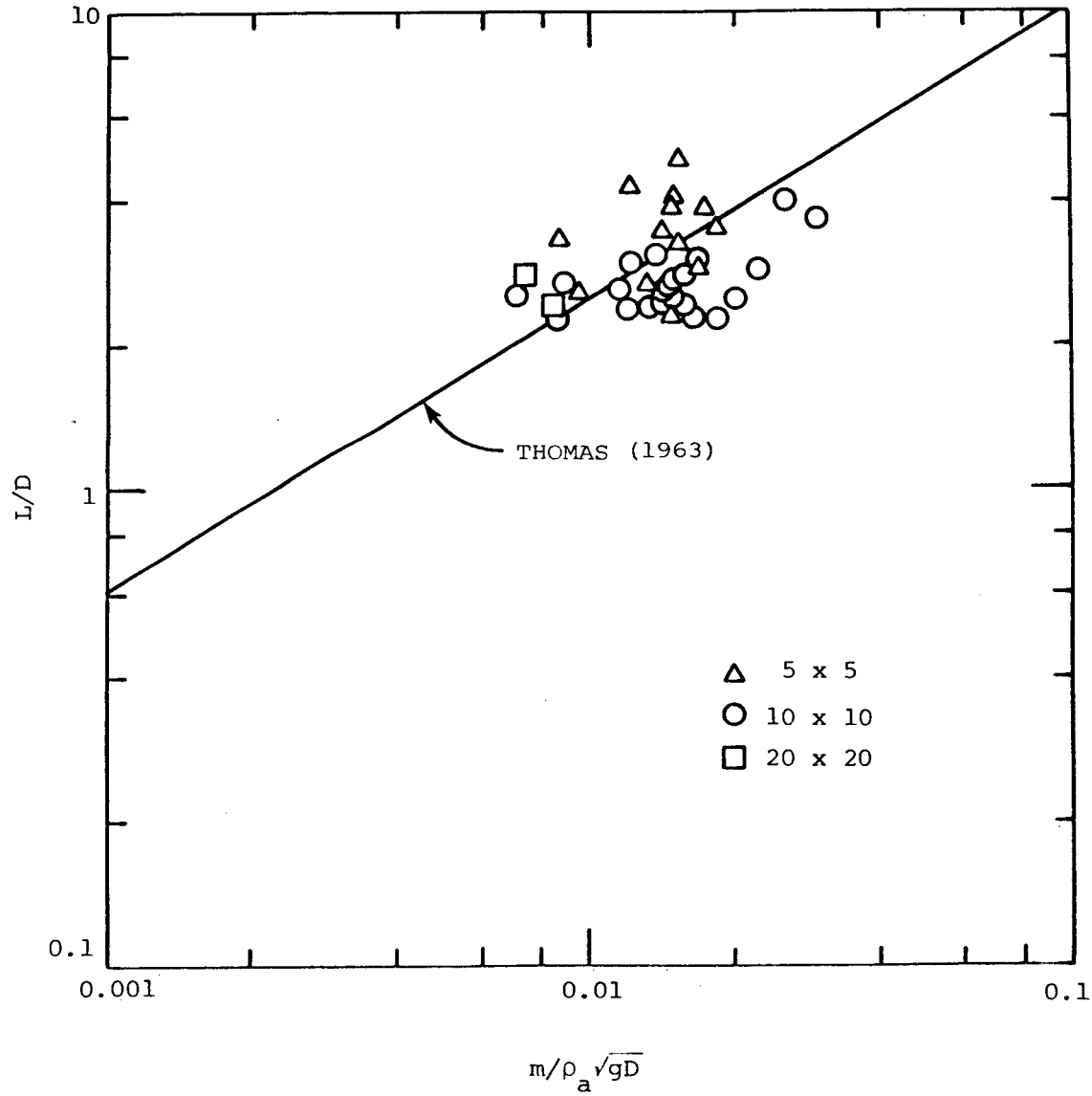

FIGURE 6. COMPARISON OF FLAME HEIGHTS WITH PREDICTION OF THOMAS (1963).

where V is the linear regression rate in in/min. Equation 13 is based on burning rates measured during the fire control and extinguishment tests (Johnson, et al., 1980).

Flame tilt angles were calculated using Equation 10 and the average wind velocities measured for the period during which the radiation measurements were made. The camera locations used to film the fires were chosen to provide coverage for determining extinguishment or control time, and the resulting photographs and movies were not useful for measuring flame tilt angles, so no comparisons of measured and predicted flame angles were possible. The flame azimuthal angles were assumed to be the same as the mean wind direction angles measured during the radiation tests.

The view factors were calculated using as basic input only the wind speed and wind direction measured during the tests and the radiometer position. All other input parameters were calculated based on previously-available information. Once the view factors had been calculated, Equation 12, based on the narrow angle radiometer data, was used to calculate the expected incident radiant flux at the wide angle radiometer locations. Table 1 includes a listing of the calculated fluxes and Figure 7 shows a comparison of measured and calculated fluxes. Figure 7 does not show all the data for cases where calculated and measured fluxes were nearly equal because of overcrowding on the graph.

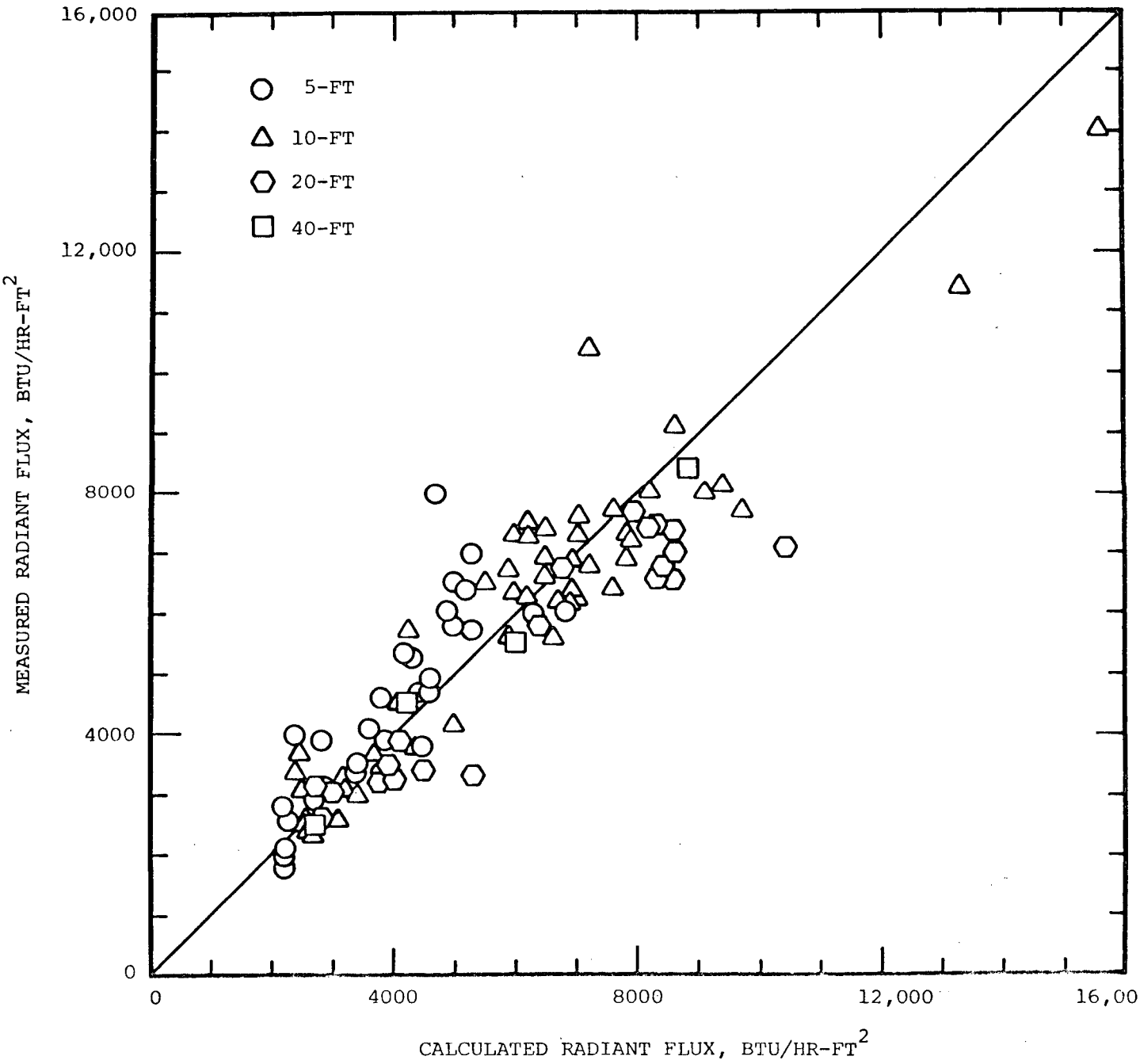

FIGURE 7. COMPARISON OF MEASURED AND CALCULATED RADIANT FLUXES

Table 1 also contains a list of the ratio of calculated flux, q_c, to measured flux, q_m. The overall average of the ratio of q_c/q_m is 0.998 with a standard deviation of about 16 percent. This result indicates that the simplified method of predicting the radiant flux from a propane fire is adequate for most purposes. If the spectral distribution of energy from a propane fire is required, the spectral emission curves for LNG fires (Raj, 1979) can be used as a good approximation.

CONCLUSIONS

The radiant fluxes from propane fires can be predicted with good accuracy using a simple flame emission model. The maximum radiant emission flux for free-burning propane diffusion flames is about 50,000 Btu/hr-ft^2, and fires from 5 to 40 ft in width follow an emission curve derived by simplifying a basic transport model. Predicted radiant fluxes incident at locations near the flame show close correlation to measured fluxes. Flame height and angle of tilt predicted by models from the literature are adequate for modeling flame geometry.

REFERENCES

1. Johnson, D. W., et al., "Control and Extinguishment of LPG Fires," Report No. DOE/EV-6020-1, U. S. Department of Energy, Washington, DC (August 1980).

2. Love, T. J., Radiative Heat Transfer, Charles E. Merrill Publishing Co., Columbus, OH (1968).

3. Shahrokhi, F., "Numerical Technique for Calculation of Radiant Energy Flux to Targets from Flames," Ph.D. Dissertation, University of Oklahoma, Norman, OK (1965).

4. Pfenning, D. B., "Radiative Transfer from Laminar Diffusion Flames," Ph.D. Dissertation, University of Oklahoma, Norman, OK (1970).

5. Markstein, G. H., "Radiative Energy Transfer from Gaseous Diffusion Flames," 15th International Symposium on Combustion, The Combustion Institute (1974).

6. Rein, R. G., et al., "Radiation View Factors for Tilted Cylinders," J. Fire and Flammability, 1, 140 (1970).

7. Howell, J. R., and R. Siegel, Thermal Radiation Heat Transfer, Vol. II, NASA SP-164, Washington, DC (1969).

8. Raj, P. P. K., "Calculation of Thermal Radiation Hazards from LNG Fires--A Review of the State-of-the-Art," Proceedings, AGA Operating Section, American Gas Association, Arlington, VA (1977).

9. Thomas, P. H., "The Size of Flames from Natural Fires," Ninth International Symposium on Combustion, Academic Press, New York (1963).

10. Welker, J. R., and C. M. Sliepcevich, "Susceptibility of Potential Target Components to Defeat by Thermal Action," University of Oklahoma Research Institute Report No. OURI-1578-FR, Norman, OK (1970).

11. Raj, P. P. K., et al., "Experiments Involving Pool and Vapor Fires from Spills of Liquefied Natural Gas on Water," Report No. CG-D-55-79, U. S. Coast Guard, Washington, DC (March 1979).

REPORT III

VAPORIZATION OF PROPANE FROM SPILLS ONTO SOLID SURFACES

INTRODUCTION

If propane or other flammable liquefied gas is spilled, it will immediately begin to vaporize. The vapor plume thus formed will be flammable for a distance from the area of the spill. The vaporization rate is one of the primary factors determining the size of the flammable plume. The vaporization rate depends on the thermal properties of the solid onto which propane is spilled and on the solid temperature. The solid substrate will usually be much warmer than the propane, but its surface will cool rapidly. The vaporization rate will decrease as the solid cools until a condition is reached where heat transfer to the liquid is balanced by the heat required to vaporize the liquid. As the heat transfer rate and vaporization rate decrease, heat transfer from the atmosphere and energy available from self-cooling of the liquid also provide energy required to vaporize the liquid. Eventually, a steady state condition may be reached in which heat and mass transfer are balanced and the vaporization rate becomes constant.

MEASUREMENT PROCEDURE

A mass balance system was constructed to weigh the substrate and propane continuously. Figure 1 is a schematic diagram of the apparatus. It consists of a steel frame balanced on a pivot. One end of the frame supports the test pit and the other is attached to a load cell. Counter-weights are placed on the end of the frame near the load cell to balance the frame and increase the sensitivity of measurement. Full scale movement of the sensing element of the load cell is less than 0.01 inches, so the frame is maintained in a level attitude at all times. The entire apparatus is mounted on an outdoor concrete pad. It can be used completely in the open, in the shade, or in the shade with sheltering to reduce wind effects. All tests were run outdoors to avoid safety problems caused by potential accumulation of flammable vapors indoors.

The output signal from the load cell was recorded on both a strip chart recorder and on magnetic tape. The apparatus was calibrated before each test by loading it with lead bricks of slightly greater mass than the mass of propane to be spilled during the test. This procedure assured use of the widest possible portion of the transducer range as well as checking for proper operation. The zero point of the load cell reading changed for nearly every test because of differences in test pit weight and balance loading, but the span calibration remained constant throughout the test

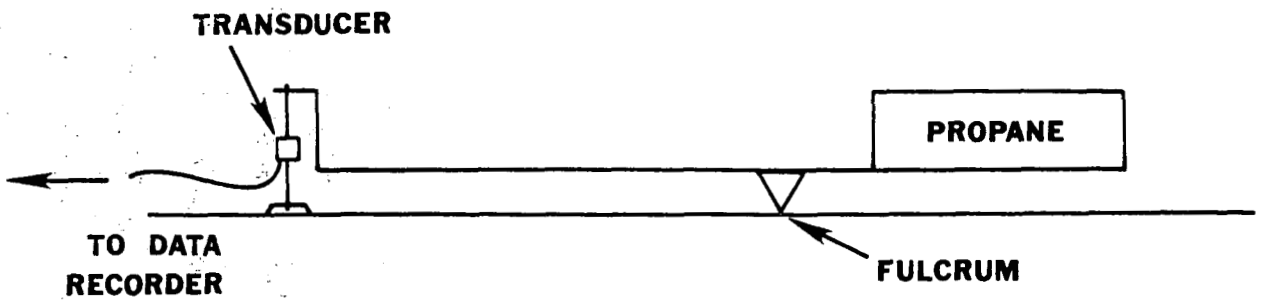

Figure 1. Apparatus for Weighing Propane During Vaporization Tests.

series. The balance system, when calibrated indoors, or outdoors under no wind conditions could record changes of about 0.05 lb, which is about 0.2 percent of the mass of the initial propane spill for most tests. Many tests were run when there was low to moderate wind, and the wind gusts caused random variation in the recorded weight because of movement of the test pit. When the test pits were partially shielded from wind effects, the weighing accuracy was about one percent of the amount of propane spilled, or about a quarter to a third of a pound. In some tests where the weighing frame and pit were not shielded and wind speed was high, random variations in recorded weight of more than 5 lb were found. In cases where the wind fluctuations were present, data were averaged over about a 10-sec period, 5 sec before the time being considered and 5 sec after. This procedure produced reasonably consistent data except for quite strong, gusty winds.

In addition to the propane weight, the propane temperature, wind speed, solar flux, and substrate temperature were measured for each test. Ambient temperature, humidity, and barometric pressure were recorded for most tests.

The general test procedure was to set up the load cell and test pit on opposite ends of the weighing frame, bias the weight so that the load cell was set near the end of its effective span, and calibrate the load cell. Propane was transferred from an ambient temperature storage tank to

a spill bucket. In the first tests, the spill bucket was insulated to minimize boiloff before the spill. However, regardless of the care used in transferring the propane, substantial subcooling occurred, so that the propane was sometimes more than 30 degrees F below its normal boiling point. Subcooling to that extent was large enough that boiling of the propane on the substrate did not raise the bulk of the liquid to the boiling point. Therefore, an uninsulated bucket was used for transferring propane during most tests. In addition, warm propane gas was bubbled through the propane liquid in the spill bucket to warm the liquid to the boiling point before it was spilled.

The usual procedure was to pour the liquid propane into the pit as rapidly as possible without splashing or sloshing. The time required depended on the amount spilled, but was usually 10 to 15 seconds for a spill of 25 to 30 lb.

The test pits were constructed from a variety of materials. Whenever practicable, thermocouples were placed in the floor of the pit to monitor the temperature profile. The floor area of the test pits was usually 5 ft^2, but in a few cases the material used for the pit bottom could not be obtained in a large enough piece, so smaller pits were constructed. The pit sides were usually about 4 inches thick and the pit bottoms were 4 to 6 inches thick. In some cases, such as when soil or sod was being tested, the pit sides were made from polystyrene foam or polyurethane foam

because of the problems encountered in making walls of the substrate material. When polystyrene foam was used for pit walls it was covered with a layer of 0.6-mil polyethylene to prevent degradation by direct contact with propane.

Many tests were run with the propane pool open to the atmosphere. When this procedure was followed, it was possible to estimate the contributions of solar radiation and atmospheric convection to the vaporization process. In other tests, the propane was poured into covered pits where the effects of the outside environment were small. The covered tests enabled the estimation of thermal conductivity and surface-to-liquid heat transfer coefficients.

In several tests granite or marble rocks were placed in the bottom of the pit to simulate the effects of gravel or rock surfaces. The very rapid vaporization of propane spilled on crushed rock surfaces caused some measurement problems because several pounds of propane could be vaporized in the 10 to 15 seconds required to pour it into the pits. A few tests were run in which rocks were poured into previously cooled propane pits.

PROPANE VAPORIZATION THEORY

When propane is spilled on a solid surface, it starts to vaporize immediately at usual ambient temperatures. In most cases the heat transfer rate from solid to liquid is fast enough that boiling occurs for a short

time until the solid surface begins to cool. Later, as heat transfer from the solid decreases, boiling stops, but vaporization continues, with the heat required for vaporization being supplied by radiation or convection from the atmosphere, or from self-cooling of the liquid, in addition to conduction from the solid surface.

The total rate of heat transfer available to cause vaporization from a propane pool on a smooth surface can be calculated from a heat balance,

$$q = q_c + q_a + q_r + q_s \qquad (1)$$

where q = heat transfer rate available for vaporization

q_c = heat conduction to solid surface

q_a = heat transfer from atmosphere

q_r = heat transfer from solar radiation

q_s = sensible heat rate from self-cooling

The heat transfer rate from the solid, q_c, is usually dominant at the start of the spill. However, as the solid surface cools, q_c decreases relatively rapidly. Both q_a and q_r are relatively constant and change primarily because of changes in ambient conditions. As the pool cools, a relatively small amount of energy is extracted from the pool itself. It's importance is usually in determining the pool temperature rather than in causing substantial vaporization of liquid. If the propane pool is deep enough to persist

longer than 15 minutes to half an hour, the atmospheric convection and solar radiation terms become dominant as source of heat.

Heat transfer from the solid surface can be found by considering a heat balance within the solid. Assume that the solid has constant thermal properties. Its temperature can then be found from

$$k \frac{\partial^2 T}{\partial x^2} = \rho c \frac{\partial T}{\partial t} \qquad (2)$$

where T = temperature within the solid

k = thermal conductivity

x = distance within the solid

ρ = solid density

c = solid heat capacity

t = time

Equation 2 is written for one-dimensional application. There is rarely a need to consider two-dimensional forms for spills of liquefied gases. Assuming that the solid is at a uniform temperature when the spill occurs,

$$T = T_o \text{ at } t = 0 \qquad (3)$$

where T_o is the initial temperature of the solid. When propane initially contacts the solid surface, the heat transfer rate is limited because by convection between the solid and liquid. Thus, one boundary condition is

$$-k \frac{\partial T}{\partial x} = h(T - T_p) \tag{4}$$

where h = convective coefficient between propane and solid

T_p = temperature of liquid propane in pool

Normally, the solid can be treated as being semi-infinite, so the second boundary condition is

$$\frac{\partial T}{\partial x} = 0 \tag{5}$$

for large values of x, i.e., at depths where the solid has not yet been cooled by propane.

The solution to Equation 2, along with its initial and boundary conditions, is

$$\frac{T - T_p}{T_o - T_p} = \text{erf}\left(\frac{x}{2\sqrt{\kappa t}}\right) + \exp\left(\frac{hx}{t} + \frac{h^2 t}{k\rho c}\right) \text{erfc}\left(\frac{x}{2\sqrt{\kappa t}} + \frac{h\sqrt{t}}{\sqrt{k\rho c}}\right) \tag{6}$$

where κ is the thermal diffusivity, $k/\rho c$.

The rate of heat transfer from the solid to the liquid propane is

$$q_c = h(T - T_p) \tag{7}$$

at x = 0 (the solid surface), so, substituting $(T - T_p)$ from Equation 6,

$$q_c = h(T_o - T_p) \exp\left(\frac{h^2 t}{k\rho c}\right) \operatorname{erfc}\left(\frac{h\sqrt{t}}{\sqrt{k\rho c}}\right) \tag{8}$$

Any consistent set of units may be used; note that $h^2 t/k\rho c$ is unitless. Equation 8 can also be written in the form

$$q_c = \frac{\sqrt{k\rho c}\ (T_o - T_p)}{\sqrt{\pi t}} \sqrt{\pi}\ Y \exp Y^2 \operatorname{erfc} Y \tag{9}$$

where

$$Y = \frac{h\sqrt{t}}{\sqrt{k\rho c}} \tag{10}$$

The function

$$f(Y) = \sqrt{\pi}\ Y \exp Y^2 \operatorname{erfc} Y \tag{11}$$

is between 0.95 and 1.0 for values of Y greater than 3, which indicates that the heat transfer coefficient h is important primarily for times

$$t < \frac{3k\rho c}{h^2} \tag{12}$$

The total heat transfer from solid to liquid over a time t can be found by integrating Equation 8. The result is

$$Q_c = h(T_o - T_p)\left(\frac{2k\rho c}{h^2}\right)\left[\frac{(\exp Y^2 \ \text{erfc}\ Y - 1)}{2} + \frac{Y}{\sqrt{\pi}}\right] \qquad (13)$$

where Q_c is the total heat transfer from the solid. At long times Equation 13 reduces to

$$Q_c = \frac{2\sqrt{k\rho ct}(T_o - T_p)}{\sqrt{\pi}} \qquad (14)$$

The elapsed time before Equation 14 applies depends on the thermal properties of the solid and the heat transfer coefficient. A value of $Y = 8$ is required to bring the value of Q_c calculated from Equation 14 to within 10 percent of the value calculated from Equation 13.

The rate of heat transfer from the atmosphere can be calculated from

$$q_a = h_a (T_a - T_p) \qquad (15)$$

where h_a = convective coefficient between air and propane

T_a = ambient air temperature

Values for h_a depend on the pool size and the wind velocity. They are typically about 1 to 2 Btu/hr-ft^2-^{o}F, so the heat transfer rate from the atmosphere to the pool is only a few

percent of that from the solid until the solid surface cools. Atmospheric heating is more important for solids with low values of the product $k\rho c$ at shorter times after the spill.

The solar radiant flux is also small compared to the initial heat transfer rate from the solid. It is about the same magnitude as the convective flux, and is important only for spills that are deep enough to be long-lasting.

The propane pool is not in equilibrium with the atmosphere, so propane will continue to vaporize even if the heat transfer from the surroundings becomes very low. The energy required to vaporize the propane can come from sensible heat released as the pool cools. The rate of sensible heat change is given by

$$q_s = \rho_L H C_L \frac{dT_p}{dt} \qquad (16)$$

where ρ_L = propane liquid density

H = pool depth

C_L = specific heat of liquid propane

If the pool temperature is at the boiling point, q_s is zero and remains zero until the heat transfer rate (primarily q_c) becomes low enough that the pool begins to cool. Until that time, the vaporization rate can be calculated from

$$m = \frac{q}{\Delta H_v} \tag{17}$$

where m = mass evaporation rate

ΔH_v = heat of vaporization of propane

The total mass evaporated up to any time before the pool cools below the boiling point is

$$M = \frac{Q_c + Q_a + Q_r}{\Delta H_v} \tag{18}$$

where

$$Q_a = q_a t \tag{19}$$

$$Q_r = q_r t \tag{20}$$

and t is the duration of the spill. Notice that both q_a and q_r are assumed to be constant.

If the pool drops below its boiling point, the vaporization rate no longer can be determined by heat transfer considerations only, because not all heat added to the pool must result in vaporization. Therefore, once subcooling begins, vaporization rates must be calculated from mass transfer considerations. For subcooled pools, the vaporization rate may be estimated from

$$m = \frac{k_g P_v}{P} \tag{21}$$

where k_g = mass transfer coefficient

P_v = vapor pressure of propane

P = atmospheric pressure

The mass transfer coefficient depends primarily on the wind velocity, but is also affected by pool size and propane properties. The vapor pressure depends only on pool temperature. Therefore, once the pool begins to cool, at a time that can be determined as

$$m < k_g \tag{22}$$

where m is calculated from Equation 17 using

$$q = q_c + q_a + q_r \tag{23}$$

the pool temperature must be found by integrating Equation 16 and finding the decrease in pool temperature caused by vaporization. The incremental quantity of propane vaporized during any period, as calculated from Equation 21, must be balanced by the quantity of equivalent energy supplied by q_c, q_a, q_r, and q_s. A stepwise calculation can be made for successive time increments to determine vaporization rates and the total quantity vaporized at any time.

Equation 13, which gives the heat transferred from the solid to the propane, is based on the assumption that the solid surface is smooth and flat. In many practical cases of interest, the surface will be covered by rocks or gravel, and the propane will vaporize rapidly until the

rocks or gravel cool. The additional heat transfer to the propane can be estimated if the rocks are small enough that they can be assumed to be at a uniform temperature as they cool following the propane spill. The uniform rock temperature is

$$\frac{T_r - T_p}{T_o - T_p} = \exp -\left(\frac{h_r A_r t}{M_r C_r}\right)$$

where h_r = convective coefficient between rocks and propane

A_r = total surface area of rocks

M_r = total mass of rocks

C_r = specific heat of rocks

The value of A_r depends on both the size and shape of the rocks and the total mass of the rocks. If the rocks are all the same shape, and uniform in size, the ratio A_r/M_r is an inverse function of rock size. If typical rock dimensions are on the order of a centimeter or two, h_r is reasonably independent of rock size and is about the same magnitude as h (for convective transfer between pit bottom and propane).

RESULTS

Figure 2 shows the result for two typical tests, in this case, spills of propane into a 5-ft^2 perlite concrete pit. In Test P-15, about 40 lb of propane was poured into the pit, which was uncovered and exposed to both sun and wind. After about 15 minutes, the vaporization rate becomes relatively constant until the propane has entirely vaporized. During this constant rate vaporization period, the liquid in the pit is subcooled, reaching a temperature of $-82^{\circ}F$. In Test P-54, about 30 lb of propane was poured into the same perlite concrete pit. However in Test P-54 the pit was covered with a polystyrene foam lid that precluded both wind and solar radiation from reaching the propane. The vaporization rate was lower for Test P-54, and only about 15 lb vaporized in the hour the test was run, compared to a total vaporization of about 40 lb for Test P-15. The lid used in Test P-54 prevented vaporization caused by non-equilibrium between the pool and the vapor above it, so the pool did not subcool. The liquid temperature after an hour of vaporization remained at the boiling point of propane.

Similar tests were run using gravel mix concrete, sand mix concrete, vermiculite concrete, clay soil, sandy soil, polyethylene foam, polystyrene foam, plywood, sod, sand, asphalt, and potting soil as the substrate materials. In a few tests granite chips or marble chips were placed on

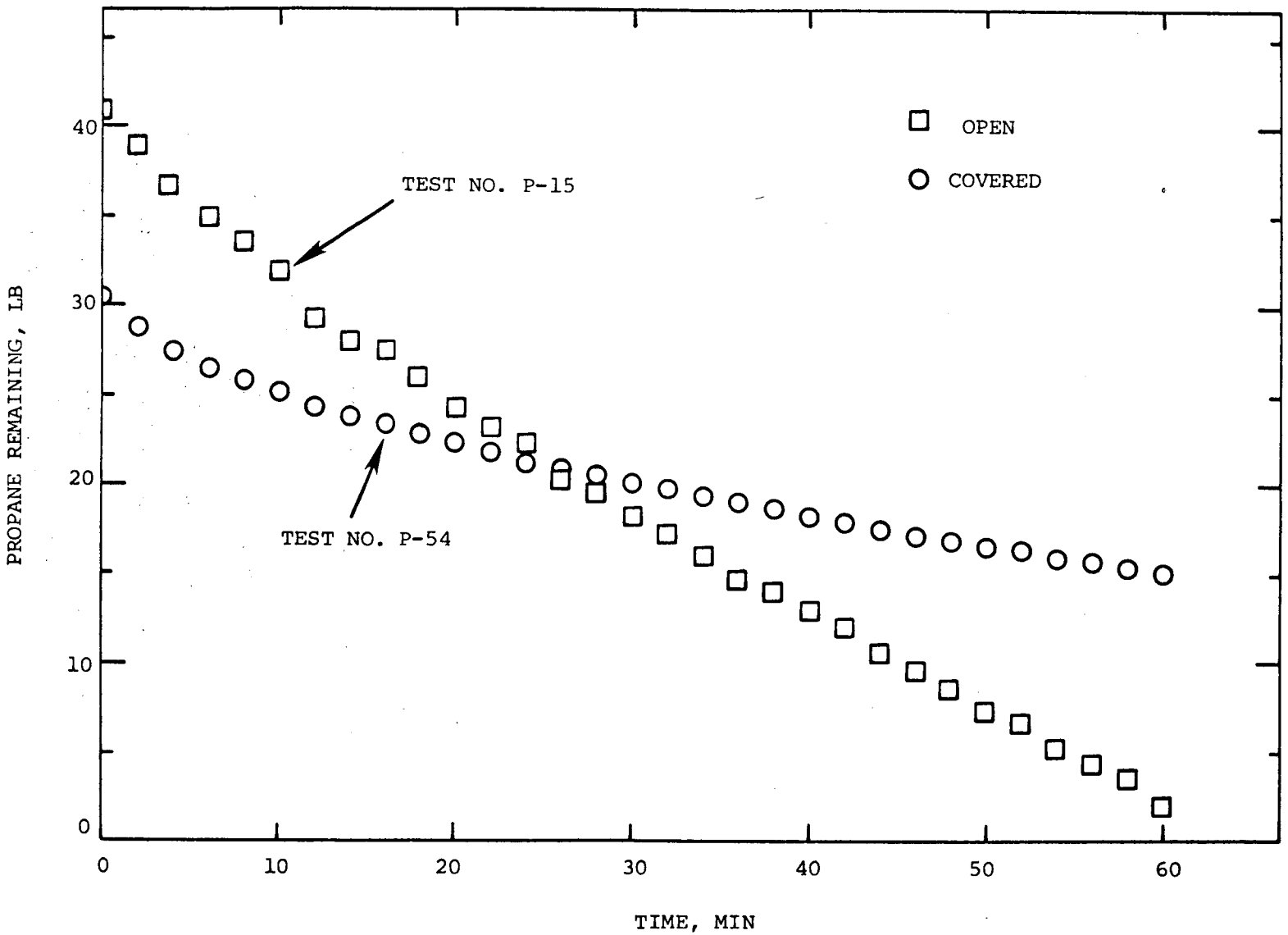

Figure 2. Weight of Propane Remaining After Spill into Perlite Concrete Pit.

the substrate surface to investigate the effects of rock coverings.

Table 1 is a summary of the results of the spill tests, giving the initial conditions, the measured thermal properties, and the steady state vaporization rate where tests were uncovered and steady vaporization rates were achieved. Table 2 is a key to the substrate abbreviations used in Table 1 and includes substrate density and heat capacity. Figures A-1 through A-79 in the Appendix are plots showing the weight of propane remaining in the test pit at any time following the spill. Test durations varied as shown in the figures and Table 1.

Ambient temperature, initial substrate temperature, propane temperature, wind speed, and solar radiation flux were measured for most tests. Summaries of the measured values are included in Table 1. In some tests the substrate temperatures were measured at various depths below the surface. Figure 3 shows the measured substrate temperatures for test P-54.

Figure 4 is the results for a test in which propane was poured onto granite chips over a perlite concrete substrate. The vaporization rate is very rapid at the start of the test, so rapid in fact that the propane was difficult to pour because of the relatively high velocity of propane vapor leaving through the pouring spout in the pit cover. By the time the pouring was complete, the granite chips,

TABLE 1. DATA FOR SPILLS OF LPG ON VARIOUS SUBSTRATES

TEST ID	PIT SIZE (SQ-FT)	TEST LENGTH (MIN)	TEMPERATURE AIR (°F)	TEMPERATURE PIT (°F)	TEMPERATURE INIT. LIQ (°F)	TEMPERATURE STEADY STATE (°F)	AVERAGE WIND SPEED (MPH)	AVERAGE SOLAR RADIATION BTU/HR-SQ-FT	STEADY STATE BOILOFF RATE LB/SEC-SQ-FT	CALCULATED THERMAL CONDUCTIVITY BTU/HR-FT-°F	BOILING HEAT TRANSFER COEFFICIENT BTU/HR-SQ-FT-°F
CG-1	5	32	86	80	-50	-55	2.8	255	0.00238	2.5-B	45
CG-3	5	44	82	78	-51	-65	5.9	150	0.00265	2.8-B	55
CG-4	5	50	85	78	-48	-48	2.7	180	0.00253	4.0-B	85
CS1-5	5	43	80	87	-50	-66	10.2	201	0.00296	3.0-B	70
CS1-7	5	54	75	82	-55	-63	5.4	184	0.00225	3.6-B	50
CS1-8	5	68	66	48	-60	-72	6.0	173	0.00208	3.8-B	60
CS1-23	5	18	66	60	-45	NA	COVERED	COVERED	0.00410-A	7.4	150
CS1-24	5	20	54	41	-45	NA	COVERED	COVERED	0.00173-A	3.6	100
CS1-26	5	14	58	30	-45	NA	8.7	141	0.00280	3.6-B	100
CS1-27	5	8	48	33	-45	NA	3.3	89	0.00333	4.0-B	100
CS1-29	5	10	62	45	-45	NA	4.9	118	0.00327	4.8-B	120
CS1-30	5	12	56	48	-45	NA	6.1	133	0.00346	4.5-B	100
CS2-33	5	11	65	62	-45	NA	2.0*	2**	0.00306	3.5-B	55
CS2-34	5	18	50	46	-45	NA	COVERED	COVERED	0.00191-A	3.7	65
CS2-36	5	15	57	26	-45	-45	COVERED	COVERED	0.00204-A	5.4	100
CS2-37	5	52	52	42	-45	-60	3.6	179	0.00176	4.6-B	55
CS2-47	5	17	78	66	-48	NA	COVERED	COVERED	0.00218-A	3.6	65
CS2-50	5	50	78	70	-50	NA	COVERED	COVERED	0.00235-A	4.7	45
CS2-75	5	30	91	90	-45	NA	COVERED	COVERED	0.00236-A	4.1	50

* - Estimated (pit was sheltered)

** - Pit was shaded from sun

NA - Not applicable

A - Long-term boiloff rate

B - determined by correcting for solar and atmospheric fluxes; see text

TABLE 1. DATA FOR SPILLS OF LPG ON VARIOUS SUBSTRATES--Continued

TEST ID	PIT SIZE (SQ-FT)	TEST LENGTH (MIN)	TEMPERATURE AIR (°F)	TEMPERATURE PIT (°F)	TEMPERATURE INIT. LIQ (°F)	TEMPERATURE STEADY STATE (°F)	AVERAGE WIND SPEED (MPH)	AVERAGE SOLAR RADIATION BTU/HR-SQ-FT	STEADY STATE BOILOFF RATE LB/SEC-SQ-FT	CALCULATED THERMAL CONDUCTIVITY BTU/HR-FT-°F	BOILING HEAT TRANSFER COEFFICIENT BTU/HR-SQ-FT-°F
P-14	5	78	75	82	-60	-82	8.1	153	0.00153	0.85-B	50
P-15	5	62	72	72	-67	-80	11.4	177	0.00180	0.90-B	45
P-38	5	14	64	47	-45	NA	COVERED	COVERED	0.00085-A	0.72	38
P-39	5	23	64	-25	-45	-60	2.2	172	0.00100	NA	NA
P-42	5	25	55	45	-48	NA	COVERED	COVERED	0.00082-A	0.84	40
P-48	5	60	59	62	-50	NA	COVERED	COVERED	0.00094-A	0.80	20
P-54	5	60	74	70	-45	NA	COVERED	COVERED	0.00085-A	0.94	20
P-73	5	55	92	95	-45	-55	2.1	246	0.00139	0.80-B	45
P-74	5	90	84	86	-45	NA	COVERED	COVERED	0.00059-A	0.96	25
V-12	5	60	65	65	-60	-76	6.7	183	0.00148	2.0-B	50
V-13	5	60	70	57	-62	-62	5.8	200	0.00160	2.0-B	30
V-32	5	10	55	55	-50	NA	14.0	125	0.00233	1.0-B	25
V-40	5	40	61	47	-45	NA	COVERED	COVERED	0.00157-A	0.72	35
V-41	5	31	61	38	-45	NA	COVERED	COVERED	0.00071-A	0.86	25
V-49	5	61	68	65	-50	NA	COVERED	COVERED	0.00087-A	0.89	20
V-83	5	30	91	85	-50	NA	COVERED	COVERED	0.00095-A	1.0	30

NA - Not applicable

A - Long-term boiloff rate

B - Determined by correcting for solar and atmospheric fluxes; see text

TABLE 1. DATA FOR SPILLS OF LPG ON VARIOUS SUBSTRATES--Continued

TEST ID	PIT SIZE (SQ-FT)	TEST LENGTH (MIN)	TEMPERATURE AIR (°F)	TEMPERATURE PIT (°F)	TEMPERATURE INIT. LIQ (°F)	TEMPERATURE STEADY STATE (°F)	AVERAGE WIND SPEED (MPH)	AVERAGE SOLAR RADIATION BTU/HR-SQ-FT	STEADY STATE BOILOFF RATE LB/SEC-SQ-FT	CALCULATED THERMAL CONDUCTIVITY BTU/HR-FT-°F	BOILING HEAT TRANSFER COEFFICIENT BTU/HR-SQ-FT-°F
CL1-20	5	57	45	48	-58	-85	10.7	87	0.00175	NA	NA
CL1-21	5	64	38	30	-63	-85	13.7	187	0.00223	NA	NA
CL2-57	5	60	76	65	-62	NA	COVERED	COVERED	0.00178-A	3.4	100
CL2-58	5	50	67	55	-50	-45	1.5	113	0.00170	2.8-B	65
CL2-59	5	40	84	80	-50	NA	COVERED	COVERED	0.00187-A	3.5	60
CL2-64	5	60	90	82	-45	NA	COVERED	COVERED	0.00121-A	3.2	50
CL2-65	5	40	80	61	-48	-53	0.9	192	0.00198	3.5-B	95
SS1-51	5	31	80	78	-48	NA	COVERED	COVERED	0.00215-A	NA	NA
SS1-52	5	16	81	78	-45	-45	2.0*	195	0.00161	NA	NA
SS1-53	5	40	78	85	-45	NA	COVERED	COVERED	0.00152-A	NA	NA
SS2-61	5	40	80	67	-46	NA	COVERED	COVERED	0.00275-A	NA	NA
SS2-62	5	30	84	77	-47	NA	COVERED	COVERED	0.00290-A	NA	NA
SS2-67	5	35	85	82	-45	-55	2.1	242	0.00287	NA	NA
PTS-19	5	48	58	53	-48	-45	3.8	137	0.02150	NA	NA

* - Estimated (pit was sheltered from wind)

NA - Not applicable

A - Long-term boiloff rate

B - Determined by correcting for solar and atmospheric fluxes; see text

TABLE 1. DATA FOR SPILLS OF LPG ON VARIOUS SUBSTRATES--Continued

TEST ID	PIT SIZE (SQ-FT)	TEST LENGTH (MIN)	TEMPERATURE AIR (°F)	TEMPERATURE PIT (°F)	TEMPERATURE INIT. LIQ (°F)	TEMPERATURE STEADY STATE (°F)	AVERAGE WIND SPEED (MPH)	AVERAGE SOLAR RADIATION BTU/HR-SQ-FT	STEADY STATE BOILOFF RATE LB/SEC-SQ-FT	CALCULATED THERMAL CONDUCTIVITY BTU/HR-FT-°F	BOILING HEAT TRANSFER COEFFICIENT BTU/HR-SQ-FT-°F
PE-44	5	35	64	73	-45	NA	COVERED	COVERED	0.00019-A	C	20
PE-45	5	167	78	78	-50	NA	COVERED	COVERED	0.00027-A	C	2
PE-46	5	40	80	-20	-64	-82	1.0*	180	0.00062	NA	NA
PS-9	5	103	74	82	-73	-94	8.5	202	0.00095	NA	NA
PS-10	5	60	70	75	-73	-100	12.8	75	0.00133	NA	NA
PS-11	5	62	48	46	-86	-92	7.9	205	0.00067	NA	NA
PS-56A	5	125	73	70	-68	NA	COVERED	COVERED	0.00006-A	C	5
PS-56B	5	60	73	-40	-62	-80	2.0*	144	0.00039	NA	NA
PS-89	5	10	58	54	-52	-68	0.5*	0.3**	0.00033	NA	NA
PL-60	4	120	78	74	-47	NA	COVERED	COVERED	0.00028-A	C	20
PL-63	4	120	84	80	-46	NA	COVERED	COVERED	0.00029-A	C	45
PL-68	4	90	88	86	-45	-72	1.9	267	0.00089	0.07-B	NA

* - Estimated (pit was sheltered from wind)

** - Pit was shaded from sun

NA - Not applicable

A - Long-term boiloff rate

B - Determined by correcting for solar and atmospheric fluxes; see text

C - Thermal conductivity could not be determined for low thermal conductivity substrates in covered tests.

TABLE 1. DATA FOR SPILLS OF LPG ON VARIOUS SUBSTRATES--Continued

TEST ID	PIT SIZE (SQ-FT)	TEST LENGTH (MIN)	TEMPERATURE AIR (°F)	TEMPERATURE PIT (°F)	TEMPERATURE INIT. LIQ (°F)	TEMPERATURE STEADY STATE (°F)	AVERAGE WIND SPEED (MPH)	AVERAGE SOLAR RADIATION BTU/HR-SQ-FT	STEADY STATE BOILOFF RATE LB/SEC-SQ-FT	CALCULATED THERMAL CONDUCTIVITY BTU/HR-FT-°F	BOILING HEAT TRANSFER COEFFICIENT BTU/HR-SQ-FT-°F
SOD-66	5	30	86	75	-45	-45	COVERED	COVERED	0.00087-A	NA	NA
SOD-69	5	20	82	79	-45	-48	1.7	187	0.00394	NA	NA
SOD-70	5	20	84	74	-45	-48	2.0*	178	0.00349	NA	NA
SOD-71	5	20	96	81	-45	-45	0.8	223	0.00406	NA	NA
SAND-17	5	52	57	57	-45	-45	4.0	153	0.00150	NA	NA
A-43	1	20	71	73	-45	NA	COVERED	COVERED	0.00157-A	2.5	95
CS/GR-76	5	30	81	86	-49	NA	COVERED	COVERED	0.00247-A	4.3	NA
P/GR-77	5	45	82	80	-45	NA	COVERED	COVERED	0.00100-A	1.1	NA
P/GR-78	5	40	96	86	-50	NA	COVERED	COVERED	0.00084-A	0.93	NA
CS/GR-79	5	30	96	90	-45	NA	COVERED	COVERED	0.00191-A	3.8	NA
P/GR-80	5	30	81	81	-45	NA	COVERED	COVERED	0.00117-A	1.3	NA
PS/GR-81	5	30	82	88	-45	NA	COVERED	COVERED	0.00005-A	C	NA
P/GR-82	5	30	90	82	-45	NA	COVERED	COVERED	0.00138-A	1.20	NA
V/GR-84	5	30	77	71	-48	NA	COVERED	COVERED	0.00094-A	1.1	NA
V/MB-85	5	20	82	70	-45	NA	COVERED	COVERED	0.00153-A	1.8	NA
V/MB-86	5	45	69	60	-45	-64	2.0*	0.5**	0.00132	NA	NA
V/MB-87	5	10	71	56	-50	NA	2.0*	1.6**	0.00123	NA	NA
V/MB-88	5	40	59	52	-45	-65	1.7	0.5**	0.00139	NA	NA
PS/MB-90	5	10	58	54	-45	NA	0.5*	0.4**	0.00018	NA	NA

* - Estimated (pit was sheltered from wind)

** - Pit was shaded from sun

NA - Not applicable

A - Long-term boiloff rate

B - Determined by correcting for solar and atmospheric fluxes; see text

C - Thermal conductivity could not be determined for low thermal conductivity substrates in covered tests.

TABLE 2. SUBSTRATE IDENTIFICATION

PIT ID	SUBSTRATE	DENSITY (LB/FT^3)	HEAT CAPACITY ($BTU/LB-^oF$)
CG	Gravel mix concrete	135	0.20
CS1	First sand mix concrete	135	0.20
CS2	Second sand mix concrete	135	0.20
P	Perlite concrete	83	0.24
V	Vermiculite concrete	77	0.25
CL1	First clay/soil	109	0.21
CL2	Second clay/soil	109	0.21
SS1	First sand/soil	95	0.19
SS2	Second sand/soil	103	0.20
PE	Polyethylene foam	2.4	0.40
PS	Polystyrene foam	0.95	0.27
PL	Plywood (fir)	30	0.65
SOD	Bermuda sod	103 *	0.20
SAND	Sand	106	0.19
A	Asphalt	144	0.20
GR	Granite chips	165	0.195
MB	Marble chips	162	0.193
PTS	Potting soil	39	0.22

* - Second sand/soil base

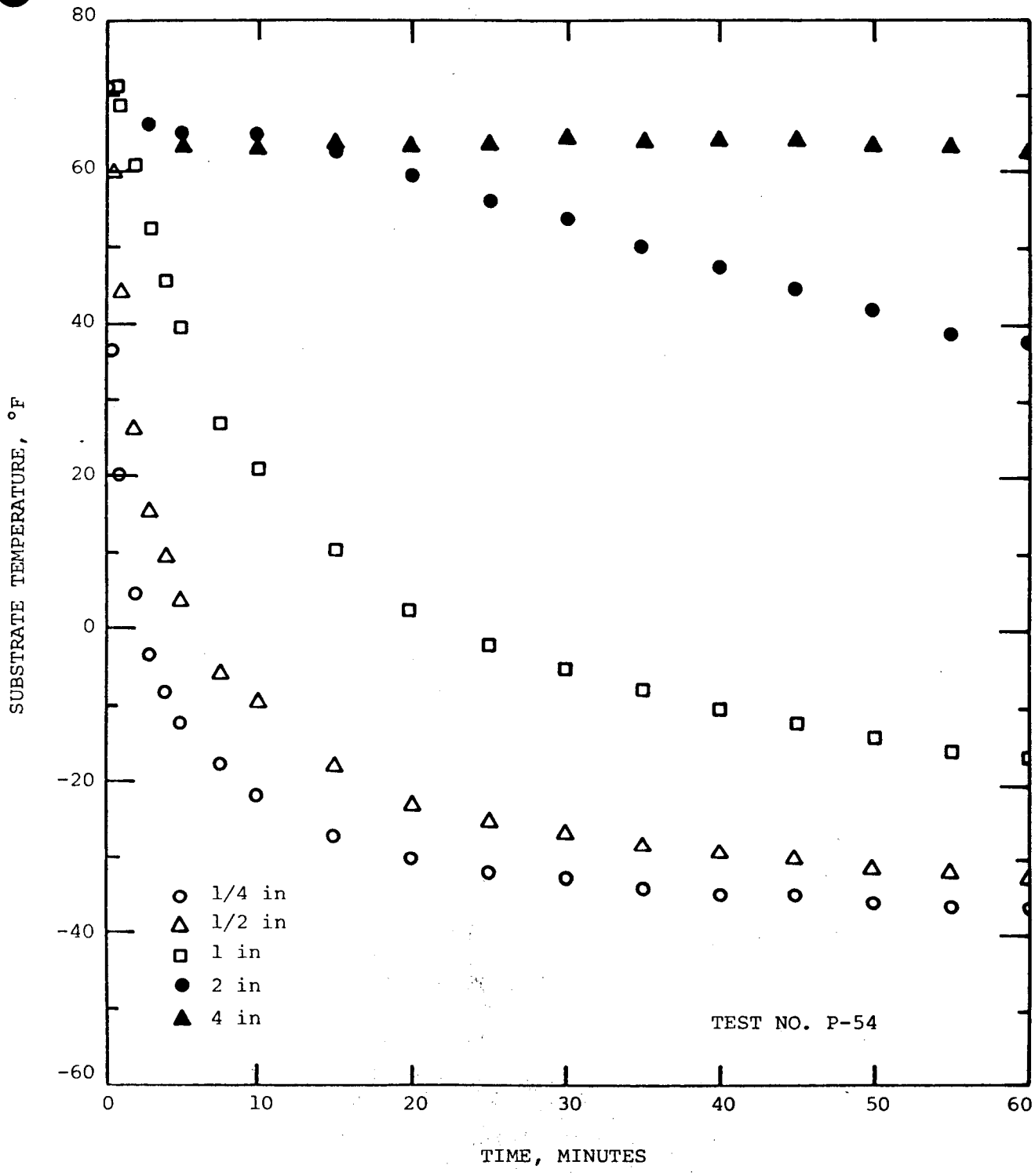

Figure 3. Substrate Temperature Profiles for Perlite Concrete.

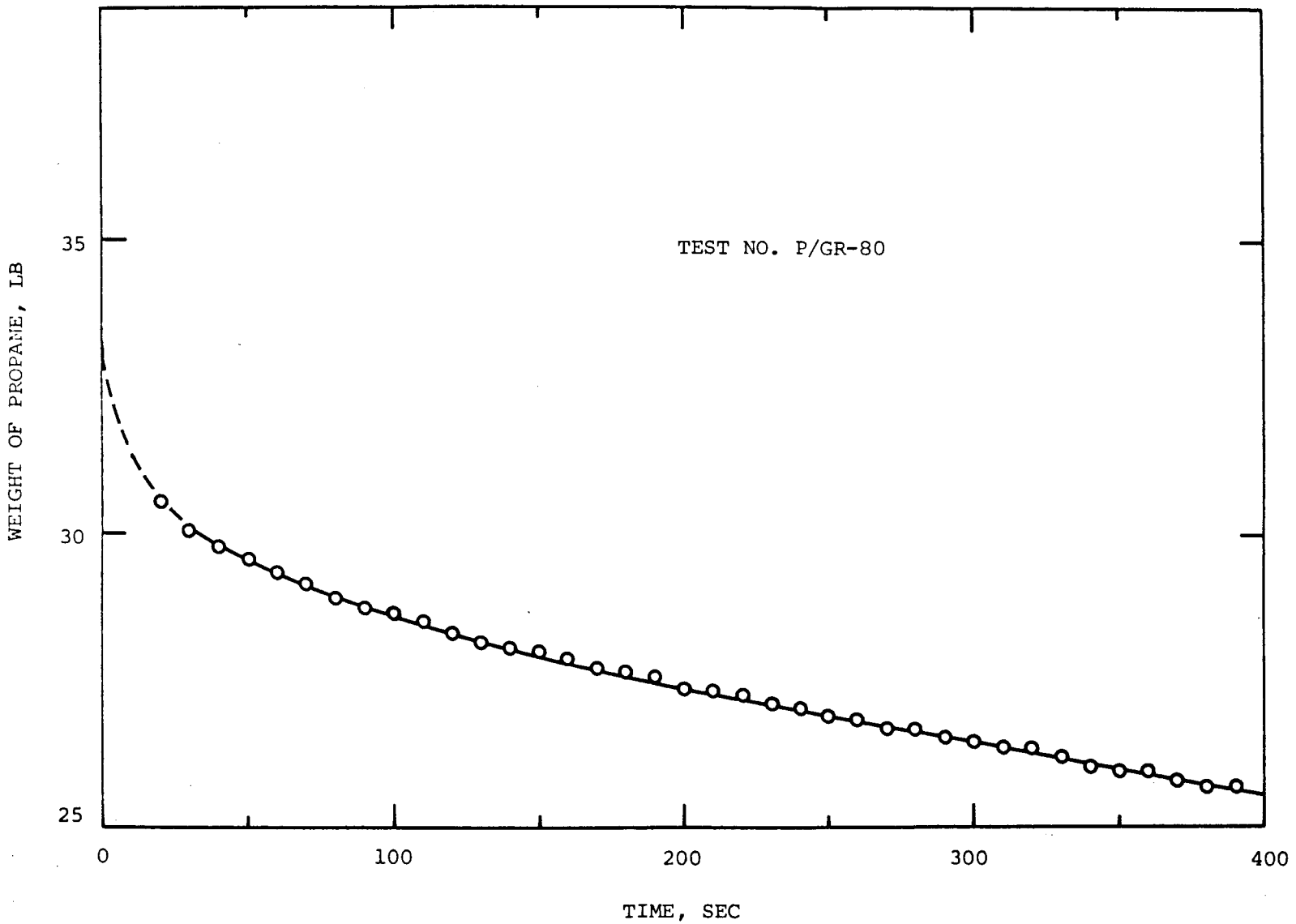

Figure 4. Weight Remaining Following Spill of Propane into Perlite Concrete Pit Containing Granite Chips.

which were about 0.15 inches in nominal size, were cooled to nearly liquid propane temperature. This very rapid boiling made it difficult to measure the initial weight of propane, because the granite chips cooled before all the propane was poured. Similar problems were encountered in tests using larger marble chips.

DISCUSSION OF RESULTS

The vaporization data shown in Figures A-1 through A-79 in the Appendix can be used in conjunction with the vaporization rate models to determine some of the effective values of heat transfer parameters required to predict vaporization rates for refrigerated propane if it is spilled on a solid surface. It should be kept in mind that if propane is spilled from ambient temperature, pressurized containers, a substantial fraction will flash to vapor immediately and an additional fraction will atomize. In fact, during these propane spill tests, careful effort was required to assure that liquid samples could be withdrawn from ambient temperature storage.

Figure 2 shows the vaporization rate for propane spilled on a solid substrate. In the test where the liquid pool was covered, vaporization was caused primarily by heat transfer by conduction through the substrate to the liquid. Equation 9 or Equation 13 can be used at long times after the spill to determine some of the thermal properties. In

these tests, the quantity of propane evaporated was measured, so Equation 13 and its long time approximation given by Equation 14 were used to estimate heat transfer parameters.

Equation 14 shows that if the values of k, ρ, c, and T_p remain constant, the total quantity of heat transferred from substrate to pool is

$$Q_c = A\sqrt{t} \tag{25}$$

The total mass of propane boiled is then

$$M = \frac{A}{\Delta H_v}\sqrt{t} \tag{26}$$

or

$$M = S\sqrt{t} \tag{27}$$

where

$$S = \frac{2\sqrt{k\rho c}(T_o - T_p)}{\sqrt{\pi}\,\Delta H_v} \tag{28}$$

and S is the slope of the line obtained by plotting M versus t. Figure 5 shows such a plot for Test No. P-54. The slope of the linear portion of the curve is 0.05 $lb/ft^2\text{-}sec^{1/2}$.

The density of perlite concrete used in the tests was 83 lb/ft^3, obtained by direct weighing and a volume

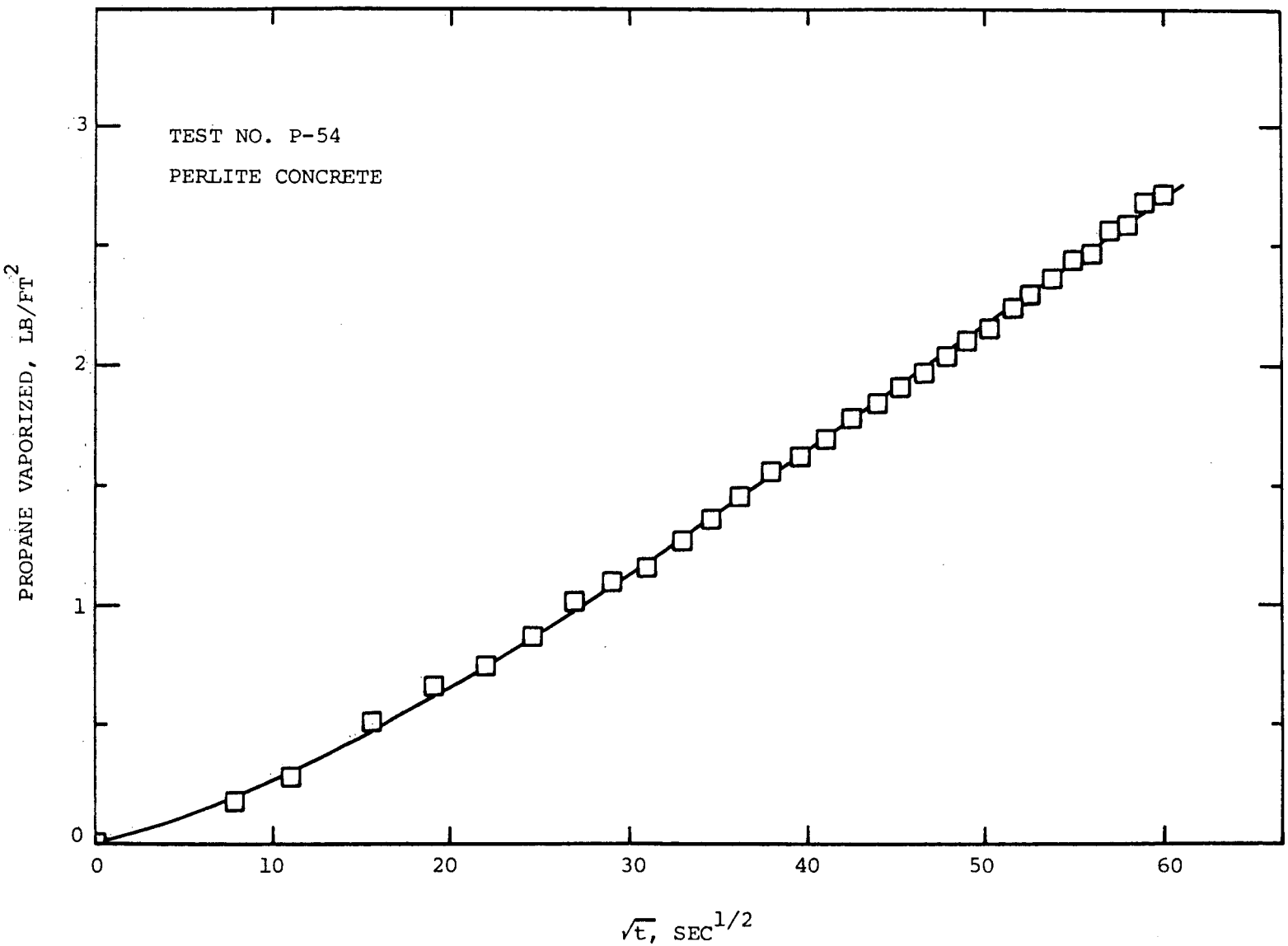

Figure 5. Weight of Propane Vaporized, Plotted Versus $\sqrt{t}$.

measured by displacement. Specific heat of perlite concrete was measured to be 0.24 Btu/lb-^{o}F. Using the initial substrate temperature of 70^{o}F and the propane boiling temperature of -45^{o}F, the effective thermal conductivity of perlite concrete was found to be 0.94 Btu/hr-ft-^{o}F.

Once the thermal conductivity has been determined from the long term vaporization data, the covective heat transfer coefficient between the substrate and the liquid can be determined by assuming a value for h and calculating the vaporization curve. The calculated curve will be parallel to the measured data points at long times, but will coincide with the measured data points only if the proper effective value for h is chosen. Figure 6 shows a comparison of calculated and measured vaporization results for Test No. P-54. The line drawn through the data points in Figure 6 was calculated using k = 0.94 Btu/hr-ft-^{o}F and h = 20 Btu/hr-ft^{2}-^{o}F, as reported in Table 1.

If a test does not run long enough for a linear relationship to develop between M and $\sqrt{t}$, the values for h and k can be approximated by fitting the curve of M versus t.

Vaporization curves calculated from the assumed values of k and h are relatively sensitive to the input values. Figure 7 shows calculated curves where k is varied by 20 percent from the effective value, using the effective value of h, and Figure 8 shows calculate curves where the

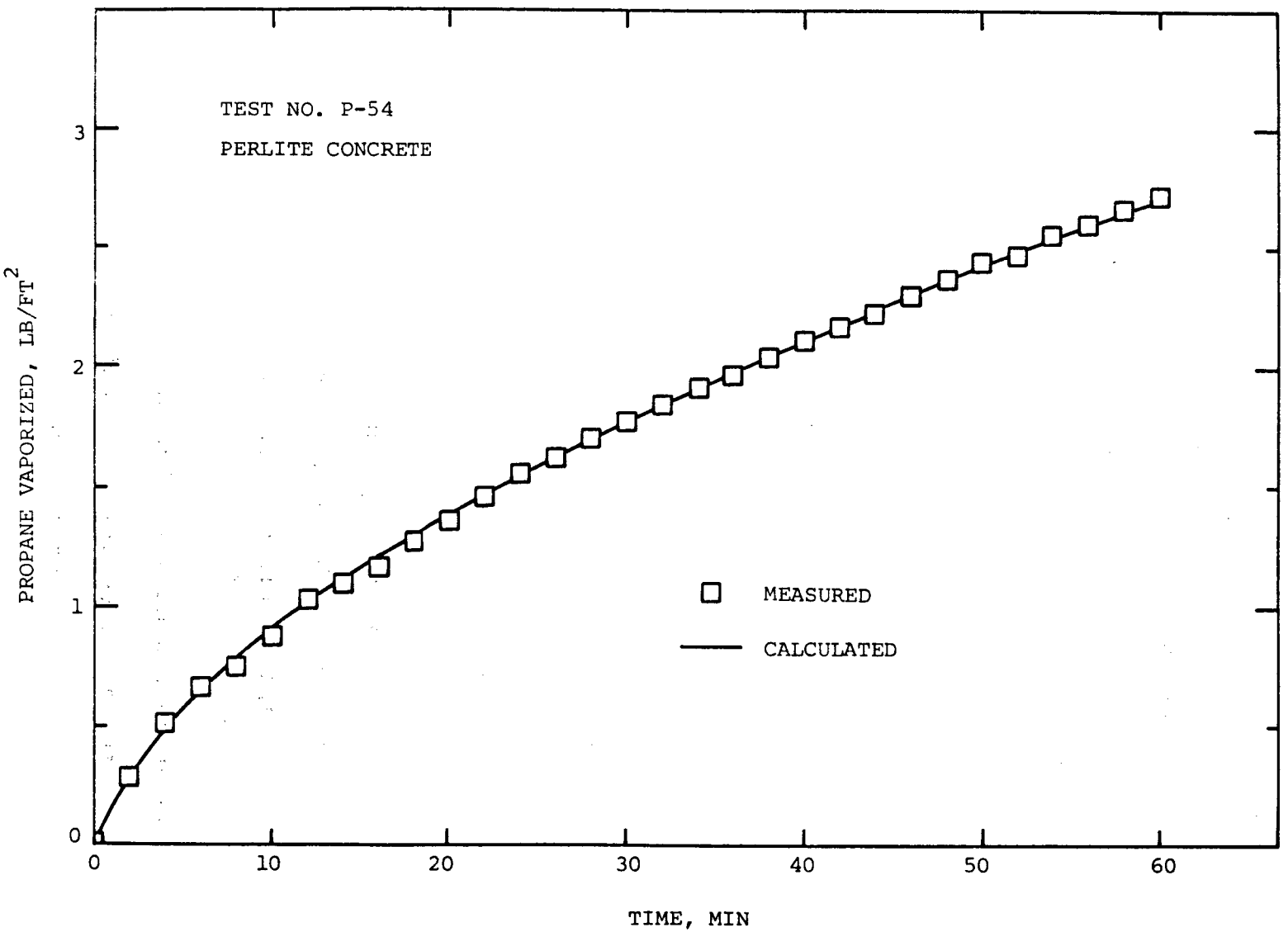

Figure 6. Comparison of Measured and Calculated Weight of Propane Vaporized for Test No. P-54.

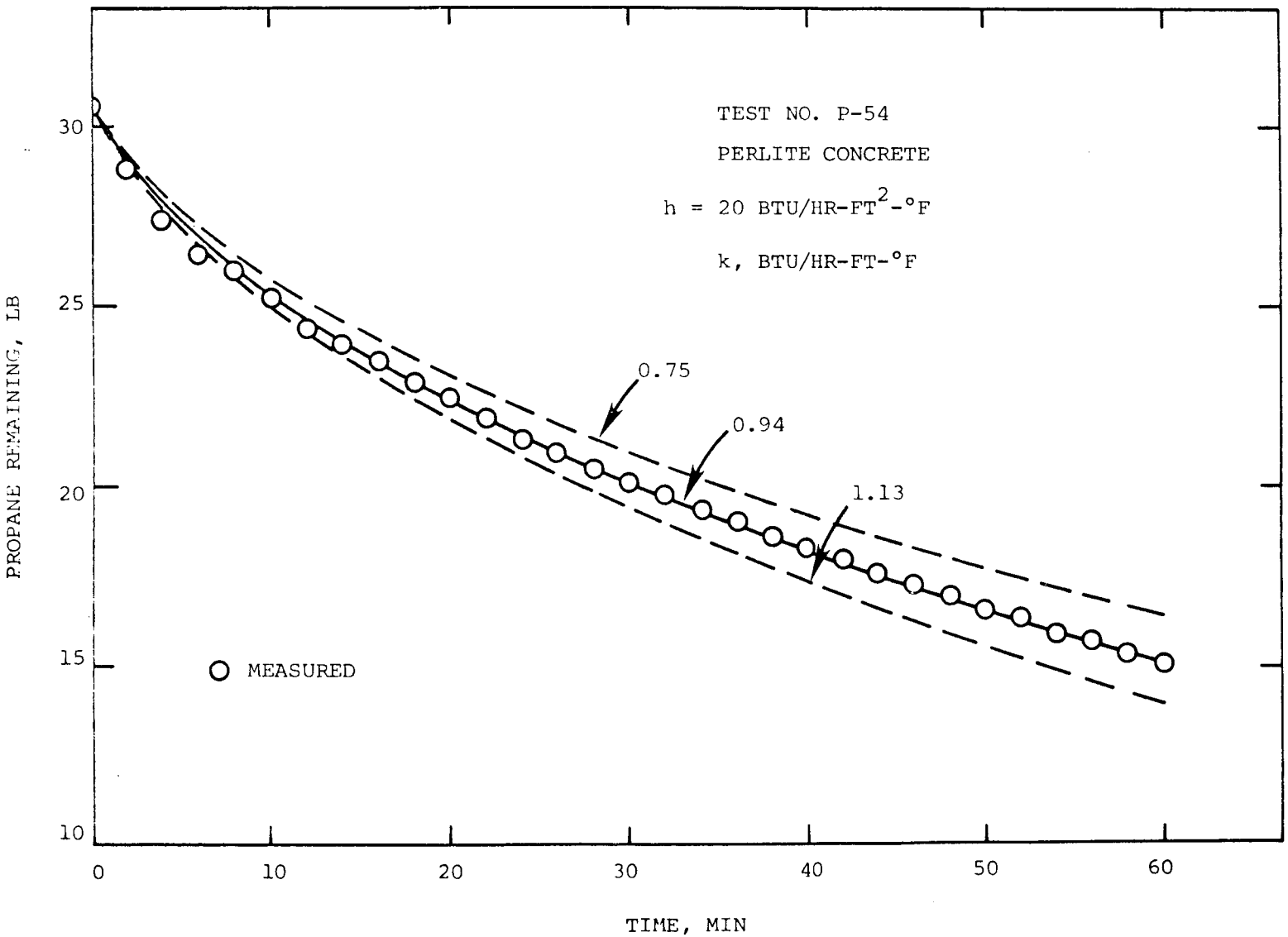

Figure 7. Effect of Thermal Conductivity on Calculated Vaporization.

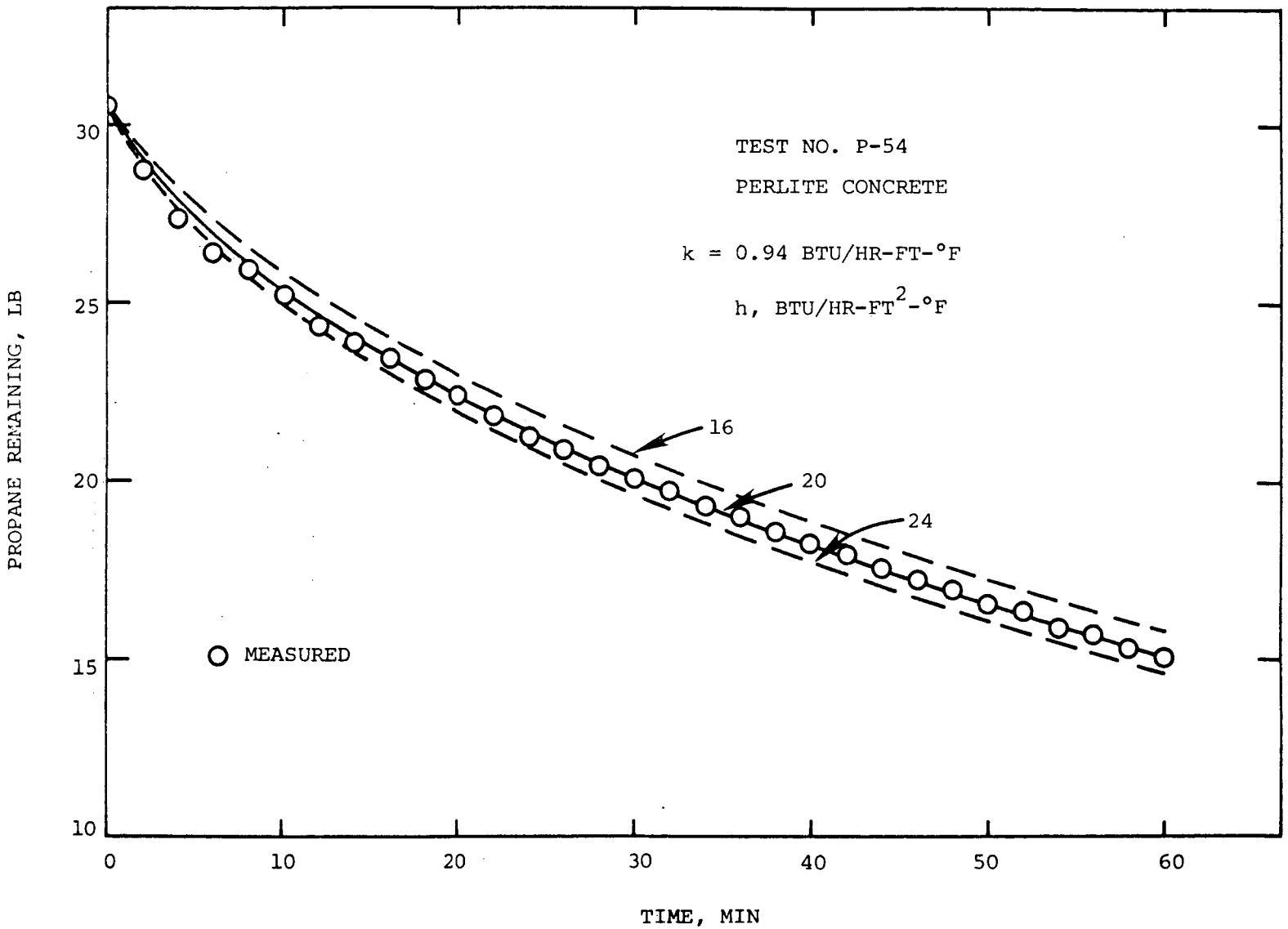

Figure 8. Effect of Heat Transfer Coefficient on Calculated Vaporization.

value of h is varied by 20 percent using a constant value of k. In Figure 7, varying the value chosen for k causes changes in the slope of the curve; so it can be inferred that the thermal conductivity is incorrect. In most cases, k was determined from the slope of the curve in a plot of M versus $\sqrt{t}$, so trial and error solutions for k were not required. If, as shown in Figure 8, the slopes of the calculated line and the data line are the same, but the magnitude differs by an approximately constant amount, adjustments in the value selected for h are required.

There were several tests for which the thermal conductivity could not be determined by the procedure discussed above. In tests such as P-15, for which vaporization data are shown in Figure 2, the cover was not placed over the pit, and the vaporization included effects of heat transfer from atmospheric convection, solar radiation, and self-cooling of the liquid propane. In a few such cases, the thermal conductivity and solid-to-liquid heat transfer coefficient were estimated by recourse to the heat transfer model that included all the effects present. The values of k and h determined were about the same as those found for the covered tests, so not all of the uncovered tests were analyzed.

The effective values for k and h are included in Table 1 for all the tests where they could be determined. Table 3 is a summary of the best values for each material.

TABLE 3. HEAT TRANSFER PROPERTIES FOR SOLID SUBSTRATES

Material	h Btu/hr-ft^2-°F	k Btu/hr-ft-°F		Reference
		Exp	Lit.	
Gravel concrete	50	2.7	2	Lentz and Monfore (1965)
Sand concrete	100	4.0		
Perlite concrete	30	0.9	0.2	Eshbach (1975)
Vermiculite concrete	30	0.9	0.2	Eshbach (1975)
Clay soil	70	3.5	3-4	Reid (1980)
Asphalt	95	2.5		

The effective value of k is compared with values for the same or similar materials from literature sources.

The thermal conductivities measured from the covered vaporization rate tests are generally higher than those reported in the literature for similar materials. Similar behavior is shown in the data of Reid (1980), where thermal conductivities of polystyrene foam were found to be in the range of 0.06 Btu/hr-ft-^{o}F, when the vaporizing liquid was LNG. That value is about 3 times the value stated by foam manufacturers for temperatures near 60 to 80^{o}F. Since thermal conductivities for foamed insulation decrease as the temperature decreases, the actual difference is greater than is immediately apparent. Reid also measured higher thermal conductivity for solid polyethylene than reported in the literature. The reason for the high thermal conductivities is not readily apparent. However, the values shown in Table 3 do represent data that are required for predicting vaporization rates for propane spills.

The heat transfer coefficients given in Table 3 are in the range to be expected, based on the work of Sciance (1966). The variability among the various substrates is probably due partly to differences in material surfaces, but may be due to the range of average temperature differences between propane and the substrate. Sciance showed that the transition region between nucleate and film boiling occurred over temperature differences of about 30 to 200^{o}F for

propane. The vaporization data used to determine heat transfer coefficients were largely in the transition region, so some differences could be expected. The values given in Table 3 should enable relatively good vaporization rate predictions to be made.

Figure 3 showed an example of the temperature profiles measured in the perlite concrete pit during Test No. P-54. The temperature near the surface decreased rapidly during the first few minutes, then decreased more slowly. The temperature 4 inches deep remained approximately constant throughout the test. It is possible to predict the temperature profiles for a solid substrate from Equation 16. Figure 9 shows the result of such calculations for Test No. P-54. The calculated temperatures, shown as solid lines, are higher than the measured temperatures at depths less than about an inch in the substrate, but lower than the measured temperatures at depths more than about an inch.

Similar plots were made for other tests; they showed poor comparisons between calculated and measured temperatures, especially for the insulating materials such as polyethylene foam and polystyrene foam. In the case of the concrete based materials, some of the deviation between measured temperatures and calculated temperatures may be due to the surface layer, which may have less vermiculite or perlite at the surface than in the bulk. However, there are

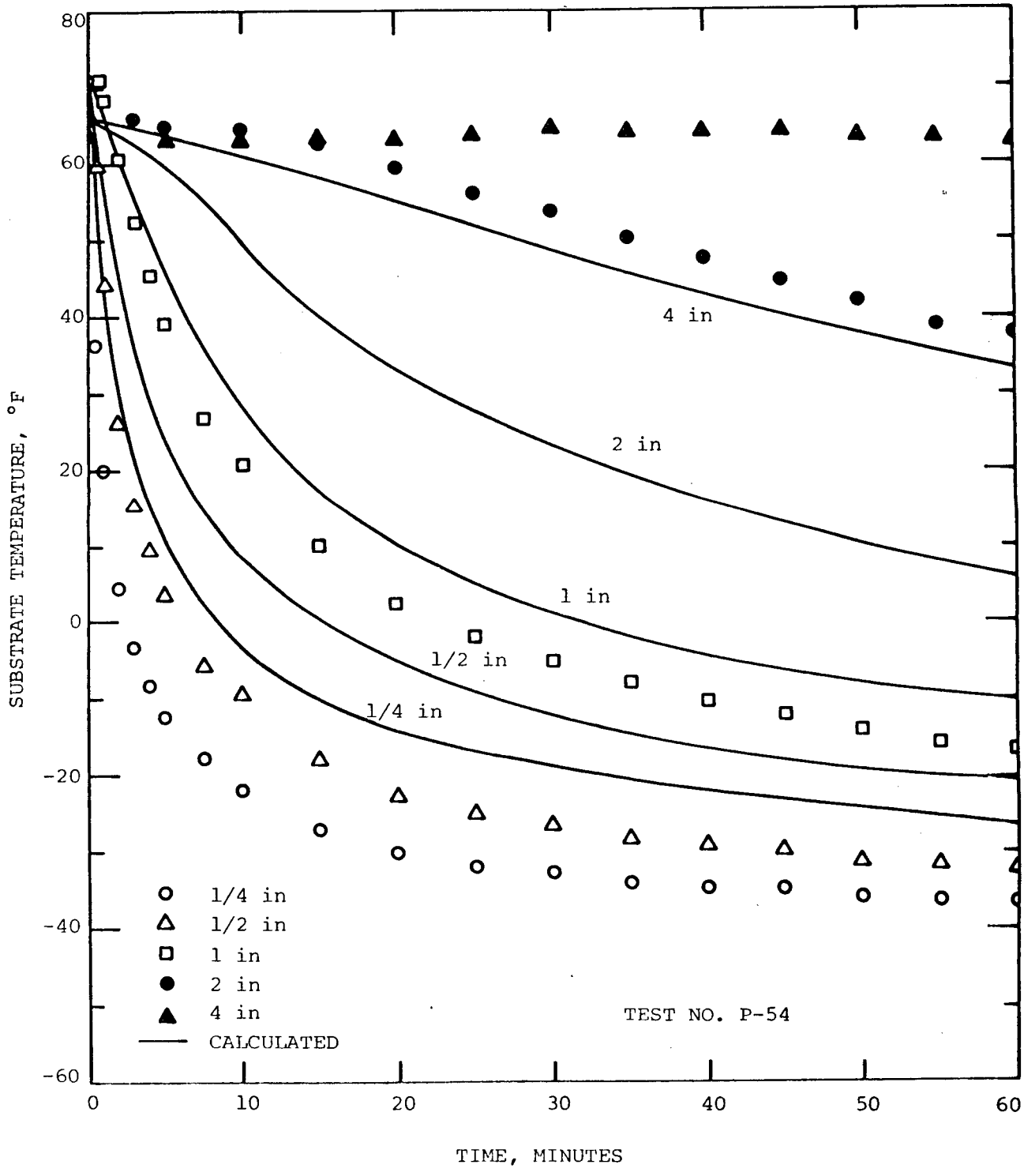

Figure 9. Comparison of Calculated and Measured Substrate Temperatures.

other non-consistent results in the data as well. For a given test pit, the ratio $(T - T_p)/(T_o - T_p)$ should be constant for a given time and depth in the pit, provided the pit properties remain constant from run to run. The temperature ratios did not remain constant from run to run, but there was no obvious reason for the changes.

Temperature profile plots could be drawn that fit the data at one or two depths but not at other depths. However, the thermal conductivities required for those calculations could differ from those found by considering the vaporization data.

The temperature profiles measured during the propane vaporization tests generally showed higher measured temperatures deep in the substrate than those predicted by Equation 6. That result implies that the thermal conductivity derived from the vaporization data is too large. However, near the surface of the substrate, the measured temperatures were lower than the calculated temperatures, which implies that the thermal conductivity derived from vaporization data is too low. In reality, the most likely explanation for the behavior is that the thermal conductivity varies with temperature, increasing as the temperature decreases. The vaporization tests provide an average thermal conductivity that is applicable for the temperature range of boiling or slightly subcooled liquid propane at atmospheric pressure. The thermal data are

therefore quite good for predicting vaporization rates, but less reliable for determining temperature profiles.

The mass transfer coefficient required for calculating vaporization rates for an open pool after boiling ceases and the liquid begins to subcool can be obtained from steady state vaporization measurements. Table 1 lists the steady state vaporization rates for the tests where the pit was uncovered and steady conditions were reached. The mass transfer coefficients were found for some of those tests. They were then used to determine the mass transfer factor defined by

$$j_m = \frac{k'_g}{G_m}\left(\frac{\mu_a}{\rho_a D}\right)^{2/3} \qquad (29)$$

where j_m = mass transfer factor

G_m = wind velocity in molar units

k'_g = mass transfer coefficient in molar units

μ_a = ambient air viscosity

ρ_a = ambient air density

D = diffusion coefficient

The mass transfer factor is determined primarily by the size of the vaporizing pool and the ambient wind velocity, combined in dimensionless form as a Reynolds number,

$$N_R = \frac{LG}{\mu_a} \qquad (30)$$

where N_R = Reynolds number

L = length (or diameter) of pool in downwind direction

G = wind velocity in mass units

Figure 10 is a plot of the mass transfer factors derived from propane vaporization data. Data are included for wind velocities from less than one mi/hr to nearly 15 mi/hr. The data points shown as open circles are for circular test pits about 2.5 ft in diameter. The pits were usually 4 inches deep, but in a few tests pits as deep as 8 inches were used. As part of a general series of propane fire extinguishment and control tests (Johnson, et al., 1980) several tests were run to measure the vaporization rates of propane in larger pits. Figure 10 includes the results of those tests as well. The large pit sizes and occasionally higher wind velocities during those tests resulted in higher Reynolds numbers, so the data extend over a range of Reynolds numbers spanning nearly two orders of magnitude. The pits 5, 10, and 20 ft square were all 2 ft deep and generally contained about 3 to 6 inches of propane during the tests. The results indicate that the amount of freeboard did not influence the vaporization rate strongly for these tests.

Three data points are included in Figure 10 from other steady state vaporization tests. Those vaporization rates were measured during a series of U. S. Coast Guard

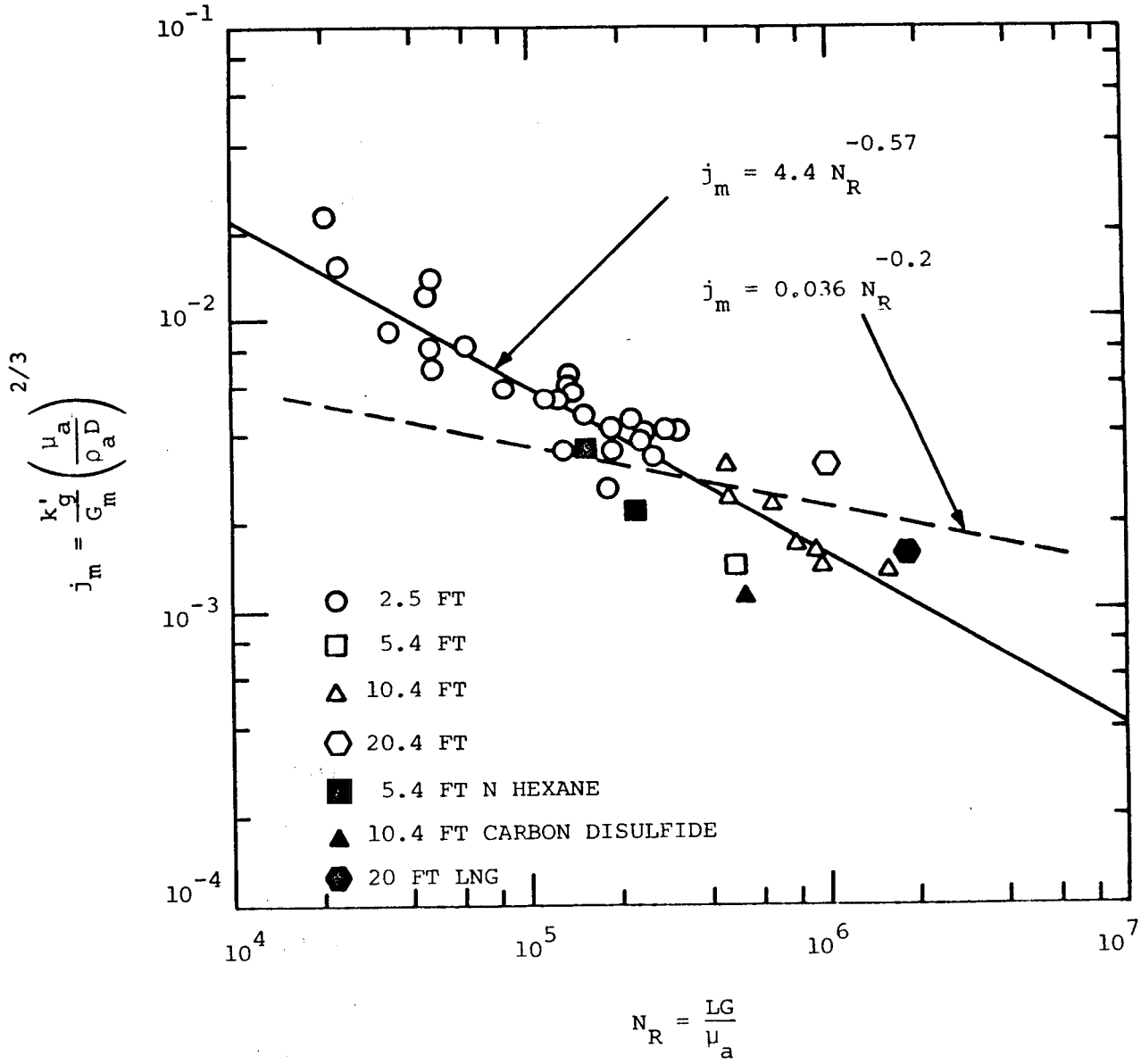

Figure 10. Mass Transfer Factors from Propane Vaporization.

fire fighting tests (Welker et al., 1980, Johnson et al., 1981). The two hexane data points were measured using the 5-ft square pit and the carbon disulfide point was taken during measurements on the 10-ft square pit. These points indicate that the mass transfer factor data measured for propane may be useful for other liquids as well. Some small amount of data are available for other liquids. Perry (1950) contains a brief summary of results from tests made mostly with water. Those data are represented by the equation

$$j_m = 0.036\ N_R^{-0.2} \qquad (31)$$

whereas the propane data fit the equation

$$j_m = 4.4\ N_R^{-0.57} \qquad (32)$$

Both lines are shown in Figure 10. For Reynolds numbers between 10^5 and 10^6, either equation passes through the propane data. However, the slope for the propane data is different from the data in Perry. The best procedure to follow in estimating vaporization rates is to use Equation 32, keeping in mind that extrapolation may lead to errors. The vaporization rates predicted by Equation 32 are in the same range as the steady state rates found for liquefied natural gas in tests where steady state rates were measured as about 0.02 in/min (about 8×10^{-4} lb/ft^2-sec) (AGA 1974).

The vaporization rate and pool temperature both change as the wind speed changes. The vaporization rate changes cannot be measured easily because the change is small when compared to the sensitivity of the measurement system. Pool temperature changes are more rapid. Figure 11 shows pool temperatures and wind velocity for a portion of Test No. P-9. There is a correlation between wind velocity and pool temperature, indicating the effect of wind velocity. The data in Test P-9 were taken during a period of nearly constant solar radiation. The changes in wind speed are relatively frequent, so the pool temperature changes are not large. The most noticeable changes occur between 1433 hours and 1436 hours, when wind speed decreases and pool temperature increases. The wind speed increase between 1436 and 1439 hours causes a decrease in pool temperature. About 1439 hours the pool temperature begins to rise as wind speed decreases, but a sudden drop in solar flux causes a drop in pool temperature.

Pool temperatures change more noticeably in response to changes in solar radiation. Figure 12 shows a plot of solar radiation and pool temperature for Test No. PE-46. The thermocouple measuring the pool temperature responds quickly to the changes in radiant flux. Both the pool thermocouple and the substrate surface may be at slightly higher temperatures than the liquid in the pool because radiant heat is absorbed more effectively by the solid

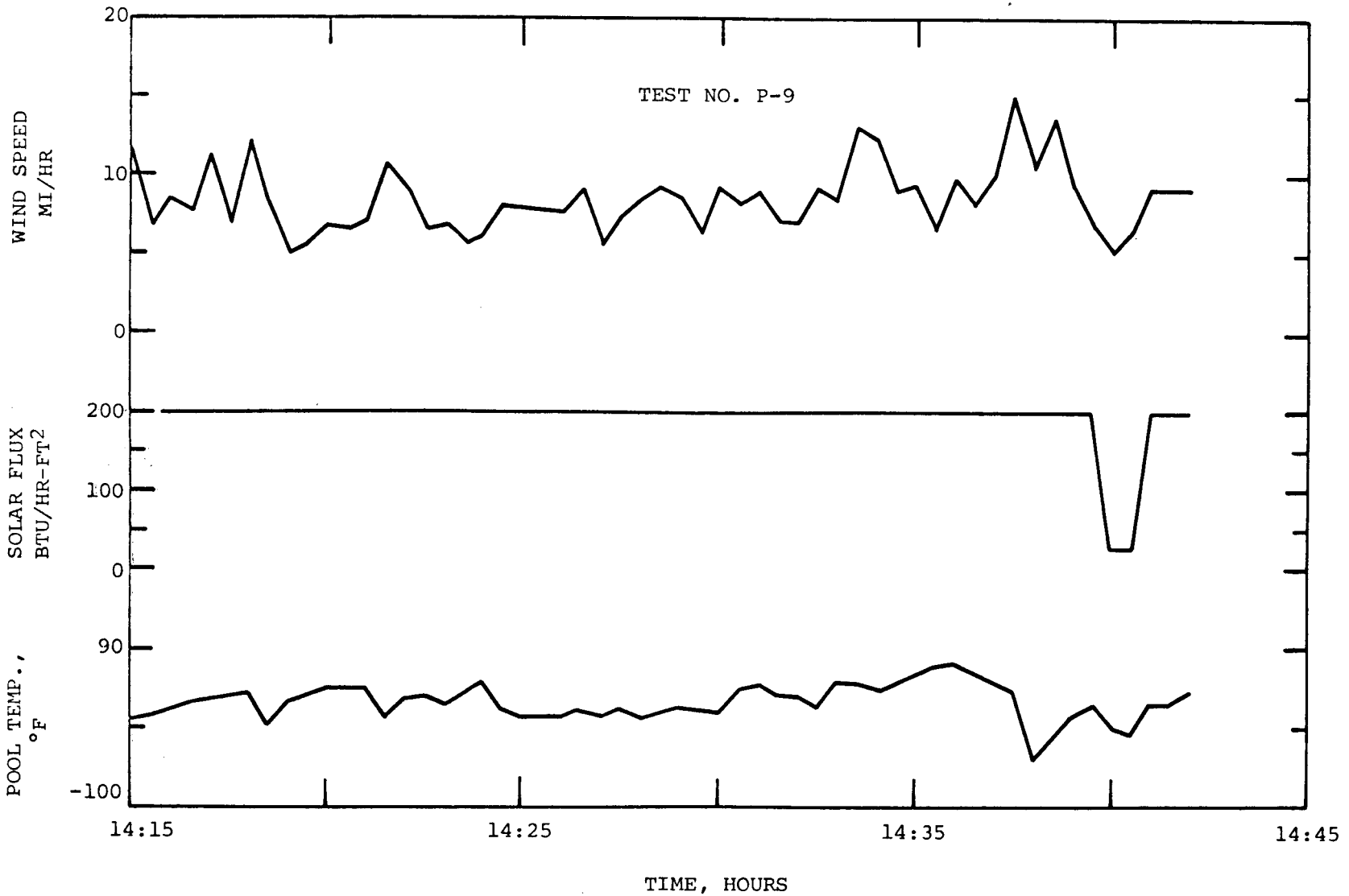

Figure 11. Effect of Wind Speed on Pool Temperature.

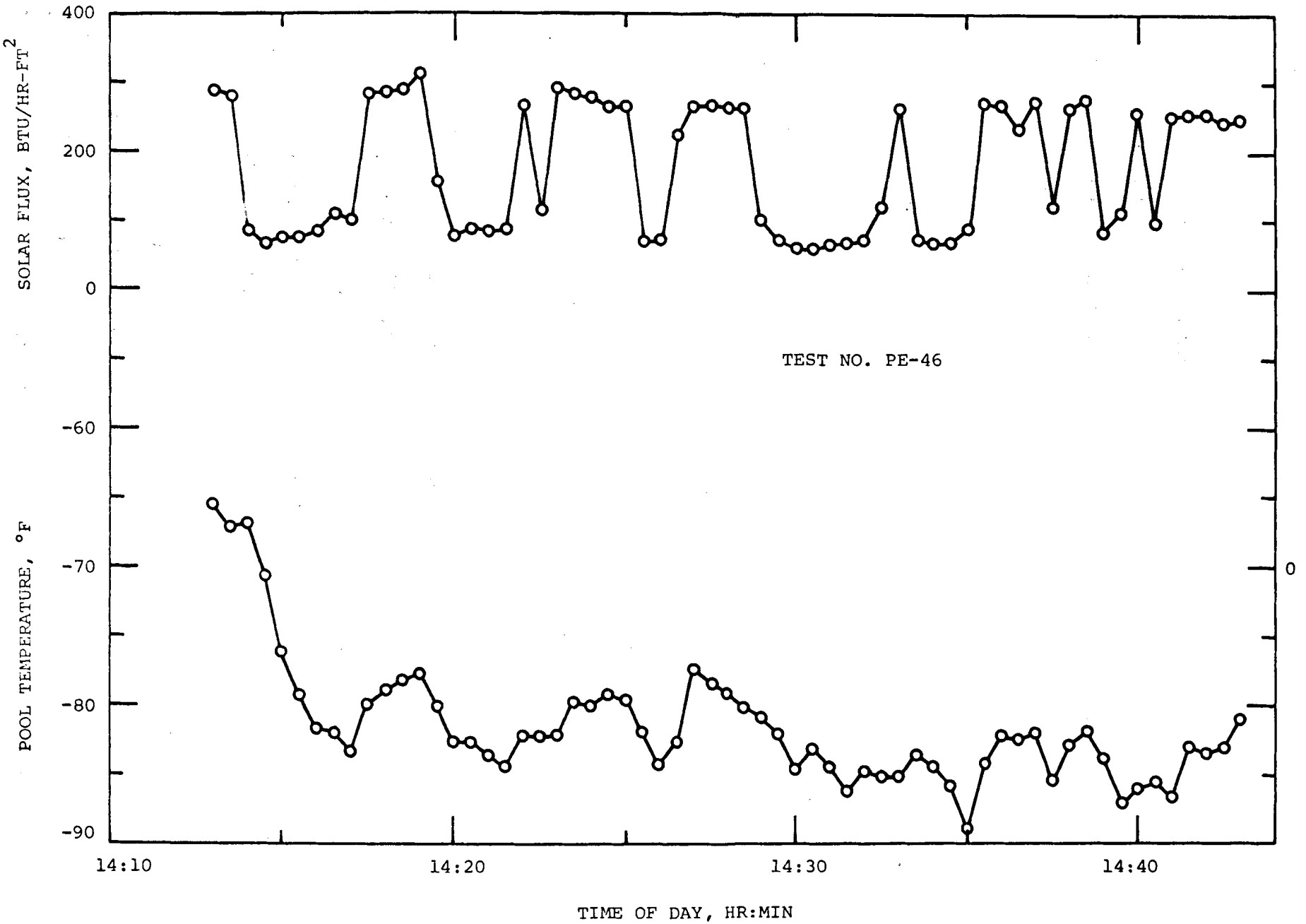

Figure 12. Pool Temperature Fluctuations Caused by Changes in Solar Radiation Level.

surfaces. In fact, solar radiation impinging on the thermocouple can change the thermocouple reading even though the pool temperature does not change. Assuming the thermocouple bead to be cylindrical, a heat balance on the bead shows that

$$d\ L\ q_s = h\ \pi\ d\ L\ (T_b - T_p) \qquad (33)$$

where d = diameter of bead

L = length of bead

T_b = bead temperature

q_s = solar flux

h = heat transfer coefficient

T_p = pool temperature

It can be shown that the minimum value of h is

$$h = \frac{2k_\ell}{d}$$

where k_ℓ is the liquid thermal conductivity. The thermocouple beads are less than 0.1 inches in diameter, so for propane, h is greater than about 20 Btu/hr-ft^2-$^\circ$F. For an absorbed solar flux of 300 Btu/hr-ft^2 on the thermocouple bead, $T_b - T_p$ can be found from Equation 33 to be about 4.8°F and for a solar flux of 100 Btu/hr-ft^2, $T_b - T_p$ is about 1.6°F. For a change in solar flux from 100 to 300 Btu/hr-ft^2, a temperature change of about 3.2°F would be expected for the thermocouple if the pool temperature did not change. The measured changes of about 5 to 7°F

therefore show that the pool temperature is changing with changes in solar flux. The pool temperature changes quite rapidly for the shallow pool used in these tests. For example, a solar flux change of 200 Btu/hr-ft^2 will heat the pool at a rate of about 5^{o}F/min for the mass of propane in the pool during Test PE-46. Deeper pools will respond more slowly to changes in radiant flux because the liquid mass is greater per unit of pool surface area.

Several tests were run in which granite or marble chips were either placed on the pit floor before propane was spilled or poured into the propane when steady state vaporization had been reached. The granite chips were about 0.15 inches in nominal size (aquarium gravel was used). The marble chips were about 0.75 inches in nominal size, although their size and shape were not as uniform as were those of the smaller granite chips. The boiloff from the granite chips, regardless of whether propane was poured onto the chips or the chips were poured into the propane, was as fast as pouring could be done. As a consequence of the rapid boiling, substantial propane was ejected directly into the atmosphere as spray or droplets. The boiloff rates could not be measured, and even measurements of beginning and ending weights were not consistent. The boiloff when using the larger marble chips was slower, but about as much propane was ejected as mist or spray as was vaporized by heating if the propane was poured onto marble chips in a

concrete pit. If marble chips were poured into a pit containing subcooled propane, boiling was less vigorous and little or no spray was ejected. The propane warmed and boiled for a few minutes before a new steady boiling period was reached. Figure 13 shows a curve for weight remaining in a pit containing sub-cooled propane when 20 lb of marble chips was added. About a quarter of a minute was required to add the rocks, and steady state vaporization was re-established in about 3 min. Although not shown in Figure 13, the steady vaporization rate continued until the propane was nearly gone. The curve drawn through the data is based on Equation 24 with the temperature history being used to calculate the heat lost from the marble rocks. Heat required to warm the pool to the boiling point and steady state mass transfer rates were both included in determining the vaporization rate. The heat transfer coefficient between the marble chips and the propane used to obtain the calculated curve shown was 20 Btu/hr-ft^2-^{o}F.

Figure 14 shows two curves. The upper curve is the vaporization when propane was poured into a polystyrene foam pit. The steady state vaporization rate is reached within a minute or two. The lower curve is for vaporization when propane was poured into the polystyrene foam pit containing 50 lb of warm marble chips. The line drawn through the lower data was calculated based on Equation 14 and the vaporization from the upper curve for a plain polystyrene

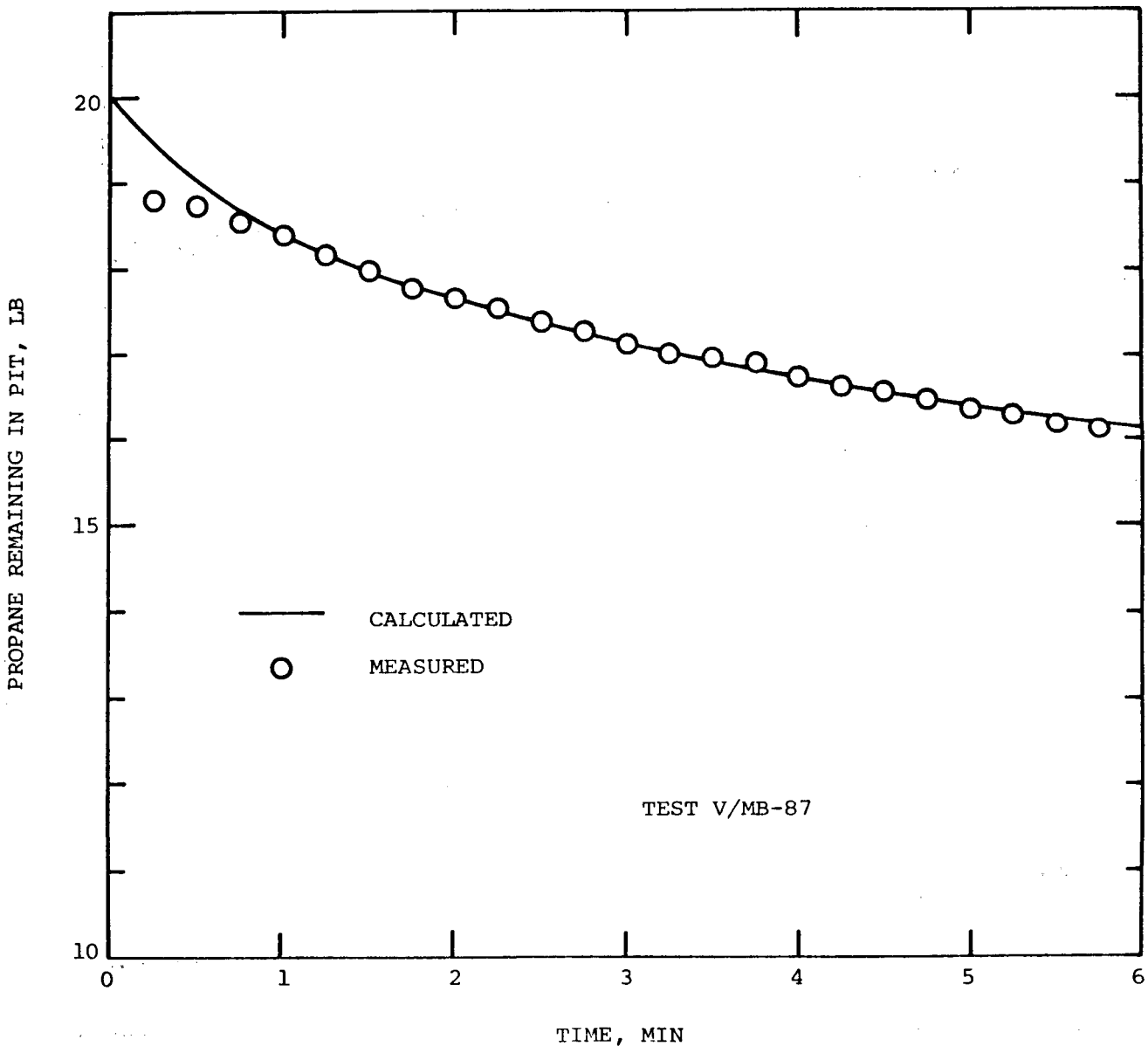

Figure 13. Propane Vaporization Following Pouring of 20 lb of Marble Chips into Propane.

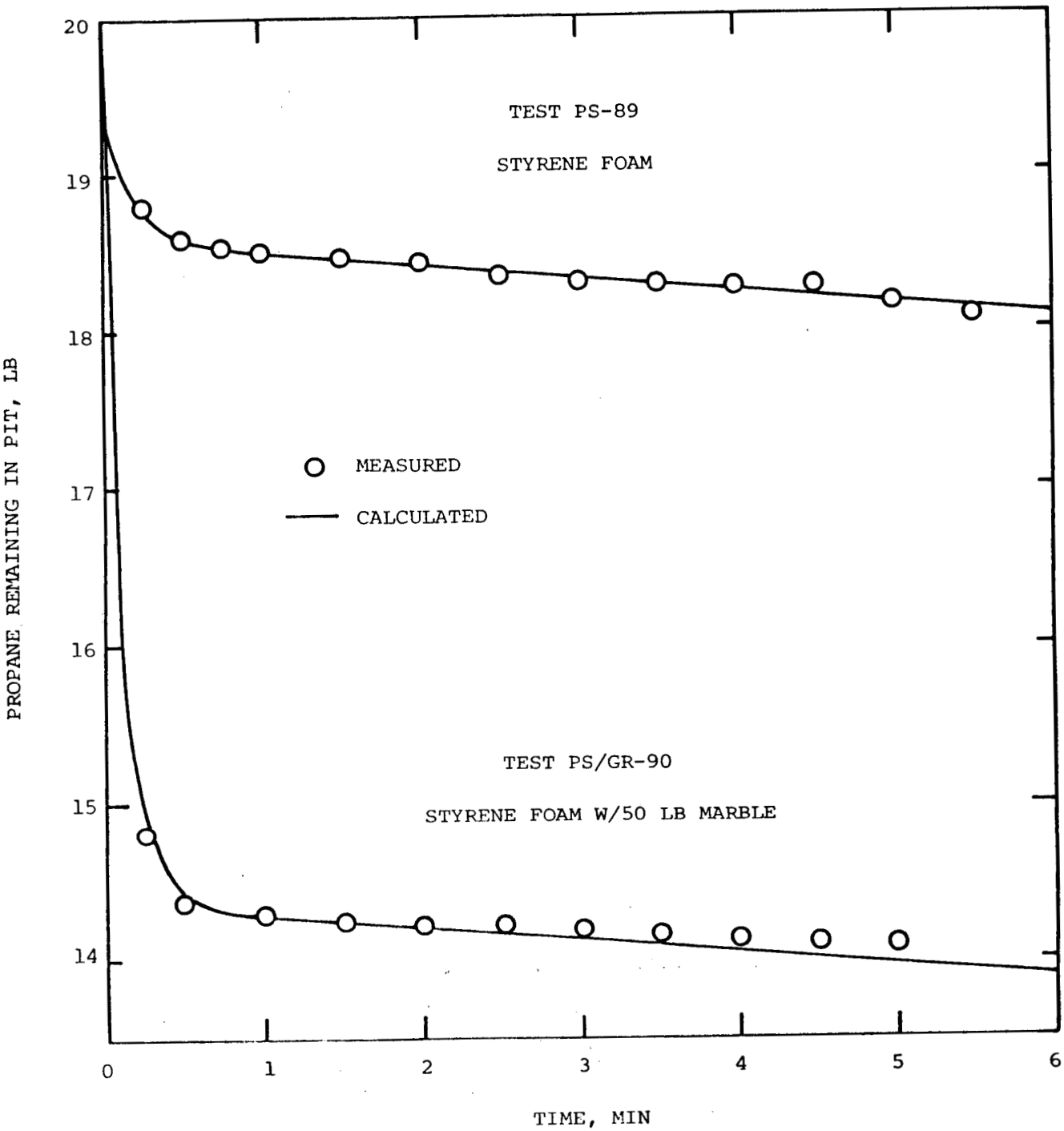

Figure 14. Propane Vaporization Following Spill into Styrene Foam Pit and Styrene Foam Pit Containing Marble Chips.

foam pit. The agreement between the curve and data is excellent. However, the heat transfer coefficient required to match calculated and measured curves was 200 Btu/hr-ft^2-^{o}F. The reason for the difference between the heat transfer coefficient for this test and the test in Figure 13 is unknown. However, the range of temperature differences between solid (pit or rocks) and boiling propane is generally in the range where transition boiling (between nucleate and film boiling) is expected for propane (Sciance, 1966). Therefore, wide variations in heat transfer coefficients may be expected.

When steady state vaporization was reached with marble chips in the pit, any marble exposed as the liquid level receded was quickly covered with a layer of frost (or hydrate). The frost layer acted as a wick, and the surface of the rocks stayed wet with propane. There was no strong effect on steady state vaporization rate that could be attributed to the wicking effect. However, it is probable that the wicking did affect the data, because a substantial fraction of the surface of the pool was taken up by the marble, reducing direct liquid to air vaporization. The wicking effect apparently added enough mass transfer area to counterbalance that lost as the liquid surface receded.

CONCLUSIONS

The vaporization tests on liquid propane showed that a conduction heat transfer model could be used to predict the vaporization rate for liquid propane spilled on solid surfaces. Two variables, the effective thermal conductivity of the solid and the heat transfer coefficient for heating from solid to liquid were derived from the test results. The effective thermal conductivities were larger than those found in the literature for similar materials. However, they were similar in magnitude to thermal conductivities found by similar techniques during LNG spill tests. The thermal conductivities of common materials such as concrete and soil vary at lower temperatures and the effective value measured from vaporization tests reflects the higher values. Temperature profiles within the substrate support this conclusion.

The steady state vaporization rate of propane depends primarily on wind velocity, and to a lesser extent, the solar radiation on the pool. A correlation of mass transfer factors was prepared. It can be used with other heat and mass transfer data to determine steady state vaporization rates. Pool temperature changes occur in response to changes in solar radiation and wind velocity. The changes are dependent on pool depth and are most pronounced for shallow pools.

REFERENCES

1. American Gas Association, "LNG Safety Program: Interim Report on Phase II Work," Project IS-3-1 (1974).

2. Eshbach, O. W., and M. Souders, Handbook of Engineering Fundamentals, 3rd ed., John Wiley & Sons (1975).

3. Johnson, D. W., et al., "Fire Control Agent Effectiveness for Hazardous Chemical Fires: Carbon Disulfide," Report No. CG-D-09-81, U. S. Coast Guard, Washington, DC (1981).

4. Johnson, D. W., et al., "Control and Extinguishment of LPG Fires," Report No. DOE/EV/06020-1, U. S. Dept. of Energy, Washington, DC (1980).

5. Maclean, J. D., "Thermal Conductivity of Wood," Heating, Piping, and Air Conditioning, 459 (1940).

6. Lentz, A. E., and G. E. Monfore, "Thermal Conductivity of Concrete at Very Low Temperatures," Journal of PCA Research and Development Laboratories, 7, 39 (1965).

7. Perry, J. H., ed., Chemical Engineers' Handbook, 3rd ed., McGraw Hill Book Company (1950).

8. Reid, Robert C., "Boiling of LNG on Typical Dike Floor Materials," Report No. GRI-79/0026, Gas Research Institute, Chicago (1980).

9. Sciance, C. T., "Pool Boiling Heat Transfer to Liquefied Hydrocarbon Gases," Ph.D. Dissertation, University of Oklahoma, Norman, Oklahoma (1966).

APPENDIX A

This Appendix contains the vaporization data for all the tests run in the 5-ft^2 test series. The data are shown in graphical form in the sequence in which they were run. The run numbers are the same as listed in Table 1 in the body of the report. The substrate for each test is noted and each figure is labeled to indicate whether the test was open or covered. Refer to Table 1 for additional data.

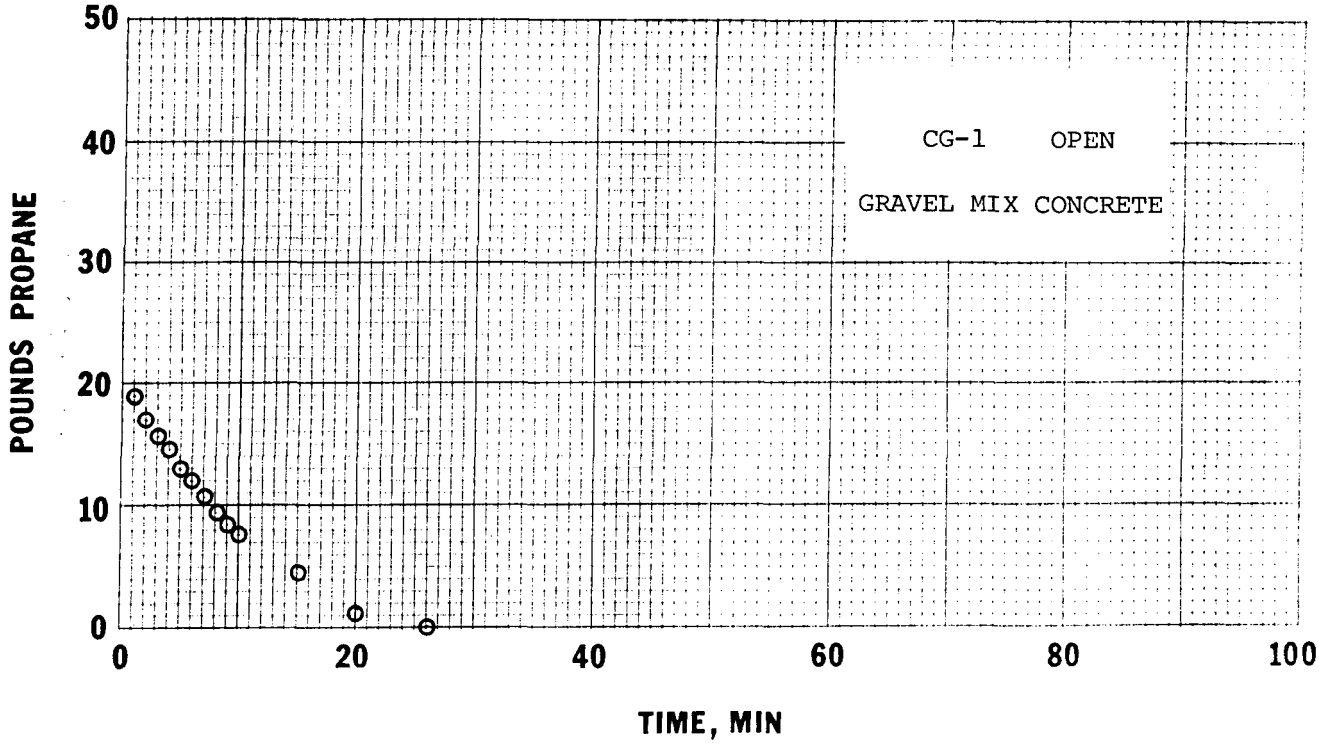

FIGURE A-1. VAPORIZATION OF PROPANE FOLLOWING A SPILL ON GRAVEL MIX CONCRETE.

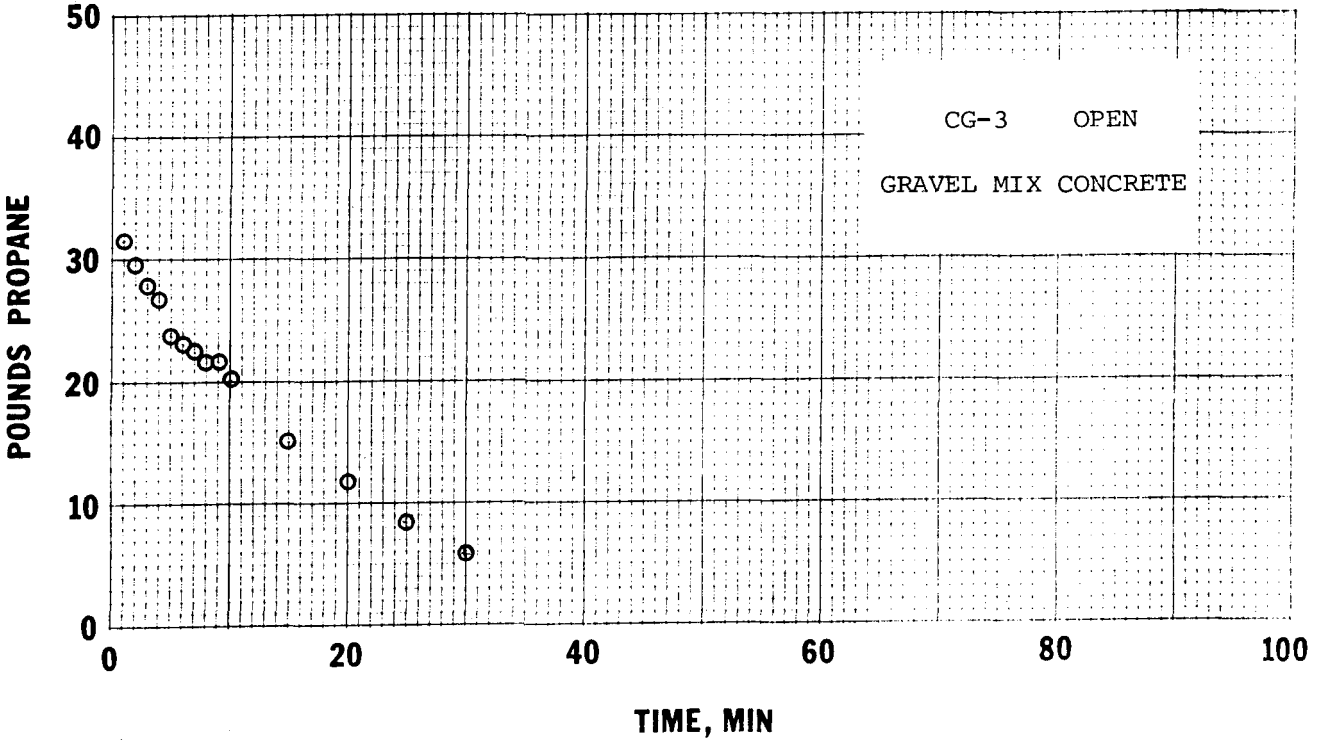

FIGURE A-2. VAPORIZATION OF PROPANE FOLLOWING A SPILL ON GRAVEL MIX CONCRETE.

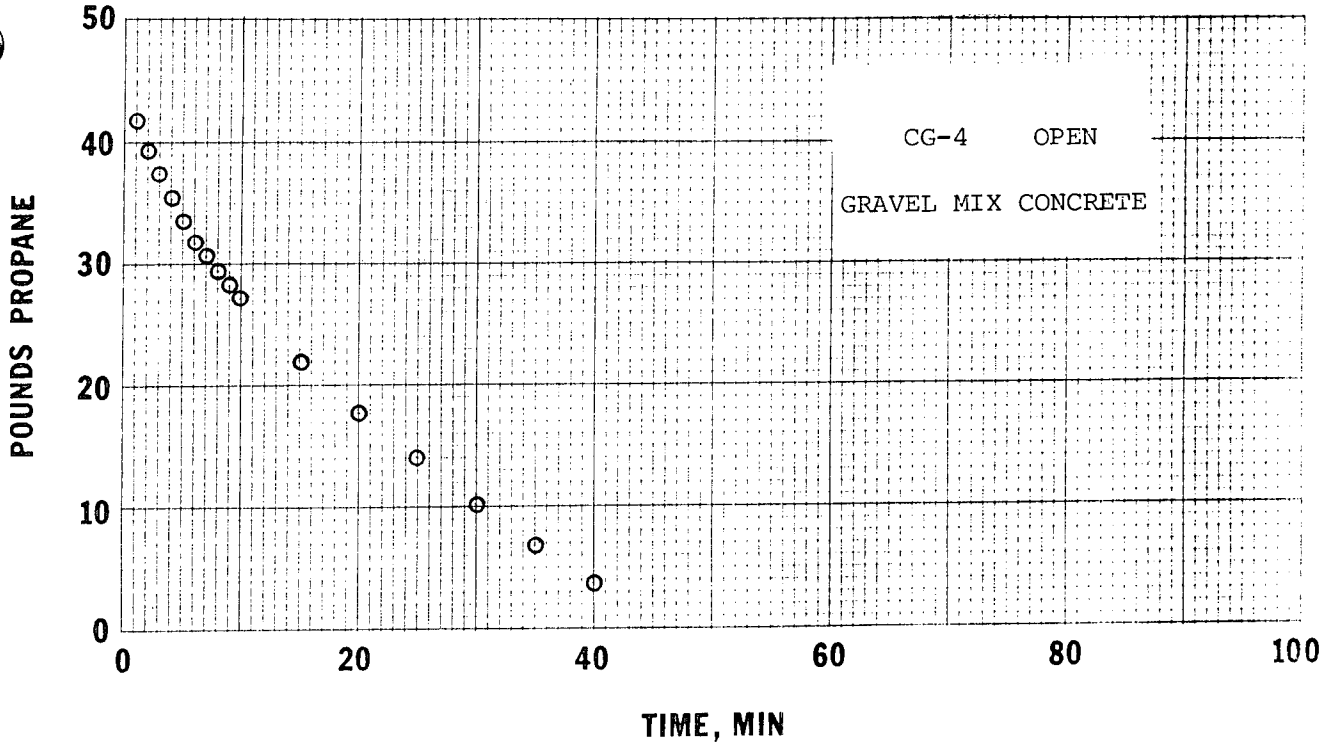

FIGURE A-3. VAPORIZATION OF PROPANE FOLLOWING A SPILL ON GRAVEL MIX CONCRETE.

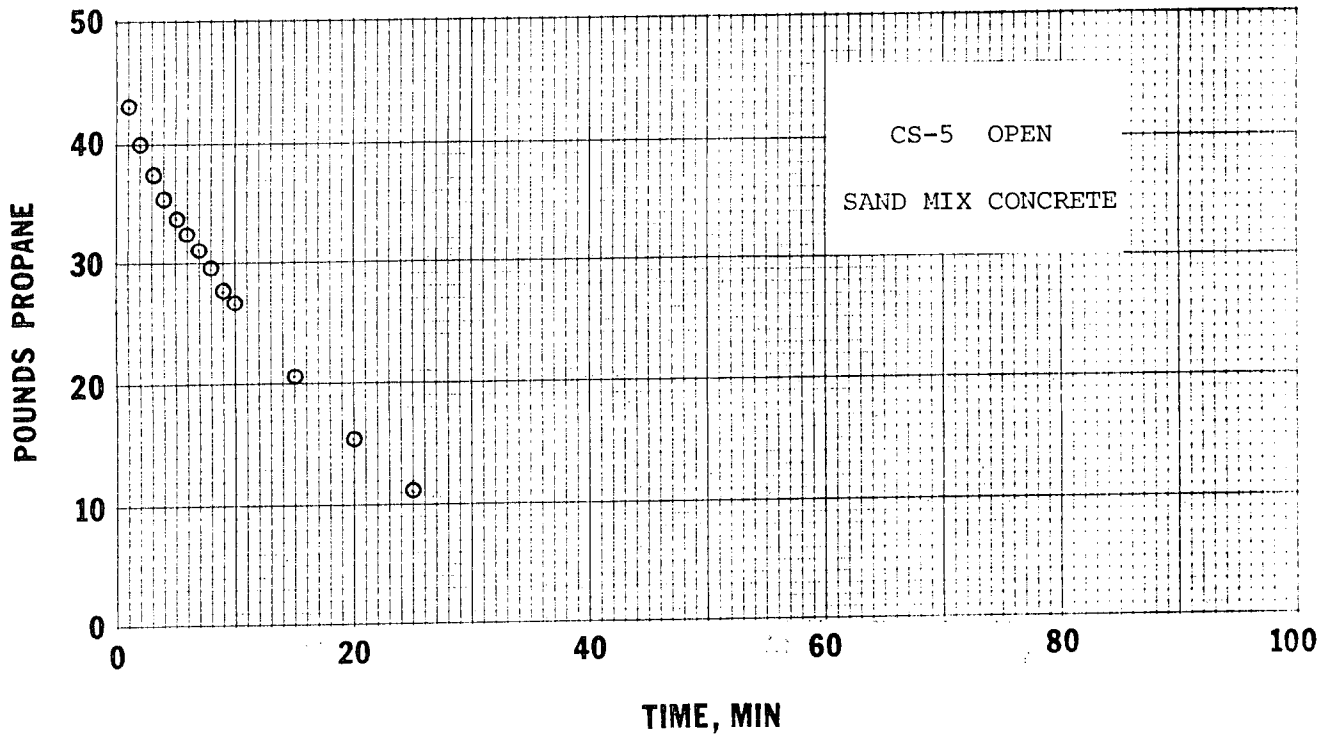

FIGURE A-4. VAPORIZATION OF PROPANE FOLLOWING A SPILL ON SAND MIX CONCRETE.

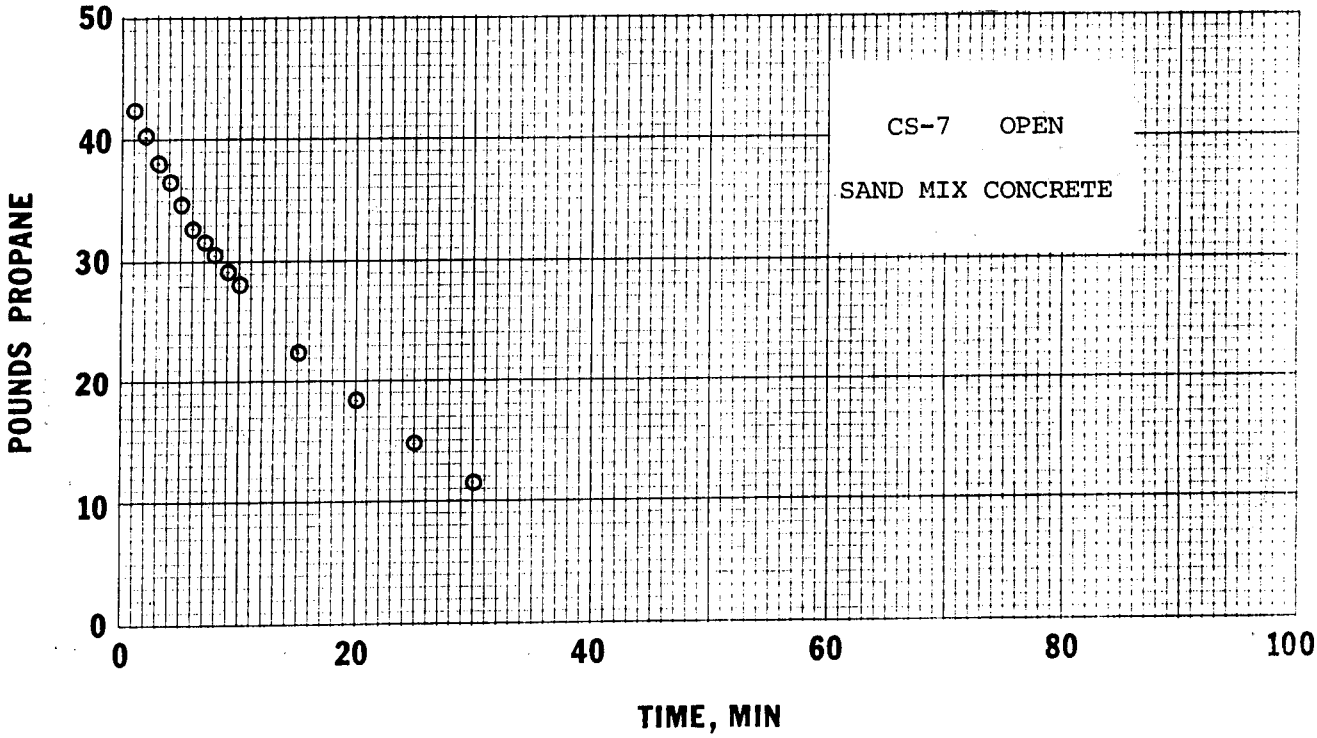

FIGURE A-5. VAPORIZATION OF PROPANE FOLLOWING A SPILL ON SAND MIX CONCRETE.

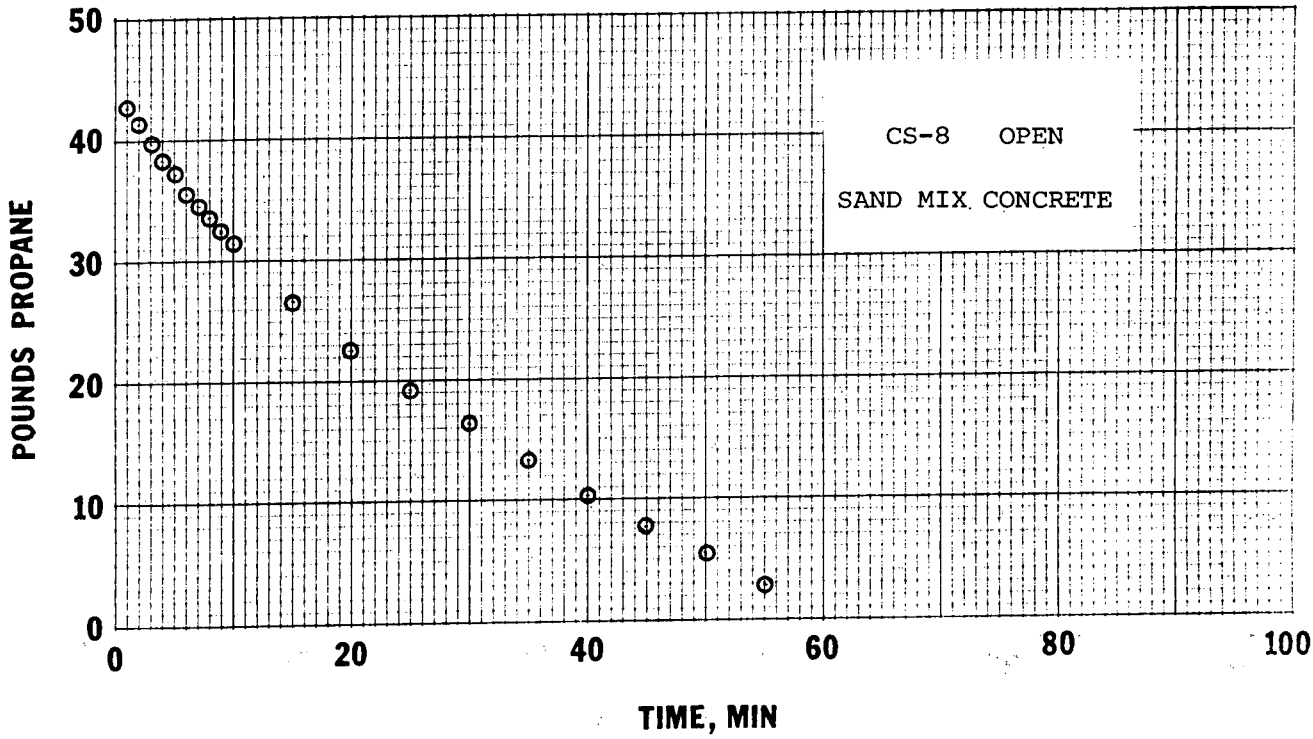

FIGURE A-6. VAPORIZATION OF PROPANE FOLLOWING A SPILL ON SAND MIX CONCRETE.

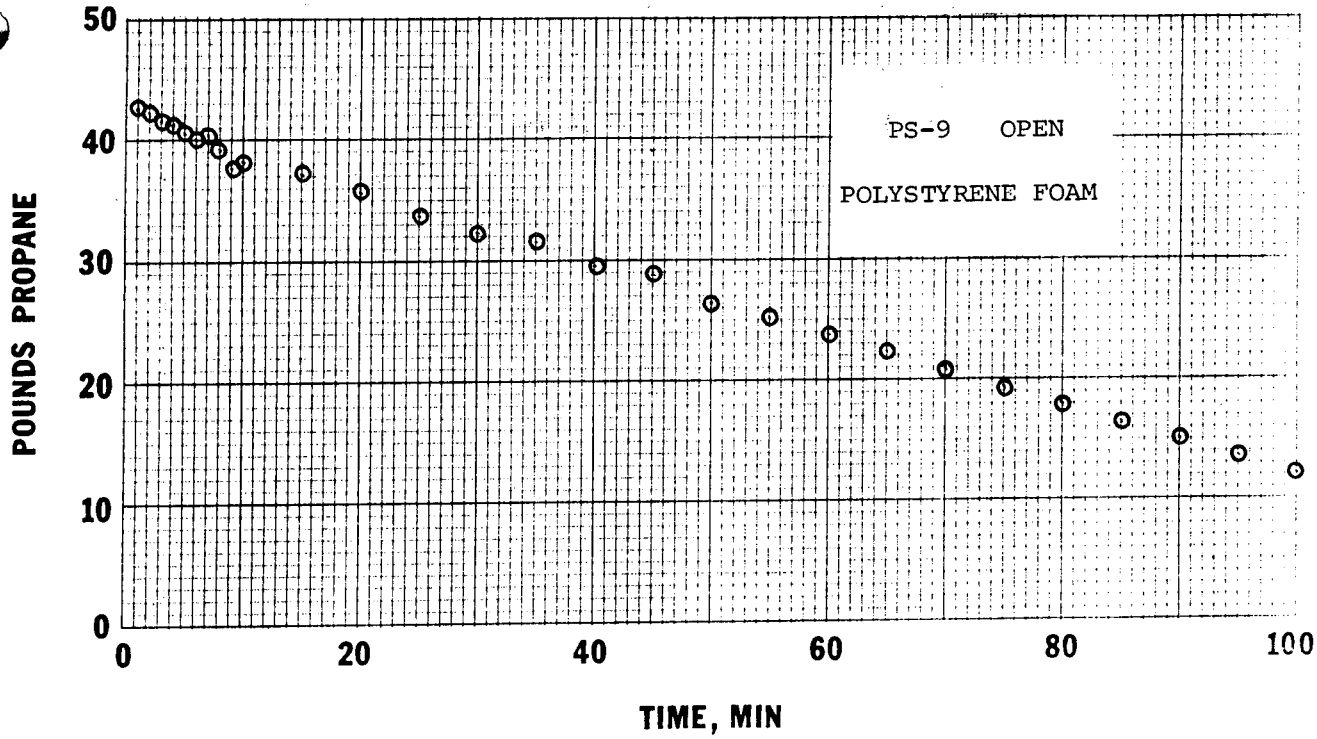

FIGURE A-7. VAPORIZATION OF PROPANE FOLLOWING A SPILL ON POLYSTYRENE FOAM.

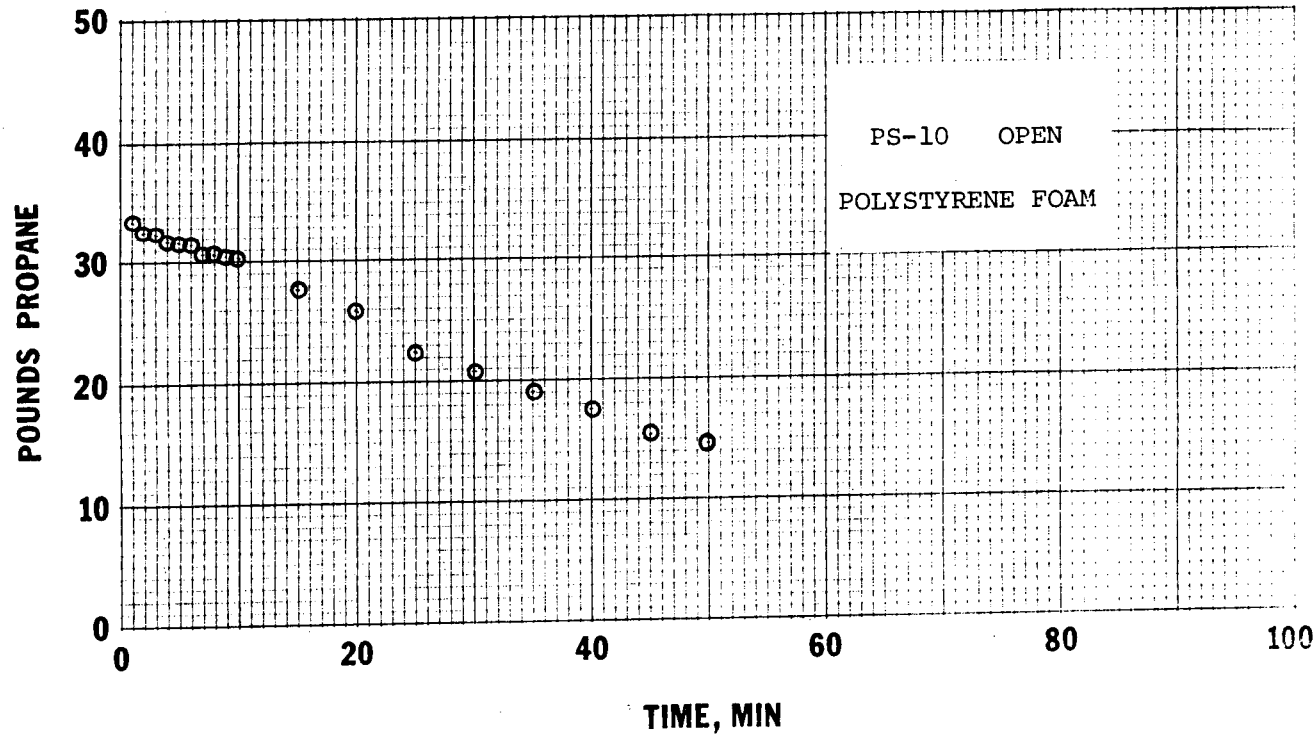

FIGURE A-8. VAPORIZATION OF PROPANE FOLLOWING A SPILL ON POLYSTYRENE FOAM.

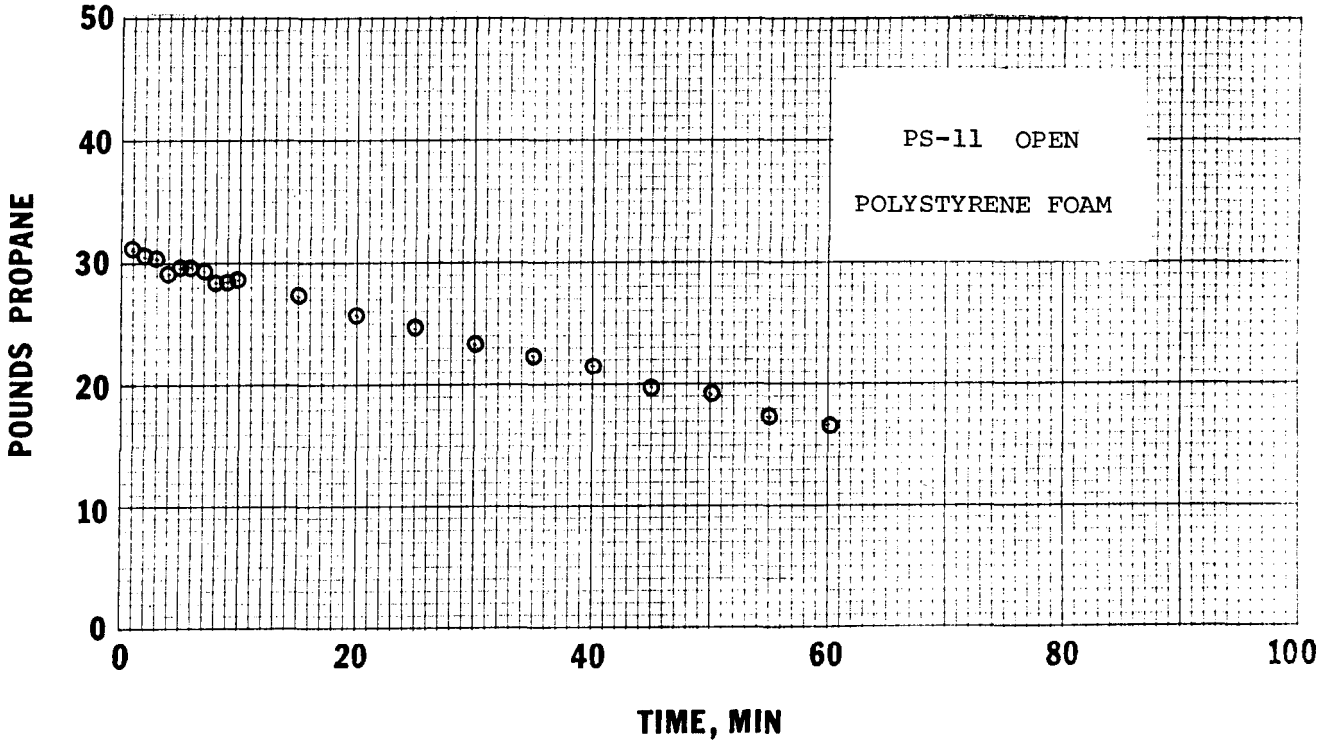

FIGURE A-9. VAPORIZATION OF PROPANE FOLLOWING A SPILL ON POLYSTYRENE FOAM.

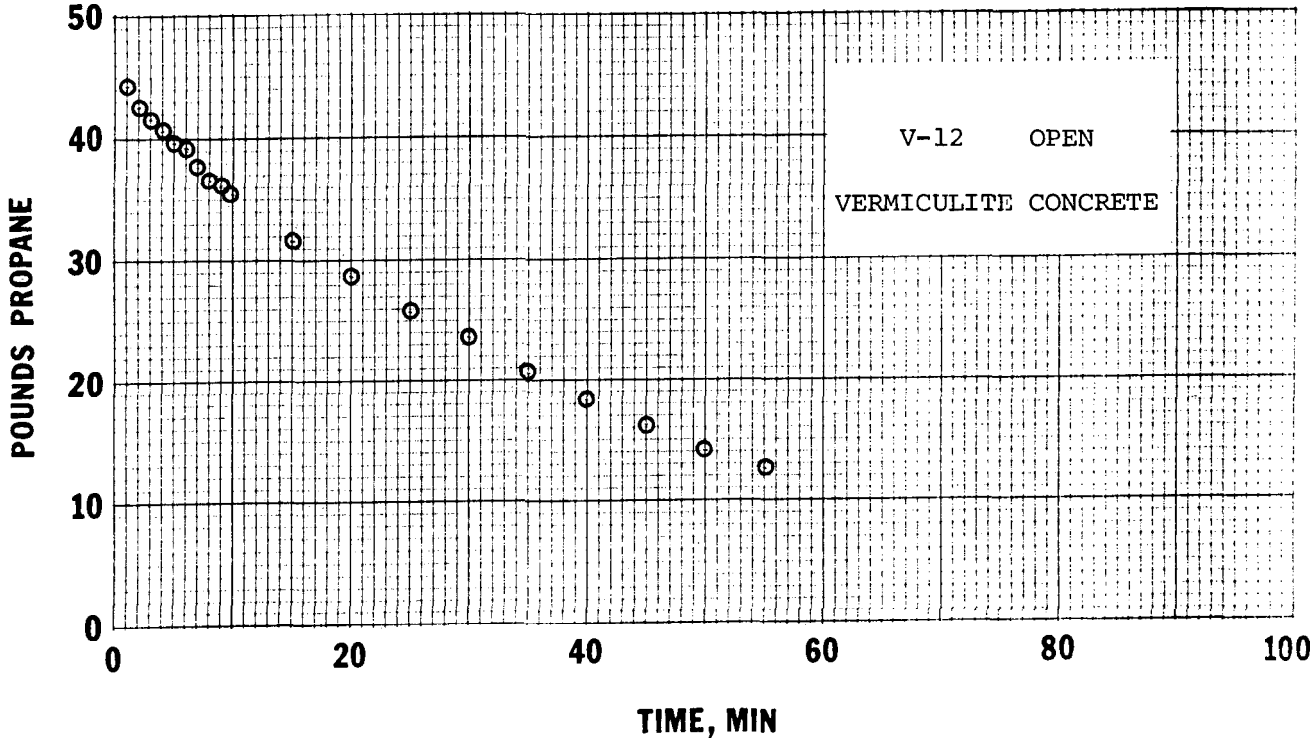

FIGURE A-10. VAPORIZATION OF PROPANE FOLLOWING A SPILL ON VERMICULITE CONCRETE.

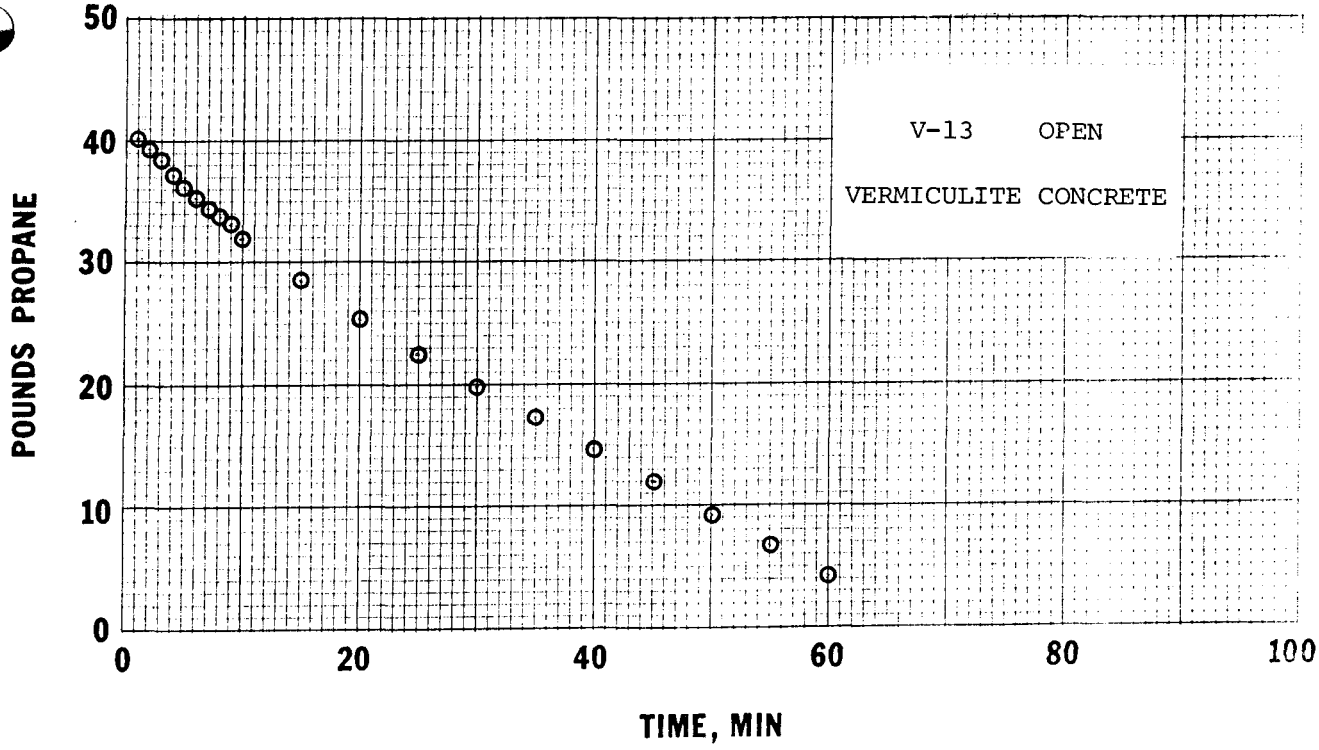

FIGURE A-11. VAPORIZATION OF PROPANE FOLLOWING A SPILL ON VERMICULITE CONCRETE.

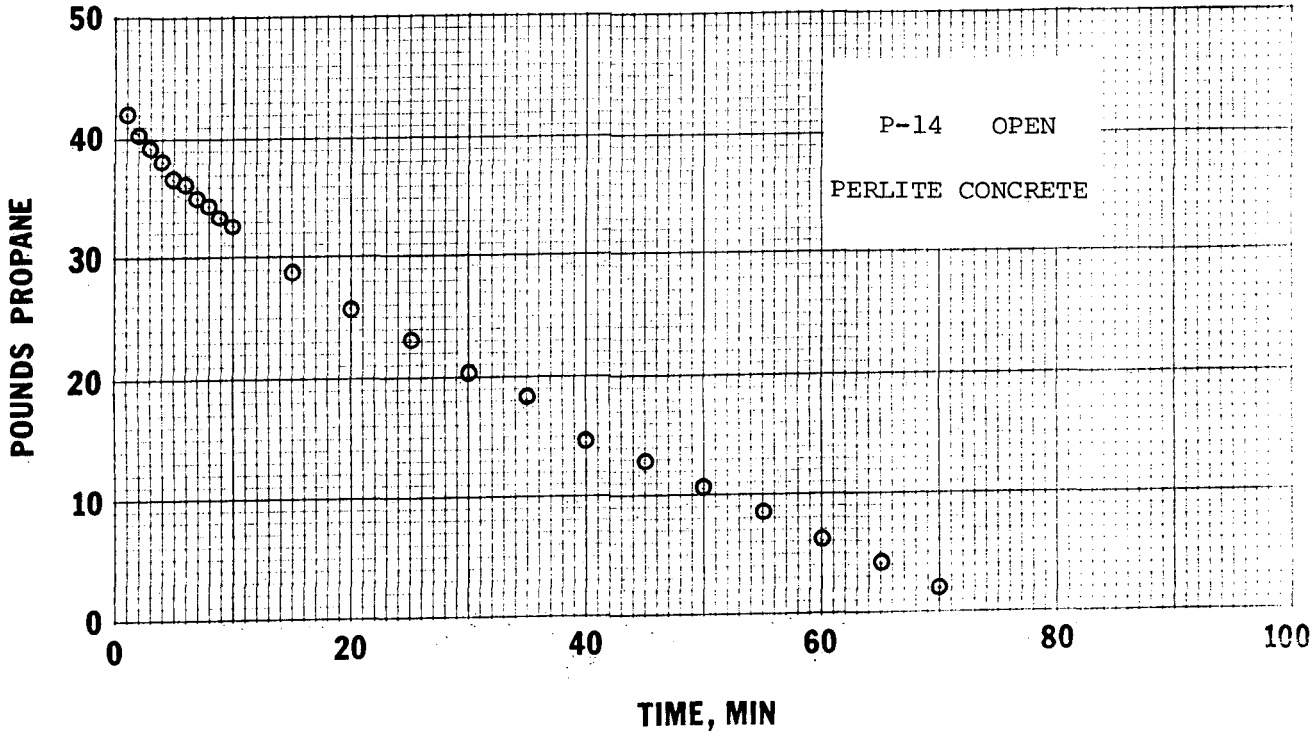

FIGURE A-12. VAPORIZATION OF PROPANE FOLLOWING A SPILL ON PERLITE CONCRETE.

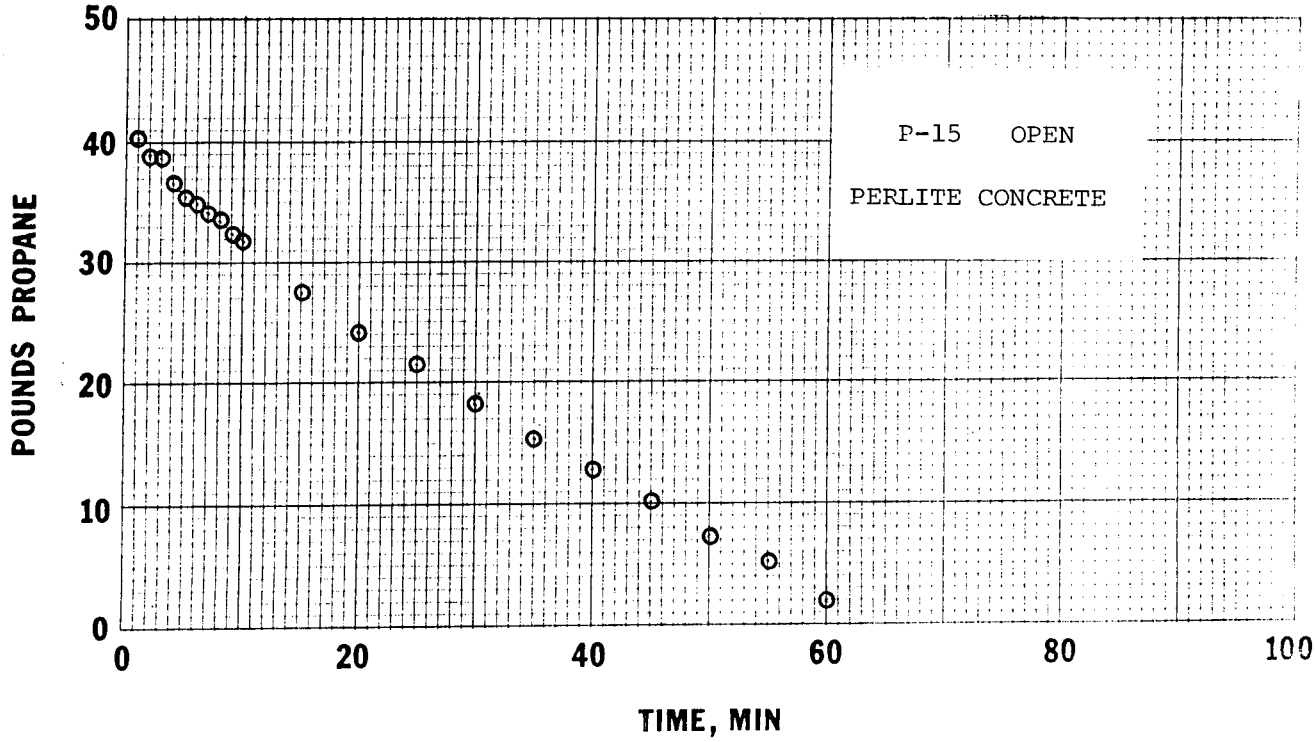

FIGURE A-13. VAPORIZATION OF PROPANE FOLLOWING A SPILL ON PERLITE CONCRETE.

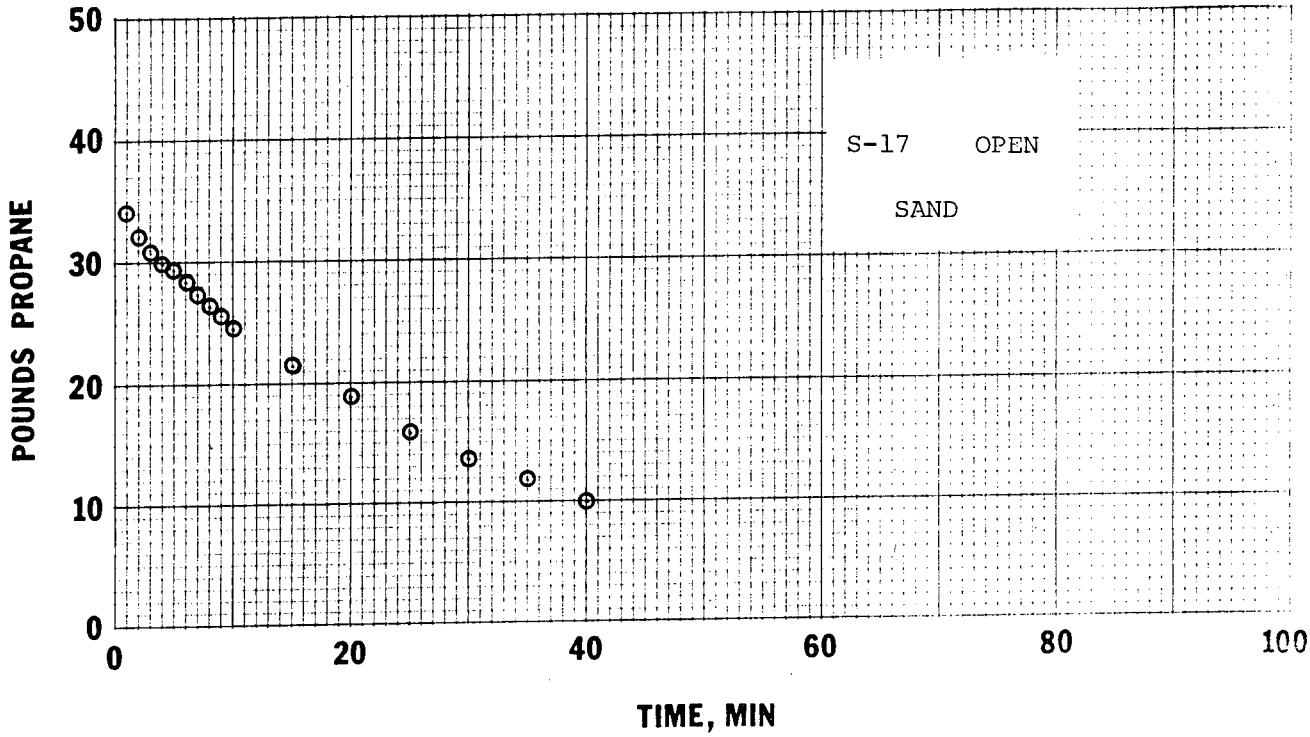

FIGURE A-14. VAPORIZATION OF PROPANE FOLLOWING A SPILL ON SAND.

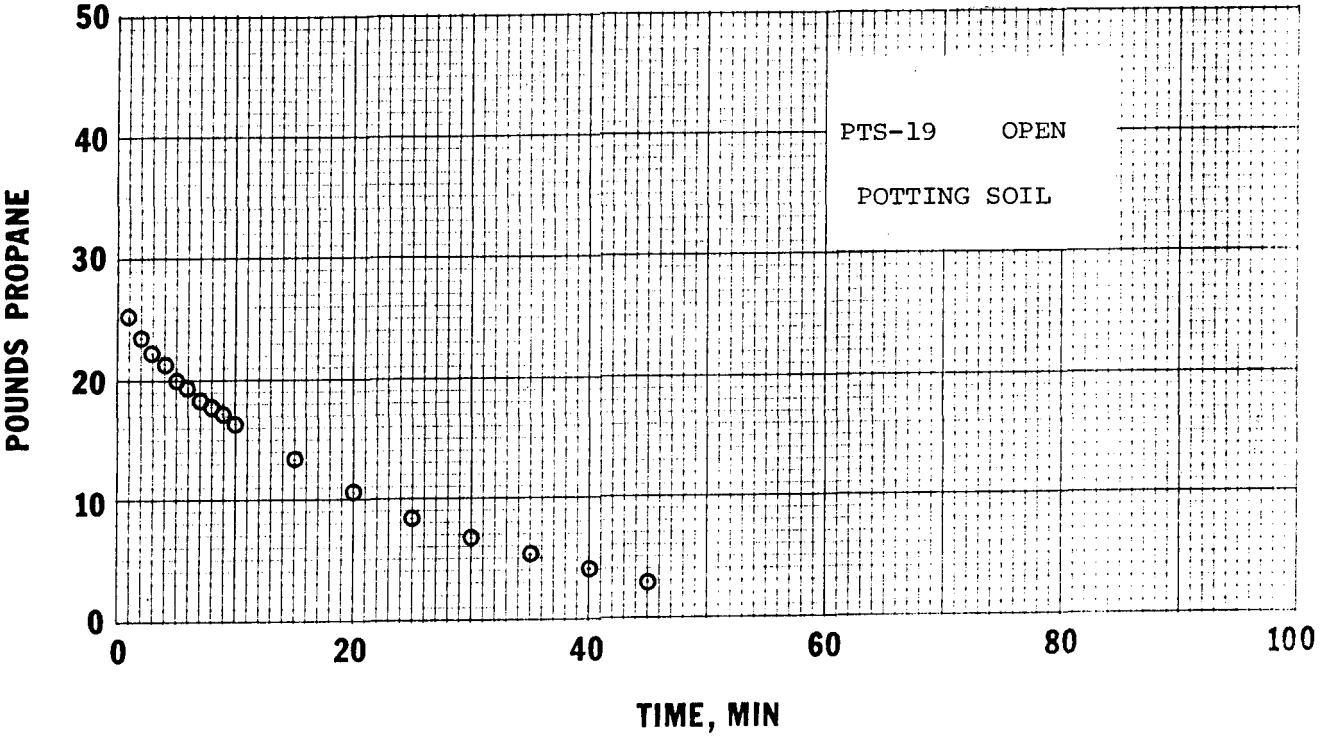

FIGURE A-15. VAPORIZATION OF PROPANE FOLLOWING A SPILL ON POTTING SOIL.

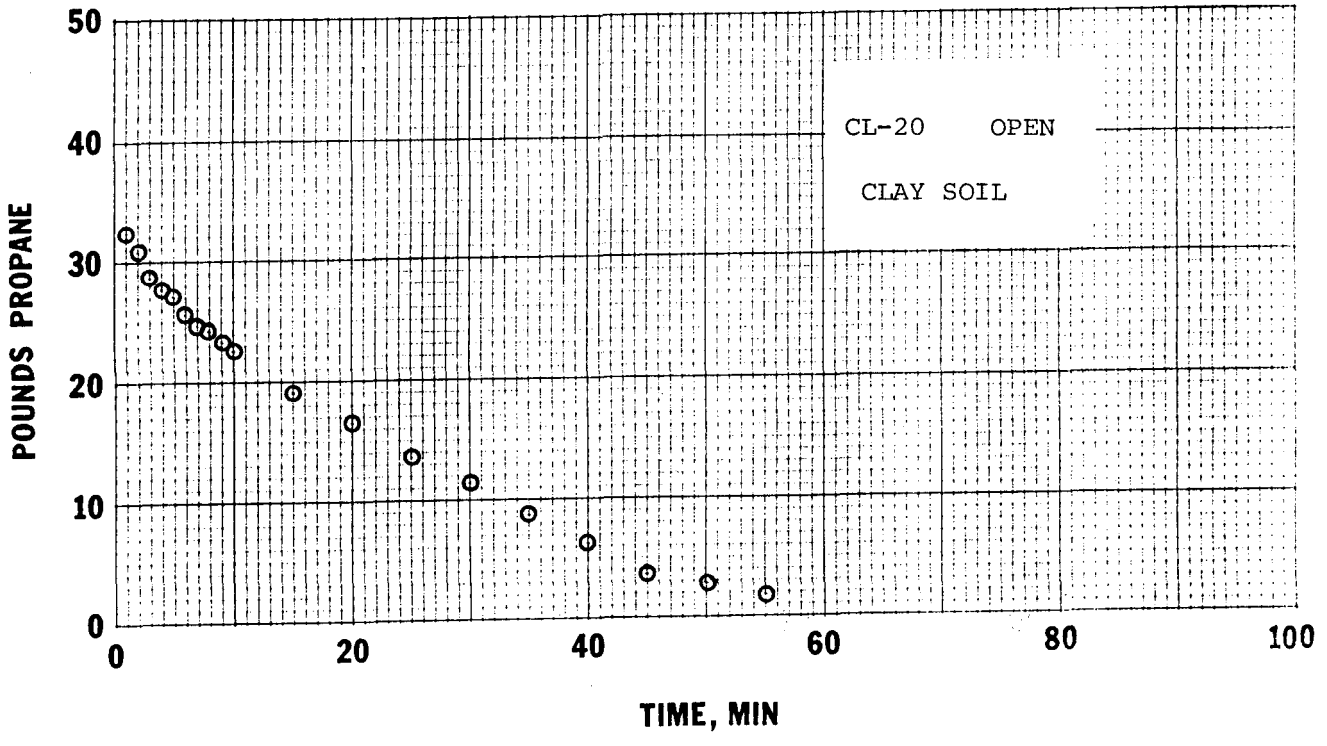

FIGURE A-16. VAPORIZATION OF PROPANE FOLLOWING A SPILL ON CLAY SOIL.

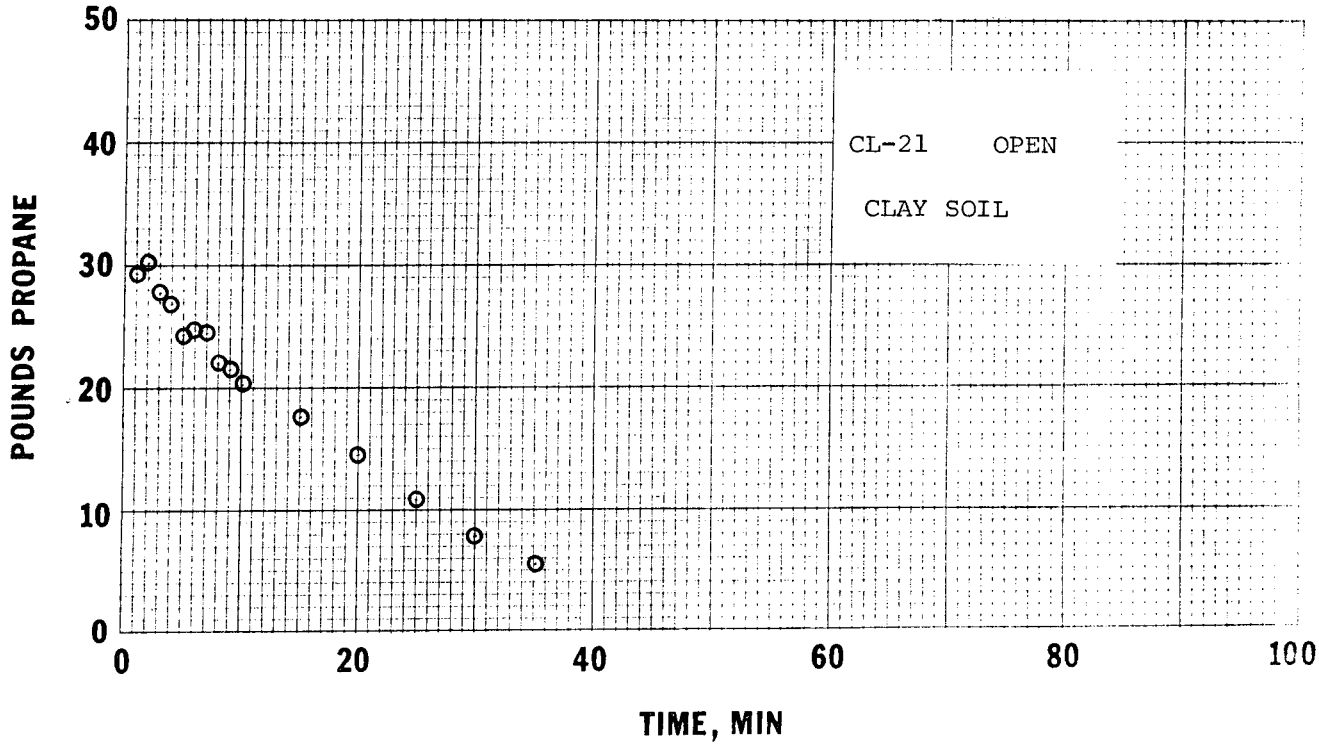

FIGURE A-17. VAPORIZATION OF PROPANE FOLLOWING A SPILL ON CLAY SOIL.

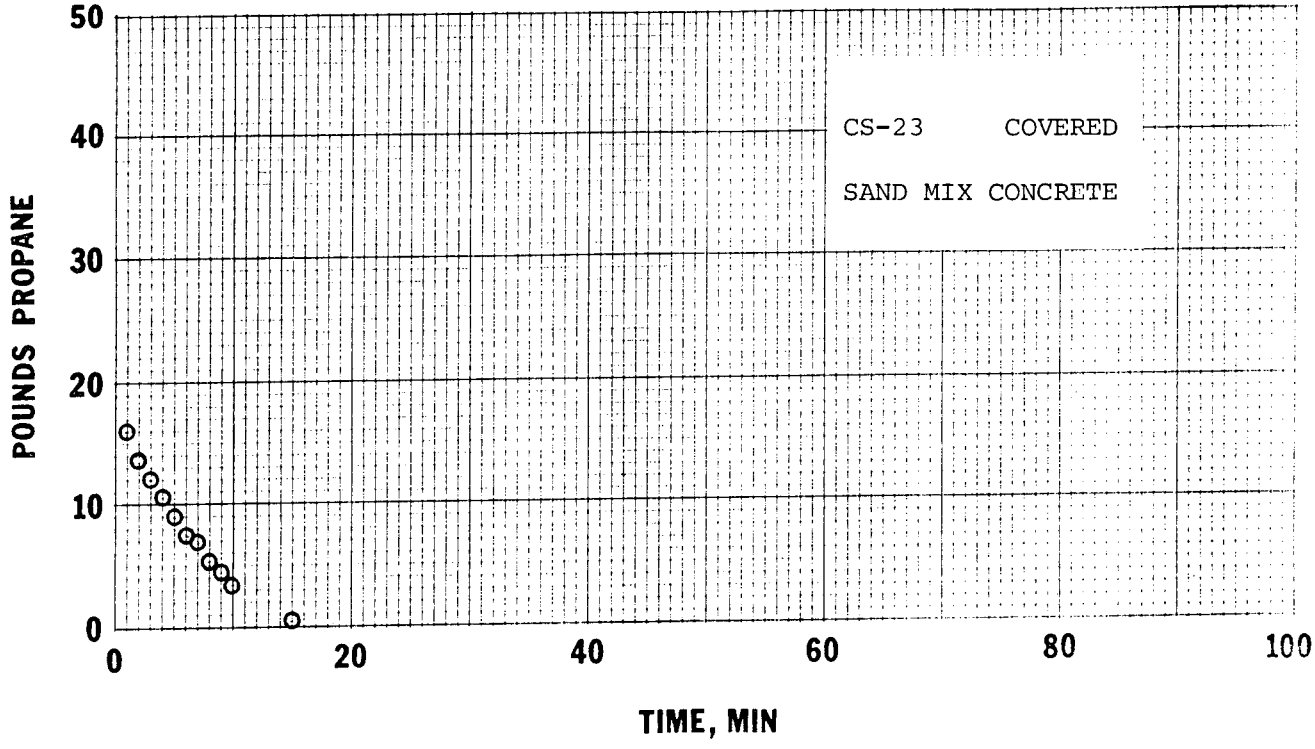

FIGURE A-18. VAPORIZATION OF PROPANE FOLLOWING A SPILL ON SAND MIX CONCRETE.

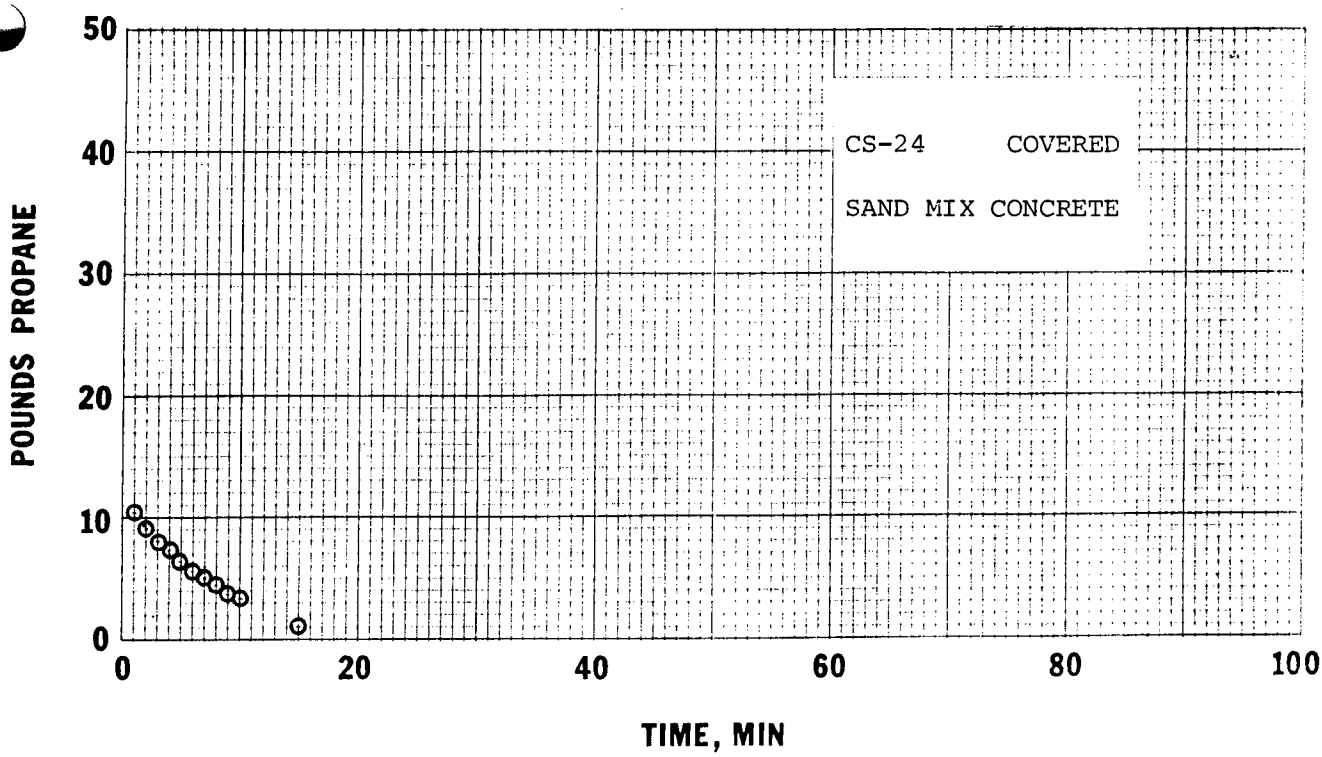

FIGURE A-19. VAPORIZATION OF PROPANE FOLLOWING A SPILL ON SAND MIX CONCRETE.

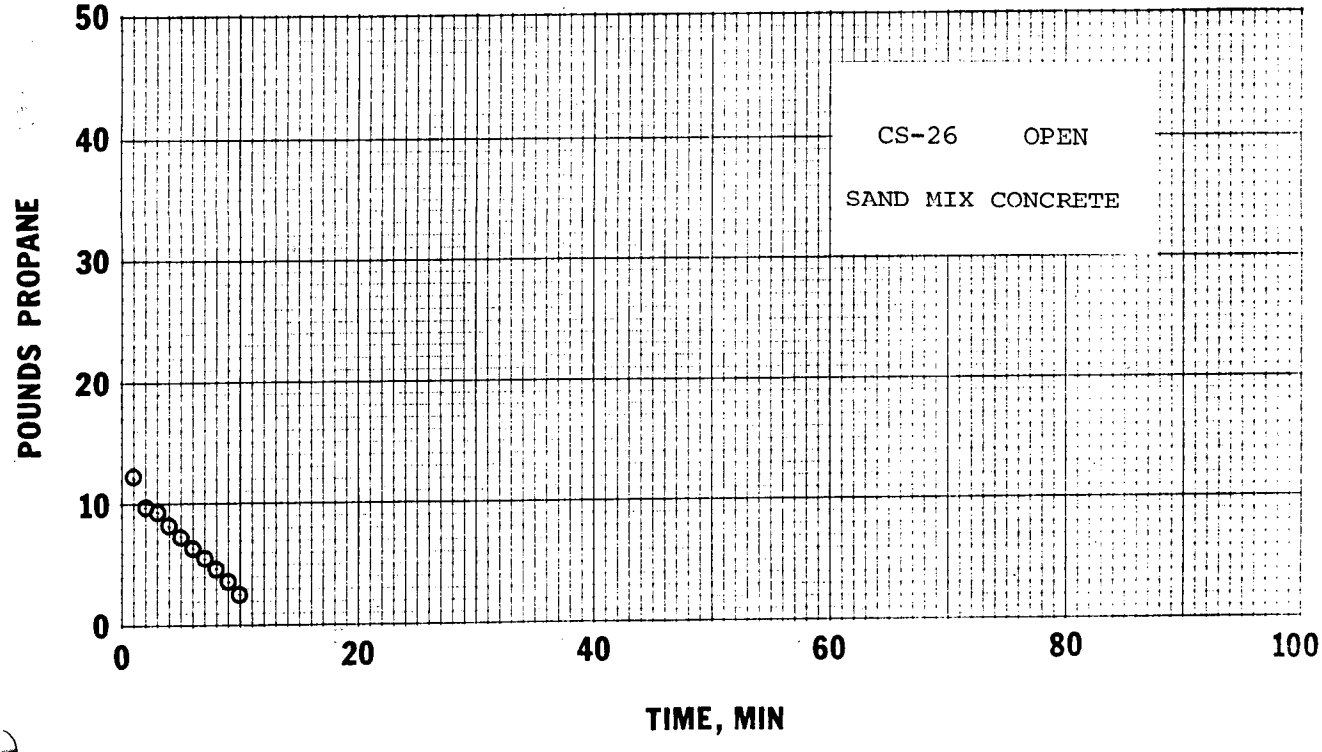

FIGURE A-20. VAPORIZATION OF PROPANE FOLLOWING A SPILL ON SAND MIX CONCRETE.

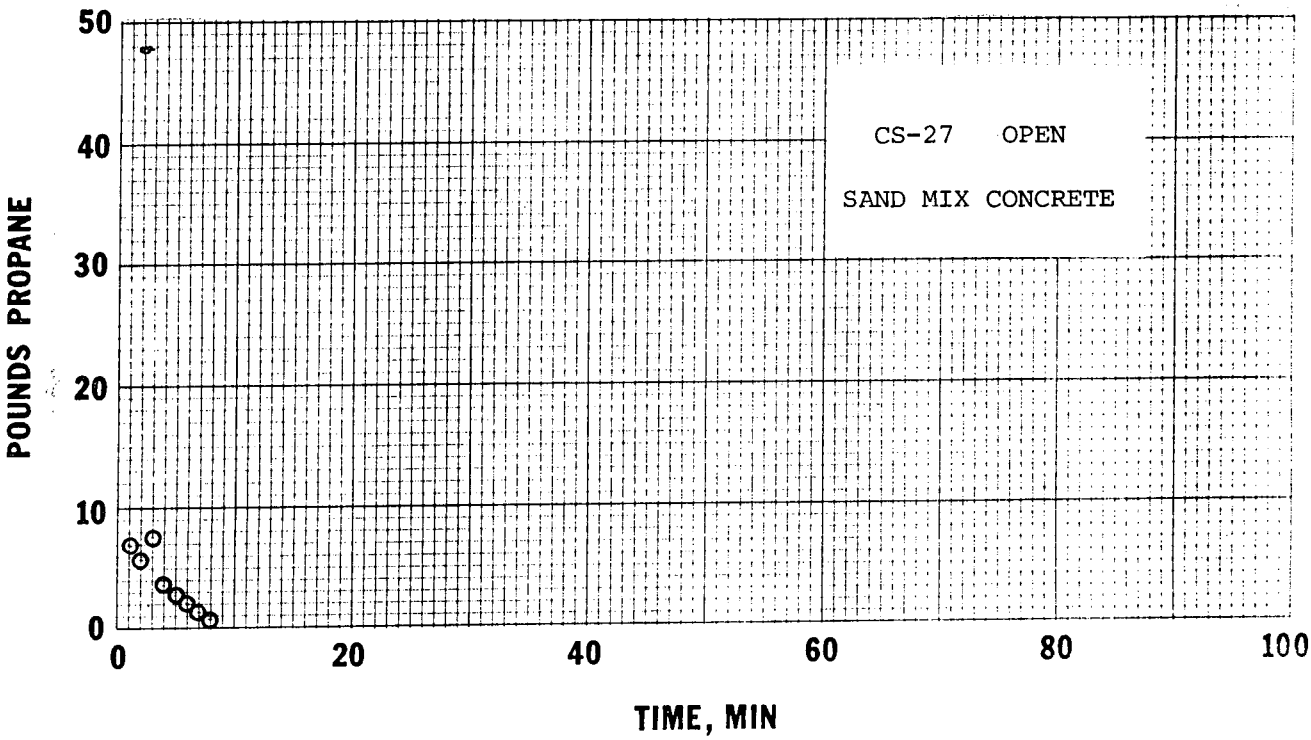

FIGURE A-21. VAPORIZATION OF PROPANE FOLLOWING A SPILL ON SAND MIX CONCRETE.

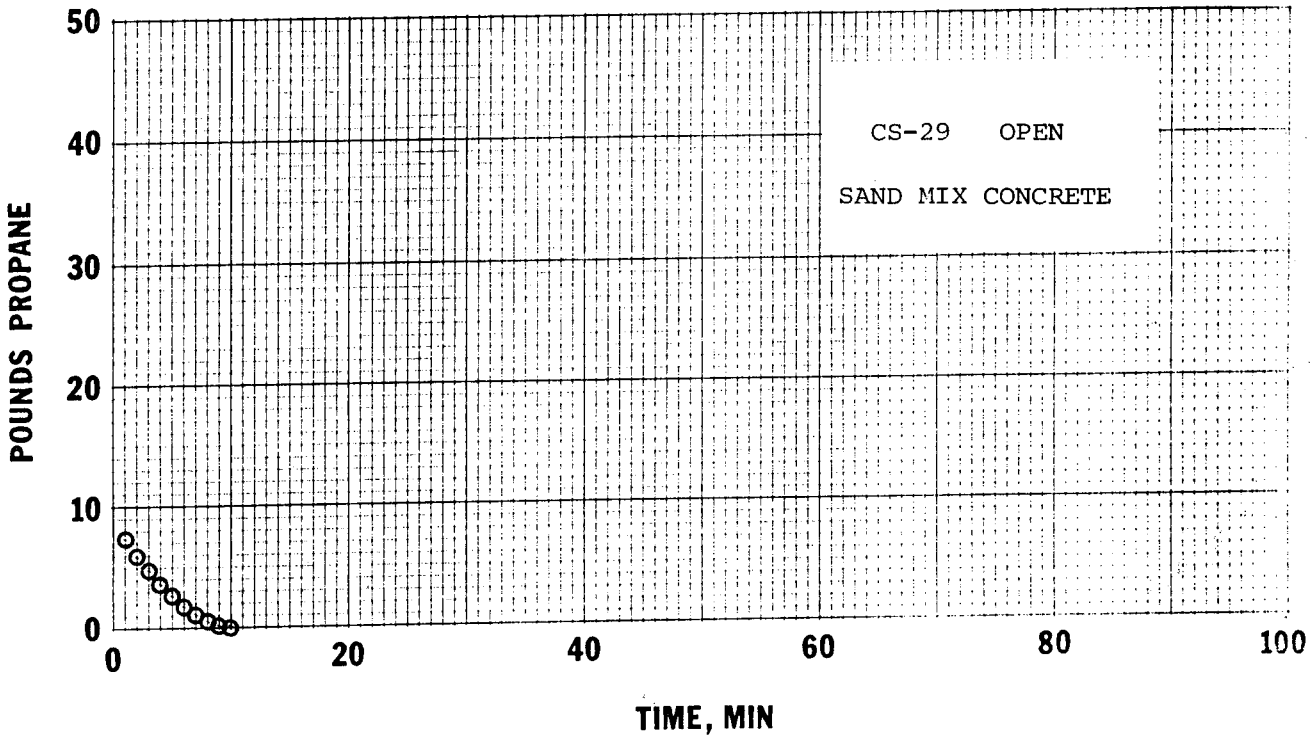

FIGURE A-22. VAPORIZATION OF PROPANE FOLLOWING A SPILL ON SAND MIX CONCRETE.

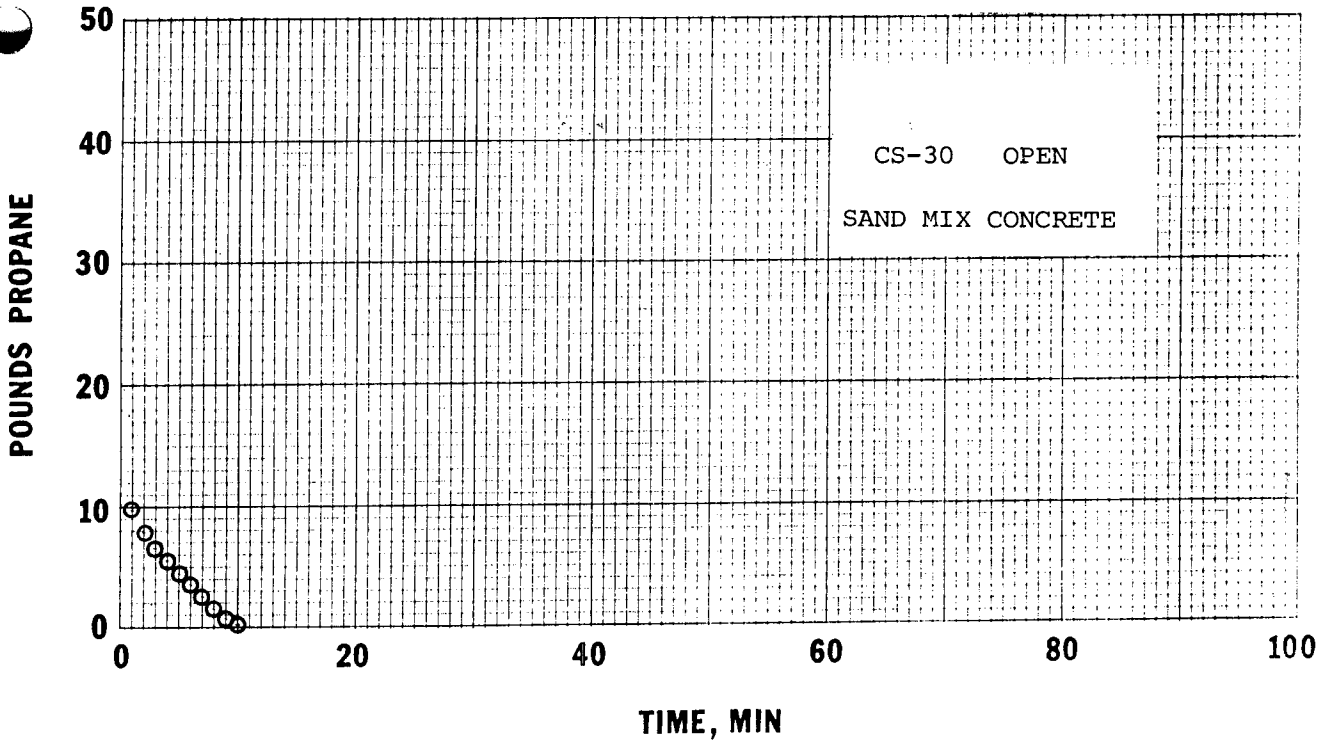

FIGURE A-23. VAPORIZATION OF PROPANE FOLLOWING A SPILL ON SAND MIX CONCRETE.

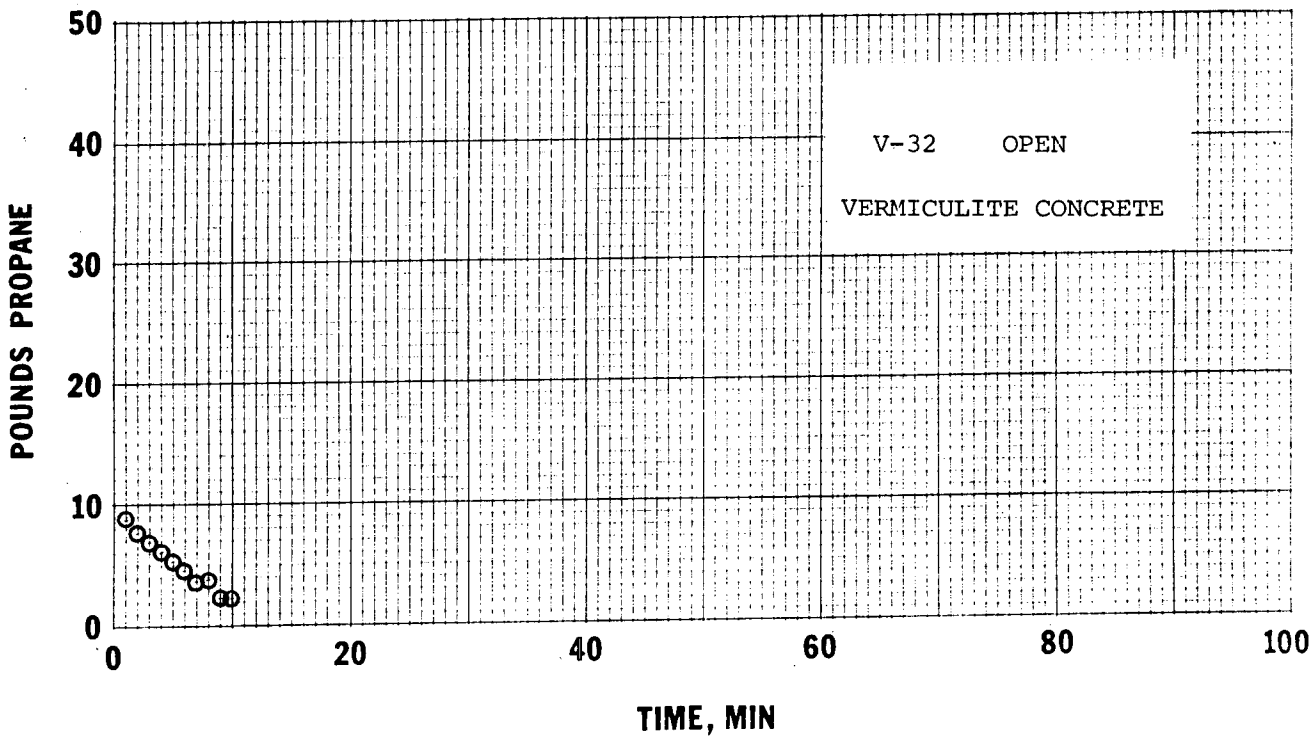

FIGURE A-24. VAPORIZATION OF PROPANE FOLLOWING A SPILL ON VERMICULITE CONCRETE.

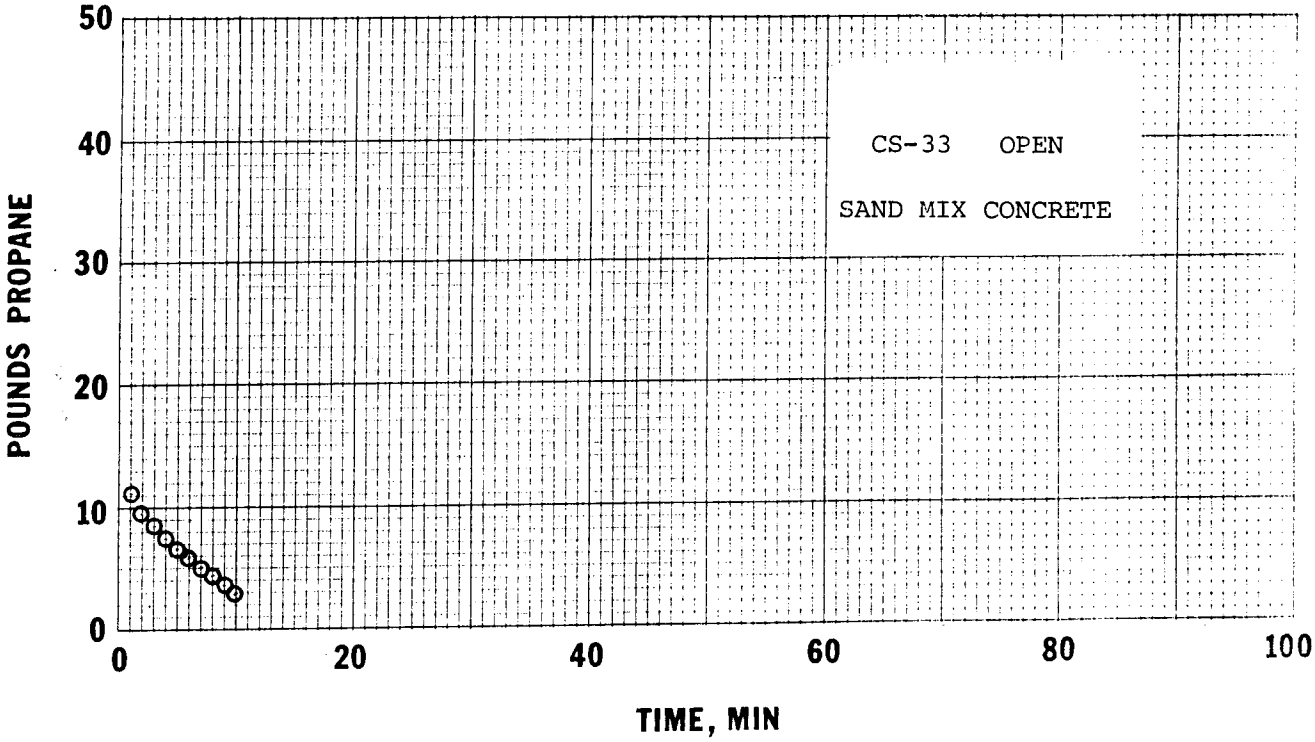

FIGURE A-25. VAPORIZATION OF PROPANE FOLLOWING A SPILL ON SAND MIX CONCRETE.

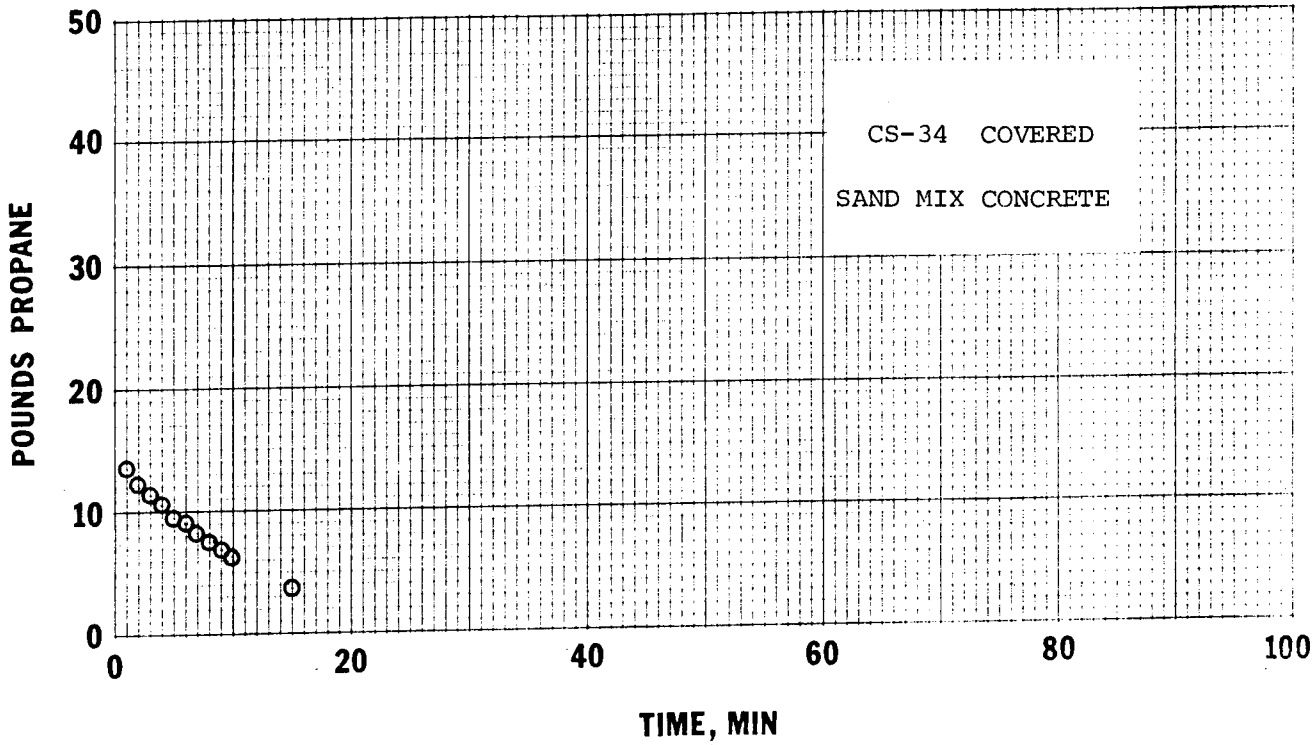

FIGURE A-26. VAPORIZATION OF PROPANE FOLLOWING A SPILL ON SAND MIX CONCRETE.

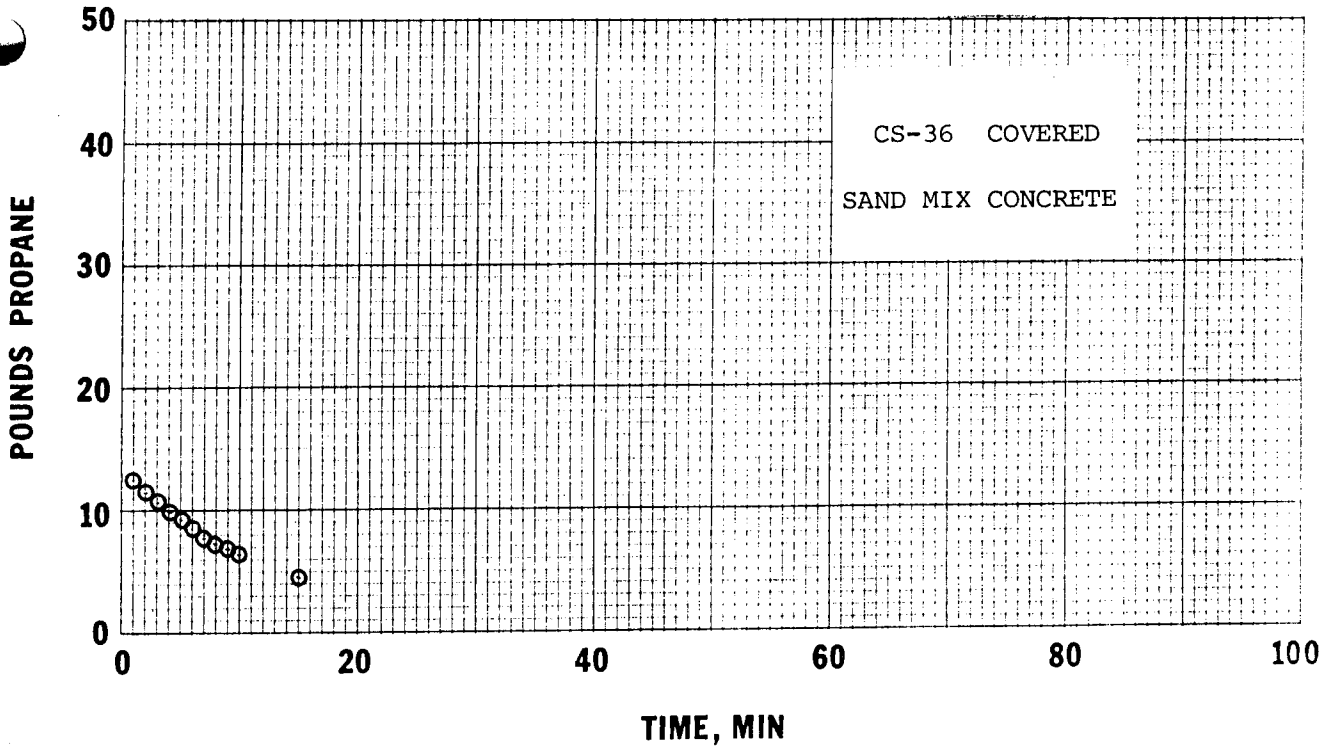

FIGURE A-27. VAPORIZATION OF PROPANE FOLLOWING A SPILL ON SAND MIX CONCRETE.

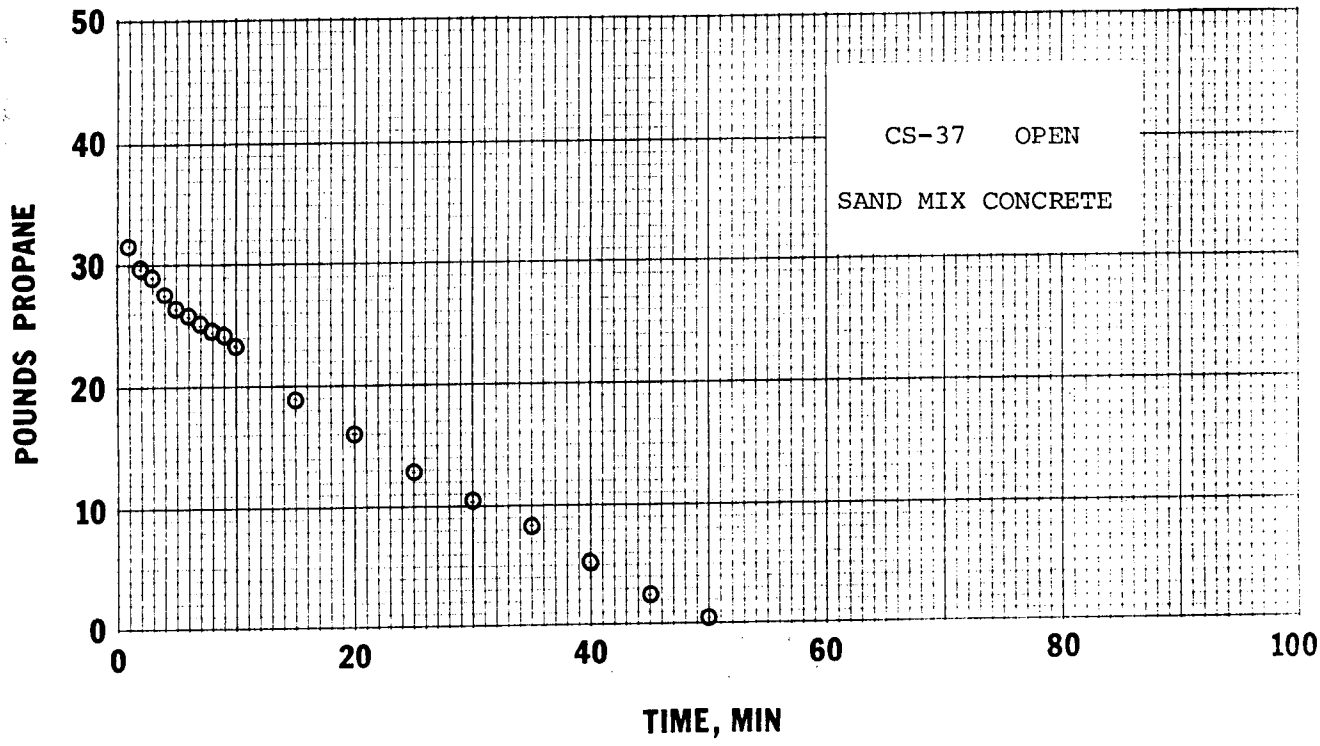

FIGURE A-28. VAPORIZATION OF PROPANE FOLLOWING A SPILL ON SAND MIX CONCRETE.

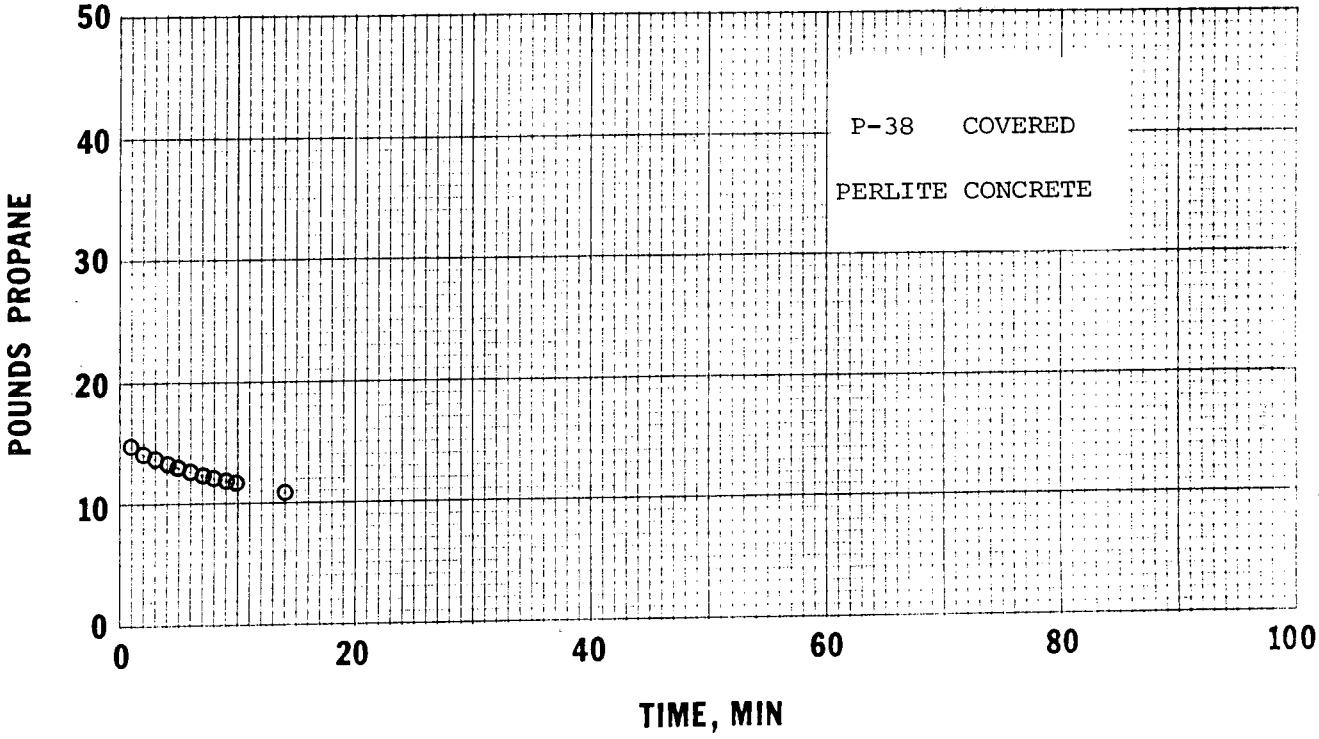

FIGURE A-29. VAPORIZATION OF PROPANE FOLLOWING A SPILL ON PERLITE CONCRETE.

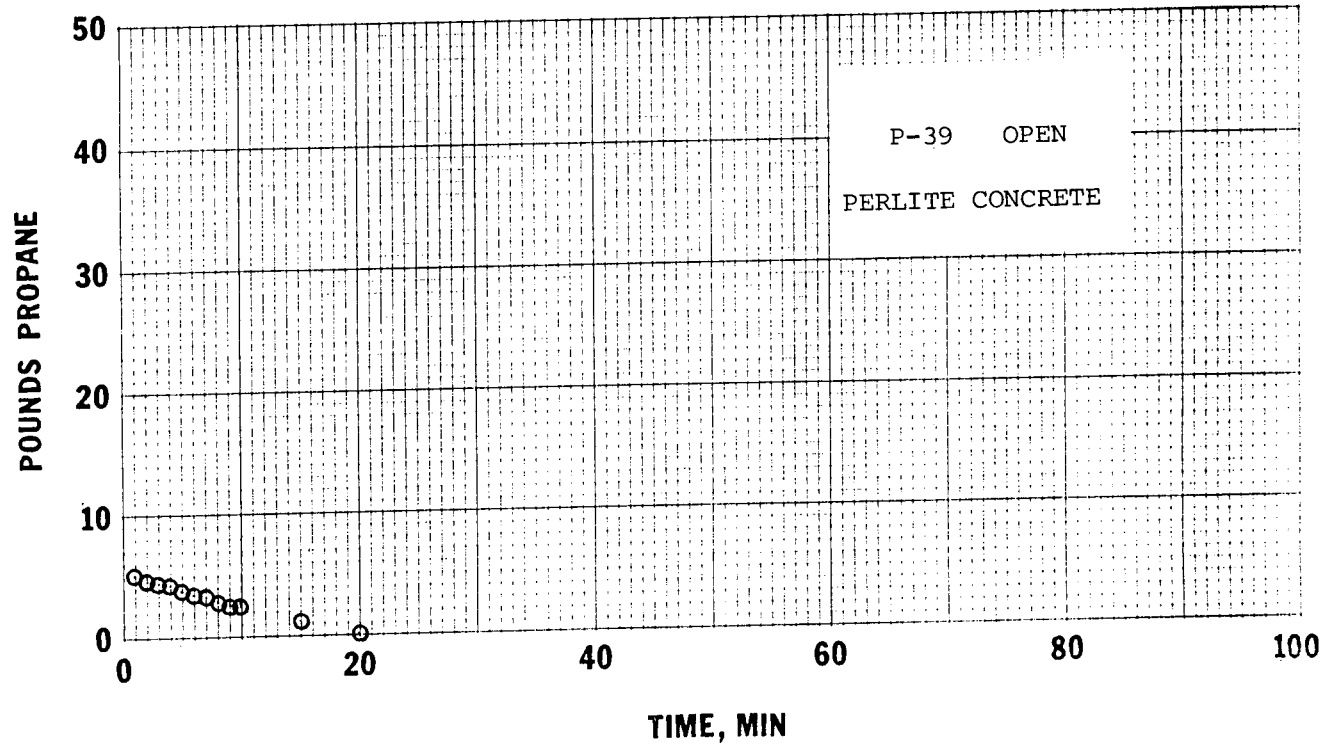

FIGURE A-30. VAPORIZATION OF PROPANE FOLLOWING A SPILL ON PERLITE CONCRETE.

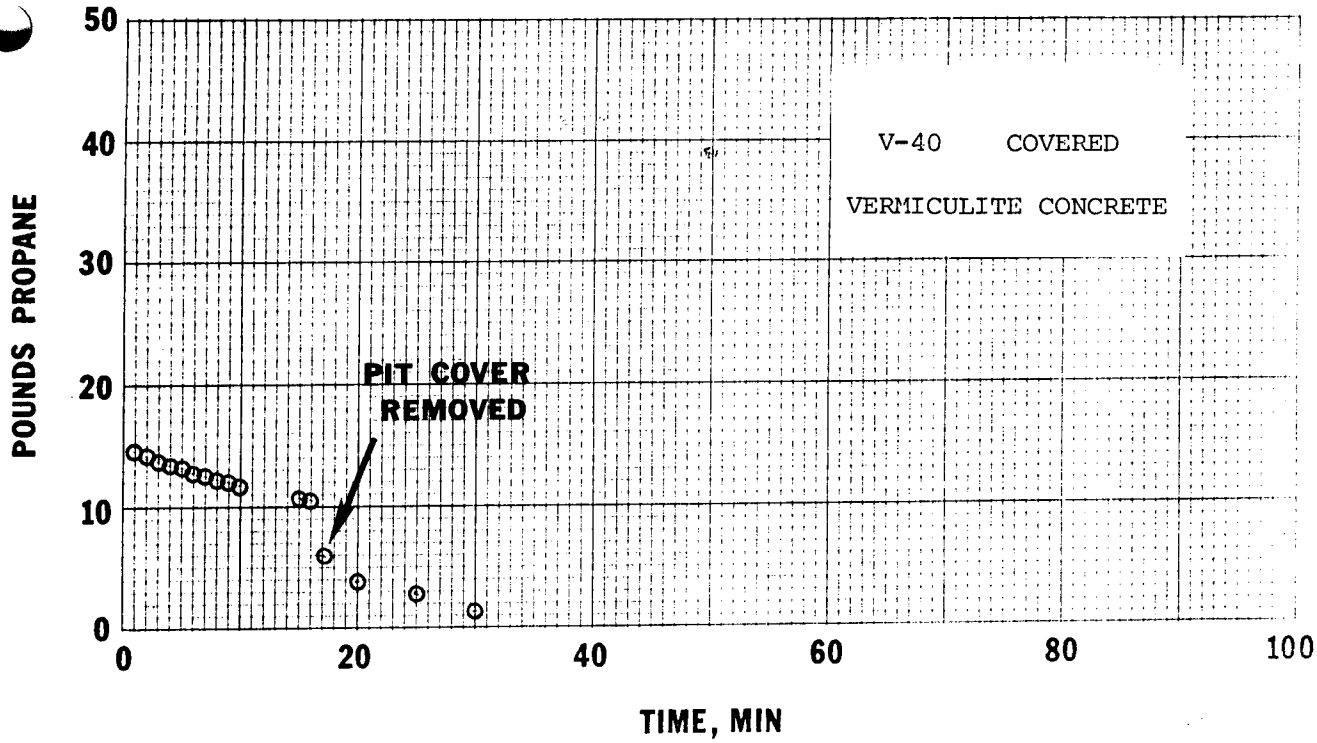

FIGURE A-31. VAPORIZATION OF PROPANE FOLLOWING A SPILL ON VERMICULITE CONCRETE.

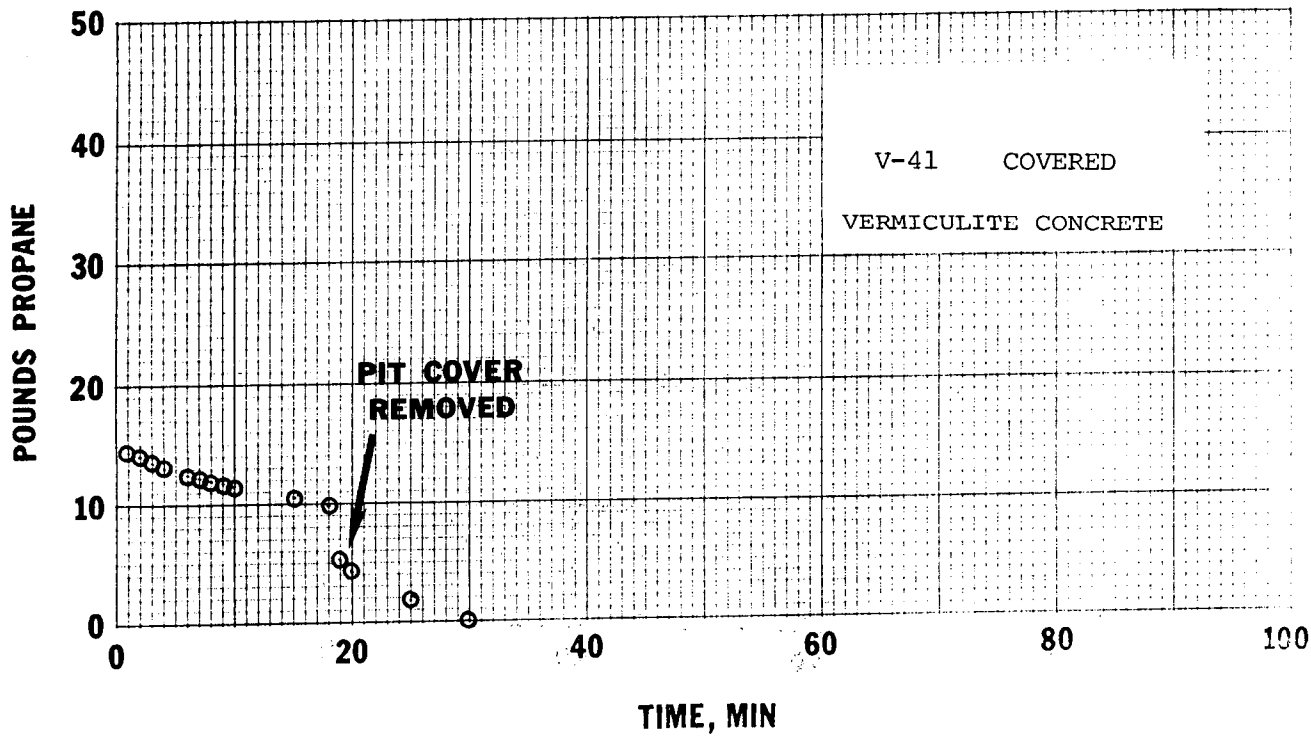

FIGURE A-32. VAPORIZATION OF PROPANE FOLLOWING A SPILL ON VERMICULITE CONCRETE.

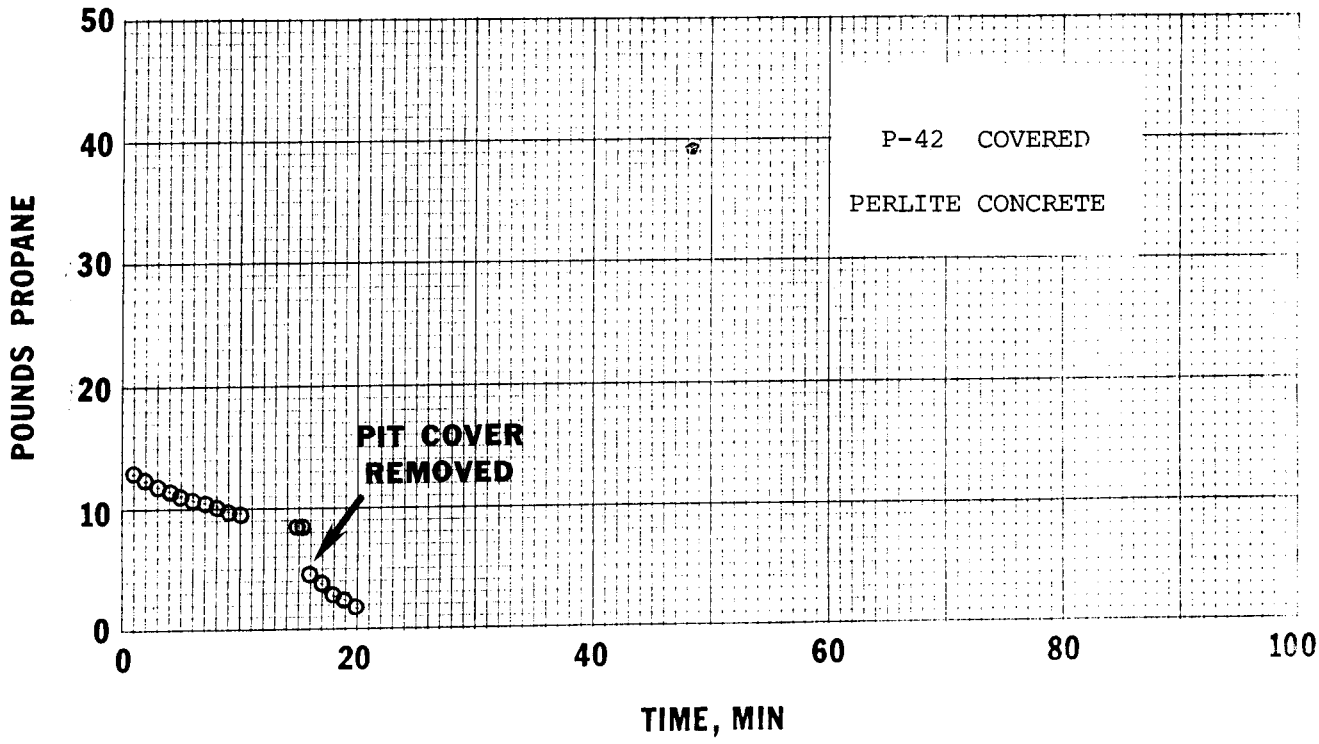

FIGURE A-33. VAPORIZATION OF PROPANE FOLLOWING A SPILL ON PERLITE CONCRETE.

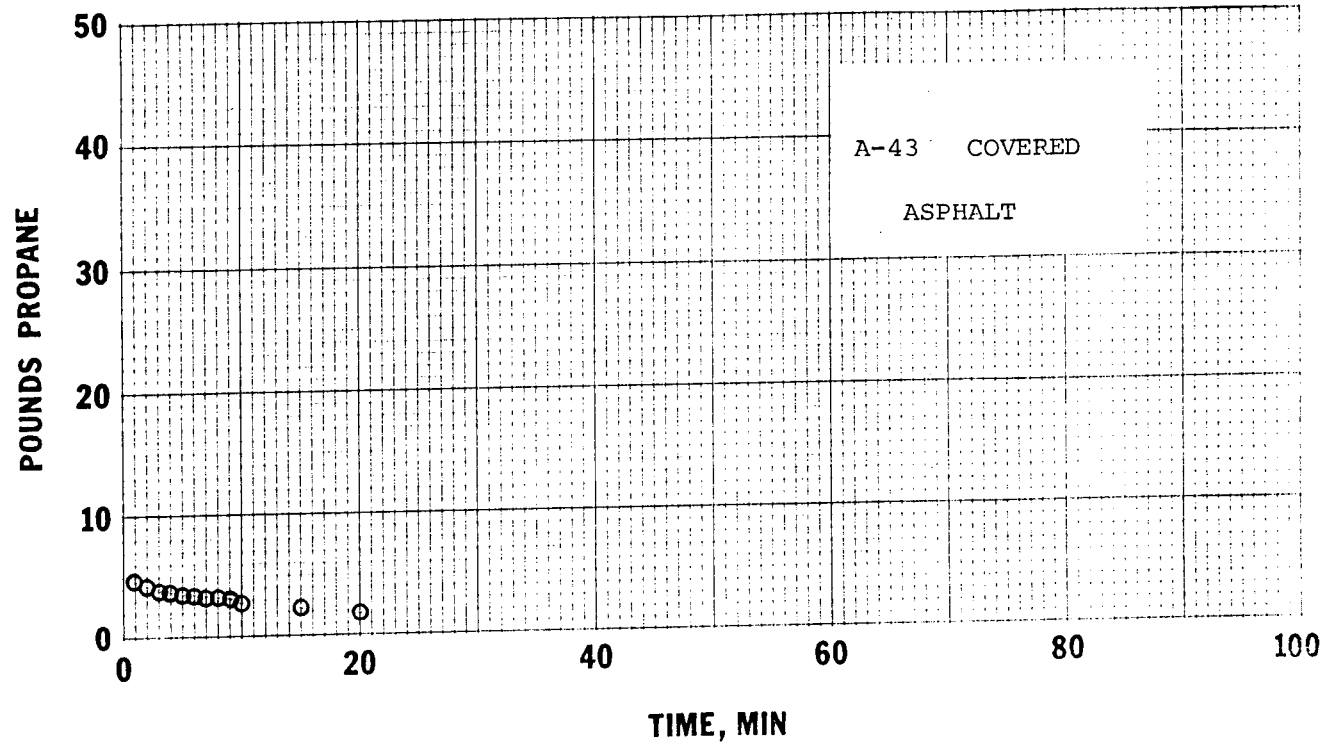

FIGURE A-34. VAPORIZATION OF PROPANE FOLLOWING A SPILL ON ASPHALT.

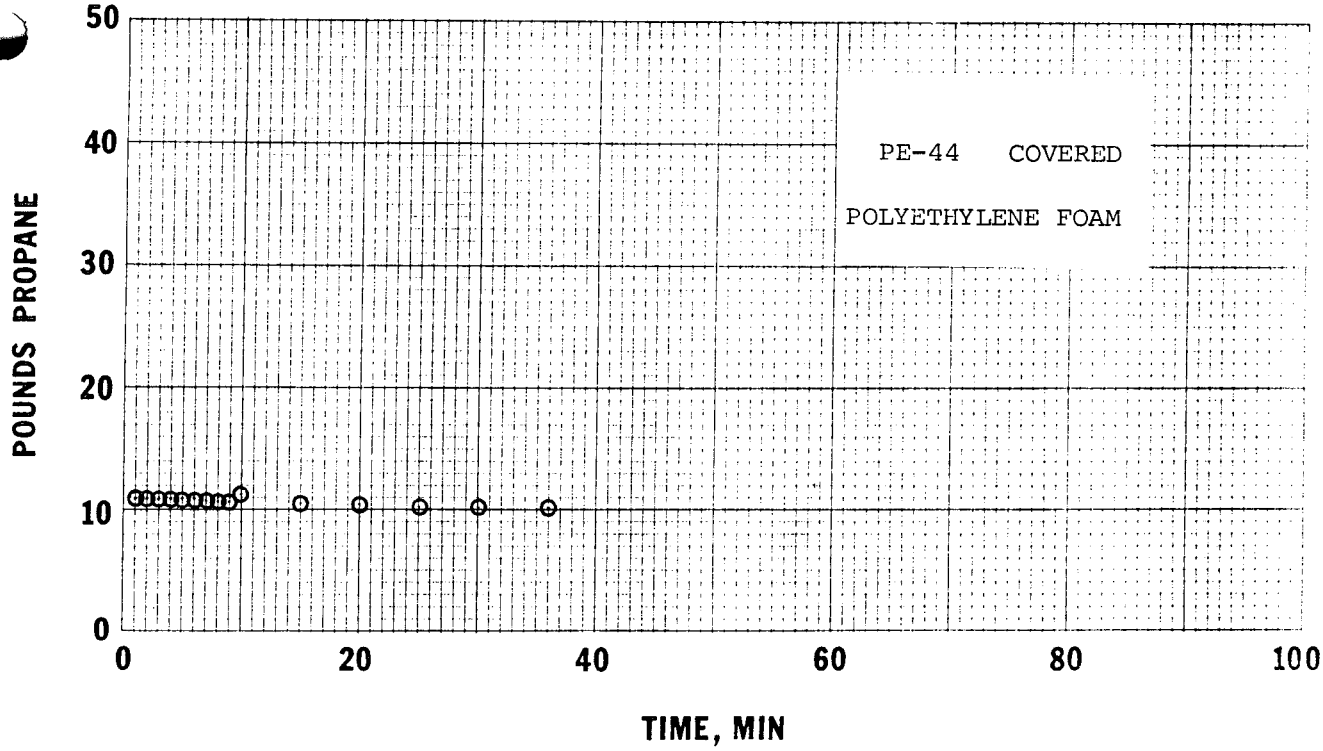

FIGURE A-35. VAPORIZATION OF PROPANE FOLLOWING A SPILL ON POLYETHYLENE FOAM.

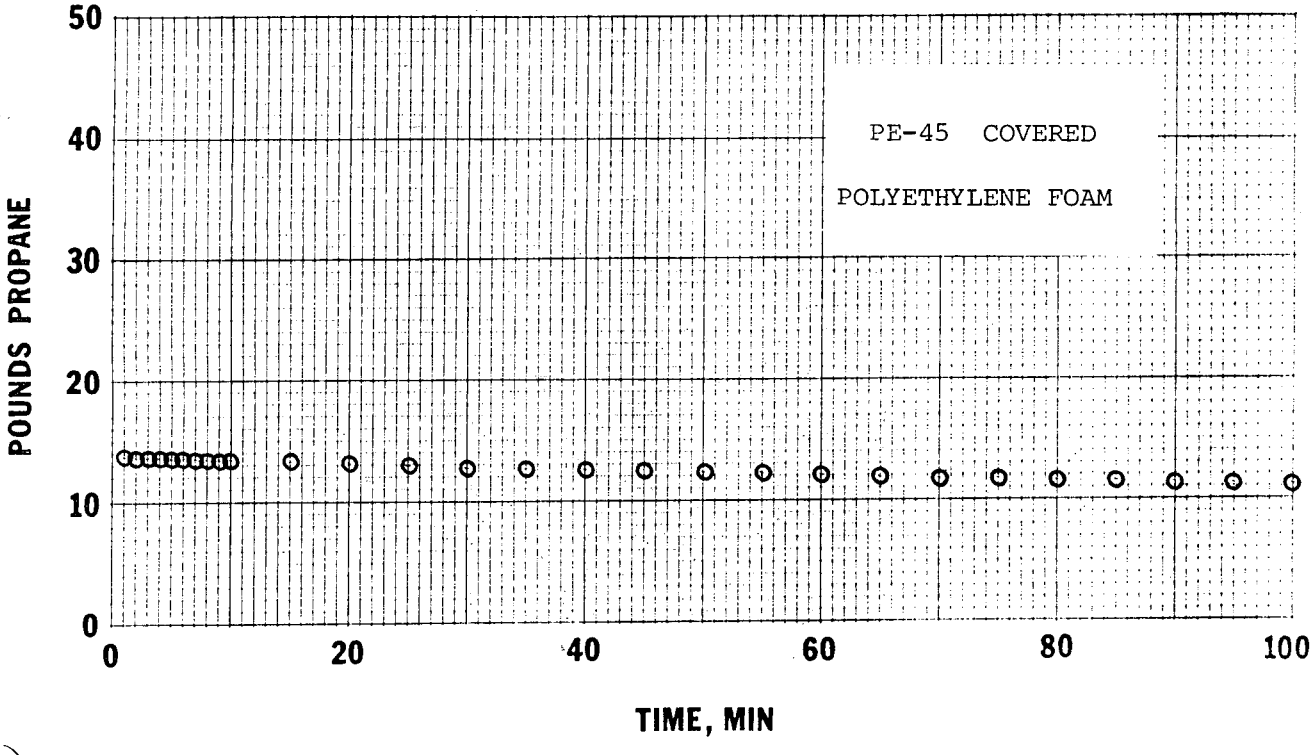

FIGURE A-36. VAPORIZATION OF PROPANE FOLLOWING A SPILL ON POLYETHYLENE FOAM.

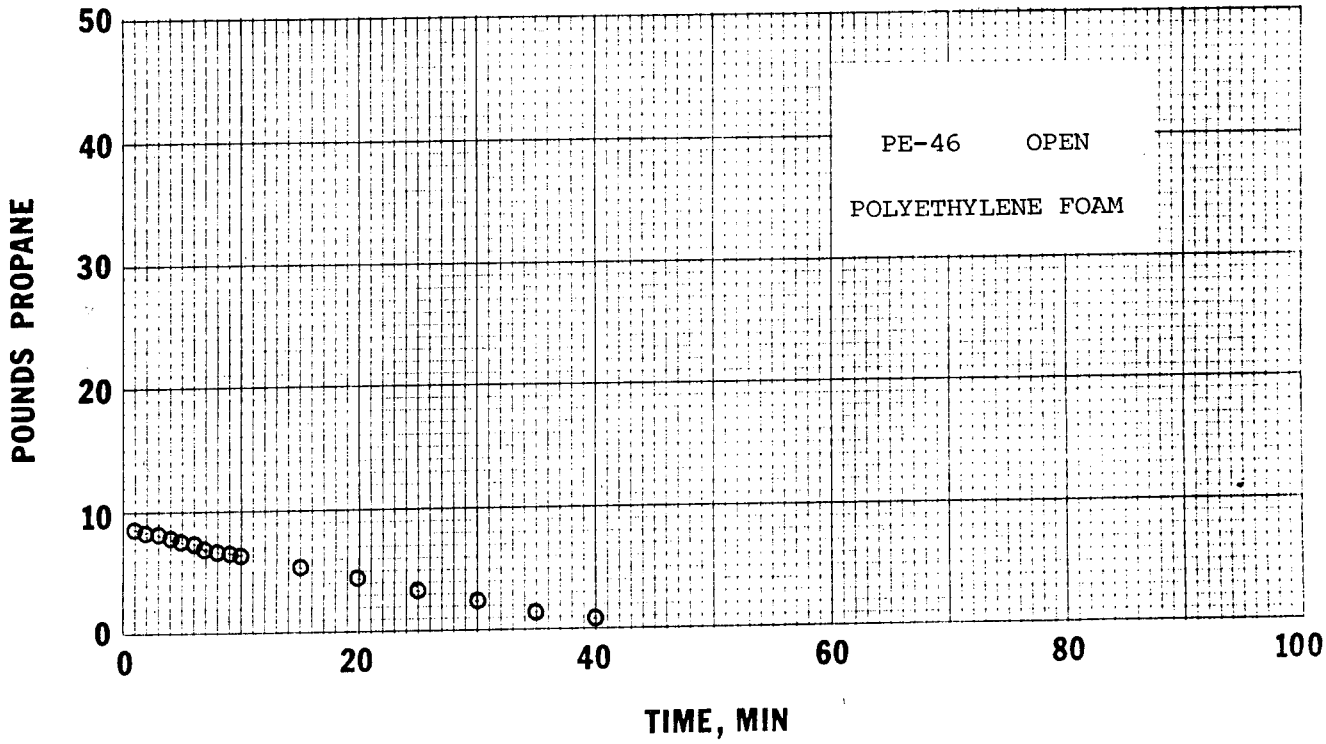

FIGURE A-37. VAPORIZATION OF PROPANE FOLLOWING A SPILL ON POLYETHYLENE FOAM.

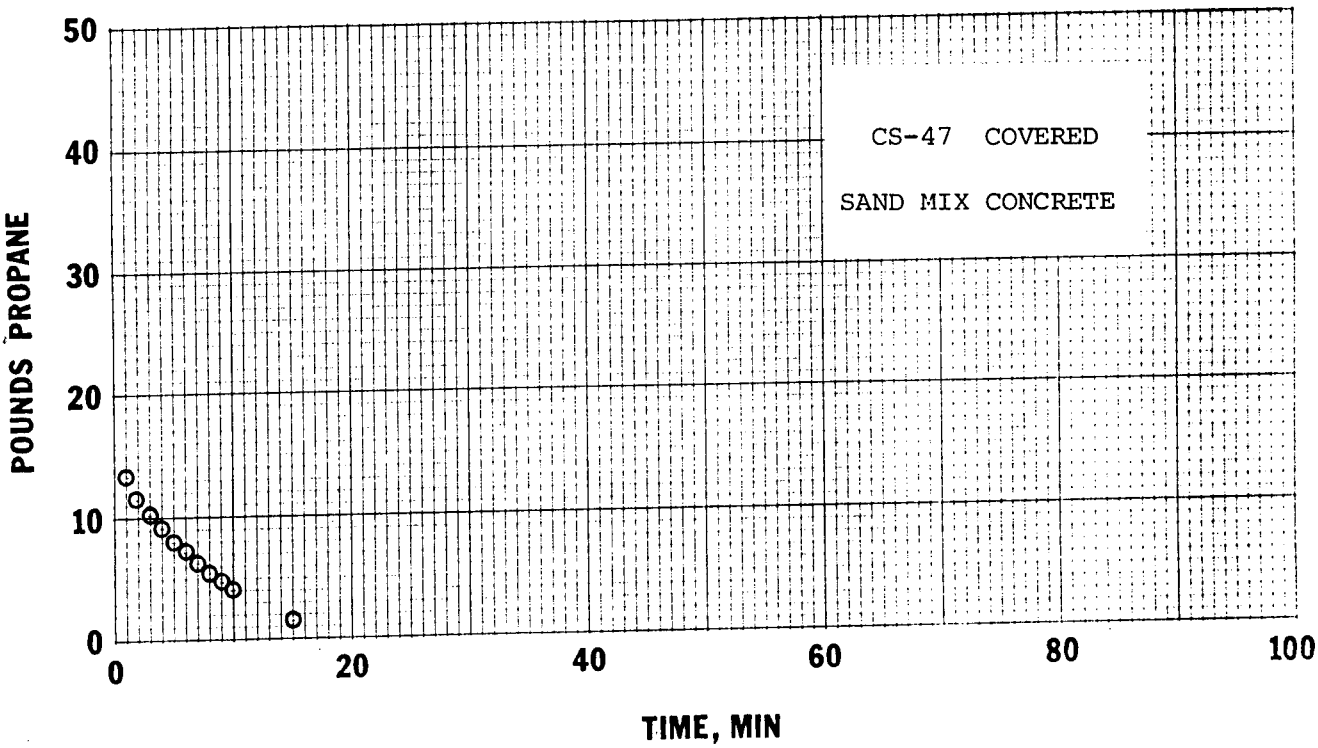

FIGURE A-38. VAPORIZATION OF PROPANE FOLLOWING A SPILL ON SAND MIX CONCRETE.

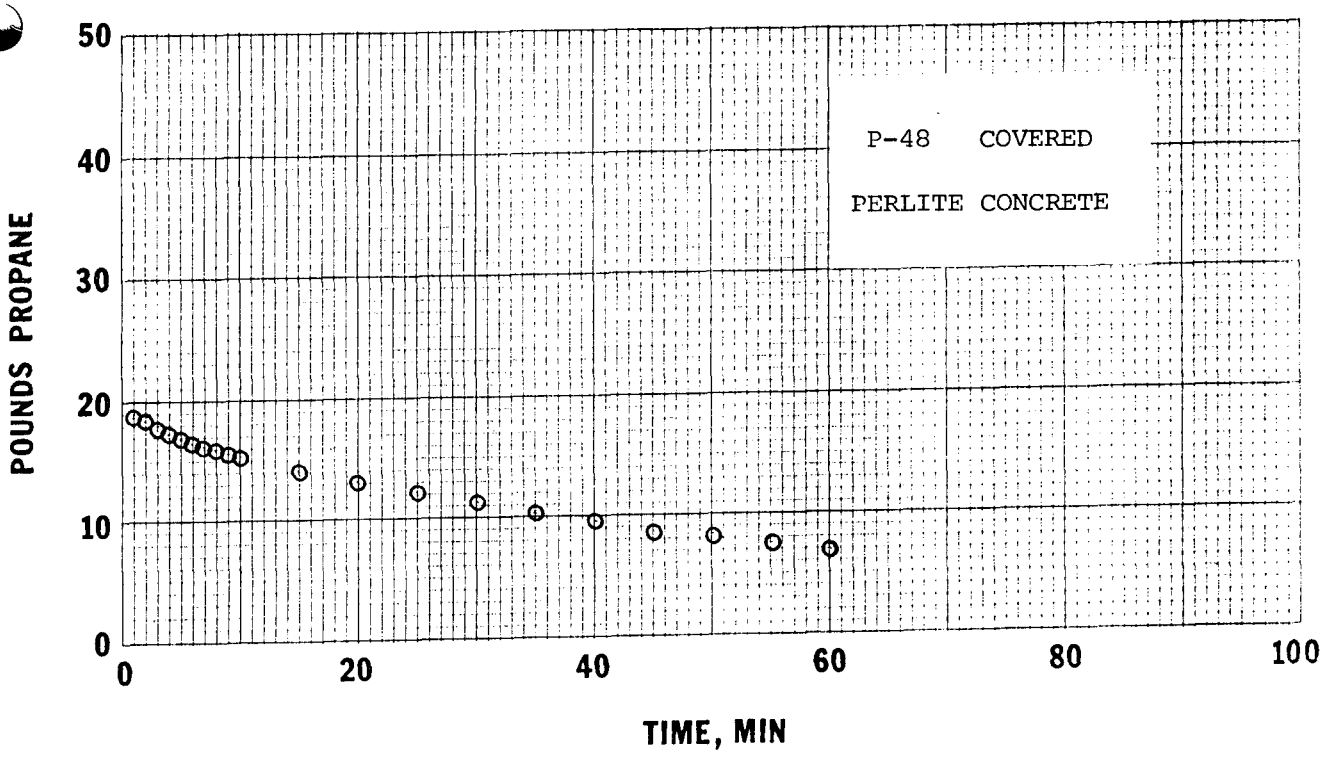

FIGURE A-39. VAPORIZATION OF PROPANE FOLLOWING A SPILL ON PERLITE CONCRETE.

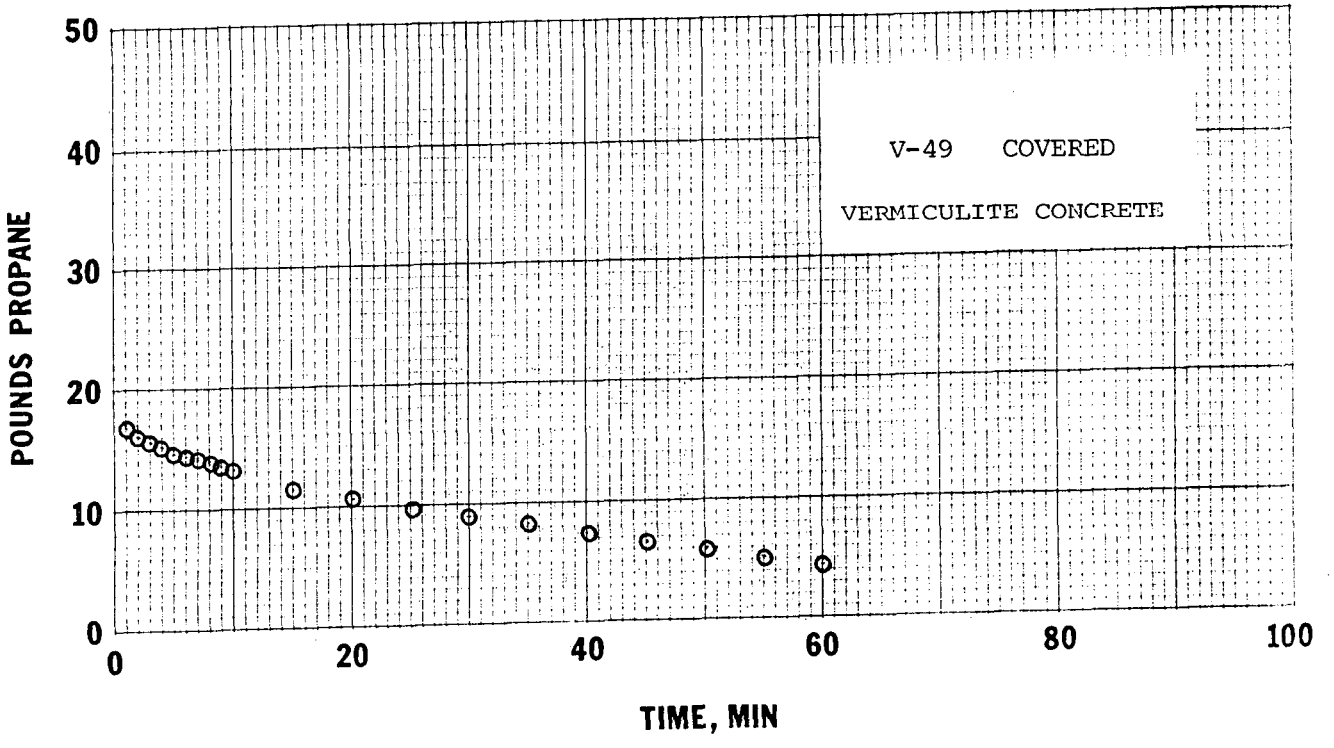

FIGURE A-40. VAPORIZATION OF PROPANE FOLLOWING A SPILL ON VERMICULITE CONCRETE.

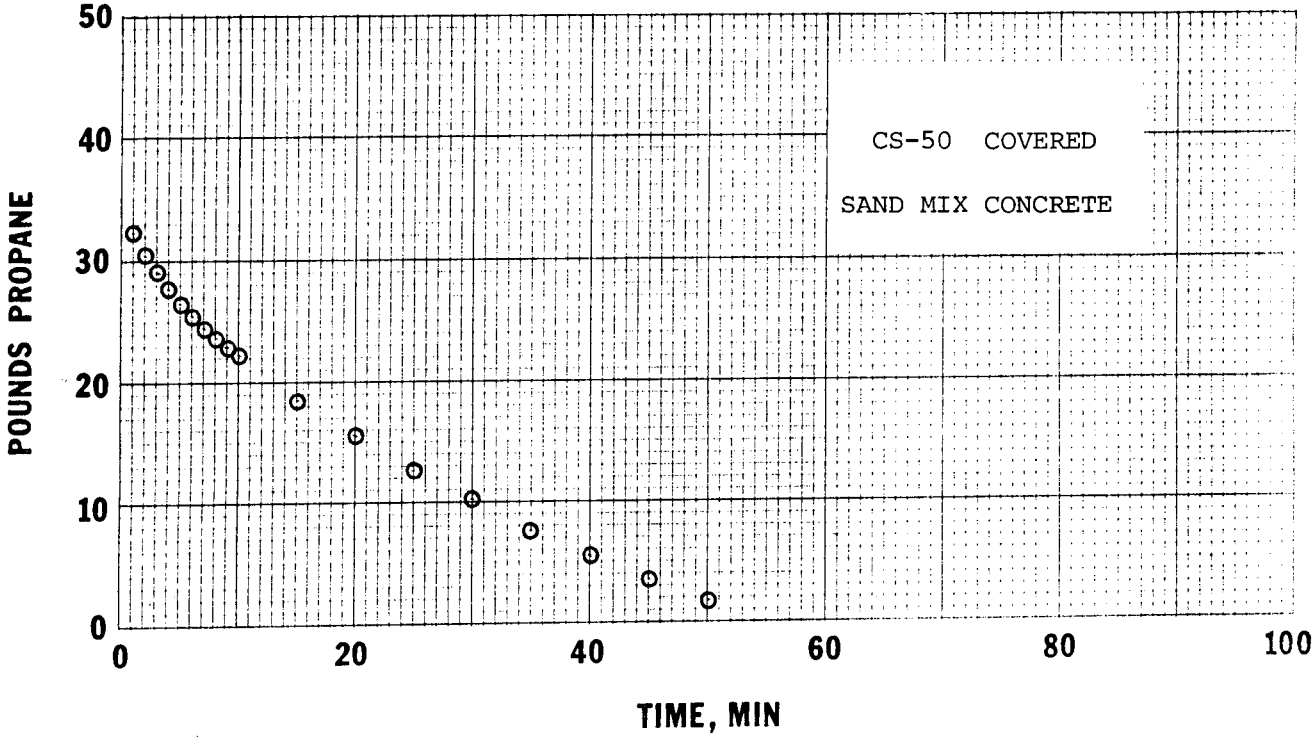

FIGURE A-41. VAPORIZATION OF PROPANE FOLLOWING A SPILL ON SAND MIX CONCRETE.

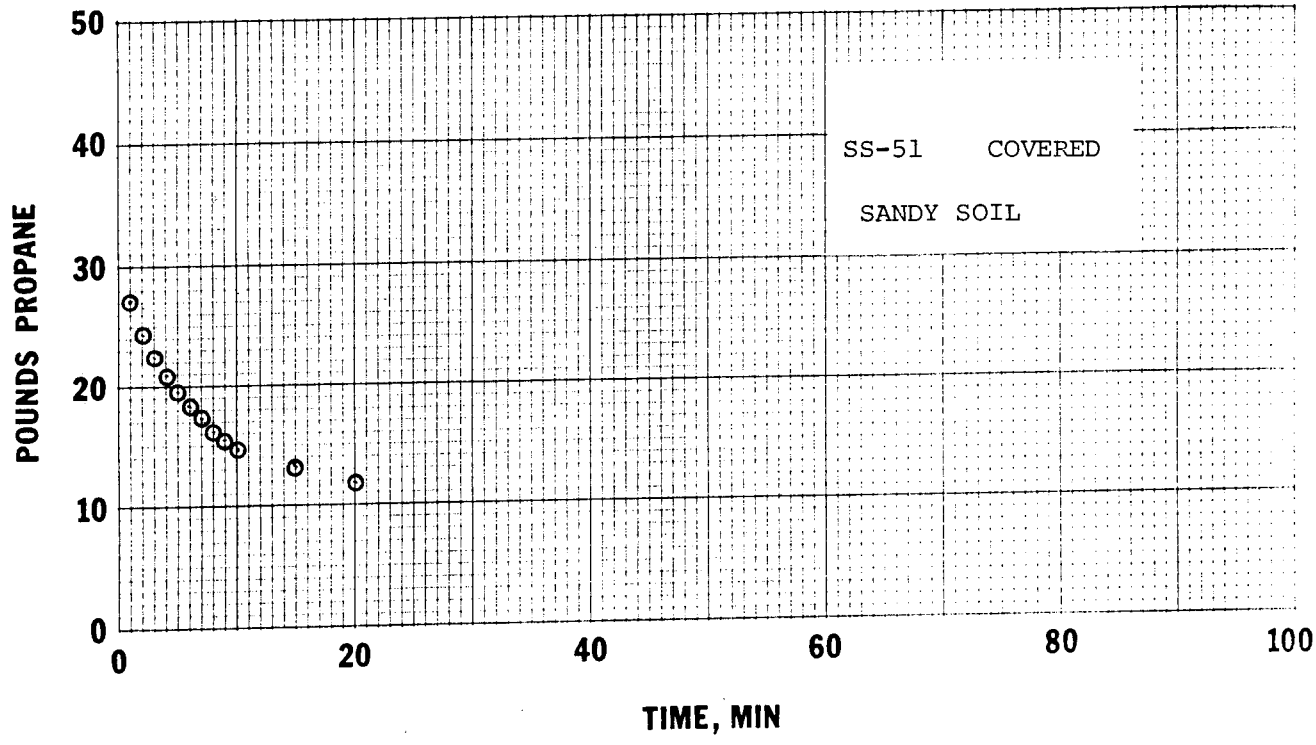

FIGURE A-42. VAPORIZATION OF PROPANE FOLLOWING A SPILL ON SANDY SOIL.

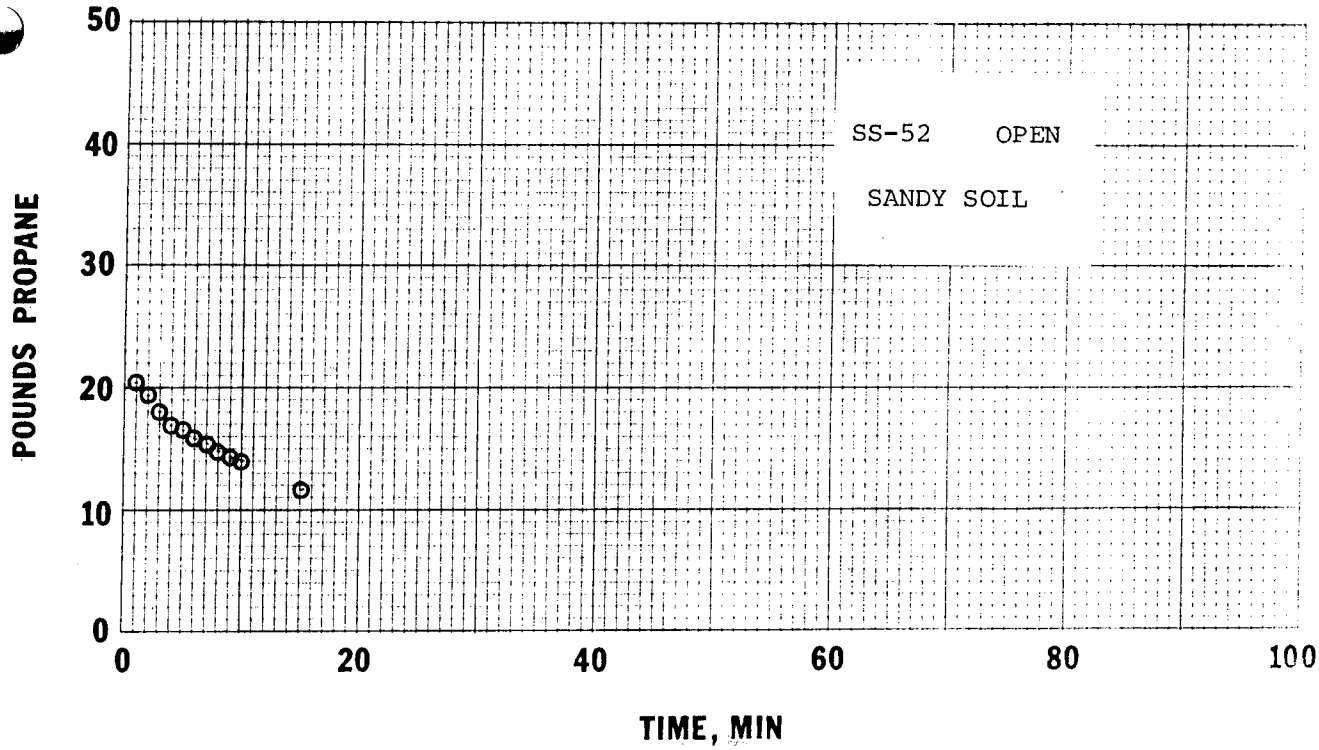

FIGURE A-43. VAPORIZATION OF PROPANE FOLLOWING A SPILL ON SANDY SOIL.

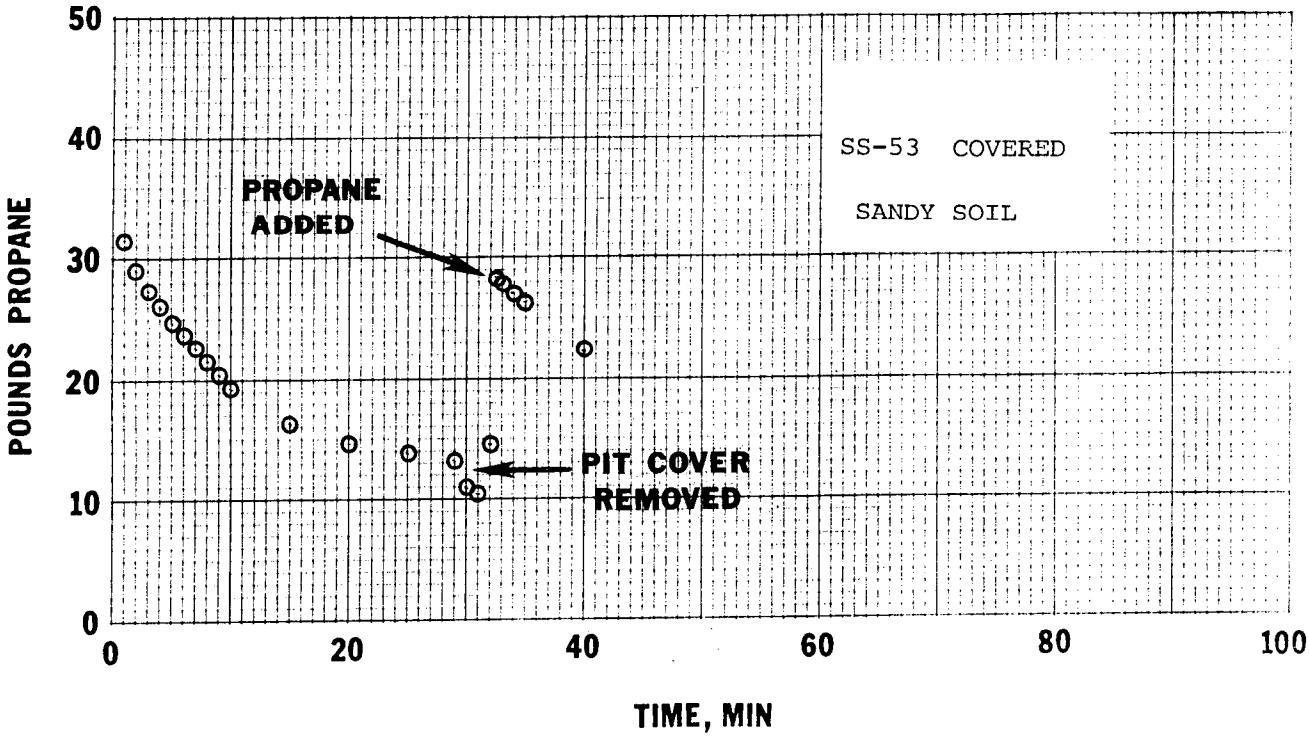

FIGURE A-44. VAPORIZATION OF PROPANE FOLLOWING A SPILL ON SANDY SOIL.

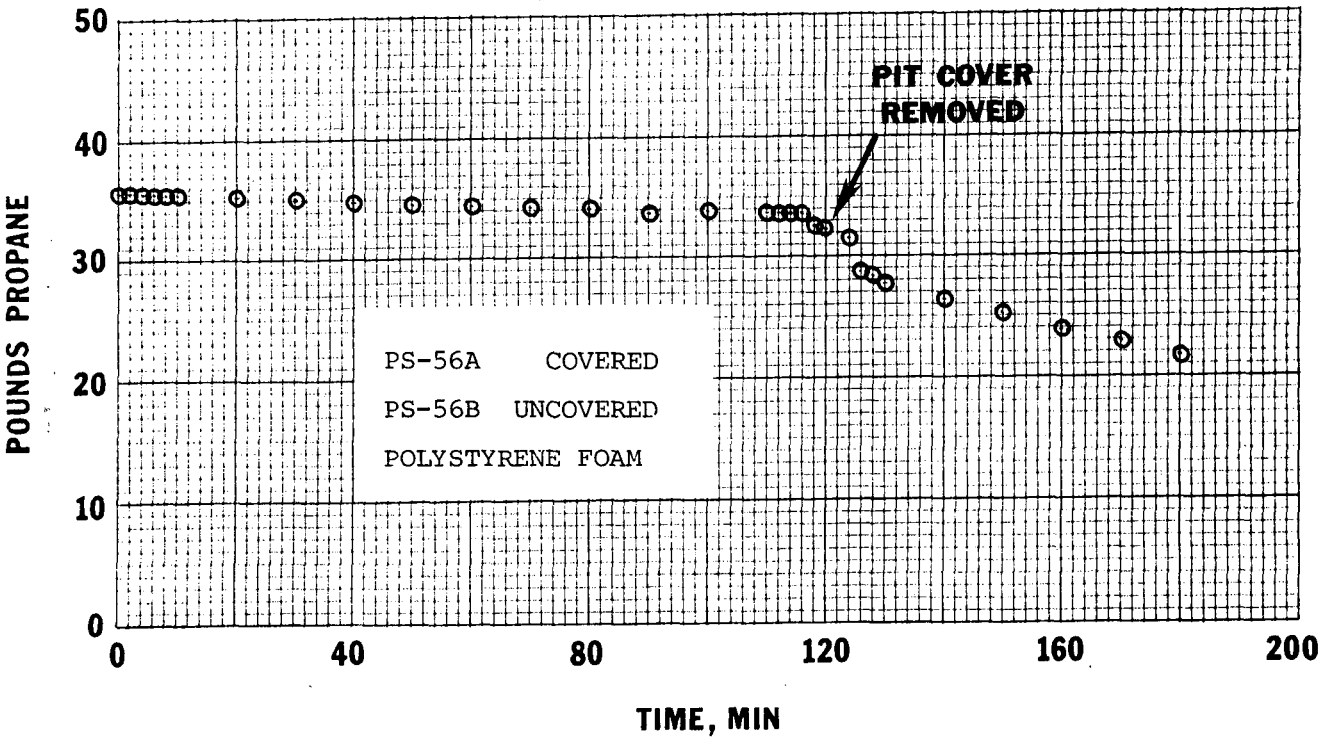

FIGURE A-45. VAPORIZATION OF PROPANE FOLLOWING A SPILL ON POLYSTYRENE FOAM.

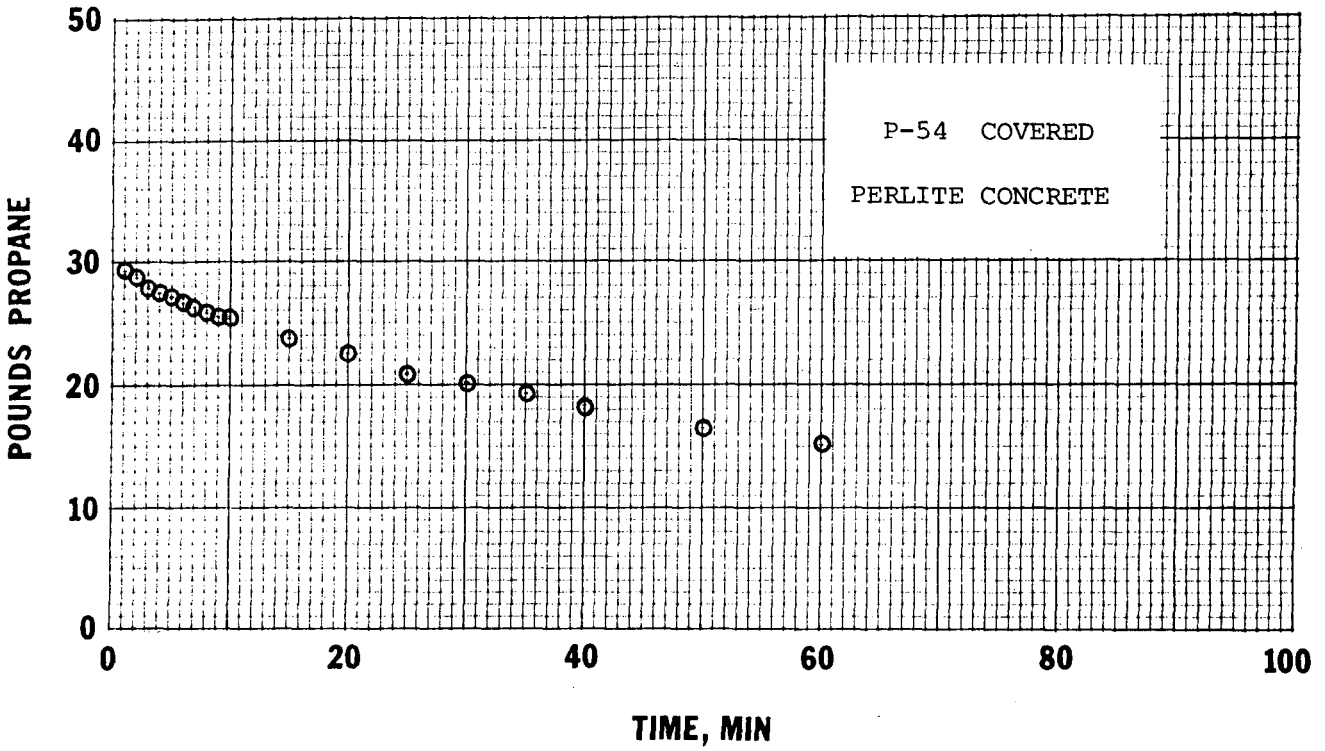

FIGURE A-46. VAPORIZATION OF PROPANE FOLLOWING A SPILL ON PERLITE CONCRETE.

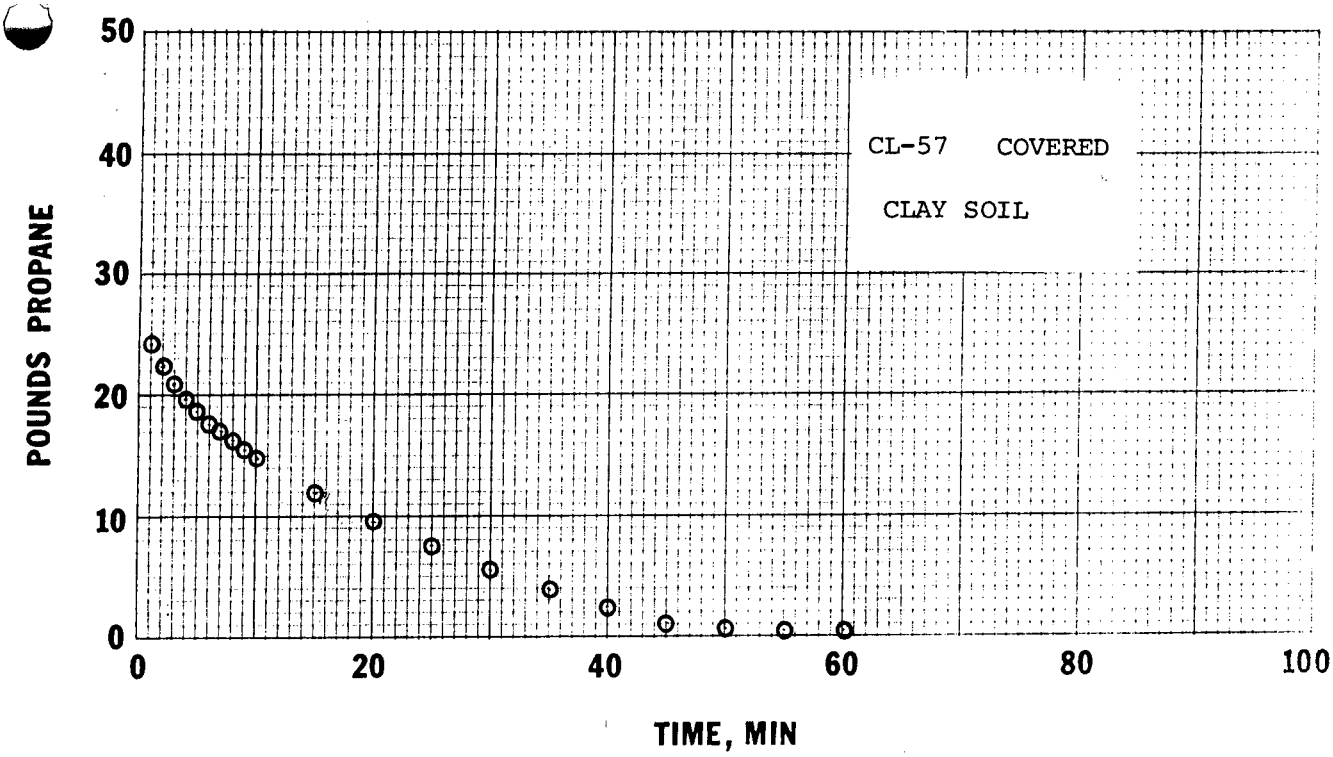

FIGURE A-47. VAPORIZATION OF PROPANE FOLLOWING A SPILL ON CLAY SOIL.

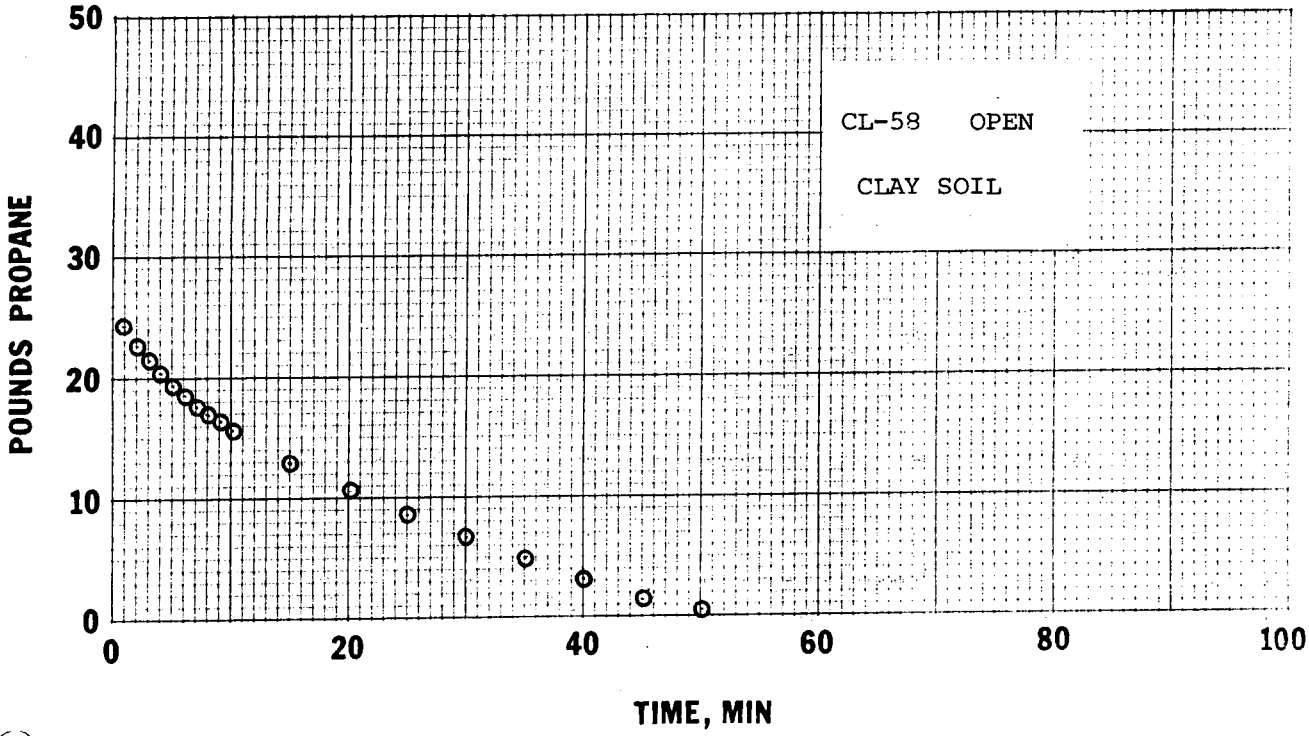

FIGURE A-48. VAPORIZATION OF PROPANE FOLLOWING A SPILL ON CLAY SOIL.

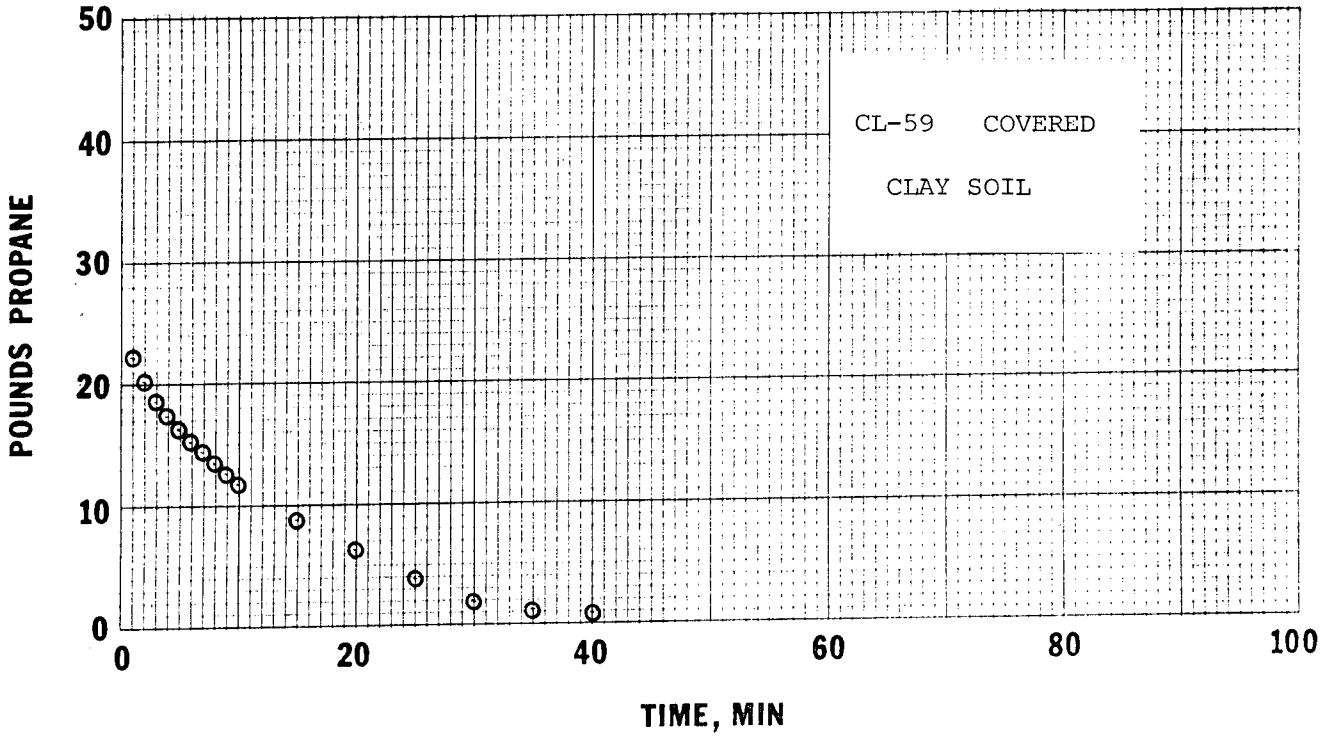

FIGURE A-49. VAPORIZATION OF PROPANE FOLLOWING A SPILL ON CLAY SOIL.

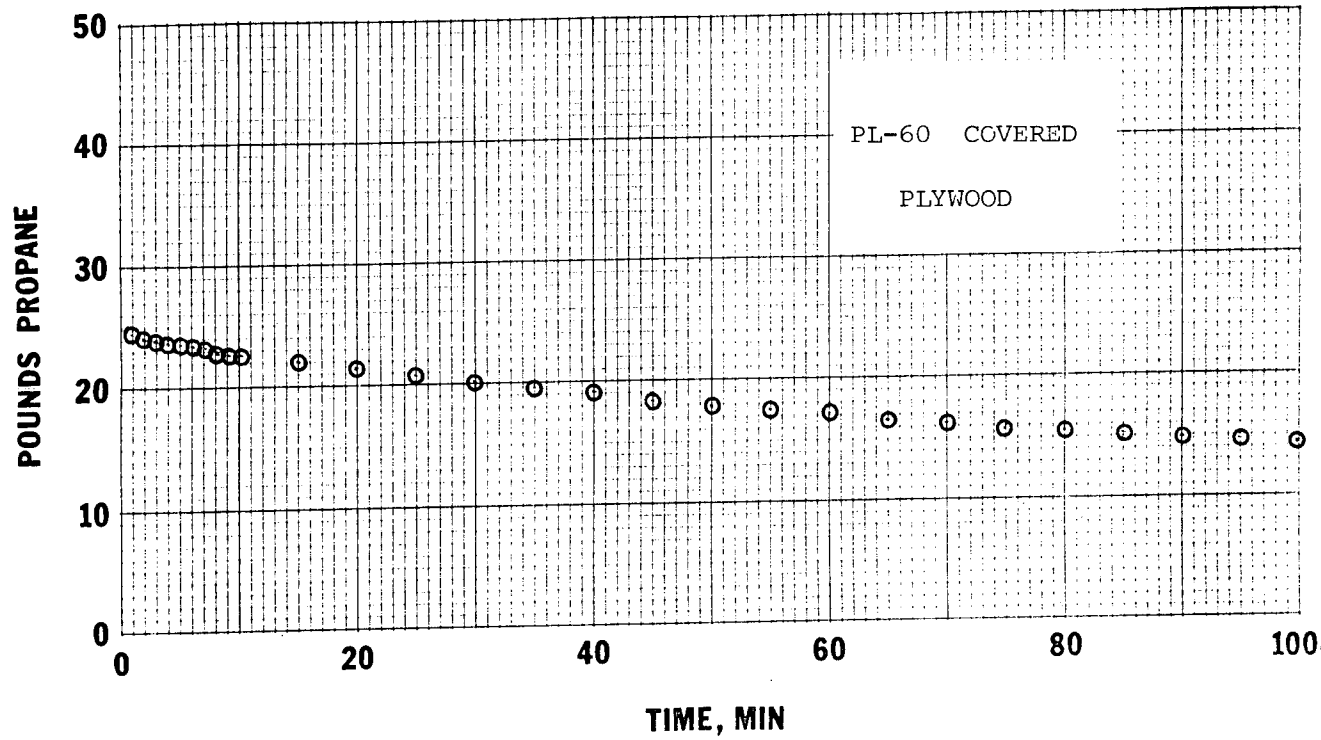

FIGURE A-50. VAPORIZATION OF PROPANE FOLLOWING A SPILL ON PLYWOOD.

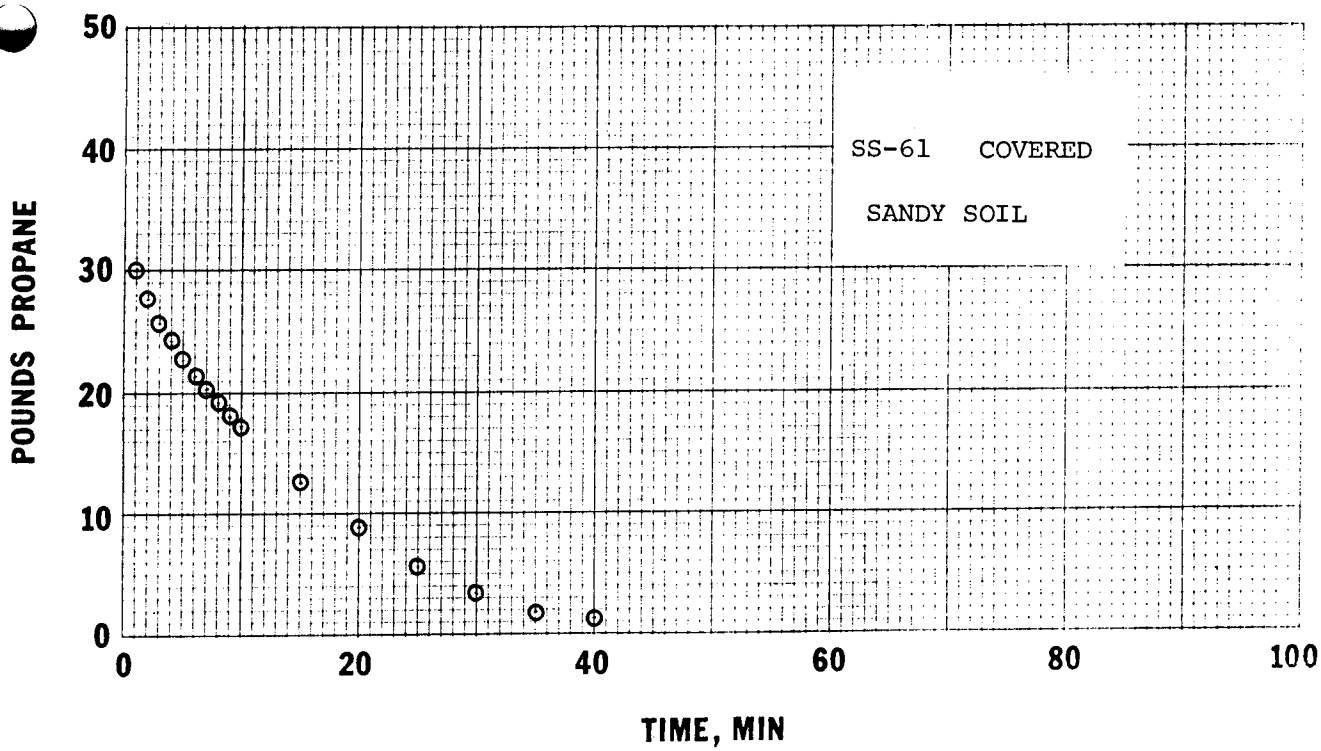

FIGURE A-51. VAPORIZATION OF PROPANE FOLLOWING A SPILL ON SANDY SOIL.

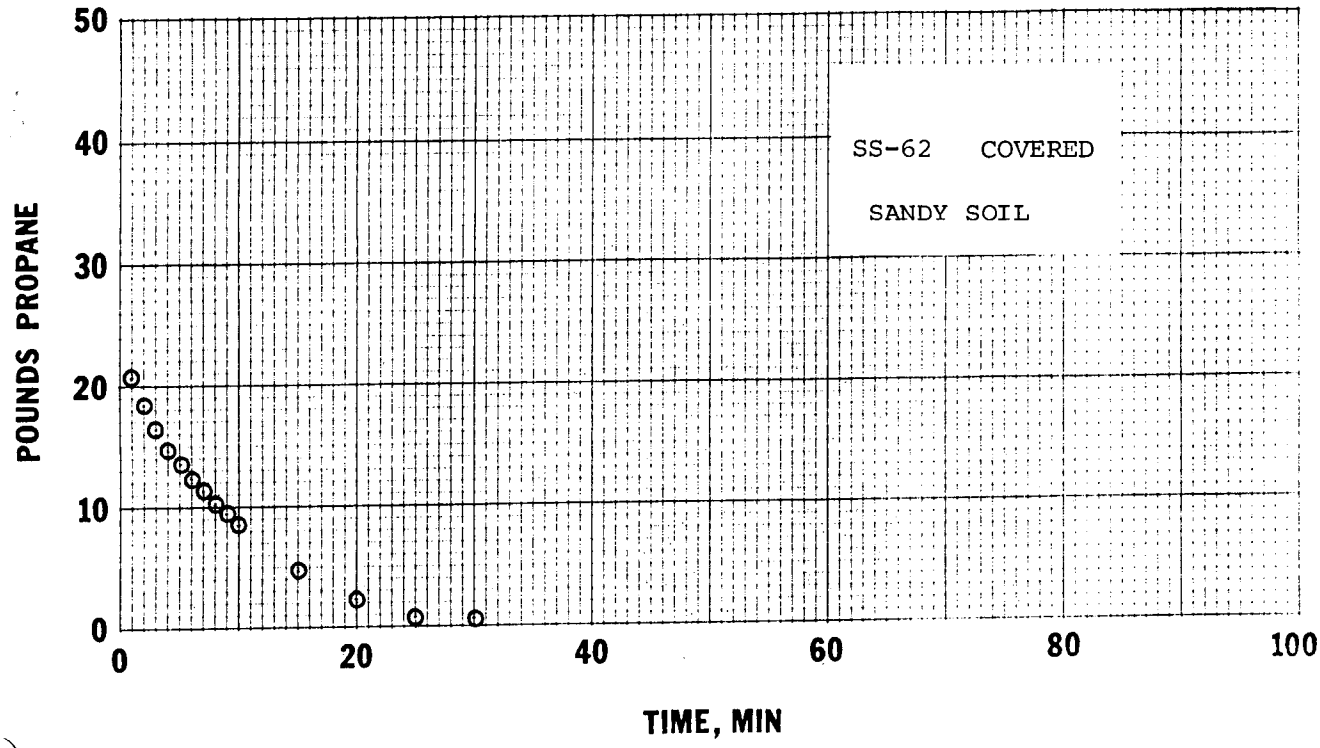

FIGURE A-52. VAPORIZATION OF PROPANE FOLLOWING A SPILL ON SANDY SOIL.

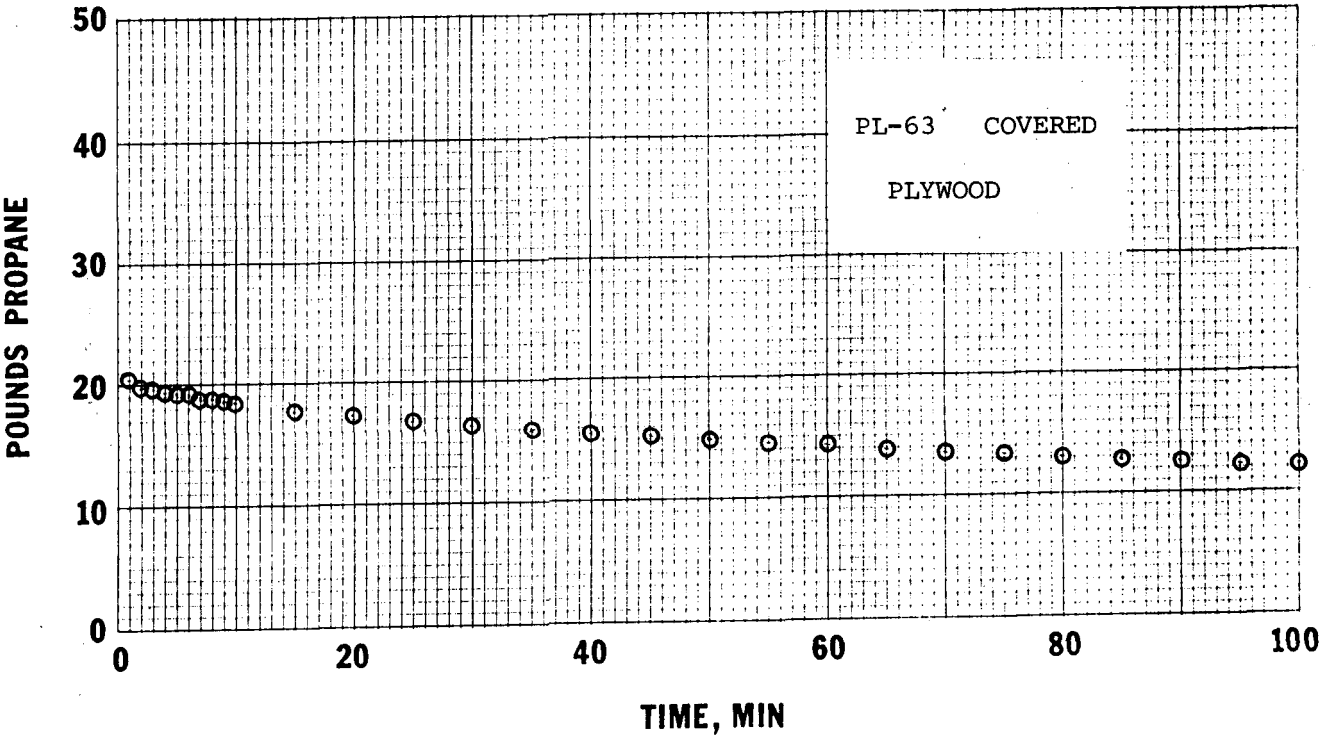

FIGURE A-53. VAPORIZATION OF PROPANE FOLLOWING A SPILL ON PLYWOOD.

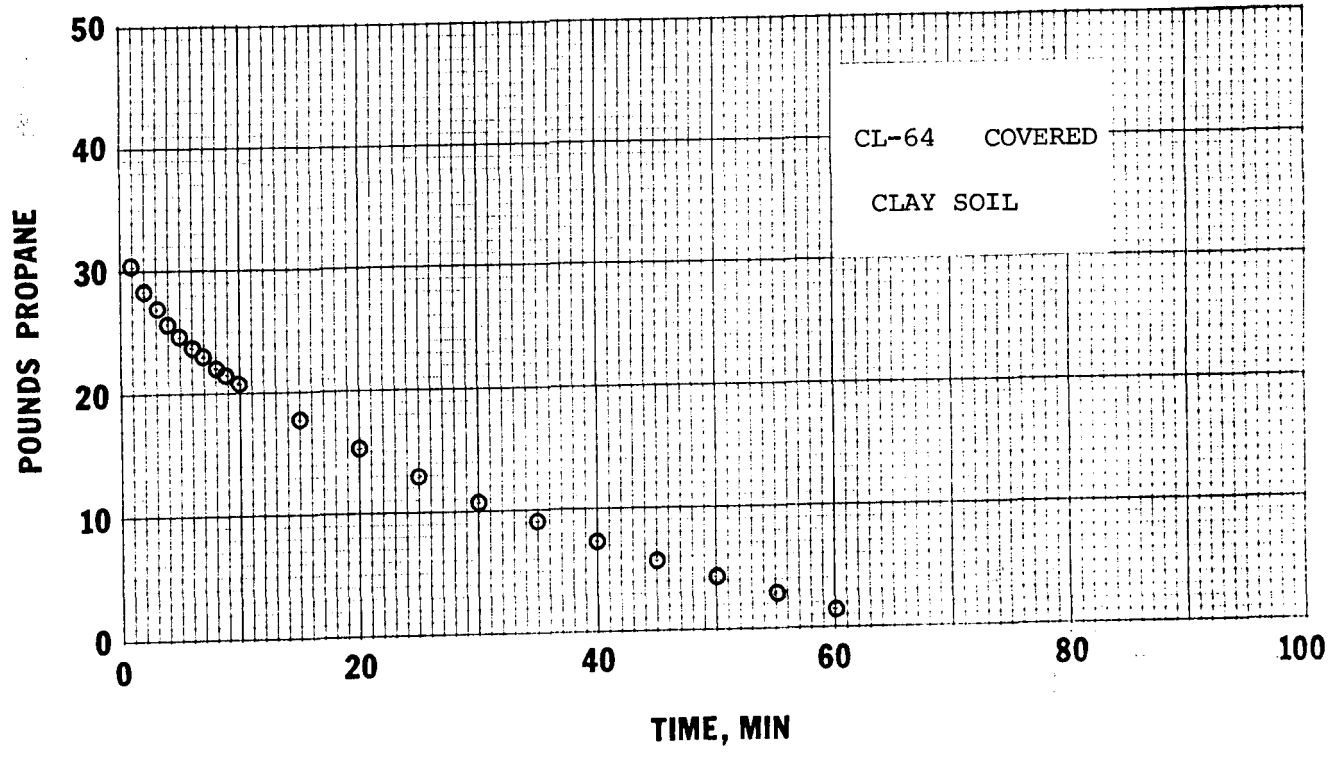

FIGURE A-54. VAPORIZATION OF PROPANE FOLLOWING A SPILL ON CLAY SOIL.

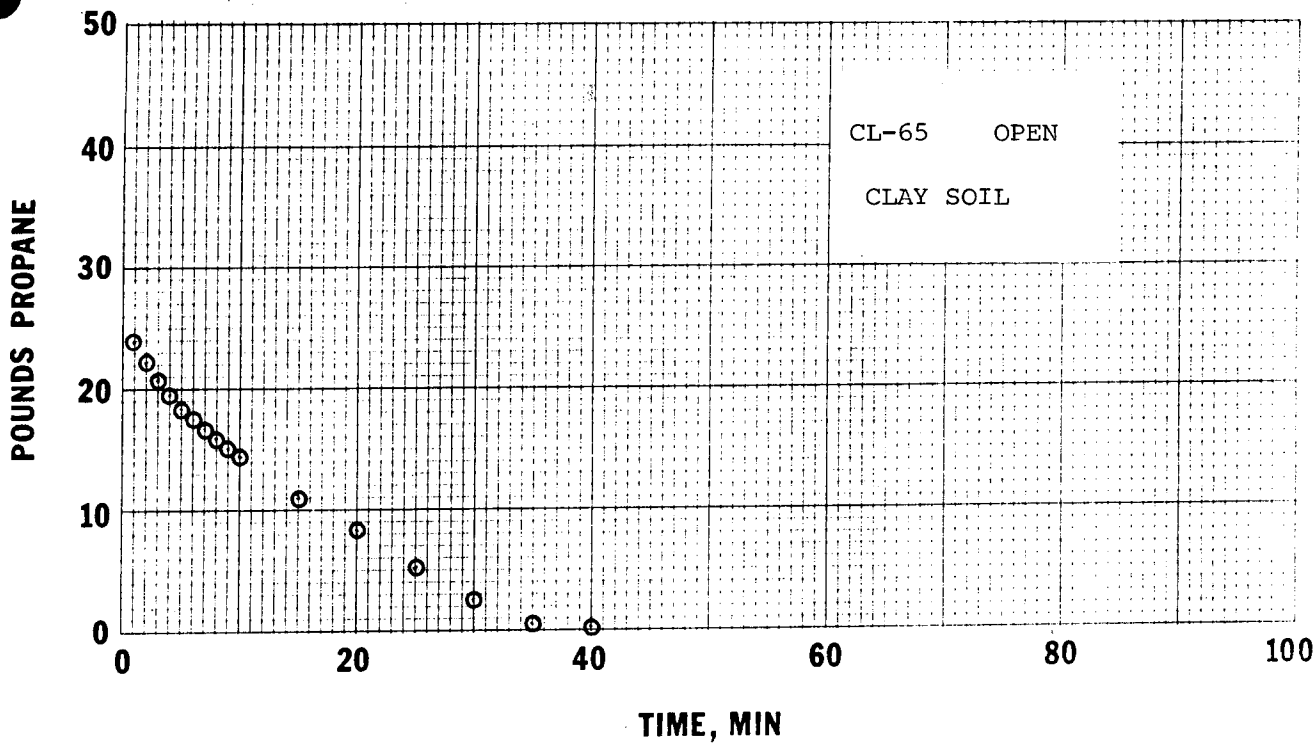

FIGURE A-55. VAPORIZATION OF PROPANE FOLLOWING A SPILL ON CLAY SOIL.

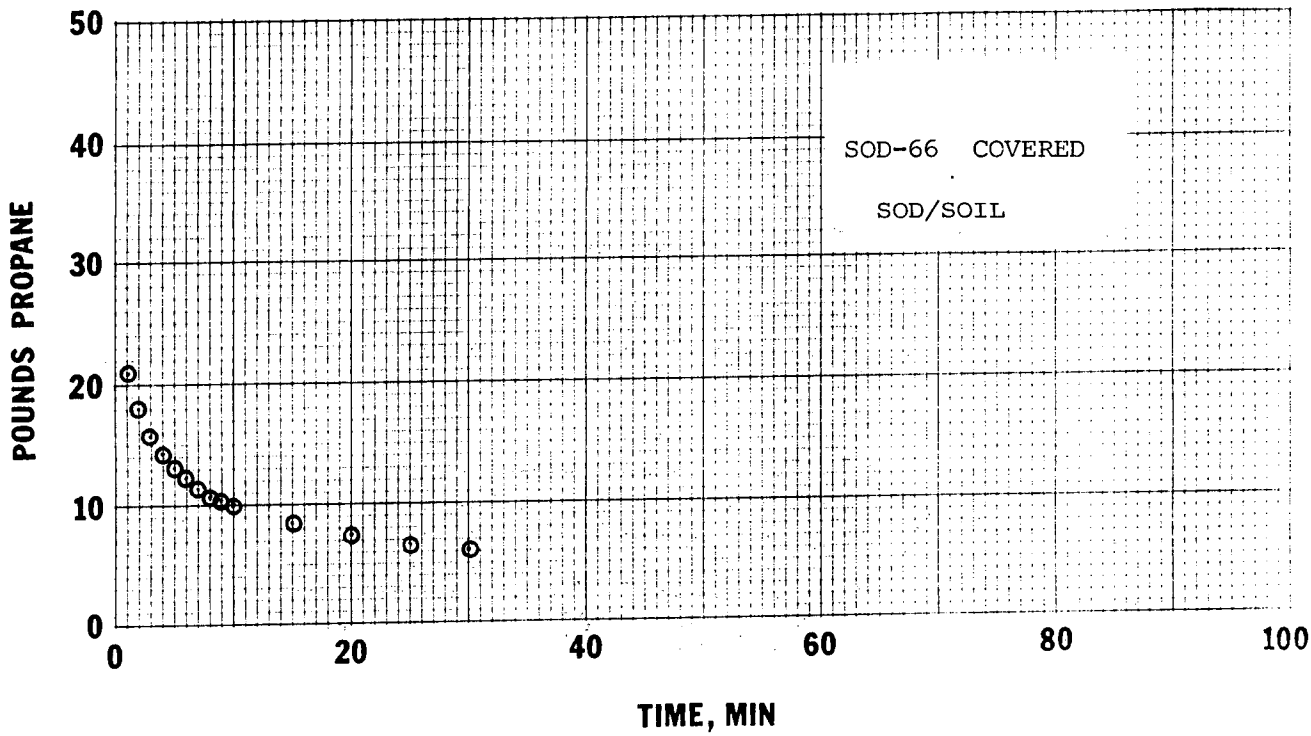

FIGURE A-56. VAPORIZATION OF PROPANE FOLLOWING A SPILL ON SOD/SOIL.

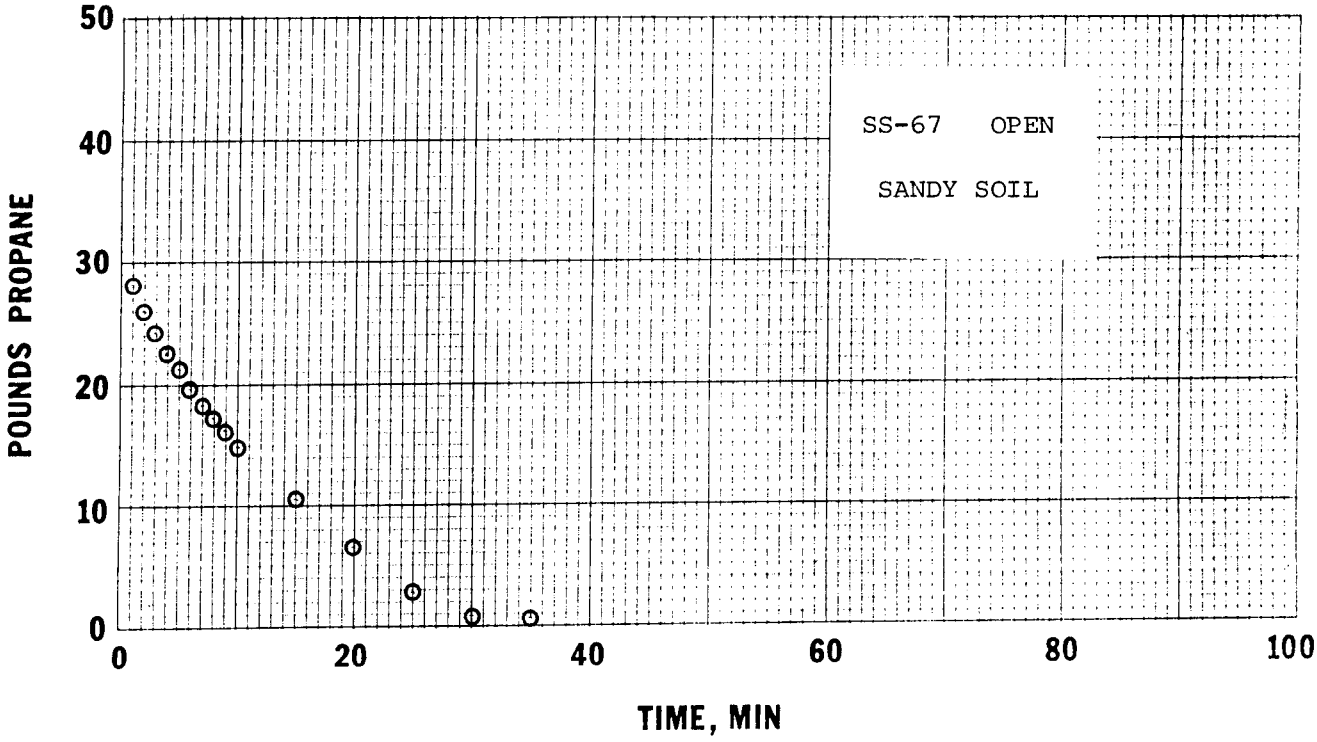

FIGURE A-57. VAPORIZATION OF PROPANE FOLLOWING A SPILL ON SANDY SOIL.

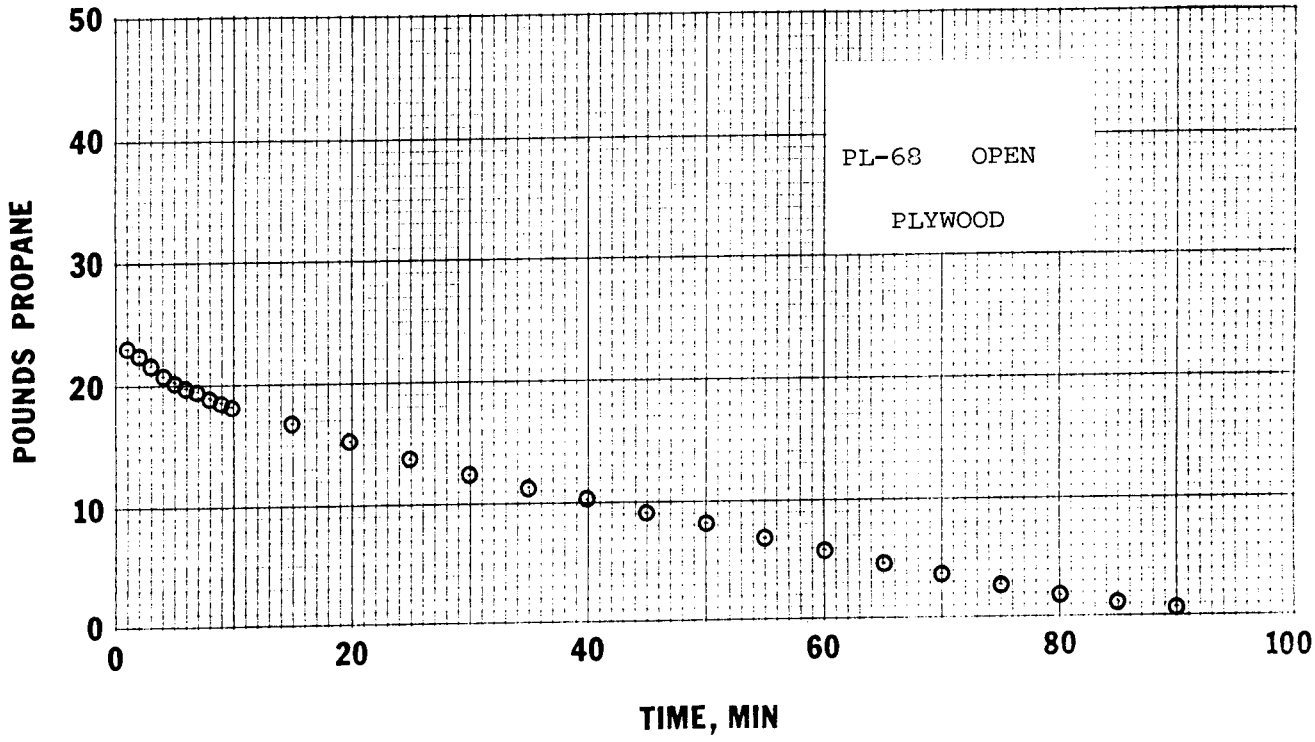

FIGURE A-58. VAPORIZATION OF PROPANE FOLLOWING A SPILL ON PLYWOOD.

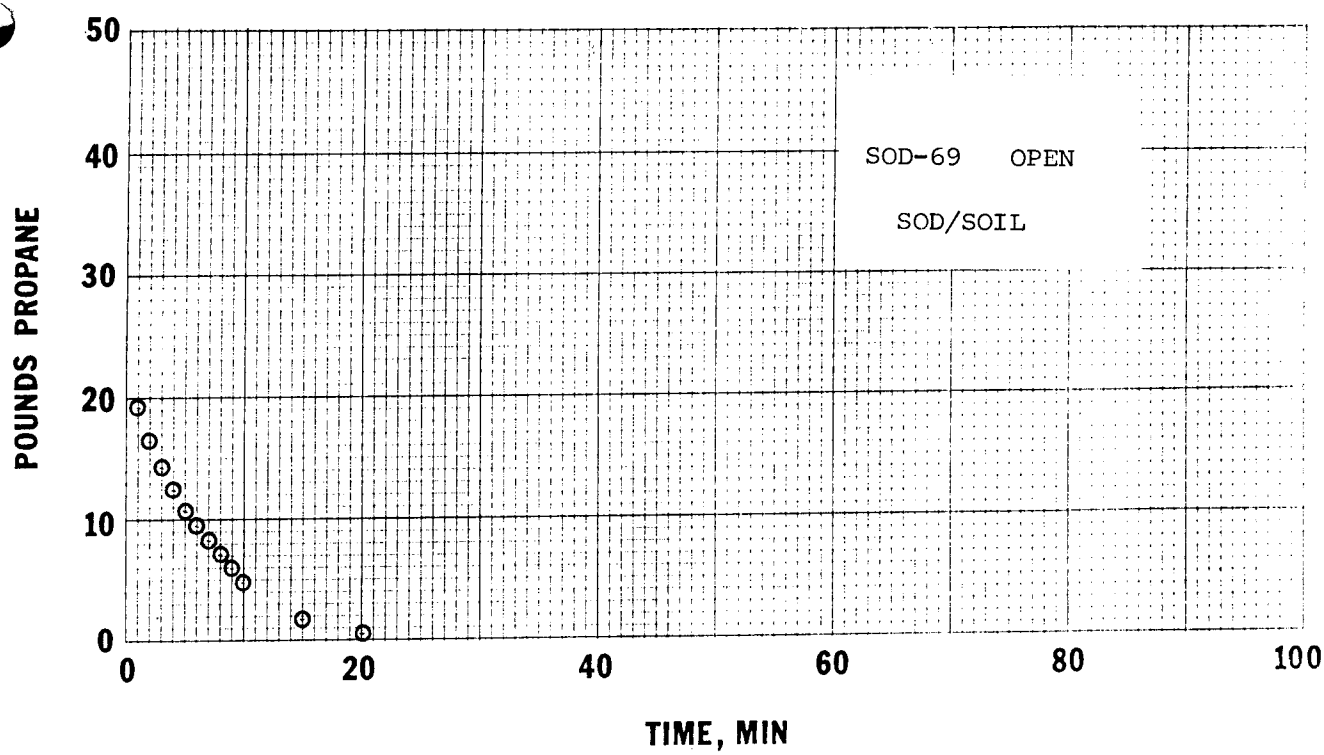

FIGURE A-59. VAPORIZATION OF PROPANE FOLLOWING A SPILL ON SOD/SOIL.

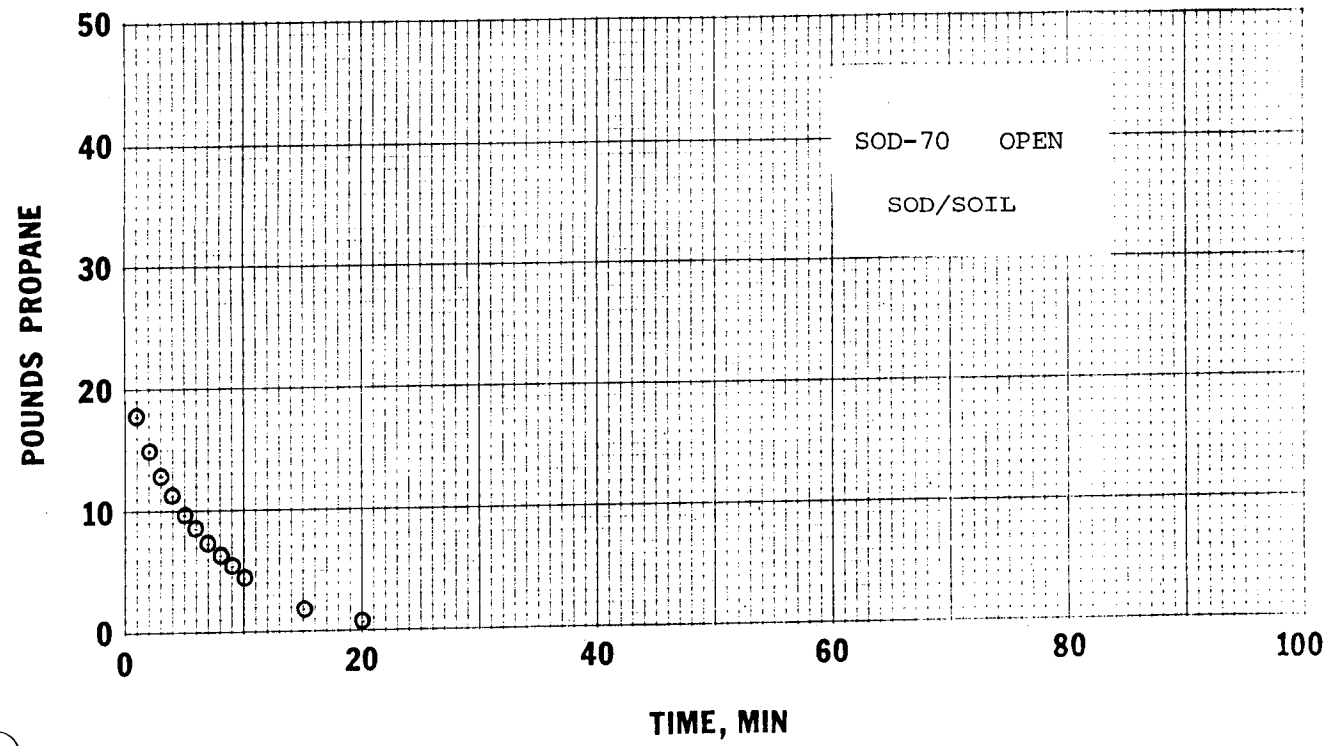

FIGURE A-60. VAPORIZATION OF PROPANE FOLLOWING A SPILL ON SOD/SOIL.

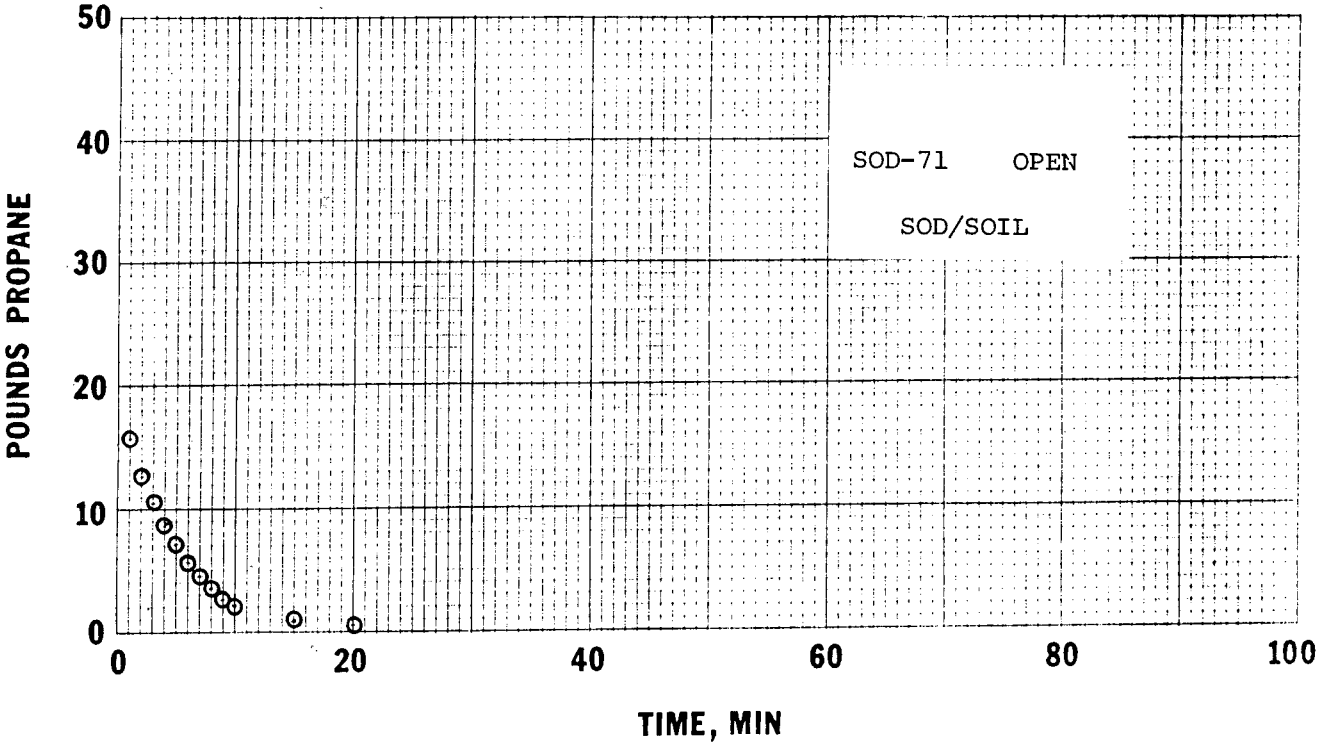

FIGURE A-61. VAPORIZATION OF PROPANE FOLLOWING A SPILL ON SOD/SOIL.

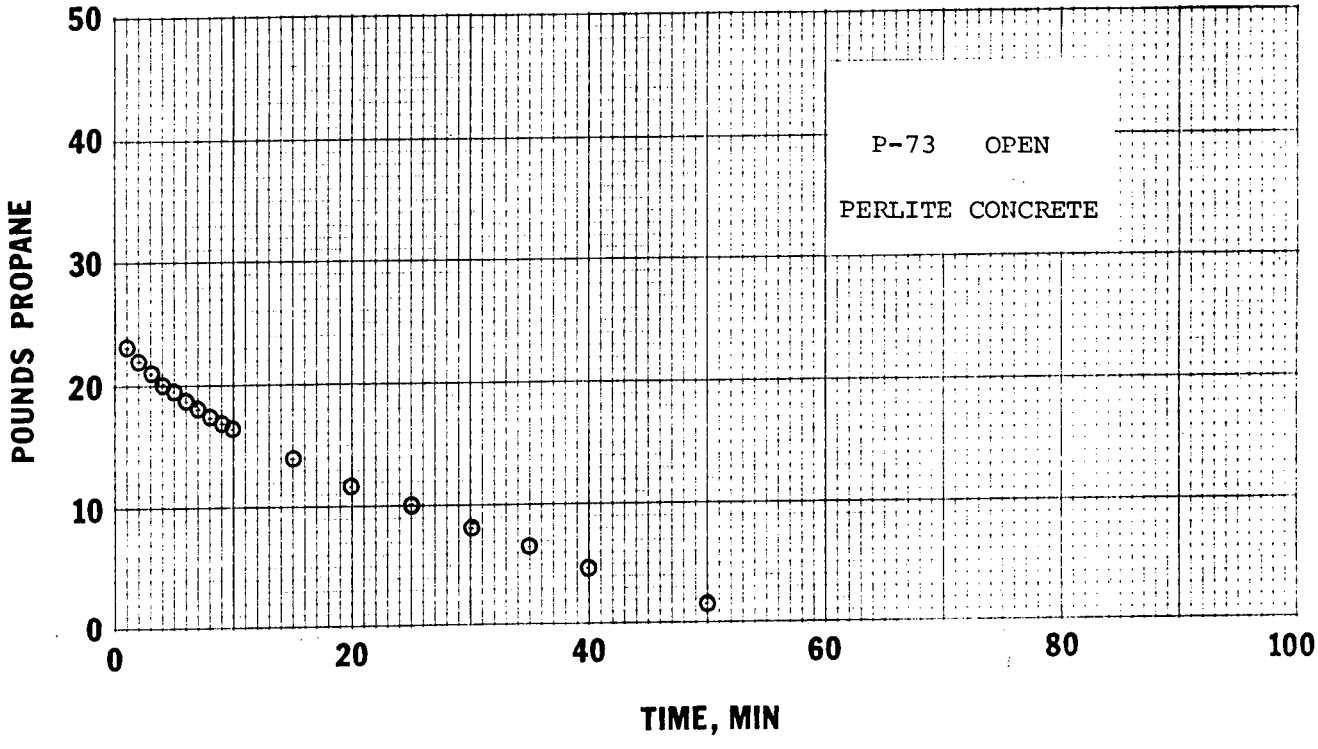

FIGURE A-62. VAPORIZATION OF PROPANE FOLLOWING A SPILL ON PERLITE CONCRETE.

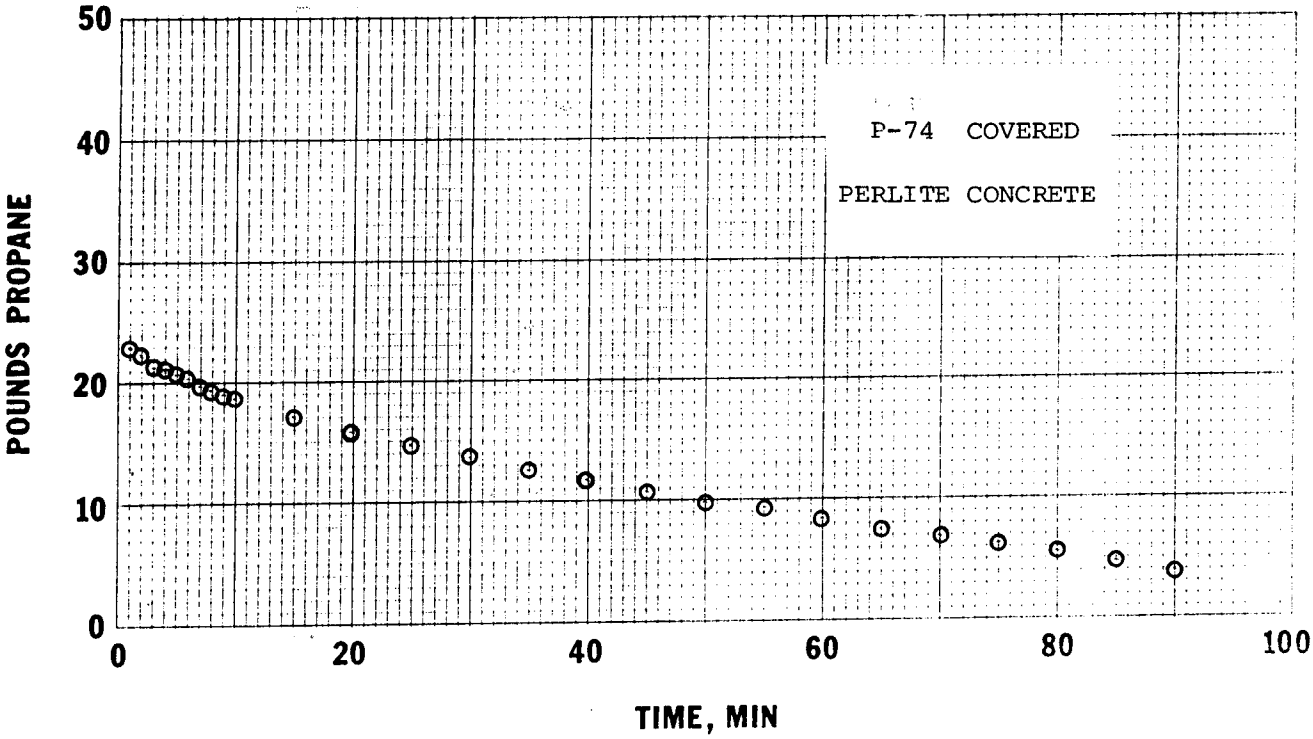

FIGURE A-63. VAPORIZATION OF PROPANE FOLLOWING A SPILL ON PERLITE CONCRETE.

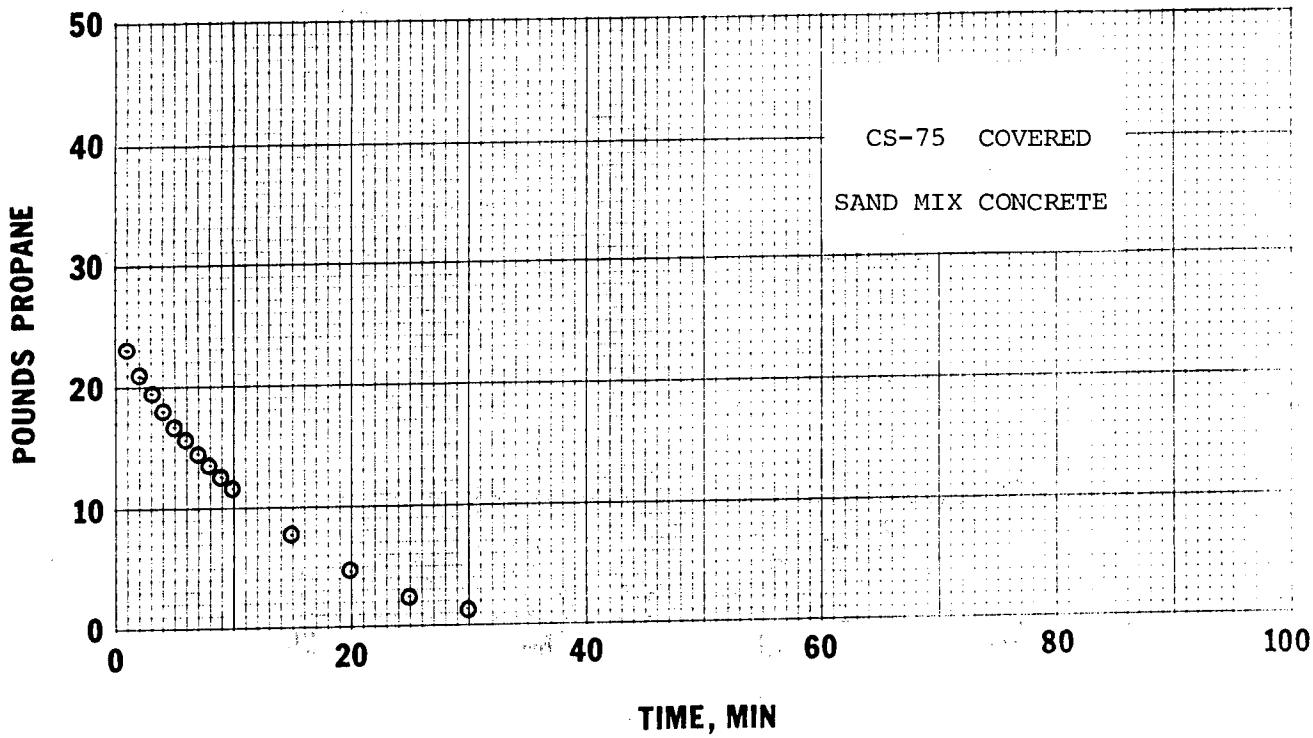

FIGURE A-64. VAPORIZATION OF PROPANE FOLLOWING A SPILL ON SAND MIX CONCRETE.

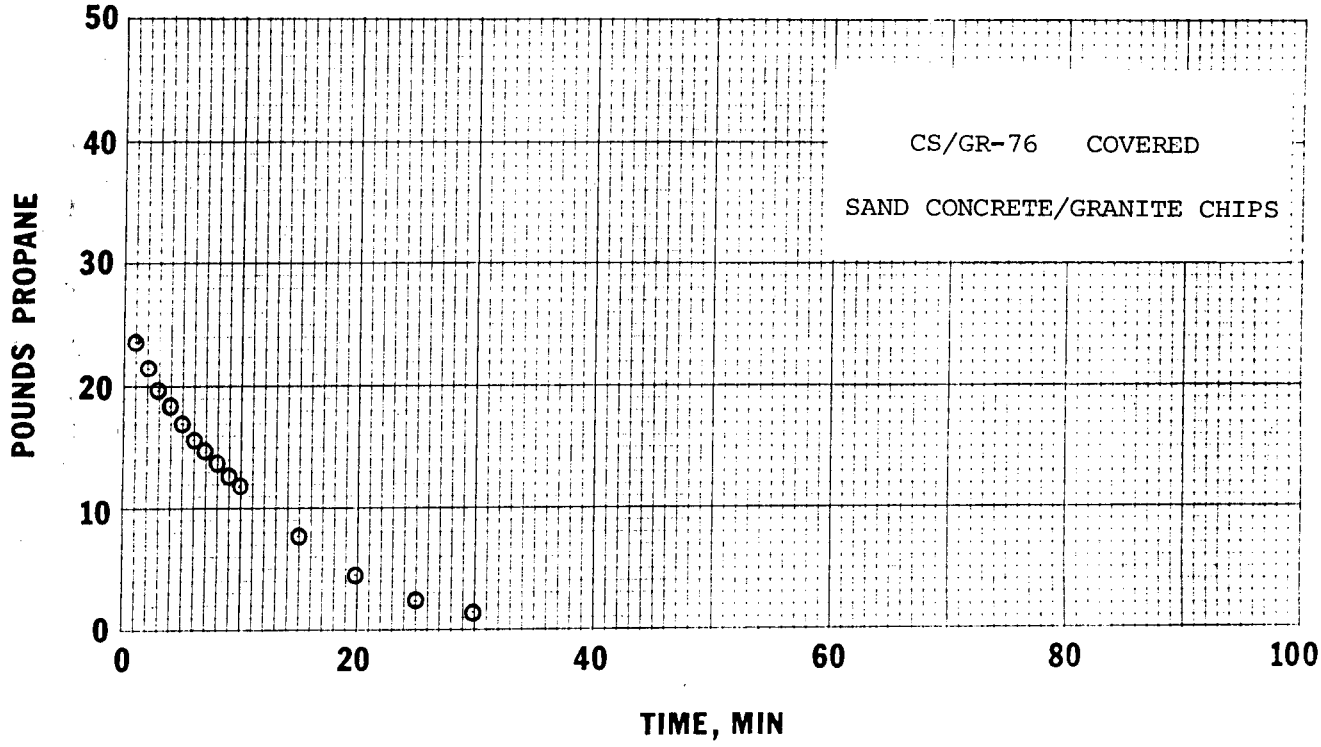

FIGURE A-65. VAPORIZATION OF PROPANE FOLLOWING A SPILL ON SAND CONCRETE/ GRANITE CHIPS.

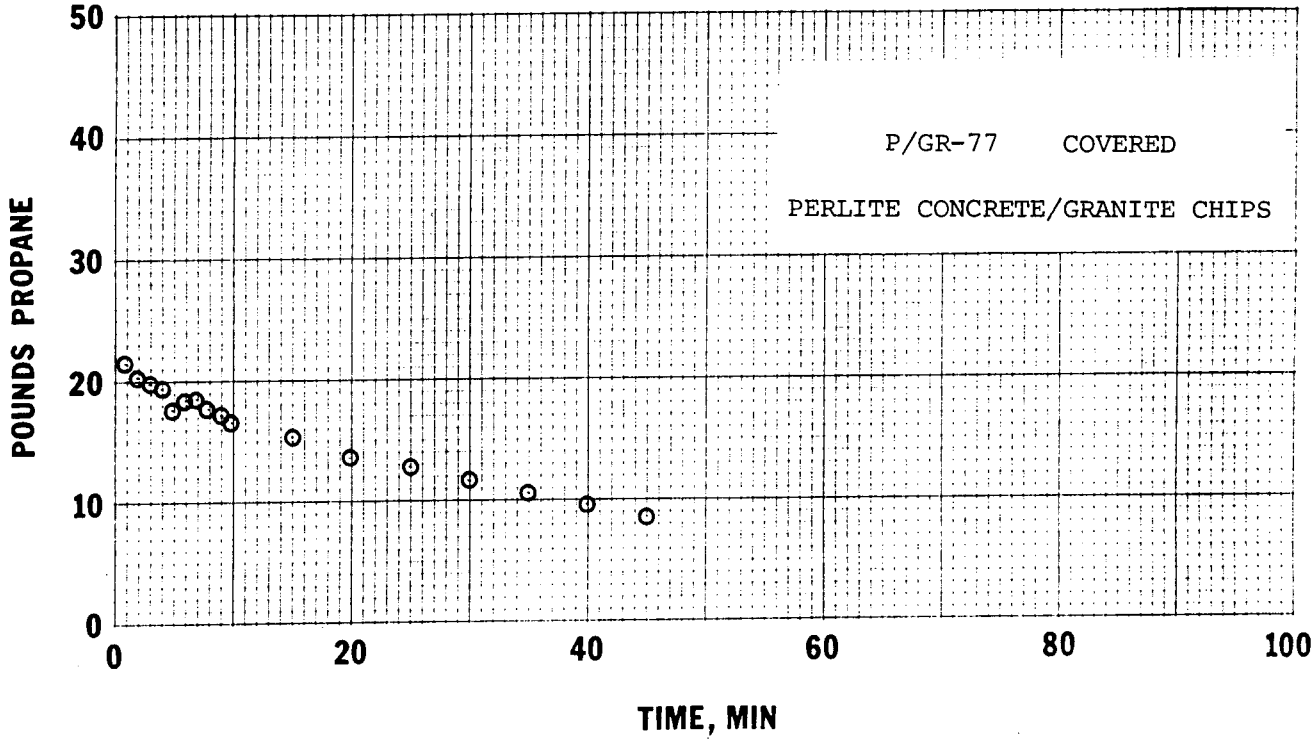

FIGURE A-66. VAPORIZATION OF PROPANE FOLLOWING A SPILL ON PERLITE CONCRETE/ GRANITE CHIPS.

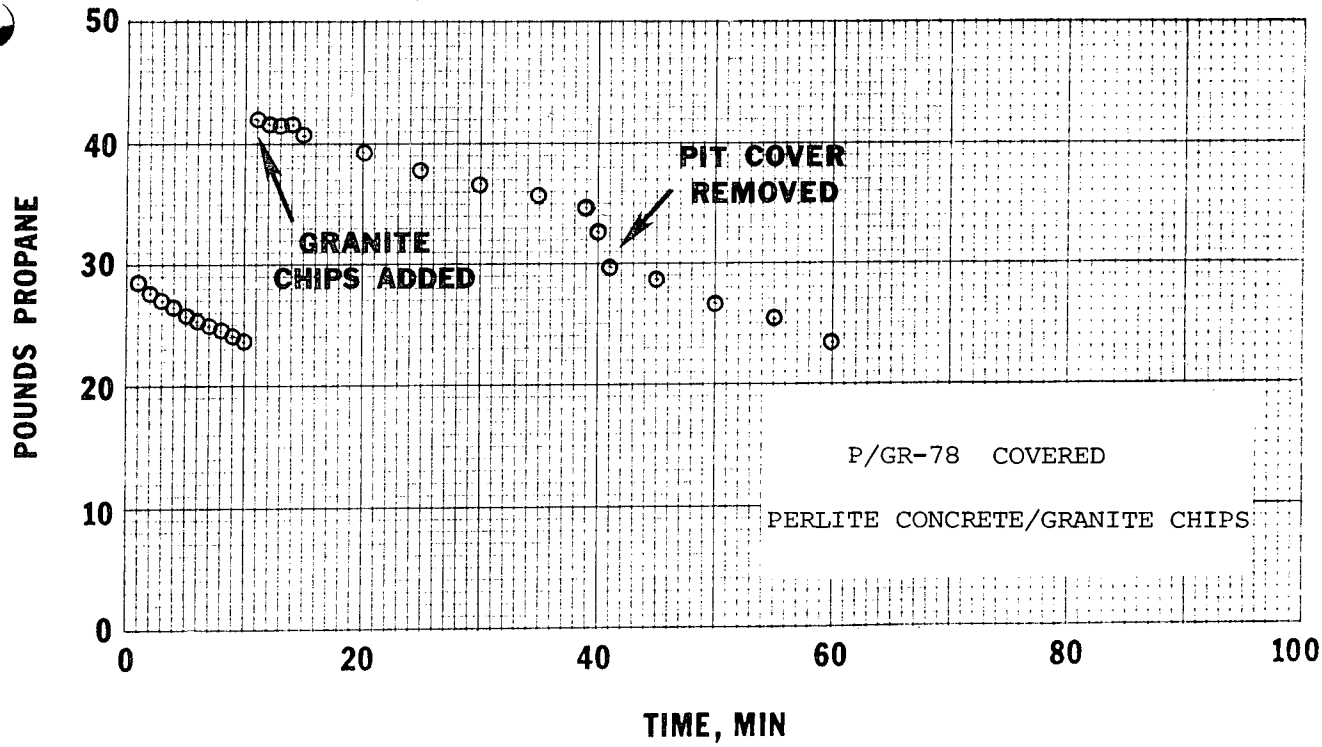

FIGURE A-67. VAPORIZATION OF PROPANE FOLLOWING A SPILL ON PERLITE CONCRETE/GRANITE CHIPS.

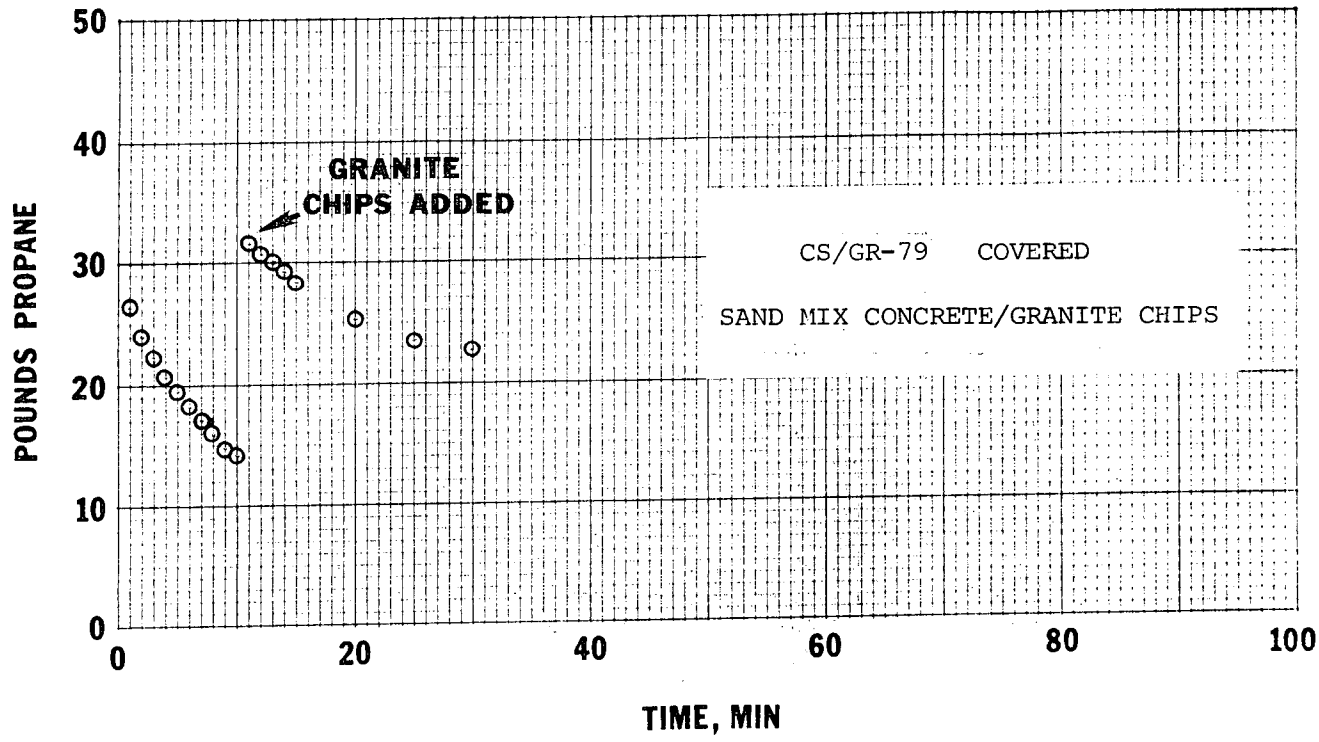

FIGURE A-68. VAPORIZATION OF PROPANE FOLLOWING A SPILL ON SAND MIX CONCRETE/GRANITE CHIPS.

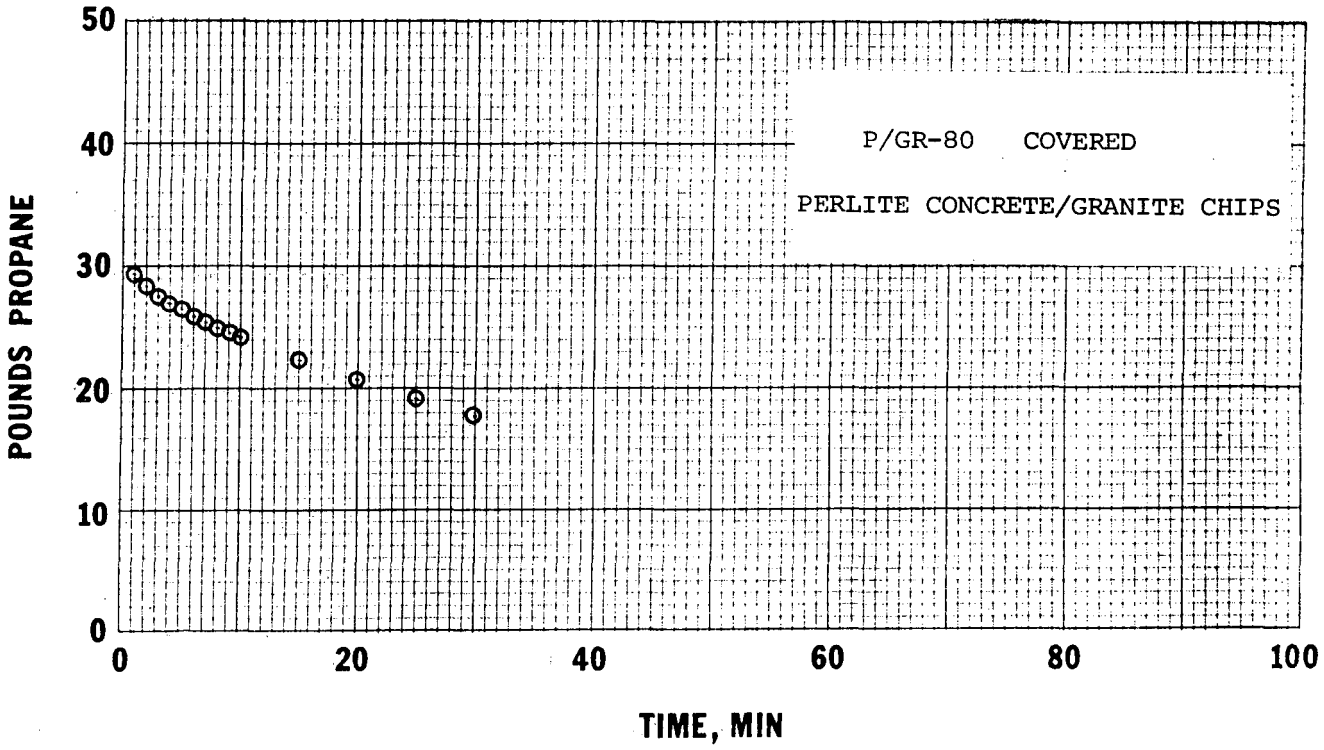

FIGURE A-69. VAPORIZATION OF PROPANE FOLLOWING A SPILL ON PERLITE CONCRETE/GRANITE CHIPS.

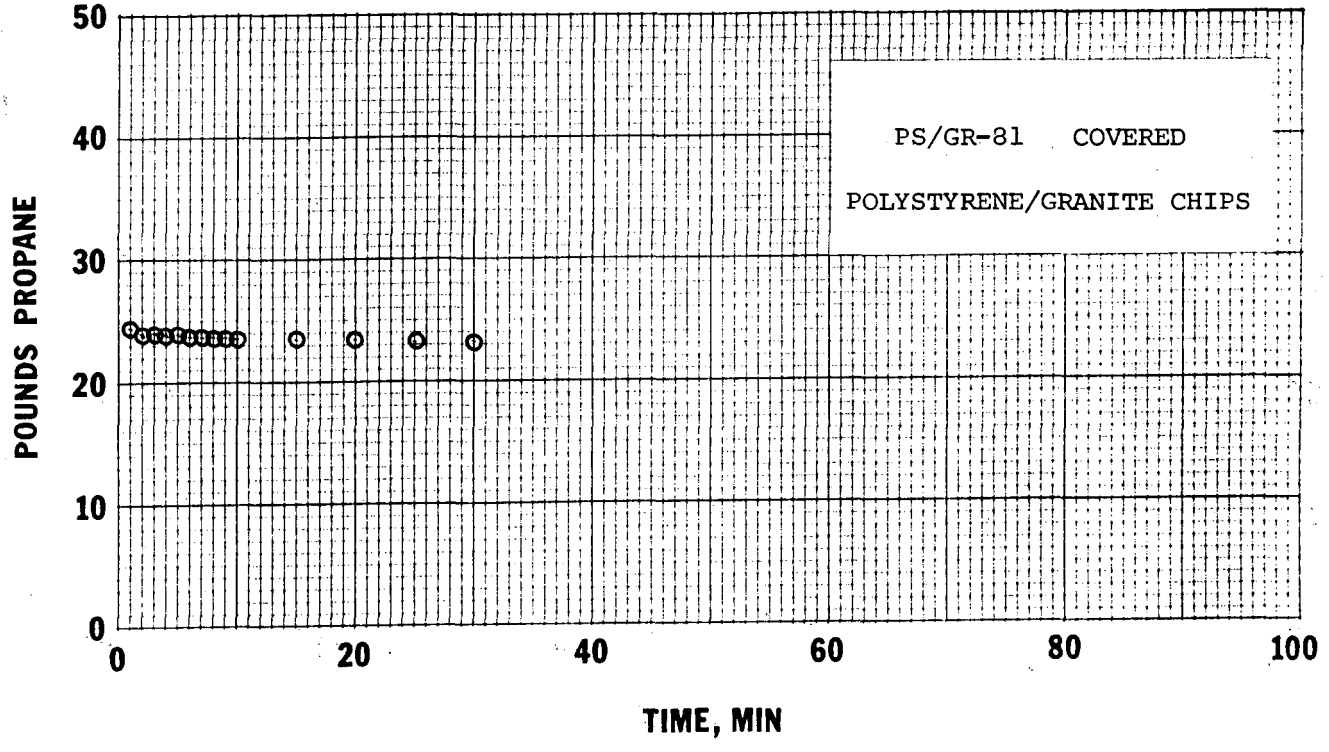

FIGURE A-70. VAPORIZATION OF PROPANE FOLLOWING A SPILL ON POLYSTYRENE/GRANITE CHIPS.

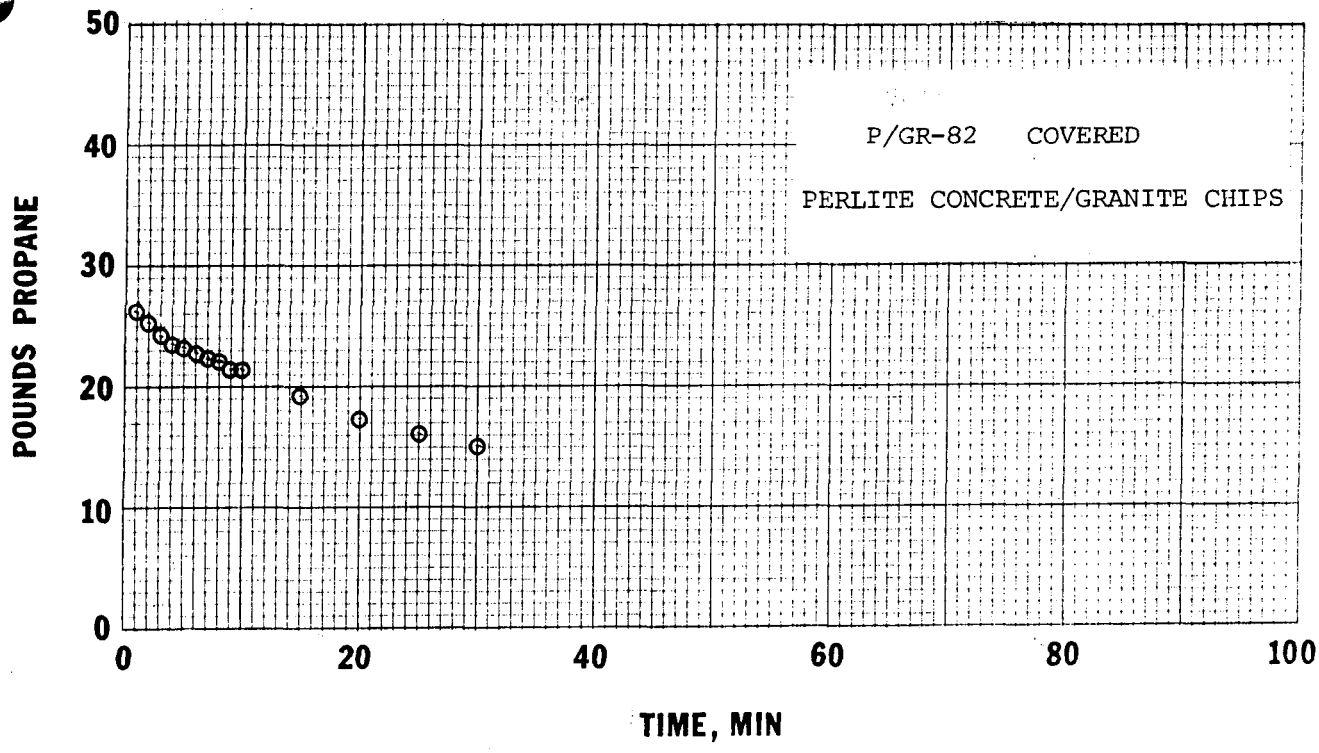

FIGURE A-71. VAPORIZATION OF PROPANE FOLLOWING A SPILL ON PERLITE CONCRETE/GRANITE CHIPS.

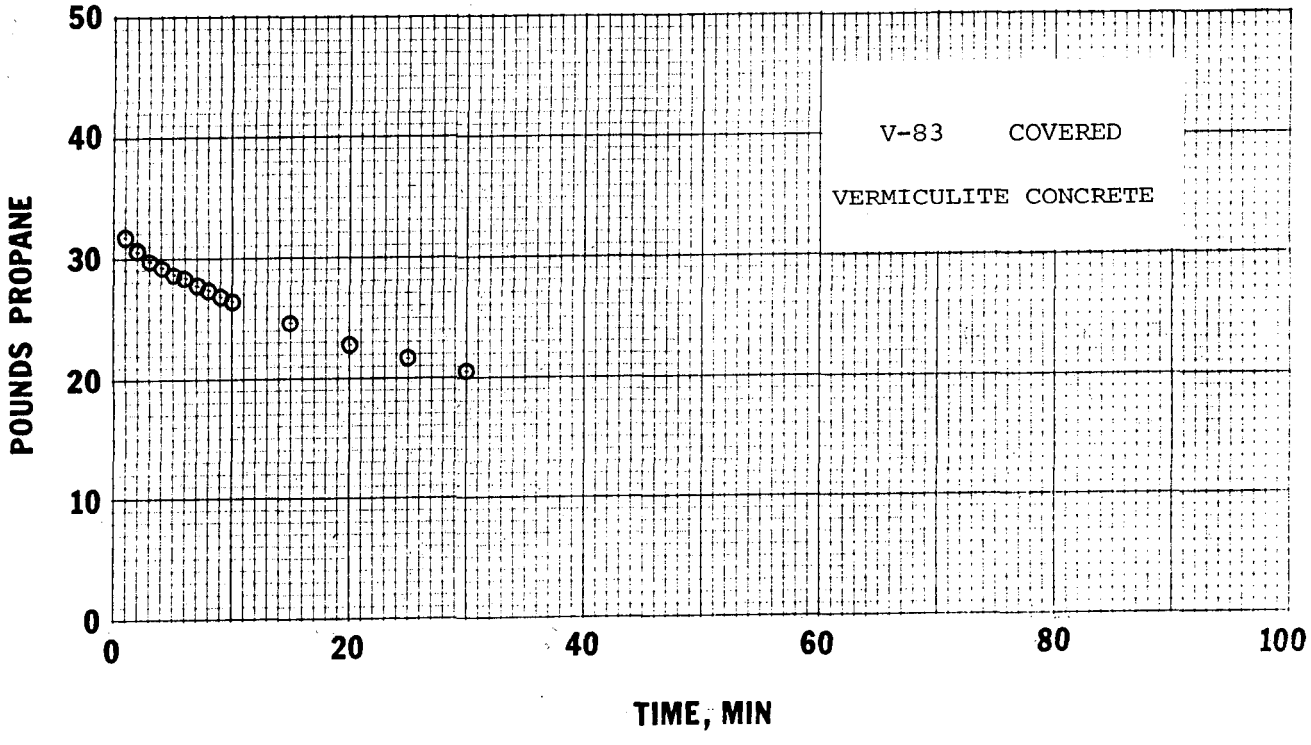

FIGURE A-72. VAPORIZATION OF PROPANE FOLLOWING A SPILL ON VERMICULITE CONCRETE.

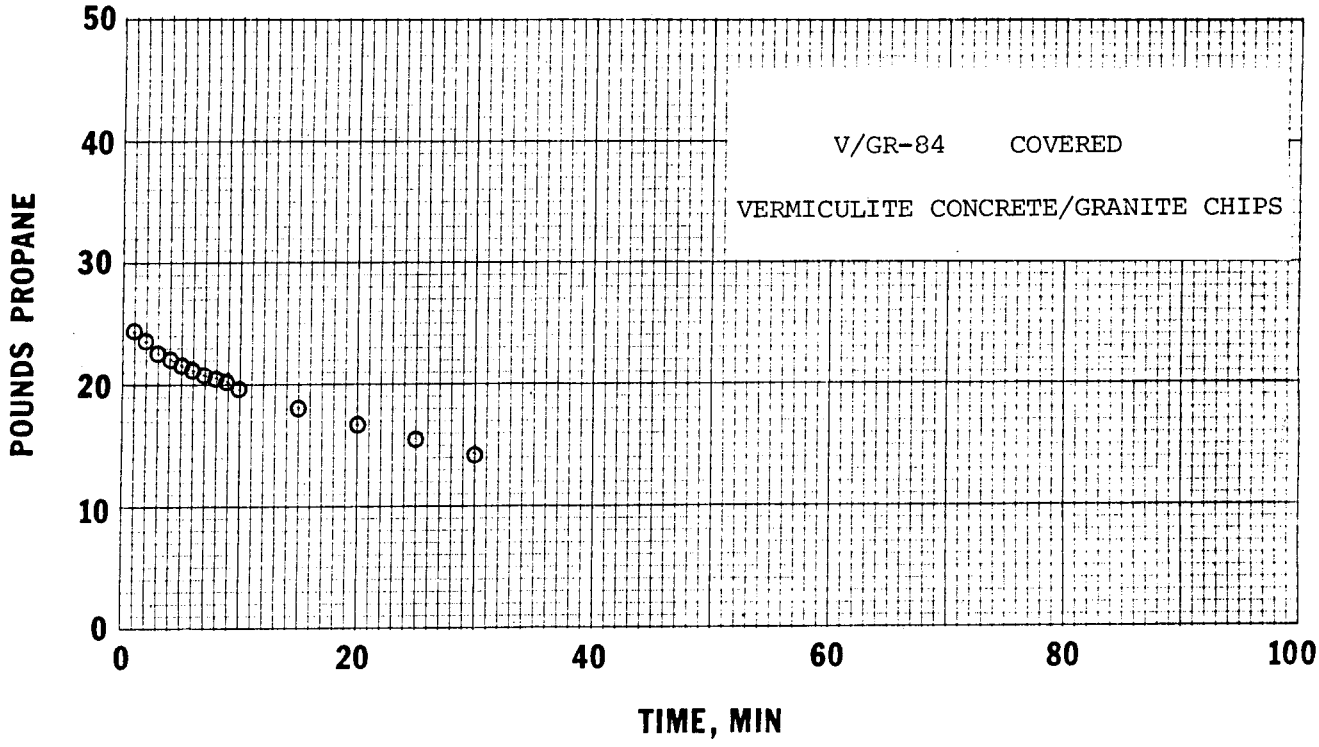

FIGURE A-73. VAPORIZATION OF PROPANE FOLLOWING A SPILL ON VERMICULITE CONCRETE/GRANITE CHIPS.

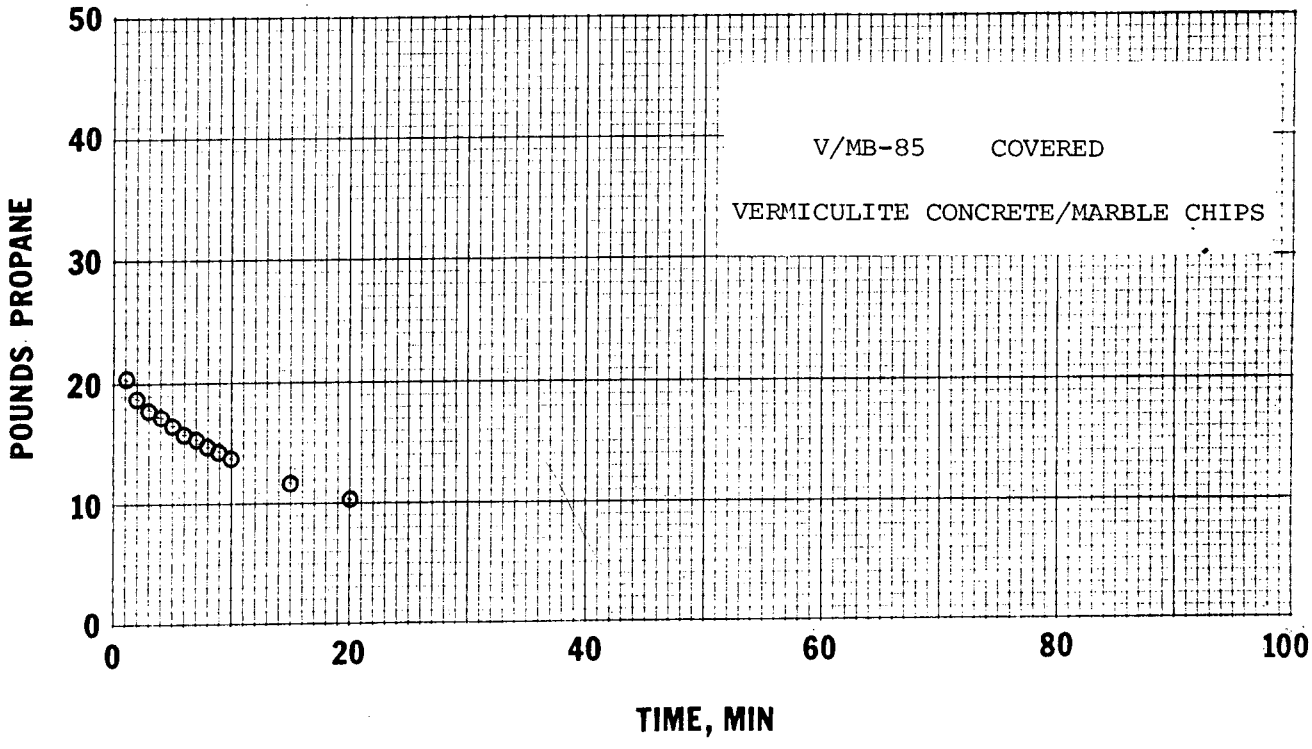

FIGURE A-74. VAPORIZATION OF PROPANE FOLLOWING A SPILL ON VERMICULITE CONCRETE/MARBLE CHIPS.

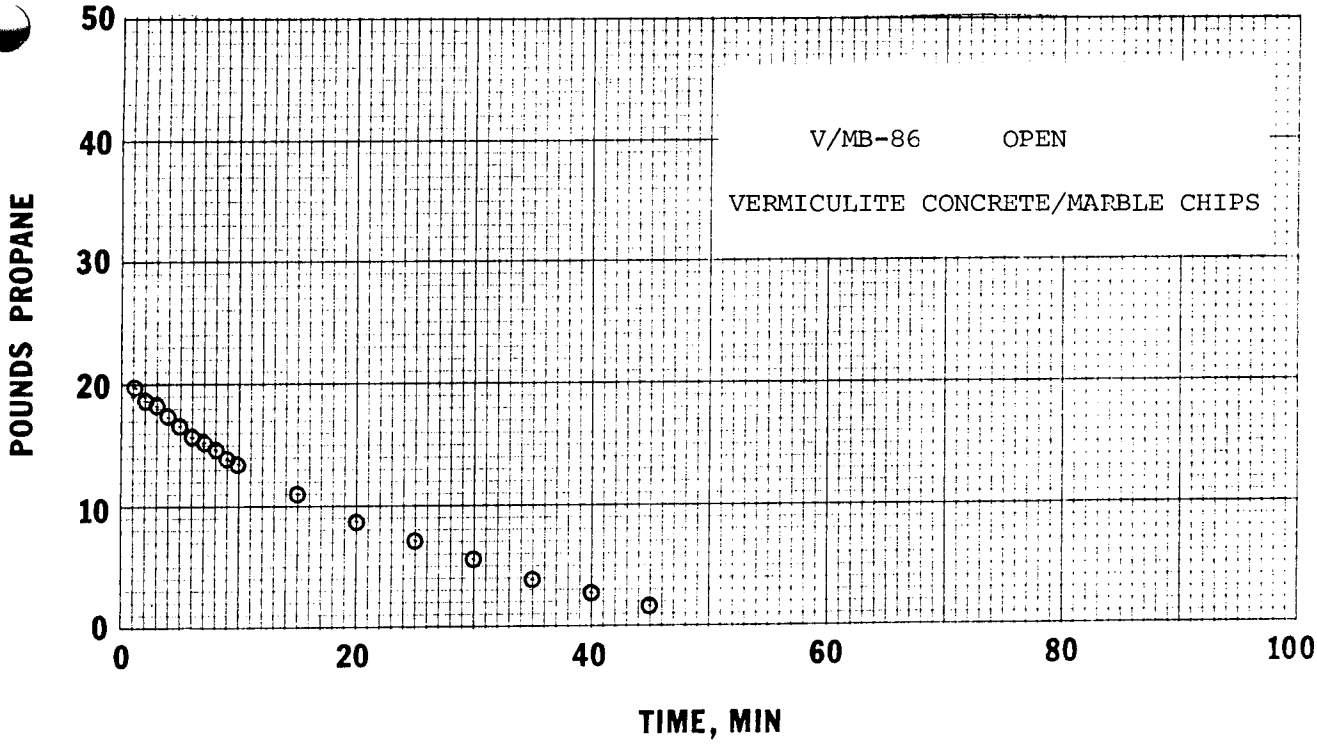

FIGURE A-75. VAPORIZATION OF PROPANE FOLLOWING A SPILL ON VERMICULITE CONCRETE/MARBLE CHIPS.

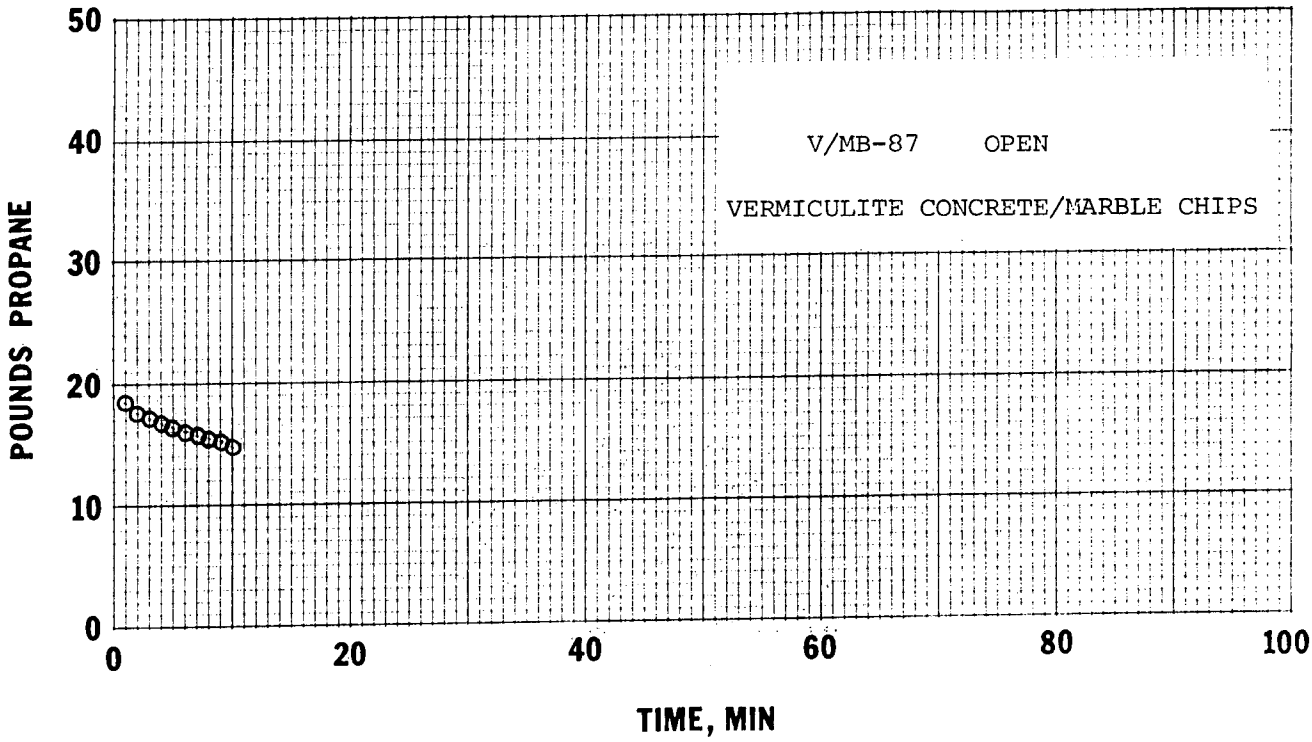

FIGURE A-76. VAPORIZATION OF PROPANE FOLLOWING A SPILL ON VERMICULITE CONCRETE/MARBLE CHIPS.

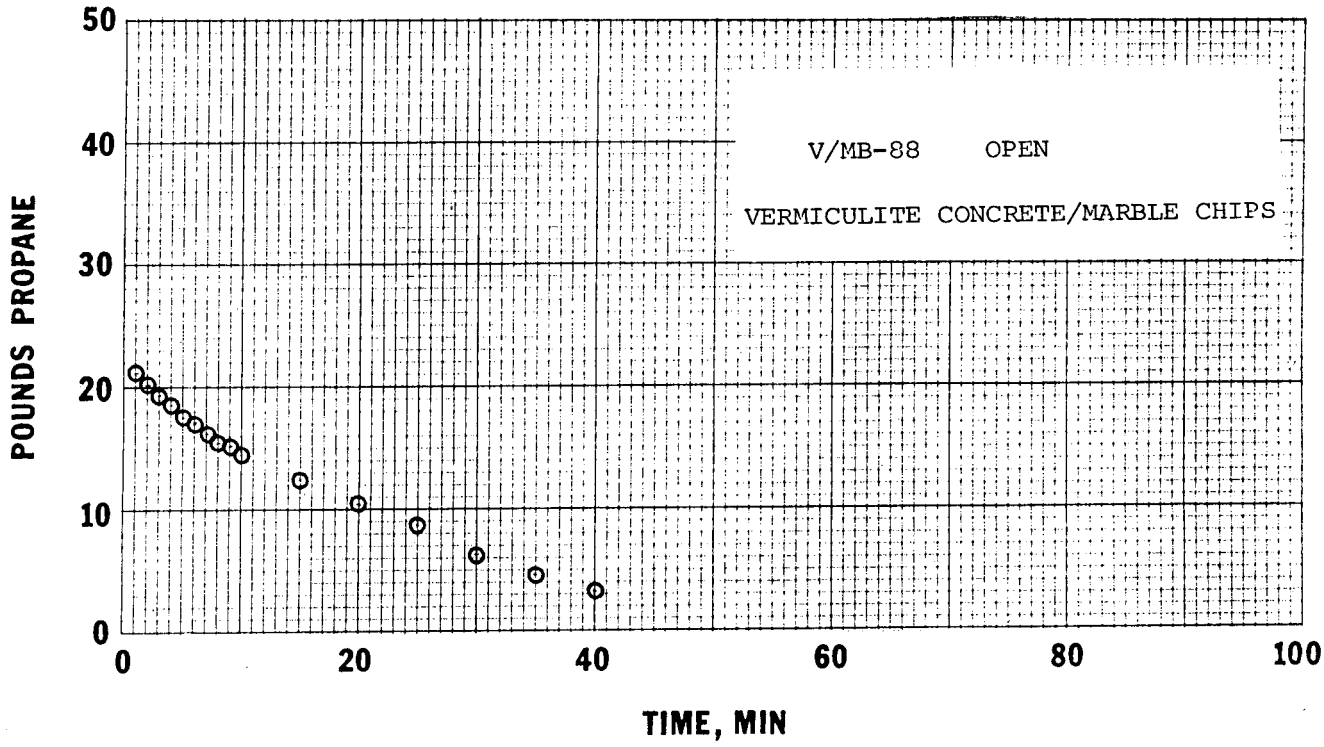

FIGURE A-77. VAPORIZATION OF PROPANE FOLLOWING A SPILL ON VERMICULITE CONCRETE/MARBLE CHIPS.

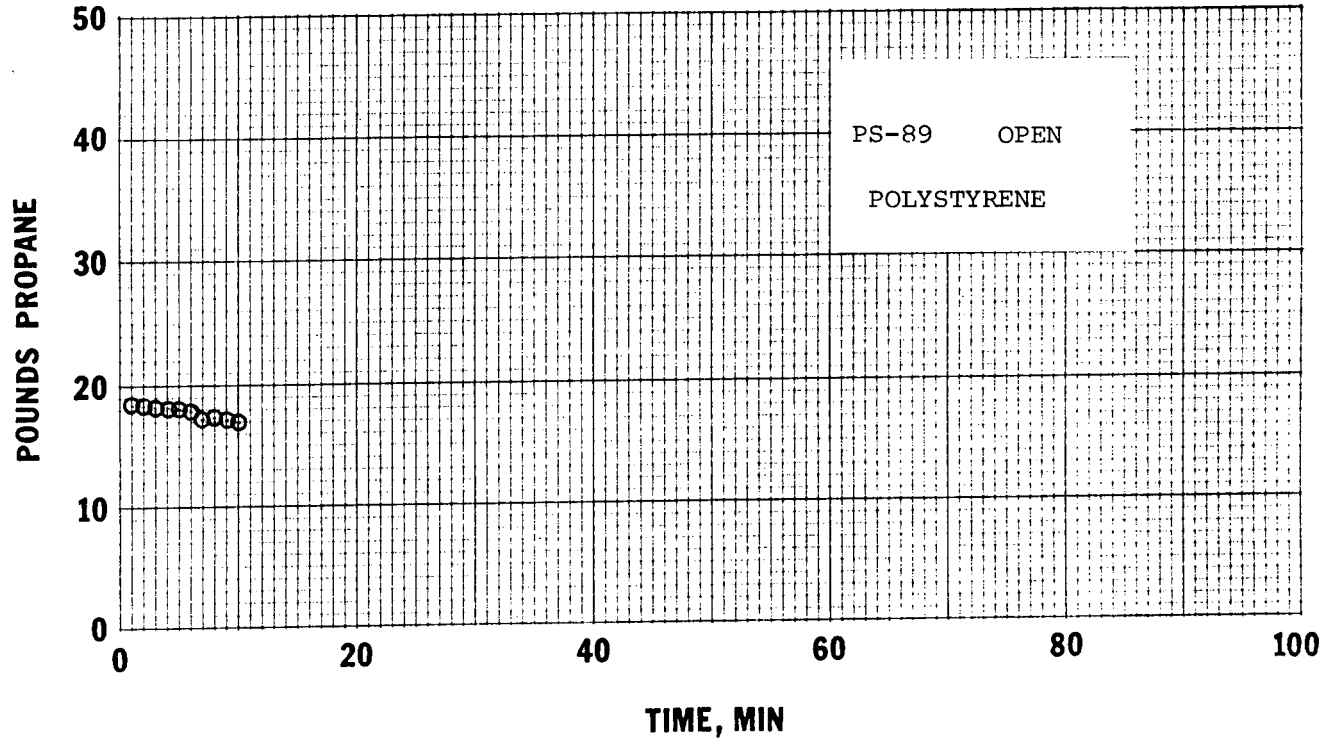

FIGURE A-78. VAPORIZATION OF PROPANE FOLLOWING A SPILL ON POLYSTYRENE.

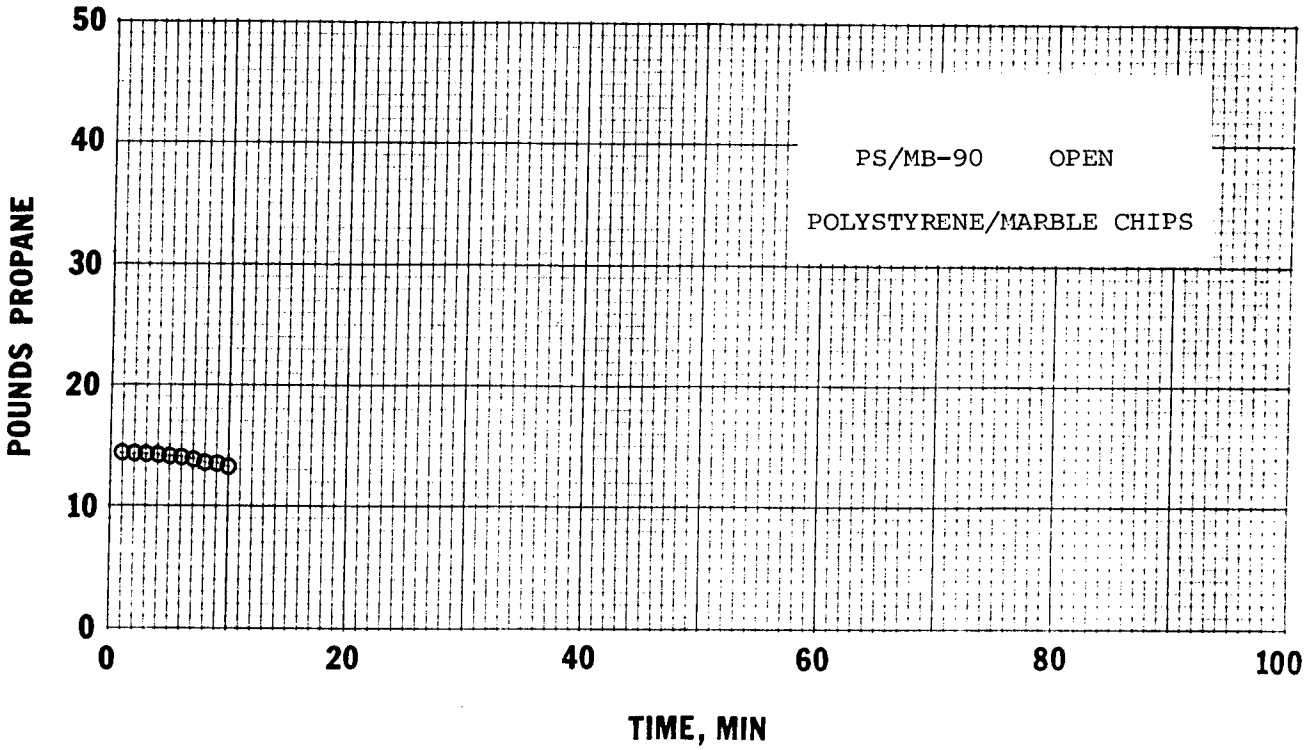

FIGURE A-79. VAPORIZATION OF PROPANE FOLLOWING A SPILL ON POLYSTYRENE/MARBLE CHIPS.

REPORT IV

SPILLS OF PRESSURIZED PROPANE

INTRODUCTION

Most propane transported in the United States is carried by rail tank car, tank truck, or pipeline. In nearly all cases, the propane is transported as a pressurized liquid at ambient temperature. If the pressure on the liquid is released suddenly, such as when a leak occurs, a substantial fraction of the liquid flashes to vapor. The fraction flashed depends on the saturation pressure before the pressure is released.

As the liquid flashes to vapor, and as it flows through a crack or valve, strong shearing forces are generated. The shearing forces break the liquid up, atomizing it into very small droplets. This section discusses tests made in an attempt to determine how much propane might accumulate following a release of pressurized propane.

PROCEDURE

Figure 1 is a schematic diagram of the test apparatus. A tank containing liquid propane was placed on one end of a balance mechanism and a weight transducer was attached to the other end. Figure 2 shows a schematic of the measuring devices that were attached. They included a thermocouple to measure liquid temperature and a pressure

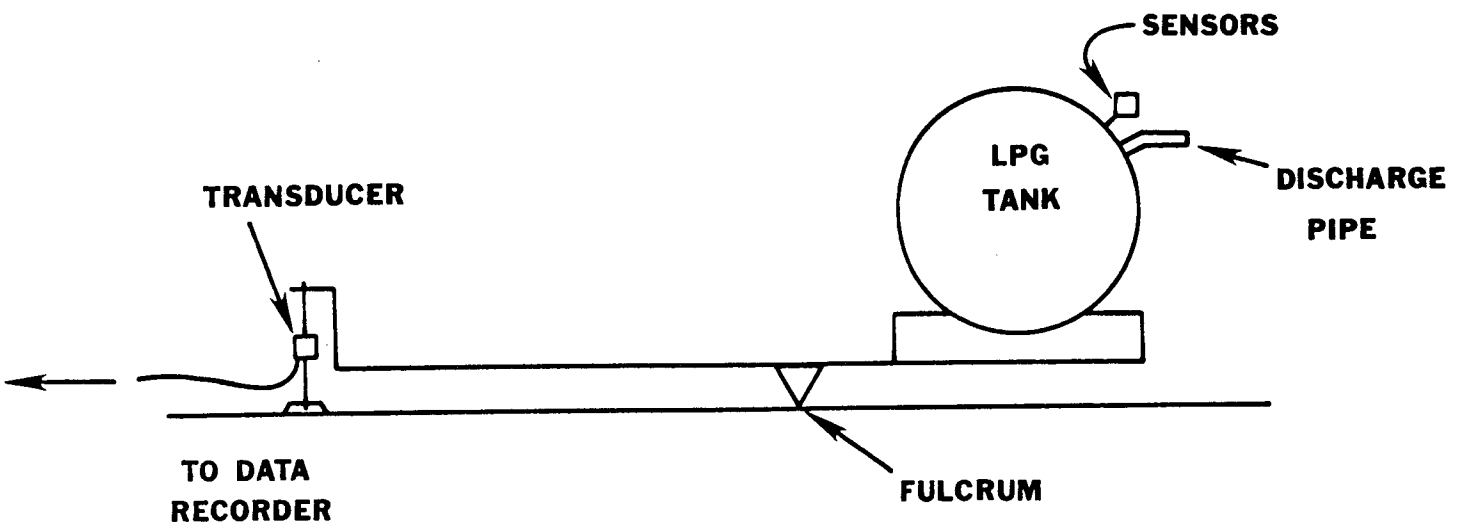

Figure 1. Setup for Propane Spray Tests.

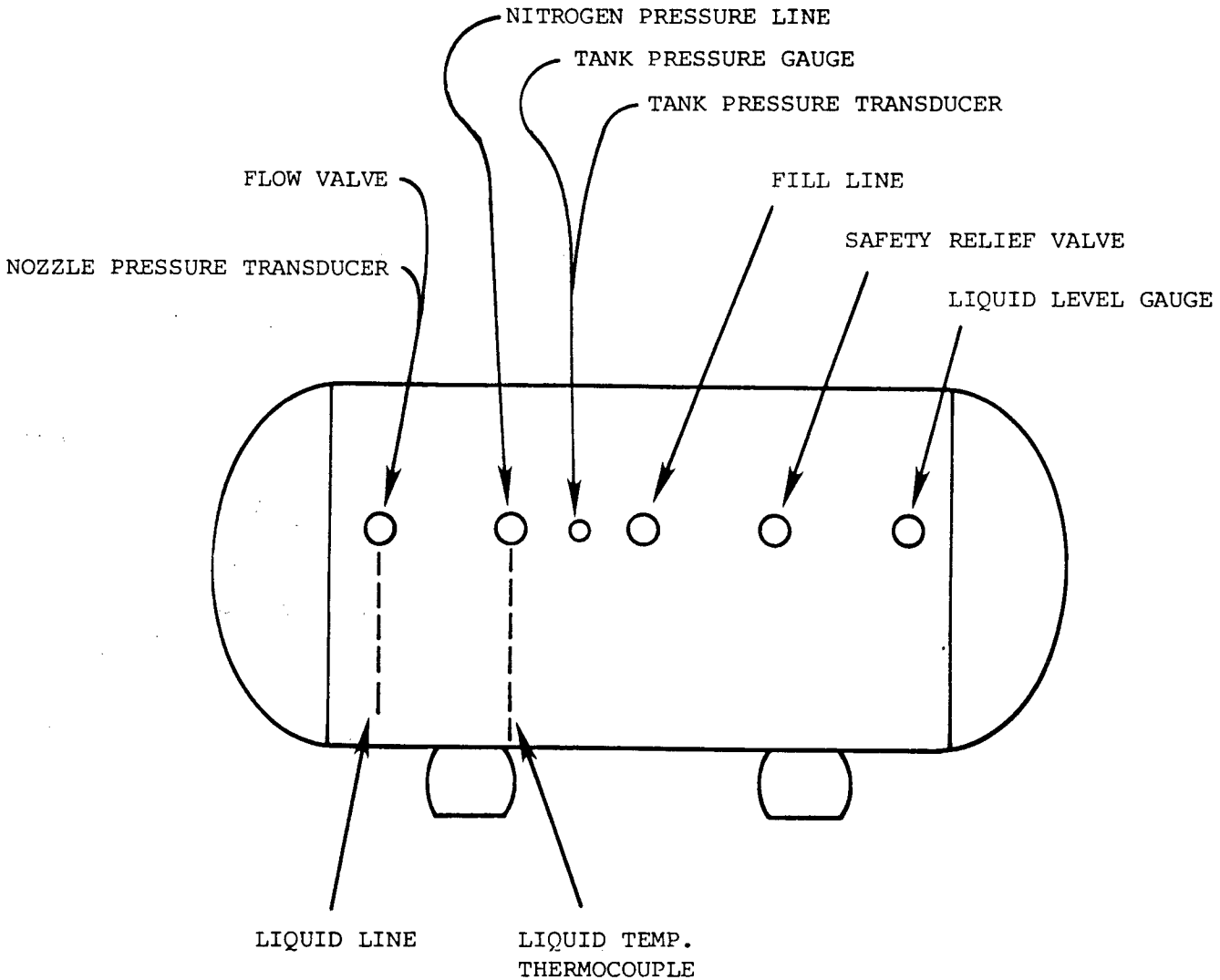

Figure 2. Location of Measuring Equipment for Propane Spray Tests.

transducer. In addition, thermocouples were positioned downstream from the discharge pipe to measure the temperature of the propane plume during discharge.

A large polystyrene foam tray was built downstream of the discharge pipe to catch propane during discharge. The tray was lined with lightweight polyethylene film to prevent loss due to seepage into the foam or foam deterioration.

Tests followed a simple pattern. The tank was charged with propane at ambient temperature and its own vapor pressure (the propane contained 0.25 percent ethane and 0.36 percent isobutane). The tank pressure was then increased by about 15 to 25 psi by dry nitrogen supplied through a regulator. After starting recording instruments, the discharge valve was opened and propane was allowed to flow out. The nitrogen pressure was maintained at the maximum regulator capacity until all liquid was discharged. Nitrogen pressure was used to aid in preventing liquid flashing upstream of the valve during discharge.

RESULTS AND DISCUSSION

Figure 3 shows the plume formed during a propane discharge test. The discharge is horizontal at a rate that stabilized at 175 lb/min after about 10 seconds of flow. The flow rate remained constant until the tank was essentially empty following the initial drop from about 400

Figure 3. Vapor Plume from Discharge of Pressurized Propane at 180 lb/min.

lb/min. It was apparent that nitrogen flow was insufficient to keep the tank pressure above the vapor pressure during the high flow rate discharge.

Figure 4 shows the weight of propane discharged during the test, the tank temperature, and the tank pressure. After an initial decrease in tank pressure about equal to the pressure added by the nitrogen cap, the pressure decreased slowly until the liquid was gone; the tank pressure was then allowed to decrease until the propane vapor and nitrogen gas were discharged. The liquid temperature in the tank remained at ambient temperature until nearly all of the propane had been discharged. At the tank temperature of about 82°F, the tank pressure was the vapor pressure of propane, again indicating that the nitrogen flow was too small to maintain tank pressure.

The thermocouples in the propane plume located 2 and 5 ft from the nozzle showed temperatures in the plume as low as -85°F during discharge. As long as liquid was being discharged, the plume temperature was less than about -70°F. The plume was therefore substantially subcooled as the small drops formed during discharge vaporized. About 50 percent of the liquid discharged would have to vaporize in order to subcool the plume. Those droplets that remained in the plume vaporized very rapidly as they mixed with the air, so that by the time the plume reached the thermocouple 10 ft from the discharge pipe, the plume temperature was 40 to 50°F, indicating that all the propane was vaporized.

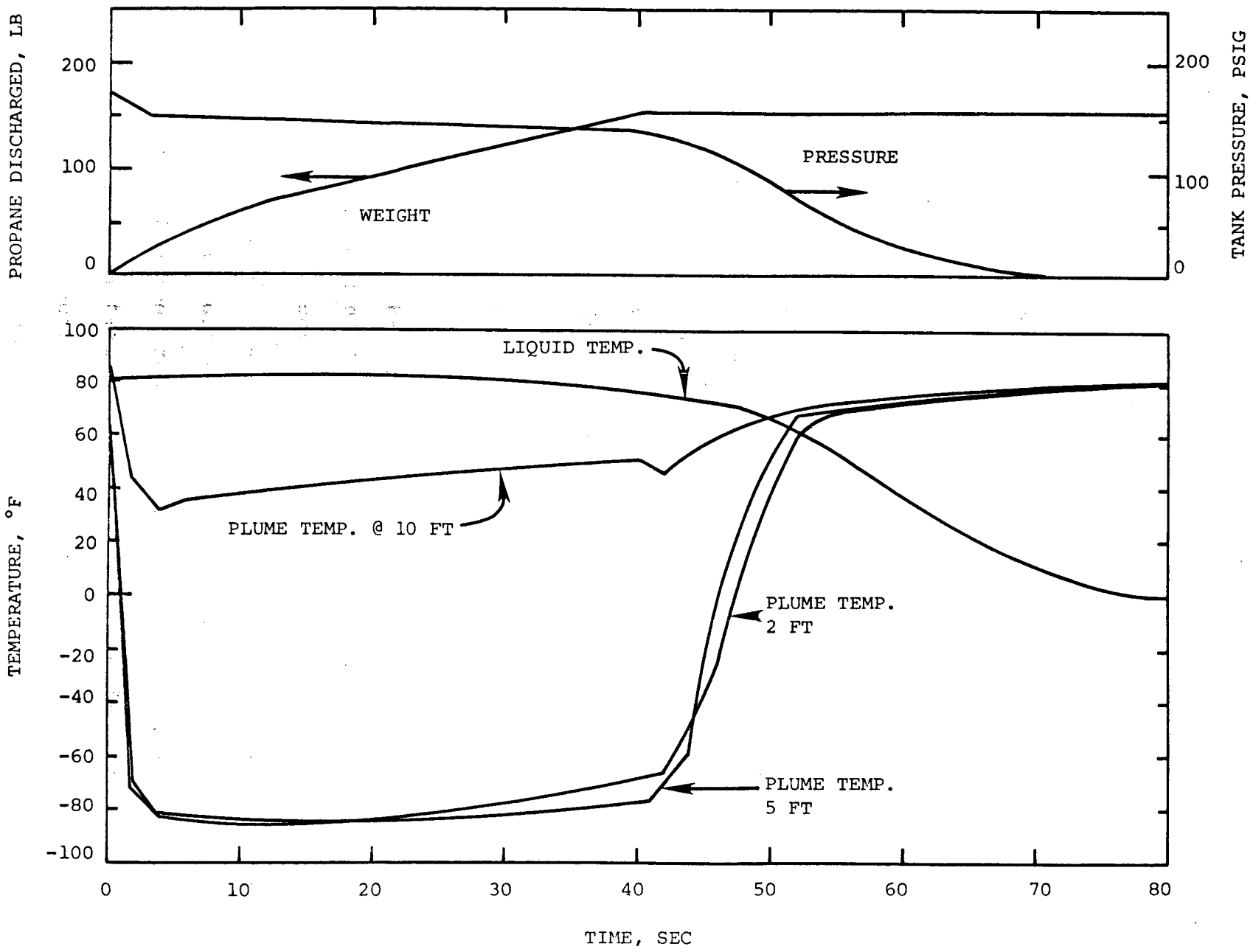

Figure 4. Temperatures, Tank Pressure, and Weight Loss for Ambient Temperature Propane Discharge.

Tests similar to that for which data are shown in Figure 4 were run for discharge rates from 13 to 180 lb/min. No propane was collected in the catch tray during any of the tests. In one test at a flow rate of 180 lb/min a deflector shield was placed 3 ft from the end of the discharge pipe to aid in catching liquid, but no liquid was accumulated. Qualitative tests were run with smaller tubes where the flow rate was 1.8 lb/min, but after 10 minutes of flow, no liquid propane was accumulated in an insulated bucket. The bottom of the bucket contained ice or hydrate, but no liquid. When propane was discharged at about the same rate with the 0.125 inch discharge tube held about 0.5 inches from a concrete surface, a puddle of propane a few inches in diameter formed after about a minute. The propane vaporized rapidly when discharge was stopped.

During the LPG test program more than 200 tests involving spills of liquid propane were made. In about half of these tests, the liquid propane was taken from ambient temperature storage. The propane was discharged into buckets, barrels, and open pits, and sufficient propane could be collected for small tests easily. Previous experience with liquefied natural gas had shown that care had to be taken, even when discharge was from a refrigerated cargo, in order to assure that the cold liquid did not simply atomize and then vaporize without forming a pool. Quantities of about 30 lb of propane could be transferred from

pressurized storage to a bucket in about 15 minutes. About two-thirds to three-quarters of the liquid flashed or atomized during filling, but once the bucket was filled, evaporation was very slow. The propane flashed to a temperature of $-70^{\circ}F$ or lower and did not warm to the boiling point unless heat was added to the liquid. The easiest way to warm the liquid was to sparge ambient temperature vapor into it. The vapor condensed into the liquid until the liquid reached its boiling point.

Most of the large scale tests used refrigerated propane as the fuel source. In those tests about one-third of the liquid boiled away or was atomized during the fuel transfer to test pits. Part of the loss was due to heat transfer from the concrete pit floor, but some loss was caused by atomization of liquid as it left the discharge pipe. An expansion chamber at the end of the discharge line prevented part of the loss caused by atomization, but the loss was still greater than expected based on equilibrium calculations for flashing vapor and heat transfer from the pit floor.

During one of the large scale tests, about 3000 gal of ambient temperature propane was flashed into a pit 10 ft square. The expansion chamber was placed around the discharge nozzle. When the discharge was stopped, less than 500 gal was in the pit, and more than 80 percent of the propane had flashed, atomized and then vaporized, or vaporized as the test pit cooled.

CONCLUSIONS

If ambient temperature propane is discharged into the atmosphere at rates up to about 200 lb/min, no accumulation of liquid will occur. If the flow is directed at the ground and continues for a long time, some accumulation of liquid may occur after the ground is frozen, but only small fractions of the total flow will remain as liquid. If more than a small fraction of the flow is to be accumulated as liquid during discharge of ambient temperature propane, an expansion chamber and container must be used to trap the spray. Except possibly for very large spills the atomized spray will evaporate before it can settle to the ground.

☆ U.S. GOVERNMENT PRINTING OFFICE: 1982-361-076:3095